ISSN 2712-8172

MAGAZINE OF CIVIL ENGINEERING

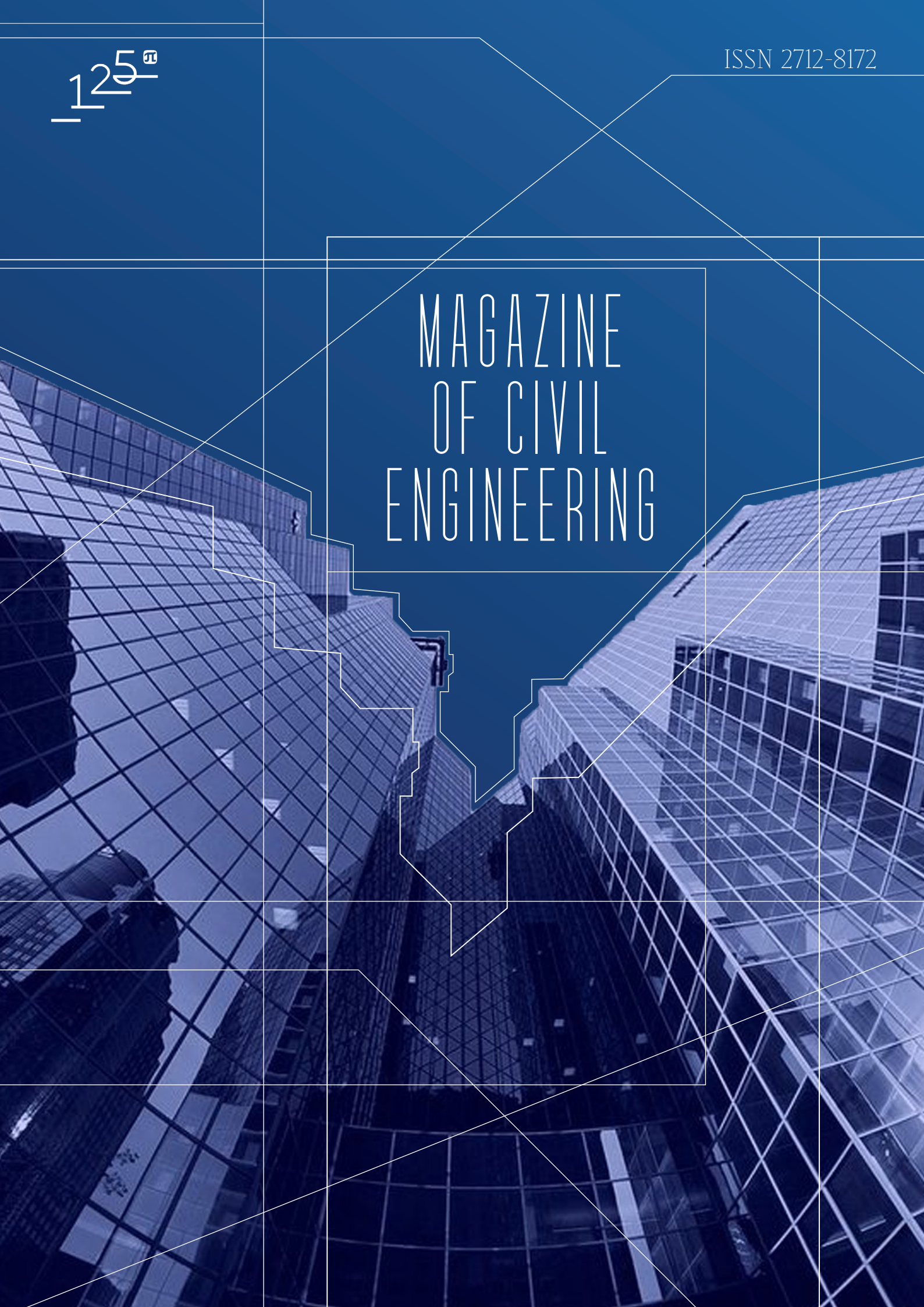

Magazine of Civil Engineering

ISSN 2712-8172

Online peer-reviewed open-access scientific journal in the field of Civil and Construction Engineering

Founder and Publisher: Peter the Great St. Petersburg Polytechnic University

This journal is registered by the Federal Service for Supervision of Communications, Information Technology, and Mass Media (ROSKOMNADZOR) in 2020. Certificate El No. FS77-77906 issued February 19, 2020.

Periodicity: 8 issues per year

Publication in the journal is open and free for all authors and readers.

Indexing: Scopus, Web of Sceince (ESCI, RSCI), DOAJ, Compendex, Google Academia, Index Copernicus, ProQuest, Ulrich's Serials Analysis System, CNKI

Corresponding address: 29 Polytechnicheskaya st., Saint Petersburg, 195251, Russia

Chief science editor:
D.Sc., Galina L. Kozinetc

Deputy chief science editors:
D.Sc., Sergey V. Korniyenko

Executive editor: Ekaterina A. Linnik

Translator, editor: Irina Ye. Lebedeva

Proofreader: Philipp Chrysanthes S. Bastian

DT publishing specialist:
Anastasiya A. Kononova

Contacts:
E-mail: mce@spbstu.ru
Web: http://www.engstroy.spbstu.ru

Date of issue: 27.06.2025

Contents

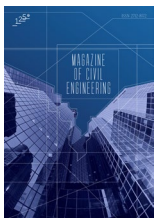

Magazine of Civil Engineering

ISSN 2712-8172

journal homepage: http://engstroy.spbstu.ru/

Research article

UDC 69

DOI: 10.34910/MCE.136.1

Early and long-term performance of green mortar made from the waste of electrical cables

Z. A. Hasan [1], ***M.S. Nasr*** [1] ✉, ***H.Z. Kubba*** [2], ***T.M. Hashim*** [3]

[1] *College of Engineering, University of Babylon, Babylon, Iraq*

[2] *Technical Institute of Babylon, Al-Furat Al-Awsat Technical University (ATU), Babylon, Iraq*

[3] *Department of Building and Construction Techniques Engineering, Al-Mustaqbal University College, Babylon, Iraq*

✉ *eng511.mohammed.nasr@uobabylon.edu.iq*

Keywords: electric cable waste, recycling, sustainable mortar, mechanical properties

Abstract. The disposal of solid waste has become one of the critical issues facing governments due to its environmental impact due to the difficulty of its decomposition. Electric cable waste (ECW) is one of these wastes. Its production increased in Iraq over time due to the demolition and reconstruction of residential and commercial homes. Therefore, reusing it in other industries, such as concrete technology, is a promising solution. Limited studies have studied the utilization of these local wastes as a replacement for natural sand in the short and long term. Therefore, the aim of this study is to investigate the properties of mortar incorporating recycled ECW as a partial replacement for sand. The fine aggregate (natural sand) was replaced by weight with ECW ranging from 0 to 25 % in the step of 5 %. Flow rate, as well as mechanical properties (compressive strength, flexural strengths, and density), were executed at 7, 28, and 360 days. It was found that the best performance was obtained at a replacement ratio of 5 % of ECW with mechanical strengths close to or slightly less than the reference sample and a 17 % reduction in density. However, regarding sustainability, it is possible to produce a lightweight structural mortar with a density lower than 1700 kg/m^3 and a compressive strength of 36 MPa at 360 days when replacing the natural sand with 25 % ECW.

Citation: Hasan, Z.A., Nasr, M.S., Kubba, H.Z., Hashim, T.M. Early and long-term performance of green mortar made from the waste of electrical cables. Magazine of Civil Engineering. 2025. 18(4). Article no. 13601. DOI: 10.34910/MCE.136.1

1. Introduction

Pollution is one of the great challenges that face humans. For that, researchers are looking for an eco-friendly solution to withstand serious problems, such as accumulating waste and non-biodegradability in addition to maintaining (natural) resources from consumption [1–5]. Recently, the world's growth and the development of electrical waste are as well-developed along one side. Electrical waste includes different materials, such as copper, aluminum, lead, iron, and plastic. The waste will react to produce a chemical toxic, which leads to spoiling human health and affects adversely the environment. The reuse of electrical cable waste (ECW) as a full or partial replacement for building substances is one of the promising solutions [6]. Plastics have wide-ranging applications, such as construction, packaging, healthcare applications, transportation, and electrical/electronic materials. Polyvinyl Chloride commonly (PVC) wire insulations are acquired from scrap vendors [7].

It is supposed that the reuse of the solid residue in concrete technology leads to less environmental damage and less demand for landfills on the one hand, as well as converting it into valuable materials on the other hand [8, 9]. Many previous works have used this plastic waste in concrete technology. For

example, Lakshmi and Nagan [10] examined the concrete compressive strength in the existence of electronic plastics. The compressive strength declined by 2.59 % when using 1 % 5 cm waste plastic. In contrast, the compressive strength increased from 6 to 11 % when the volume of waste plastic was reduced to 3 cm. Tensile strength was also improved by 4.5 % when embedding 3 cm of waste plastic compared to 5 cm. Raghatate Atul [11] reported that by incorporating waste e-plastics into concrete, mechanical properties were improved and the compressive strength was boosted by up to 20 %. However, the splitting tensile strength showed a marginal increase of 0.8 % after a 20 % substitution. Gull and Balasubramanian [12] explored the ability to use waste plastics (insulation wire) as fibers after shredding them into defined shapes with a size range of 3–5 cm. Samples were treated for 7, 14, and 28 days. The results revealed that at 1% e-plastic, the compressive strength increased by 5.9 and 10.6 % after using 4 and 3 cm sizes of waste plastic, respectively. In contrast, the reduction was 2.59 % with a size of 5 cm. However, at the same percentage addition, the tensile strength improved by 2.3 % for 5 cm of e-plastic and increased by 4.6 % for 4 cm in 28 days. Grinys et al. [13] investigated concrete's mechanical, fracture, and microstructural properties containing 5 % ECW. Bulk density reduced 6.1–6.3 % in 5–10 % of waste electrical cables compared to conventional concrete.

Manjunath [14] investigated the ability to use electrical waste in concrete as fine and coarse aggregate with different replacement ratios: 0, 10, 20, and 30 %. Results showed that the compressive strength of 10 % e-plastic gave an improved performance. In contrast, by increasing the proportion of the e-plastic content of coarse aggregate to 20 %, the concrete's mechanical properties (compression, tensile, and flexural strengths) showed a decrease related to the reference mixture. The mechanical characteristics of the concrete were reduced when the e-plastic was used as a fine aggregate throughout the curing stages. Yildirim and Duygun [15] studied the effect of Waste Electric Cable Rubber (WECR), in which sand replaces concrete at 5, 10, and 15 % of the total volume. It was recorded a rise in the concrete workability due to the poor adhesion between the WECR and the cement paste. The mechanical properties recorded a decline in their performance. An increase in WECR reduces the mechanical strengths of the concrete at 3, 7, and 28 days, leading to a decrease in adherence, especially at 15 % WECR.

Based on the existing literature, few research have used locally sourced ECW as a fine aggregate during the early and long-term periods. Moreover, waste aggregates (e-plastics) have a lighter weight than conventional natural aggregates, which is important for reducing the unit weight of the mortar. Thus, the main objectives of the current study include the production of environmentally friendly structural lightweight mortar by reducing the amount of fine aggregate (natural sand) in the mixture and replacing it with ECW. Furthermore, it aims to study its mechanical properties in the short and long term. Moreover, this research aims to recommend the best-performing substitution ratio for future research to better understand the behavior of this waste as an alternative to the natural resources in the construction sector. Therefore, in the present research, ECW in proportions of 5, 10, 15, 20, and 25 % substituted the sand in mortar. The flow and mechanical characteristics of mortars were studied at 7, 28, and 360 days. The reuse of this solid waste in the construction sector (especially concrete technology) as an alternative to raw materials contributes to enhancing sustainability by reducing the consumption of natural resources as well as limiting its environmental damage, in addition to reducing the need for landfill spaces.

2. Methods

Commercially available Ordinary Portland cement (CEM II/A-L 42.5R) was used, conforming to Iraqi specification No. 5 [16]. The chemical composition and physical and mechanical characteristics of cement are given in Table 1. Natural sand with a fineness modulus of 3, water absorption of 1.2 %, bulk density of 1650 kg/m^3 and specific gravity of 2.65 was provided by local quarries and employed as a fine aggregate. It conforms with the Iraqi specification No. 45 [17]. The particle size of the sand was ranged between 1.18 and 0.15 mm as illustrated in Table 2. The local tap water was used for mixing all ingredients. Superplasticizer type A and F, Glenium 54 (manufactured by BASF Company), was utilized to adjust the flowability of the mortar mixtures. Glenium 54 complies with ASTM C494 [18]. ECW was replaced with sand at different percentages. ECW was collected from waste cables. The outer wire sheaths, which consisted of plastic only (did not contain copper or aluminum), were shredded into small pieces and then, ground with a grinder. After that, they were sieved within the range 1.18–0.15 mm, to be ready for substitution with natural fine aggregate (sand), as presented in Fig. 1. The density of ECW is 1048 kg/m^3.

Table 1. The properties of the utilized cement.

Oxides	Content, %
CaO	62.9
Al_2O_3	4.7
Fe_2O_3	3.8
SiO_2	20.3
MgO	3.2
SO_3	1.75
Insoluble residue	1.15
Loss on Ignition	3.0
Free lime	0.8
Physical properties	
Setting time (min)	
Initial	54
Final	**222**
Compressive strength (MPa)	
3 days	**28.2**

Table 2. The sieve analysis outcome of the fine aggregate.

Sieve opening (mm)	Iraqi standard (No. 45)	Passing percentage, %
2.36	85–100	100
1.18	75–100	100
0.60	60–79	71.8
0.30	12–40	35.1
0.15	0–10	3.7

Different blends were cast to investigate mortar's fresh and mechanical properties with and without ECW. The mixture that served as the control was composed entirely of natural sand, while the other mixtures incorporated ECW by 5, 10, 15, 20, and 25 %, respectively, as a substitute for sand. The water/cement and superplasticizer dosages were 0.38 and 3.5 %, respectively. Table 3 shows the proportions mix details for mortar in this work.

Table 3. Mix proportions details of mortars in grams (for three prisms with dimensions of 40×40×160 mm^3).

Mix designation	Cement	Fine aggregate	ECW aggregate	Water/Cement	SP*
ECW0	500	1375	0	190	17.5
ECW5	500	1306	69	190	17.5
ECW10	500	1237.5	137.5	190	17.5
ECW15	500	1169	206	190	17.5
ECW020	500	1100	275	190	17.5
ECW025	500	1031.5	343.5	190	17.5

* SP – superplasticizer

A mechanical mixer that complied with ASTM C305 [19] was used for mixing the mortar components. The mixing period was five minutes. Firstly, the dry materials were mixed for 0.5 minutes at a low-speed rate (140 rpm). The water and superplasticizer were supplemented with the mixer, and all ingredients were blended for two minutes at 140 rpm. Then, the mixer was paused for half a minute. After that, the mixer was operated for final mixing at 285 rpm for two minutes. After mixing directly, the flow test of the fresh mortar was conducted following ASTM C1437 [20]. The fresh mixtures were cast 40×40×160 mm^3 standard molds and vibrated using an electrical vibrator. Molds were removed after 24 hours, and the specimens were stored in a water tank (at room temperature) until the test time. Many tests were conducted for the hardened mortar, including flexural strength, compressive strength and bulk density at 7, 28, and 360 days. The density was determined by dividing the mass of the prism by its geometric volume [21], while the compressive and flexural strengths were determined following BS EN 196-1 [22].

Figure 1. ECW aggregate.

3. Results and Discussion

3.1. Flow Rate

Fig. 2 shows the results of flow rates for all mixtures. Overall, the results reported that the existence of ECW aggregates reduced the flow rate of the mortar mixtures. The greater the percentage of substitution with natural sand, the higher the reduction rate. The decreasing values ranged from 2.5 % for ECW5 to 50 % for ECW25 compared to the control mixture (ECW0). The sharp edges and irregular shape of ECW grains may be the reason for reducing the flow of mortar, as this reduces the fluidity within the fresh mixture and increases the friction between its components [23]. When the waste content in the mixture increases, the friction between the components also increases, which results in a proportional decrease in flow. The literature has also revealed similar findings [24].

3.2. Compressive Strength

Figs. 3, 4, and 5 display the compressive strength of mortar mixtures after 7, 28, and 360 days, respectively. In general, the results showed that replacing the fine aggregate with ECW led to a drop in the compressive strength of the hardened mortar and that the decline grew as its proportion in the mixture increased. In other words, the lowest strength reduction was recorded for the ECW5 mixture, while the highest decrease was recorded for the ECW25 mixture. This behavior has been observed for all early and late ages. The reduction rates ranged from 6.92 to 45.54 %, from 4.55 to 37.06 %, and from 2.3 to 40.82 % for ECW5 and ECW25 mixtures at 7, 28, and 360 days, respectively. The softer waste strength compared to surrounding cement paste and its low compressive strength compared to the natural sand may explain the reduction in compressive strength [13].

In addition, this phenomenon occurs due to the enlargement of plastic particles and the weakening of the bonding force between the cement paste and the plastic aggregate surface. Plastic is also a hydrophobic substance, which limits the amount of water needed for the cement hydration [25, 26]. Similar results have been documented in the existing literature [13, 15, 27].

Moreover, it was observed that the decrease in compressive strength at 28 and 360 days is less than that at 7 days age compared to the control mixture. The reason for this may be that, over time, the hydration increases, which enhances the bond between the matrix and the ECW particles and, as a result, leads to a reduction in the strength losses.

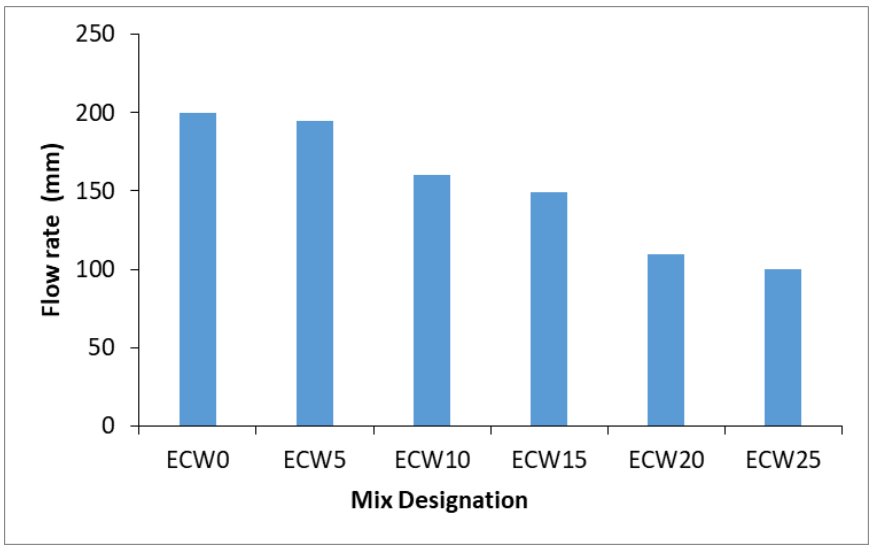

Figure 2. Flow rate results of fresh mortar mixtures.

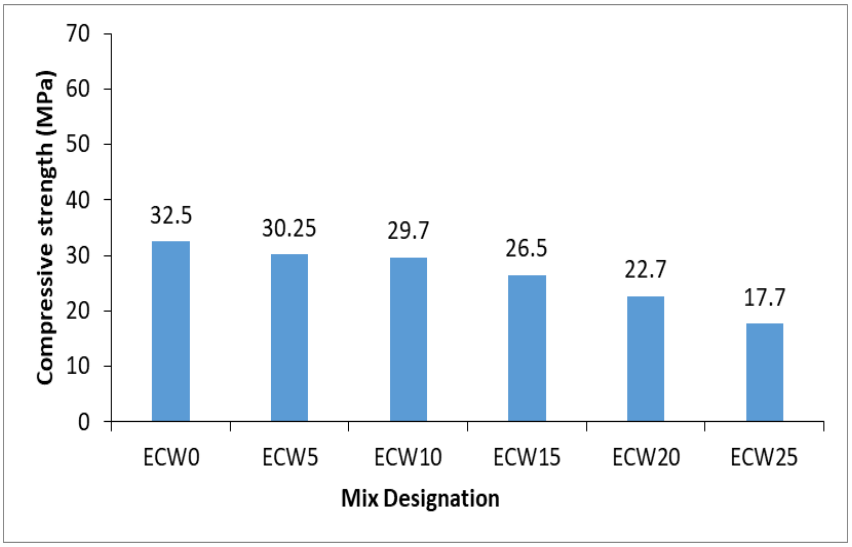

Figure 3. The 7-days compressive strength findings of ECW mortars.

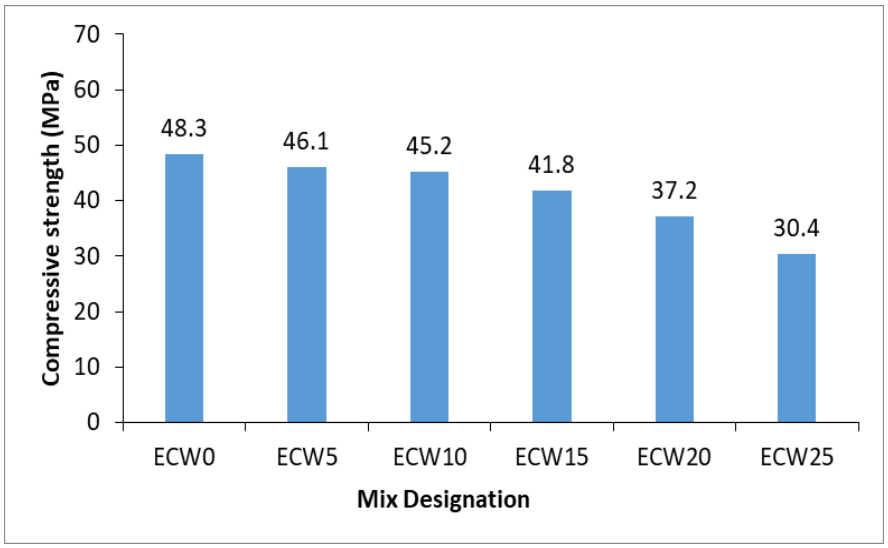

Figure 4. The 28-days compressive strength findings of ECW mortars.

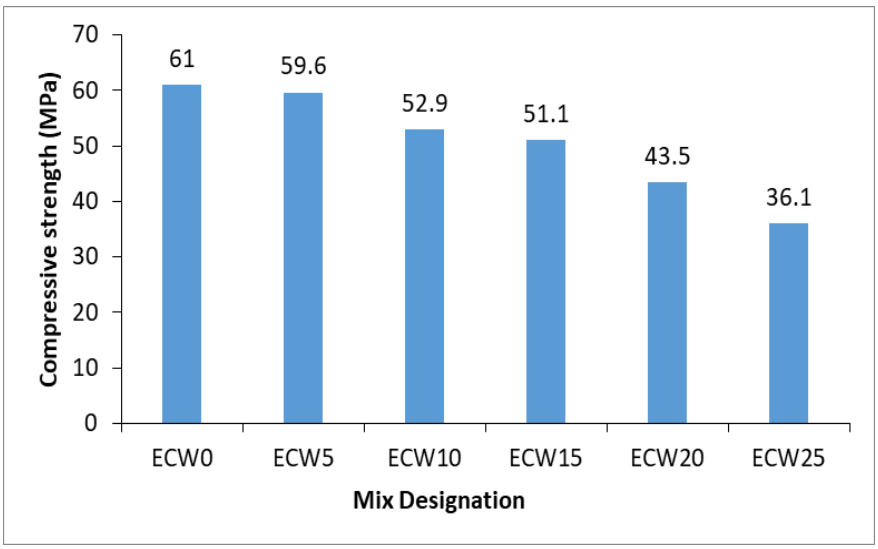

Figure 5. The 360-days compressive strength findings of ECW mortars.

3.3. Flexural Strength

Figs. 6 to 8 display the results of flexural strength examination. The results of the flexural strength showed a comparable tendency as in the compressive strength, where the strength decreased when using ECW. The higher the amount of waste in the mixture, the lower the flexural strength. The minimum decreasing rates were given by ECW5, 10, 15, and 5.56 % at 7, 28, and 360 days, respectively. In contrast, the highest drop percentages were found in ECW25: 50, 43.75, and 22.22 % in the same periods mentioned above. Comparable trends were obtained in previous works [13, 15, 27]. Among the reasons for the low flexural strength may be due to the flexible and unbreakable nature of the waste under loading [28]. The poor workability of the mixture and the weakness of the interfacial transition zone (ITZ) between the cement paste and the waste may be another reason for the low value of the flexural strength [29].

Moreover, it is noted that the decrease in flexural strength is higher than that in compressive strength for the same replacement values. The reason for this is that the flexural strength is more affected by the structure of voids and cracks inside the ITZ compared to the compressive strength [30]. Therefore, the effect on the flexural strength is greater.

3.4. Bulk Density

The bulk density results of the hardened mortars are illustrated in Figs. 9 to 11. Results disclosed that the density decreased after using ECW as a substitute for aggregates. Also, the reduction in density is proportional to the replacement rate. These results are agree with Yildirim and Duygun [15] and Ruiz-Herrero et al. [27]. The reason for reducing the density is due to the low density of these wastes (1048 kg/m^3) related to the natural aggregate (1650 kg/m^3). Similar findings for plastic waste were found in the literature [27]. Moreover, when observing the behavior of the density with age, it is noted that the reduction percentage of the given replacement percentage is almost constant regardless of the age of the examination (early or late). For example, the percentage of reduction for the ECW5 mixture (the lowest replacement percentage) was about 17 % for all ages, as well as for the ECW25 mixture (the highest replacement percentage), it was about 30 % for ages 7, 28, and 360 days, which indicates the homogeneity of the distribution of the substance in the mixture.

It is also noted that at the age of 360 days, by replacing 25 % of the waste, the density value was 1664.1 kg/m^3 compared to 2386.7 for the reference mixture. Upon observing the corresponding compressive strength value (36.1 MPa), it can be reported that a lightweight structural mortar has been produced.

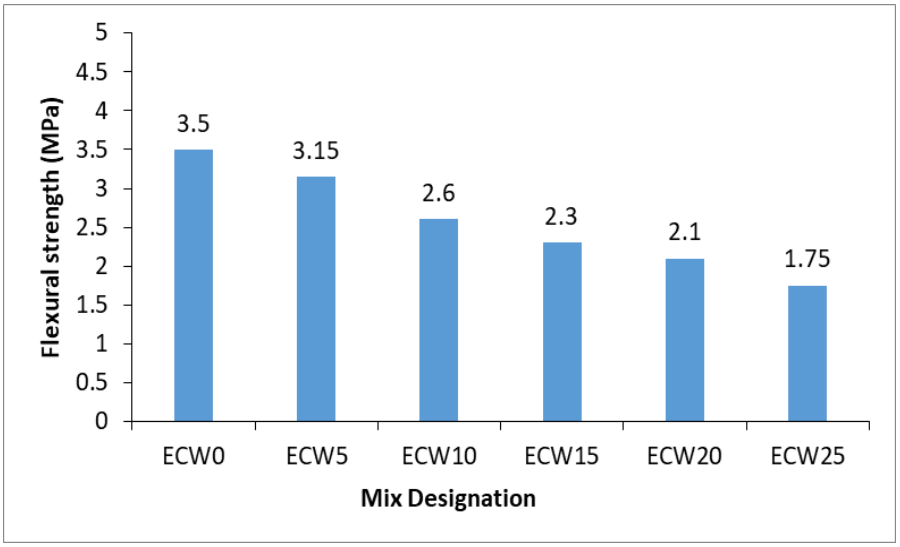

Figure 6. The 7-days flexural strength findings of ECW mortars.

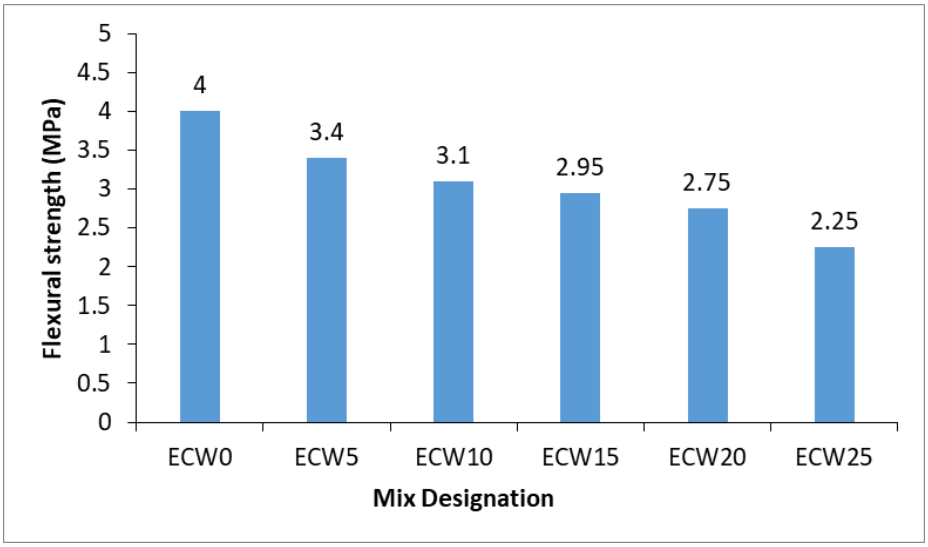

Figure 7. The 28-days flexural strength findings of ECW mortars.

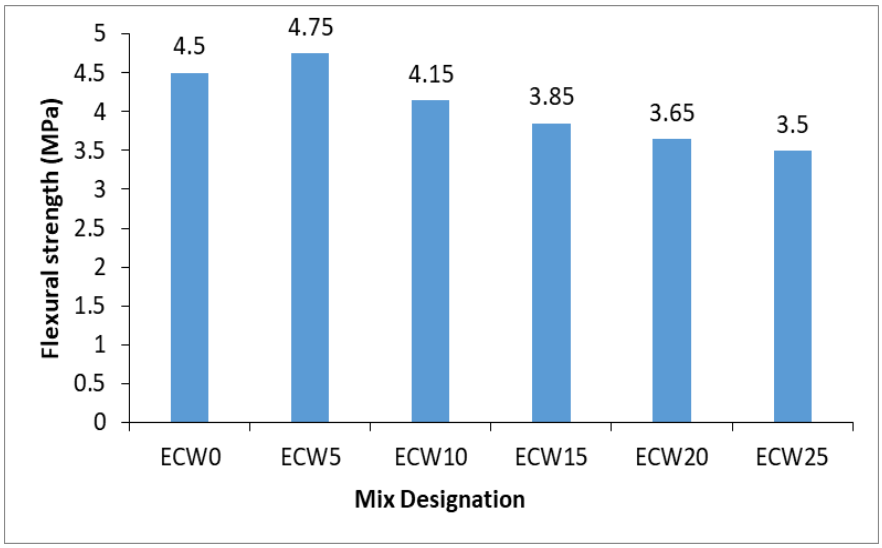

Figure 8. The 360-days flexural strength findings of ECW mortars.

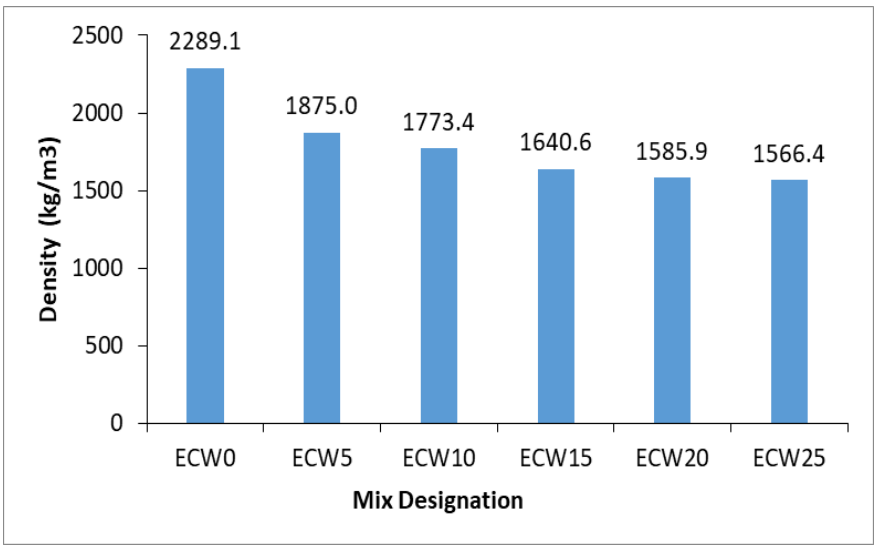

Figure 9. Density results of ECW mortars at 7 days.

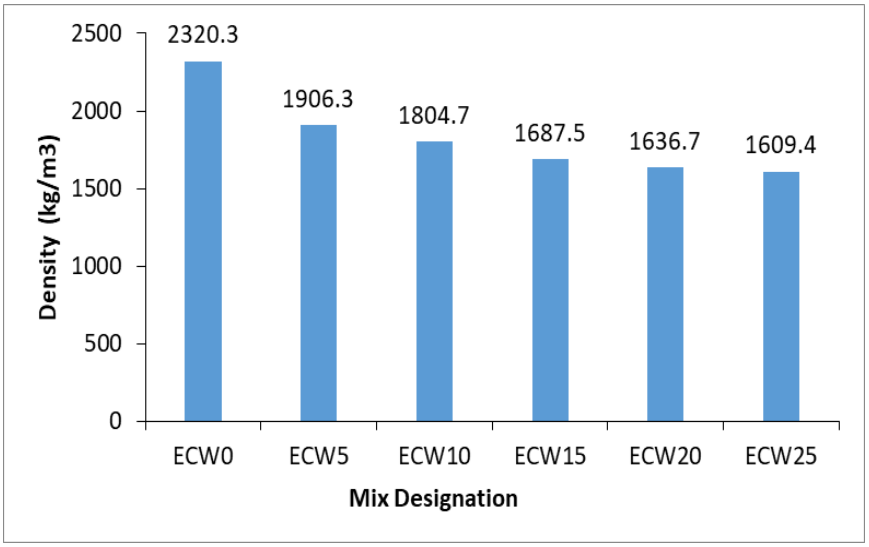

Figure 10. Density results of ECW mortars at 28 days.

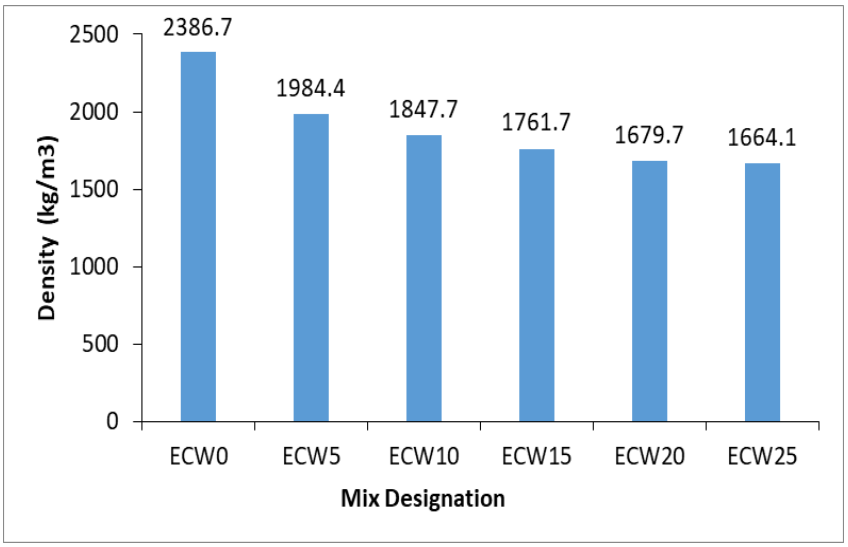

Figure 11. Density results of ECW mortars at 360 days.

3.5. Correlation

For mortars containing ECW ranging from 0 to 25 %, the compressive strength-flexural strength, compressive strength-dry density, and compressive strength-flow rate relationships have been developed

for each testing age (7, 28, and 360 days) as shown in Table 4 and Figs. 12 to 14. A polynomial equation (X^2) relationship was chosen for all the after-mentioned properties. The results revealed that a strong correlation between the compressive strength – flexural strength and compressive strength – flow rate have been recorded with a correlation coefficient (R^2) of not less than 0.91 for each corresponding age, which indicates that these properties are directly related to the compressive strength. That is, with an increase in the compressive strength, the density and flexural strength increase proportionally. Moreover, a good relationship was observed for the compressive strength with the density for ages 7, 28, and 360 days, with R^2 values in the range of 0.856 to 0.916.

Table 4. The equations and corresponding correlation coefficients of the developed equations for ECW-based mortars.

Age (days)	Relationship type					
	Compressive strength-flexural strength		Compressive strength-dry density		Compressive strength-flow rate	
	Equation	R^2	Equation	R^2	Equation	R^2
7	$Y = 0.008X^2 – 0.292X + 4.4452$*	0.940	$Y = 6.2181X^2 – 271.97X + 4467.9$	0.916	$Y = 0.3451X^2 – 10.11X + 168.64$	0.938
28	$Y = 0.0042X^2 – 0.2447X + 5.9026$	0.917	$Y = 4.2181X^2 – 300.83X + 6890.5$	0.878	$Y = 0.3127X^2 – 18.688X + 377.81$	0.950
360	$Y = 0.0016X^2 – 0.1038X + 5.2147$	0.927	$Y = 1.6518X^2 – 138.07X + 4516.4$	0.856	$Y = 0.0932X^2 – 4.8087X + 149.61$	0.991

Y – compressive strength; X – other property

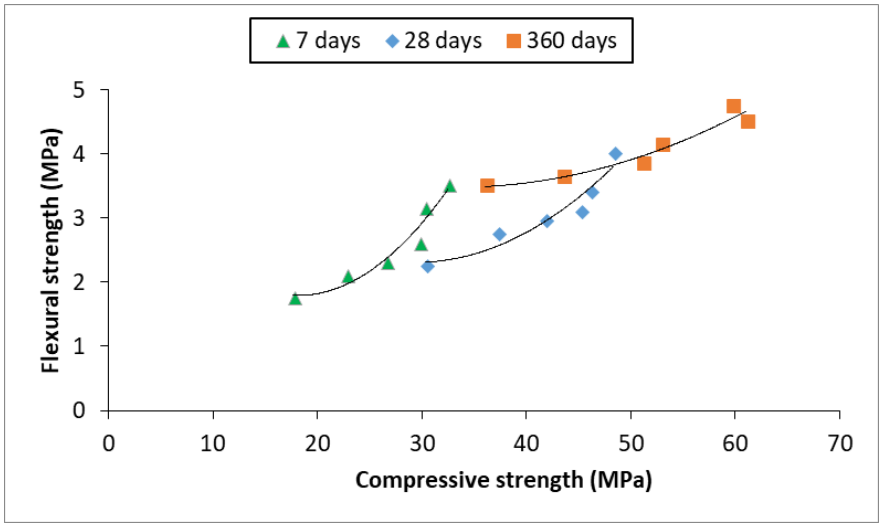

Figure 12. The compressive strength and flexural strength correlations of ECW-based mortars for 7, 28, and 360 days.

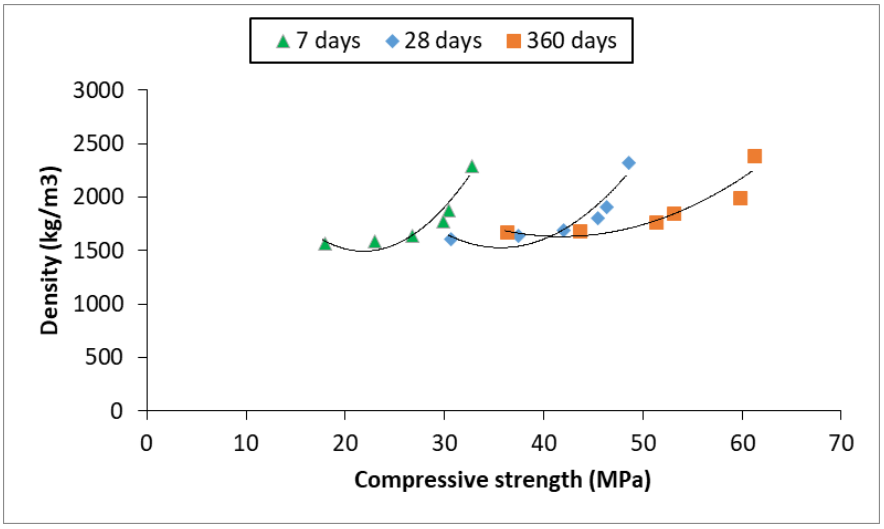

Figure 13. The compressive strength and density correlations of ECW-based mortars for 7, 28, and 360 days.

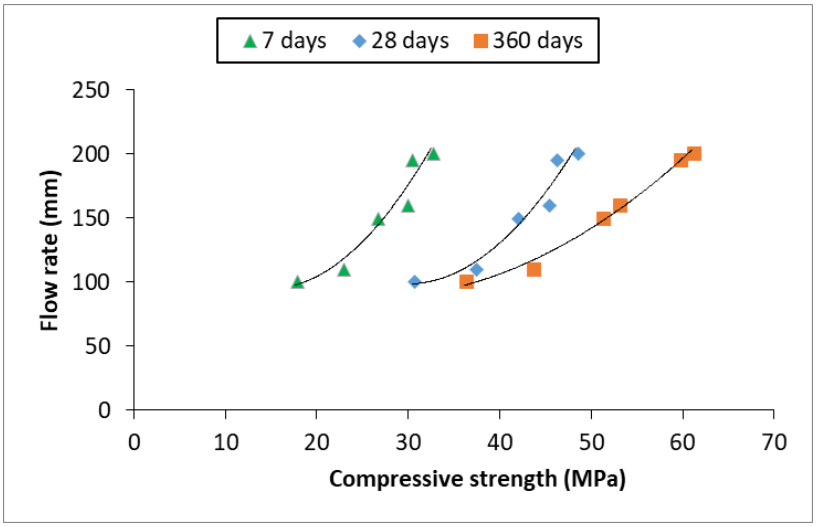

Figure 14. The compressive strength and flow rate correlations of ECW-based mortars for 7, 28, and 360 days.

4. Conclusion

In this experimental study, the influence of ECW was investigated as an alternative to the natural sand in mortar at early and late ages. Through the flowability and mechanical characteristics results, the following have been concluded:

1. The presence of ECW as sand replacement material can reduce the flowability of flesh mortar and the reduction rate increases with the ECW content in the mix.
2. Replacing sand with ECW contributed to reducing the mechanical properties of mortar for all ages (7, 28, and 360 days). The lowest reduction percentage was for ECW5 (2.3 and 15 % for compressive and flexural strength, respectively, at 360 days). On the other hand, the ECW25 mix recorded the highest reduction amount, reaching 40.82 % in compressive strength and 22.22 % in flexural strength at the age of 360 days.
3. ECW caused a decrease in solid density of approximately 17 % at a 5 % replacement rate and about 30 % at a 25 % replacement rate compared to the reference sample for all ages of examination. This indicates the production of lightweight mortar suitable for structural applications.
4. The correlations developed between the compressive strength property and each flow rate, flexural strength, and density revealed good second-order polynomial equations with a correlation coefficient (R^2) between 0.856 to 0.991.

In summary, considering all the tests carried out, the best performance of using ECW was at a 5 % substitution ratio with flow values and strengths equivalent to or slightly less than those of the reference mix with a density value of lower than 2000 kg/m^3. Moreover, it is possible to obtain a lightweight, structural, and environmentally friendly mortar with a density of less than 1700 kg/m^3 when replacing 25 % of the natural sand with ECW. It can be utilized for different construction purposes, as its compressive strength is 36 MPa at 360 days.

References

1. Abeer, S.Z., Hasan, Z.A., Abdulridha, S.Q. Investigation some properties of recycled lightweight concrete blocks as a fine aggregate in mortar under elevated temperature. Periodicals of Engineering and Natural Sciences. 2020. 8(1). Pp. 400–412.
2. Hasan, Z.A., Abdulridha, S.Q., Abeer, S.Z. Sustainable Mortar Made with Local Clay Bricks and Glass Waste Exposed to Elevated Temperatures. Civil Engineering Journal. 2021. 7(8). Pp. 1341–1354. DOI: 10.28991/cej-2021-03091729
3. Karkush, M.O., Yassin, S. Using sustainable material in improvement the geotechnical properties of soft clayey soil. Journal of Engineering Science and Technology. 2020. 15(4). Pp. 2208–2222.
4. Karkush, M.O., Yassin, S. Improvement of Geotechnical Properties of Cohesive Soil Using Crushed Concrete. Civil Engineering Journal. 2019. 5(10). Pp. 2110–2119. DOI: 10.28991/cej-2019-03091397
5. Karkush, M. O., Sabaa, M.R., Jaffar, G. S., Al Kubaisi, O. K. Effect of Embankment on the Behavior of Rigid Passive Pile Group in Sandy Soil. In Geotechnical Engineering and Sustainable Construction (pp. 329–341). Springer Nature; 2022.
6. Meyer, C. The greening of the concrete industry. Cement and concrete composites. 2009. 31(8). Pp. 601–605. DOI: 10.1016/j.cemconcomp.2008.12.010
7. Rochman, Ch.M., Browne, M.A., Halpern, B.S., Hentschel, B.T., Hoh, E., Karapanagioti, H.K., Rios-Mendoza, L.M., Takada, H., Teh, S., Thompson, R.C. Classify plastic waste as hazardous. Nature. 2013. 494(7436). Pp. 169–171. DOI: 10.1038/494169a

8. Kubba, H.Z., Nasr, M.S., Al-Abdaly, N.M., Dhahir, M.K., Najim, W.N. Influence of Incinerated and Non-Incinerated waste paper on Properties of Cement Mortar. IOP Conference Series: Materials Science and Engineering. 2020. 671. Article no. 12113. DOI: 10.1088/1757-899X/671/1/012113
9. Abdulridha, S.Q., Nasr, M.S., Al-Abbas, B.H., Hasan, Z.A. Mechanical and structural properties of waste rope fibers-based concrete: An experimental study. Case Studies in Construction Materials. 2022. 16. Article no. e00964. DOI: 10.1016/j.cscm.2022.e00964
10. Lakshmi, R., Nagan, S. Utilization of waste E plastic particles in cementitious mixtures. Journal of Structural Engineering. 2011. 38(1). Pp. 26–35.
11. Raghatate Atul, M. Use of plastic in a concrete to improve its properties. International Journal of Advanced Engineering Research and Studies. 2012. 1(3). Pp. 109–111.
12. Gull, I, Balasubramanian, M. A new paradigm on experimental investigation of concrete for e-plastic waste management. International Journal of Engineering Trends and Technology. 2014. 10(4). Pp. 180–186. DOI: 10.14445/22315381/IJETT-V10P234
13. Grinys, A, Vaičiukynienė, D, Augonis, A, Sivilevičius, H, Bistrickaitė, R. Effect of milled electrical cable waste on mechanical properties of concrete. Journal of Civil Engineering and Management. 2015. 21(3). Pp. 300–307. DOI: 10.3846/13923730.2015.1005019
14. Manjunath, B.T.A. Partial Replacement of E-plastic Waste as Coarse-Aggregate in Concrete. Procedia Environmental Sciences. 2016. 35. Pp. 731–739. DOI: 10.1016/j.proenv.2016.07.079
15. Yildirim, S.T, Duygun, N.P. Mechanical and physical performance of concrete including waste electrical cable rubber. IOP Conference Series: Materials Science and Engineering. 2017. 245. Article no. 22054. DOI: 10.1088/1757-899X/245/2/022054
16. Iraqi Standard No. 5. Portland Cement. Central Organization for Standardization and Quality Control. Baghdad, 1984.
17. Iraqi Standard No. 45. Aggregate from Natural Sources for Concrete and Building Construction. Central Organization for Standardization and Quality Control. Baghdad, 1984.
18. ASTM C494/C494M. Standard Specification for Chemical Admixtures for Concrete. ASTM International. West Conshohocken, PA, 2013.
19. ASTM C305. Standard practice for mechanical mixing of hydraulic cement pastes and mortars of plastic consistency. ASTM West Conshohocken, PA, 2014.
20. ASTM C1437. Standard Test Method for Flow of Hydraulic Cement Mortar. ASTM International. West Conshohocken, PA, 2013.
21. Raini, I., Jabrane, R., Mesrar, L., Akdim, M. Evaluation of mortar properties by combining concrete and brick wastes as fine aggregate. Case Studies in Construction Materials. 2020. 13. Article no. e00434. DOI: 10.1016/j.cscm.2020.e00434
22. BS EN 196–1. Methods of testing cement. Determination of strength. British Standards Institution-BSI and CEN European Committee for Standardization, 2005.
23. Abu-Saleem, M., Zhuge, Y., Hassanli, R., Ellis, M., Rahman, M., Levett, P. Evaluation of concrete performance with different types of recycled plastic waste for kerb application. Construction and Building Materials. 2021. 293. Article no. 123477. DOI: 10.1016/j.conbuildmat.2021.123477
24. Rao, M.M., Patro, S.K., Acharya, P.K. Utilisation of Plastic Waste as Synthetic Fiber and Aggregate in Concrete – A Review. The Open Civil Engineering Journal. 2023. 17(1). Article no. e187414952301100. DOI: 10.2174/18741495-v17-e230113-2022-HT31-3975-4
25. Bahij, S., Omary, S., Feugeas, F., Faqiri, A. Fresh and hardened properties of concrete containing different forms of plastic waste – A review. Waste Management. 2020. 113. Pp. 157–175. DOI: 10.1016/j.wasman.2020.05.048
26. Ismail, Z.Z., Al-Hashmi, E.A. Use of waste plastic in concrete mixture as aggregate replacement. Waste Management. 2008. 28(11). Pp. 2041–2047. DOI: 10.1016/j.wasman.2007.08.023
27. Ruiz-Herrero, J.L., Nieto, D.V., López-Gil, A., Arranz, A., Fernández, A., Lorenzana, A., Merino, S., De Saja, J.A., Rodríguez-Pérez, M.Á. Mechanical and thermal performance of concrete and mortar cellular materials containing plastic waste. Construction and Building Materials. 2016. 104. Pp. 298–310. DOI: 10.1016/j.conbuildmat.2015.12.005
28. Sharma, R., Bansal, P.P. Use of different forms of waste plastic in concrete – a review. Journal of Cleaner Production. 2016. 112(1). Pp. 473–482. DOI: 10.1016/j.jclepro.2015.08.042
29. Jain, A., Siddique, S., Gupta, T., Jain, S., Sharma, R.K., Chaudhary, S. Fresh, Strength, Durability and Microstructural Properties of Shredded Waste Plastic Concrete. Iranian Journal of Science and Technology: Transactions of Civil Engineering. 2019. 43(1). Pp. 455–465. DOI: 10.1007/s40996-018-0178-0
30. Zhang, H., Ji, T., He, B., He, L. Performance of ultra-high performance concrete (UHPC) with cement partially replaced by ground granite powder (GGP) under different curing conditions. Construction and Building Materials. 2019. 213. Pp. 469–482. DOI: 10.1016/j.conbuildmat.2019.04.058

Information about the authors:

Zaid Ali Hasan, *PhD*

E-mail: eng679.zaid.ali@uobabylon.edu.iq

Mohammed Salah Nasr, *PhD*

ORCID: https://orcid.org/0000-0003-0866-8526

E-mail: msn_alamar@yahoo.com

Huda Zuhair Kubba

E-mail: inb.huda@atu.edu.iq

Tameem Mohammed Hashim

E-mail: tameemmohammed@mustaqbal-college.edu.iq

Received 25.01.2023. Approved after reviewing 08.12.2024. Accepted 10.12.2024.

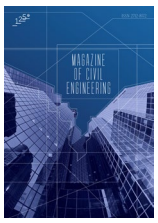

Magazine of Civil Engineering

ISSN 2712-8172

journal homepage: http://engstroy.spbstu.ru/

Research article

UDC 69

DOI: 10.34910/MCE.136.2

Production of glass-alkali binder for construction purposes by recycling of cullet

A.P. Prisyazhnyuk ✉, ***V.M. Vorontsov***,
Belgorod State Technological University named after V.G. Shukhov, Belgorod, Russian Federation

✉ *vosxod1962@mail.ru*

Keywords: cullet, glass-alkali binder, recycling, compressive strength, water resistance

Abstract. Municipal solid waste poses significant environmental challenges due to its wide range and potential contaminating impact. Finding sustainable solutions for its disposal is imperative. Moreover, certain types of municipal solid waste can serve as valuable resources in the construction sector. This study introduces a novel non-firing binder, devoid of cement, crafted from cullet, caustic alkali, water, and a plasticizing additive. These constituents undergo collaborative wet grinding in a ball mill, achieving a specific surface area of 500–550 m^2/kg. Concurrently during milling, glass particles are ground, and amorphous silica is leached with an alkaline solution, yielding a viscous-fluid adhesive mass enriched with siliceous compounds. This mass fills metal mold cells; upon attaining stripping strength, samples undergo heat treatment (drying) up to 90ºC. During this process, sols transform into polysilicic acid gels, which, after 5–6 hours, partially crystallize, achieving requisite strength. The resulting binder, produced without firing, boasts a compressive strength of approximately 25 MPa and a water resistance coefficient of 0.89. Suitable for low-grade concrete production (including glass concrete, fine-grained concrete, and foam concrete), its microstructure was analyzed via scanning electron microscopy, affirming the effective utilization of cullet in construction materials.

Funding: This work was realized in the framework of the Program “Priority 2030” on the base of the Belgorod State Technological University named after V.G. Shukhov. The work was realized using equipment of High Technology Center at BSTU named after V.G. Shukhov.

Citation: Prisyazhnyuk, A.P., Vorontsov, V.M. Production of glass-alkali binder for construction purposes by recycling of cullet. Magazine of Civil Engineering. 2025. 18(4). Article no. 13602. DOI: 10.34910/MCE.136.2

1. Introduction

The work is devoted to the development of the composition and technology for producing glass-alkaline binder, which promotes the development of environmentally friendly building materials at lower hardening temperatures.

Annually, the Russian Federation generates approximately 35–40 million tons of municipal solid waste, with 8–10% comprising glass waste, a valuable but underutilized by-product. Challenges in glass waste utilization include its heterogeneous chemical composition, presence of contaminants, and the high cost associated with its extraction from mixed waste streams. Concurrently, addressing issues related to industrial waste disposal while enhancing resource efficiency and improving the technical properties of construction materials has spurred interest in utilizing cullet from various types of unsorted glass, such as window, container, and household glass.

Cullet is waste glass that is crushed and ready to be remelted. It is an important component in the glass recycling process, used to make new glass bottles and other products. The main consumer for the recycled vitreous material (cullet) is the glass manufactory industry.

Currently, over 2.5 million tons of cullet accumulate in Russian landfills, with volumes steadily increasing. Active research endeavors seek to explore diverse avenues for cullet utilization. Crushed cullet finds application in plastics and various construction materials, including foam glass production, concrete and bitumen additives, and the manufacture of porous facing materials, tiles, panels, artificial slate, and roofing materials, road beds, pavement, trench fill, drainage medium, etc.; and in general use applications including abrasives, fluxes/additives, manufacturing of fiberglass insulation and foam insulation.

When used as sand replacement, there is some indication that there can be a noticeable reduction in compressive strength [1]. This is, however, not consistently observed [2, 3].

Concretes made from alkali-activated fly ash with pulverized glass have also been investigated [4].

Alkali-activated Class F fly ash cement with glass aggregates called “ashcrete” has also been studied [5]. The issue of alkali-silica reaction induced expansion is not a significant problem with alkali-activated fly ash cement mortar in comparison to the use of glass aggregate in normal mortar and concrete. This “ashcrete” has high strength and develops high early strength, which makes it very suitable for the precast concrete industry.

In the work [6], the alkaline solution formed with the glass waste will be use like alkaline activation agent for the blast furnace slag to produce cementitious materials.

Notably, cullet can serve not only as an aggregate, filler or alkaline activator but also as a component of binders, enabling the production of multifunctional materials.

Literature underscores the potential of finely crushed cullet, modified with additives, and subjected to heat and moisture treatment, to serve as a hydraulic binder for diverse construction applications.

Soda-glass cullet powder with specific surface area up to 400 m^2/kg has been used to produce geopolymers [7]. In contrast to fly ash or metakaolin-based geopolymers, water glass is not needed for the setting of glass cullet geopolymers.

Hence, there is a pressing need to develop a binder composition based on cullet capable of achieving strength under ambient conditions or through heat treatment at temperatures up to 100 °C. Grinding methods, including wet grinding, are explored to obtain finely dispersed powders with high specific surface areas, enhancing material chemical activity through surface effects.

When formulating the binder composition, the authors drew upon previous research findings by A.D. Bogatov et al. [8] and S.N. Bogatova et al. [9], who successfully developed non-autoclave composite building materials utilizing glass cullet mixed with alkaline solutions, resulting in enhanced resistance to aqueous acid solutions and biologically active media. However, their approach involved dry grinding of cullet followed by treatment with an alkaline solution with mechanical stirring, leading to partial extraction of amorphous silica solely from the surface of glass cullet particles. In contrast, this study employed grinding of cullet in a concentrated alkaline solution, enabling simultaneous breakdown of glass particles and dissolution of amorphous silica throughout the particle volume. This method ensured a higher concentration of silica gel formation.

The utilization of industrial waste, particularly cullet, in binder and concrete production, represents a promising frontier in modern materials science, gaining significance in recent years. Despite discussions dating back to the 1970s regarding the potential recycling of broken glass in the building materials industry, practical research in this domain has been limited. Presently, several Russian [10] and international universities and research institutes are actively engaged in developing building alkali activated composites (AAC) in general [11], and utilizing waste glass [12–14] and glass cullet [15, 16] in AAC.

The primary objective of this study is to develop effective technologies enabling the use of glass cullet not only as a filler but also as an independent binder, aligning with previous work by Y. Liu et al. [12], J.X. Lu et al. [13], A.B. Pascual et al. [14], R. Vinai et al. [15], J. Giro-Paloma and M. Soutsos [16], N.I. Kozhukhova et al. [17], V.G. Klimenko et al. [18]. Noteworthy contributions from foreign researchers include studies on the effective substitution of cement with finely dispersed glass [19–21].

However, the above-mentioned authors obtained a glass cullet-based binder by dry grinding the glass cullet to a fine dispersion similar to that of Portland cement, and then mixed the grinding product together with an aqueous solution of caustic alkali. In this case, the dissolution of amorphous silica occurred only on the surface of the particles in the glass cullet, which does not ensure its high concentration in the total mass of the binder.

Considering the high energy intensity and associated cost of such technological processes, the development of the use of cullet in the construction industry is relevant – the production of binders and concrete that can harden at temperatures up to 90 °C.

The purpose of this research is to develop a glass-alkali binder using energy-efficient technology: wet grinding of glass cullet in alkaline solution, which allows the use of technogenic raw materials and temperatures below 90 °C while maintaining the performance properties of the final product.

Research objectives: development of glass-alkaline binder compositions based on cullet with improved strength and water resistance; development of compositions of fine-grained concrete based on the obtained binder and glass cullet as a fine aggregate while maintaining strength characteristics; development of technology that allows producing glass-alkaline binder at a temperature up to 90 °C.

2. Materials and Methods

The primary glass component for the binder comprised cullet sourced from window and/or container glass.

The alkaline activator utilized was technical caustic soda (NaOH) conforming to the Russian Standard GOST–R 55064–2012, or potassium hydroxide (KOH) as per Russian Standard GOST 24363–80.

As a plasticizer, Melflux 2651 F manufactured by BASF Construction Additives, Germany, was employed. Melflux 2651 F, a spray-dried powder product based on modified polyester carboxylate, exerted a thinning effect on the binder mass, reducing the required mixing water while simultaneously increasing the alkali concentration in the solution. Tap water served as the solvent [22–24].

Table 1 presents the average chemical composition of the cullet used in the study.

Table 1. Chemical composition of glass cullet (wt. %).

Sourse of glass cullet	Oxide content (wt. %)					
	SiO_2	Al_2O_3	Fe_2O_3	CaO	MgO	Na_2O+K_2O
Window glass	69.0–72.5	1.5–4.2	0.1–0.8	7.5–8.7	2.5–3.5	13.2–14.0
Container glass	71.5–73.7	0.2–3.3	0.8–1.7	5.2–9.1	0.1–0.6	14.0–14.8

3. Results and Discussion

The cullet sourced from window and/or container glass underwent crushing using a jaw crusher with an outlet size of 2.5–5 mm. Approximately 500 g of crushed glass cullet was then introduced into a porcelain ball mill along with an alkaline solution containing dissolved caustic alkali and a plasticizer. The mixture underwent wet grinding in the designated spherical mill. The components were wet-milled in the specified milling unit for 2–8 h. During this process, the specific surface area of the milled product and the average particle size were measured (Table 2).

Table 2. Change in glass cullet dispersion depending on grinding time.

№	Grinding time, hours	Specific surface area, m^2/kg	Average particle diameter, μm
1	2	386.4	5.9
2	4	516.6	4.6
3	6	541.2	4.3
4	8	550.8	4.2

The results of the experiment (Table 2) showed that an intensive increase in the specific surface area is observed during 6 hours of grinding. Then, the increase slows down, and after 8 hours it becomes ineffective. Thus, the optimal grinding duration was 6 hours. As a result, the specific surface area of the cullet, serving as the primary component of the glass-alkali binder, reached 500–550 m^2/kg, with an average particle size ranging from 4.4–4.6 μm. The resultant milled product exhibited a viscous-fluid adhesive mass, utilized to fill the cubic cells of metal molds [25–27].

Following an exposure period of 16–18 hours under ambient conditions, during which the mixture acquired stripping strength, cube-shaped samples were extracted from the molds. Subsequently, these samples underwent heat treatment in a drying chamber at temperatures ranging from 85–90ºC for 5–6 hours. Post-heat treatment, the cooled samples were measured, weighed, and subjected to tests evaluating density, compressive strength, and water resistance. The outcomes of these tests are detailed in Table 3.

Table 3. Composition of glass-alkali binder and its physical and mechanical characteristics.

Mix ID	Mixes of glass-alkali binder, wt. %			Physical and mechanical characteristics							
	Glass cullet	Alkali component	W/C ratio	Average density, kg/m^3		Compressive strength, MPa				Water-resistance coefficient	
						in dry state		in water saturated state			
				NaOH	KOH	NaOH	KOH	NaOH	KOH	NaOH	KOH
1	98.5	1.5	0.2	1802	1800	17.5	17.5	14.7	15.2	0.84	0.87
2	98.3	1.7		1809	1806	20.3	19.6	16.2	15.8	0.80	0.81
3	98.0	2.0		1816	1813	21.6	20.1	18.6	16.8	0.86	0.84
4	97.7	2.3		1823	1819	22.4	20.3	20.2	18.5	0.90	0.91
5	97.5	2.5		1828	1820	23.1	20.4	20.3	17.7	0.88	0.87
6	97.2	2.8		1838	1835	26.4	25.8	23.5	22.9	0.89	0.89
7	97.0	3.0		1823	1818	22.5	21.8	19.8	19.0	0.88	0.87
8	96.7	3.3		1818	1810	21.6	20.3	18.6	18.2	0.86	0.90

The results depicted in Table 3 reveal that samples of the glass-alkali binder, post-drying, exhibit a compressive strength ranging from 17.5 to 26.4 MPa, with their water-resistance coefficient (the ratio of strength in a water-saturated state to the strength of dry samples) varying between 0.80 and 0.91, respectively. Notably, Mix 4 emerges as optimal, displaying the highest compressive strength and water resistance.

Microstructural analysis of fresh specimen fragments, obtained post-strength testing, was conducted utilizing a high-resolution scanning electron microscope TESCAN MIRA 3 LMU. Examination of the microstructure revealed that during cullet grinding in the presence of an alkali solution, finely dispersed amorphous silica dissolves from the glass melt. The resultant polysilicic acid gel, formed through polycondensation reactions, exhibits high adhesion, capable of binding incompletely dissolved glass particles together. Subsequent heat treatment (up to 90°C) induces the crystallization of the polysilicic acid gel, elucidating the relatively elevated values of density, compressive strength, and water resistance observed in glass-alkali binder samples. This phenomenon was documented in SEM images obtained for mixes employing potassium and sodium alkalis [28–30].

As illustrated in micrographs (Fig. 1) captured at various magnifications, the microstructure of the glass-alkali binder resembles a stone-like substance interspersed with partially crystallized silica gel (filamentous and lamellar fragments), with undissolved glass phase particles tightly adjoining them. This configuration facilitates the formation of a compacted and reinforced structure, irrespective of the alkali type used.

a **b**

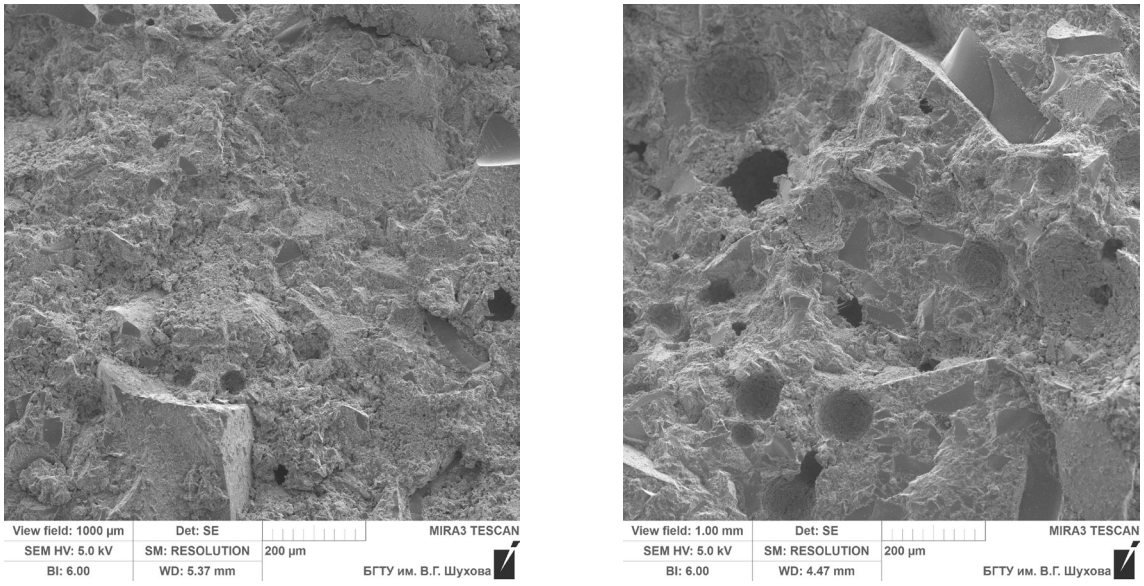

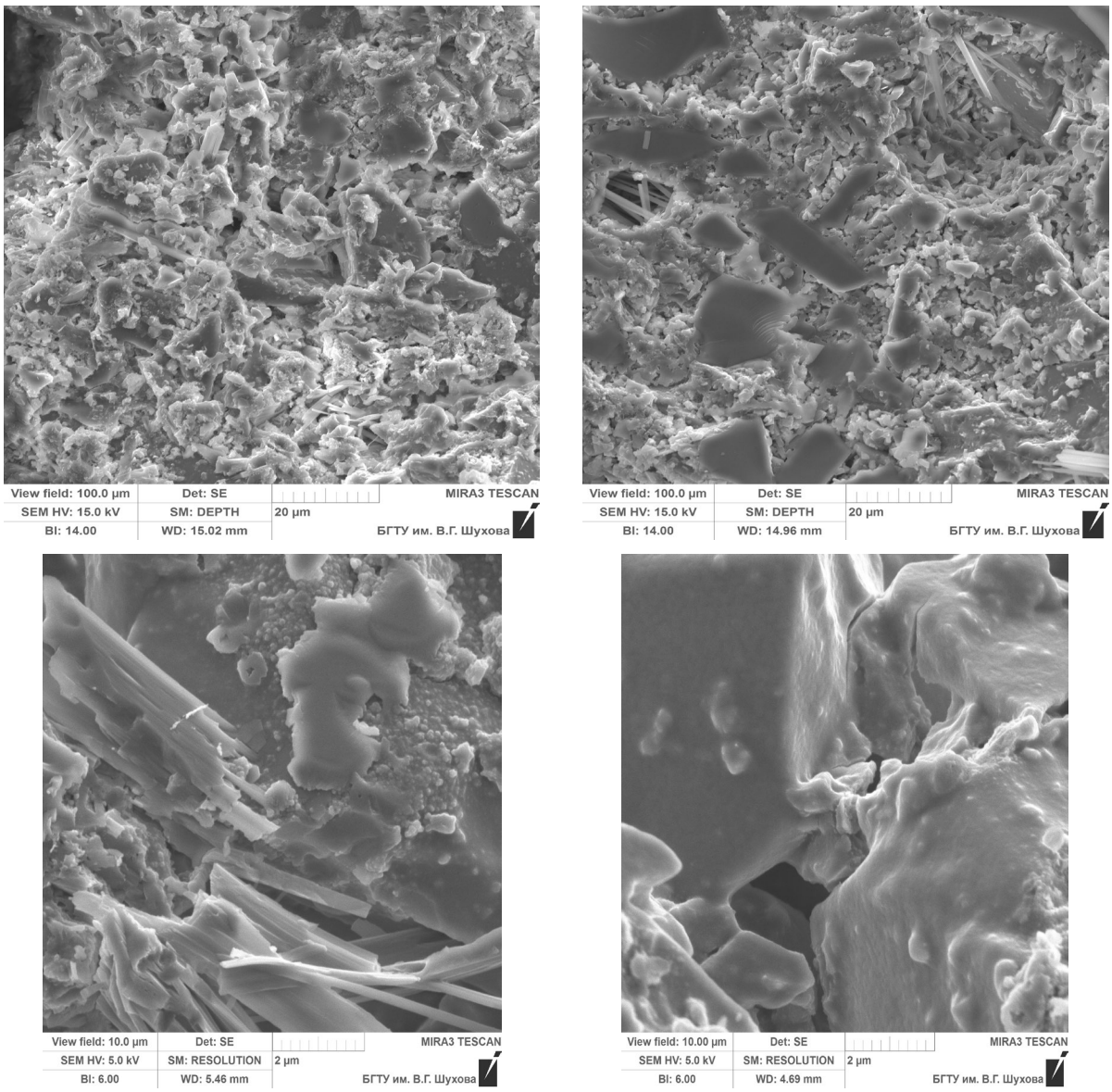

Figure 1. Microstructure of the glass-alkali binder Mixes: a) using KOH; b) using NaOH.

The results of X-ray phase analysis revealed crystalline phases of potassium silicates – $K_6Si_2O_7$, K_4SiO_4, $K_4Si_8O_{18}$, $K_2Si_2O_5$ and K_2SiO_3 – in the hardened binder modified with KOH aqueous solution (Fig. 2).

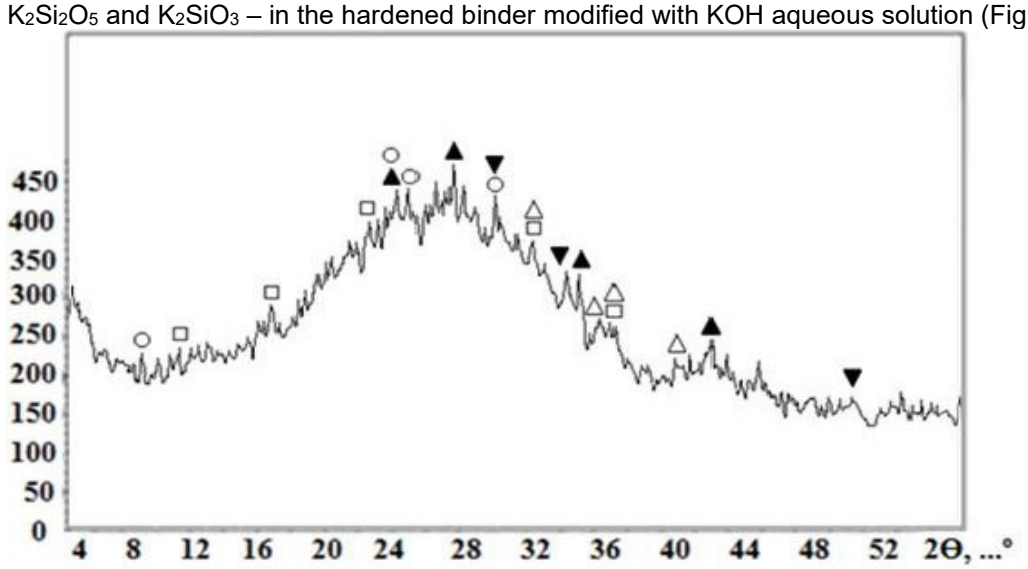

Figure 2. X-ray profile of glass-alkali binder modified with KOH aqueous solution: Δ – $K_6Si_2O_7$; ▼ – K_4SiO_4; □ – $K_4Si_8O_{18}$; ○ – $K_2Si_2O_5$; ▲ – K_2SiO_3.

In samples modified with NaOH solution, sodium silicates such as the following are observed: Na_2SiO_3, $Na_6Si_{40}O_{83}$, Na_4SiO_4 и $Na_2Si_3O_7$ (Fig. 3).

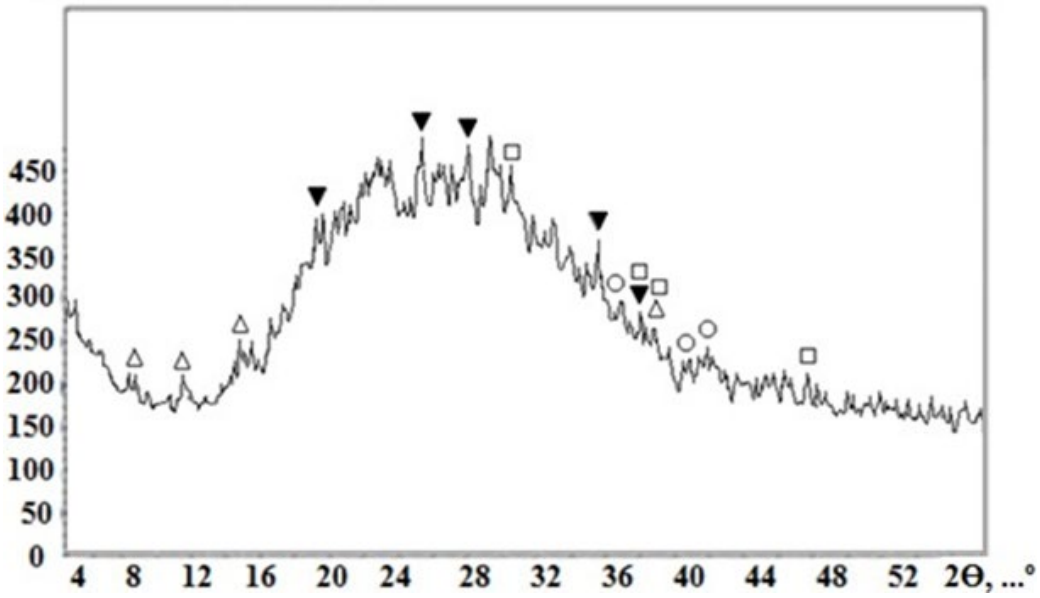

Figure 3. X-ray profile of glass-alkali binder modified with NaOH aqueous solution: □ – Na_2SiO_3; ∆ – $Na_6Si_{40}O_{83}$; ○ – Na_4SiO_4; ▼ – $Na_2Si_3O_7$.

Fine aggregates comprised quartz sand and crushed cullet with possessing a grain size of up to 1.25–0 mm. This fraction was selected considering workability and exhibiting the highest strength indicators in preliminary investigations.

The developed Mixes and the associated manufacturing method offer a pathway to create a binder without reliance on cement, lime, or other calcined binders, thereby circumventing the need for calcination and hydrothermal (autoclave) technologies, while minimizing energy consumption. The total curing time (until maximum strength is achieved) is 24 hours. The proposed glass-alkali binder holds promise for serving as a binder in the production of building materials and products, such as glass concrete, fine-grained concrete, and foam concrete. Utilizing household waste in the form of cullet as a predominant binder component, exceeding 80%, suggests the potential for significant-scale recycling of this waste.

In further studies, glass-alkali binder, Mix 6 (according to Table 3), based on NaOH at different W/C ratios in the range of 0.15–0.25, was used to obtain fine-grained silicate concrete. As a fine aggregate, quartz sand or glass cullet were used. Each aggregate was used separately. Fine aggregate was blended with a specific amount of glass-alkali binder. The resultant mixture was then shaped into metal molds with dimensions of 3×3×3 cm, compacted on a shaking table, and left to set overnight to gain stripping strength. Upon demolding, the samples underwent heat treatment in a drying chamber at temperatures ranging from 85–90ºC for 6 hours. Subsequently, the heat-treated samples underwent physical and mechanical testing, the outcomes of which are outlined in Table 4.

Table 4. Physical and mechanical characteristics of fine-aggregate concrete based on glass-alkali binder.

Mix ID	Solid components, wt. %			W/C ratio	Average density, kg/m^3	Compressive strength, MPa
	Glass-alkali binder	Quartz sand	Glass cullet			
1	75	25	–	0.15	1929	23.31
2	75	–	25		1926	22.44
3	75	25	–	0.18	1943	25.02
4	75	–	25		1938	24.52
5	75	25	–	0.20	1906	20.67
6	75	–	25		1884	18.85
7	75	25	–	0.25	1844	14.41
8	75	–	25		1836	14.08

The experimental findings presented in Table 3 demonstrate that the cement-free glass-alkali binder yields fine-grained concrete with strength properties ranging from 14–25 MPa when employing either quartz

sand or crushed cullet as fine aggregates. The subsequent concrete curing process involves drying at temperatures up to 90ºC, eliminating the need for energy-intensive heat, moisture, and autoclave treatments. This innovative approach minimizes energy and steam consumption while achieving robust concrete properties.

4. Conclusion

As a result of the studies, samples of glass-alkaline binder with a compressive strength from 17.5 to 26.4 MPa and a water resistance coefficient from 0.80 to 0.91 were obtained.

Based on the developed glass-alkaline binder, fine-grained concrete mixes with compressive strength values of 14–25 MPa were developed. The results obtained do not depend on the type of fine aggregate: quartz sand or glass waste – crushed glass cullet.

Thus, the conducted research indicates the feasibility of utilizing a cement-free and non-fired binder in the production of fine-grained concrete (utilizing quartz sand as aggregate) and glass concrete (employing cullet as aggregate). The manufacturing process of this binder is characterized by its low energy consumption, offering a sustainable alternative to traditional cement-based binders.

Moreover, the development of the glass-alkali binder facilitates the utilization of a substantial portion of household waste, specifically cullet, exceeding 80%. This presents an opportunity for large-scale waste disposal, thereby significantly mitigating the adverse environmental impact. By incorporating innovative materials and production techniques, this approach aligns with sustain-able development goals, promoting both environmental stewardship and resource efficiency.

References

1. Cement Concrete and Aggregates Australia. Use of recycled aggregates in construction. NSW. Mascot, 2008.
2. Oliveira, L.A., Castro-Gomes, J.P., Santos, P. Mechanical and Durability Properties of Concrete with Ground Waste Glass Sand. Proceedings of the 11th International Conference on Durability of Building Materials and Components. 1. Istanbul, 2008. P. 5.
3. Taha, B., Nounu, G. Utilizing Waste Recycled Glass as Sand/Cement Replacement in Concrete. Journal of Materials in Civil Engineering. 2009. 21(12). Pp. 709–721. DOI: 10.1061/(ASCE)0899-1561(2009)21:12(709)
4. Berry, M., Stephens, J., Cross, D. Performance of 100% fly ash concrete with recycled glass aggregate. ACI Materials Journal. 2011. 108. Pp. 378–384
5. Xi, Y., Li, Y., Xie, Z. and Lee, J. S. Utilization of solid wastes (waste glass and rubber particles) as aggregates in concrete. Proceedings of the International Workshop on Sustainable Development and Concrete Technology. Beijing, 2004. Pp. 45–54.
6. Torres, J., Palacios, M, Hellouin, M., Puertas, F. Alkaline chemical activation of urban glass wastes to produce cementitious Materials. Proceedings of the 1st Spanish National Conference on Advances in Materials Recycling and Eco – Energy. Madrid, 2009. Pp. 111–114.
7. Cyr, M., Idir, R., Poinot, T. Properties of inorganic polymer (geopolymer) mortars made of glass cullet. Journal of Materials Science. 2012. 47. Pp. 2782–2797. DOI: 10.1007/s10853-011-6107-2
8. Erofeev, V., Rodin, A., Yakunin, V.V., Bogatov, A.D., Bochkin, V.S., Chegodajkin, A.M. Alkali-activated slag binders from rock-wool production wastes. Magazine of Civil Engineering. 2018. 82. Pp. 219–227. DOI: 10.18720/MCE.82.20
9. Erofeev, V.T., Bogatov, A.D., Bogatova, S.N., Smirnov, V.F., Rimshin, V.I., Kurbatov V.L. Bioresistant building composites on the basis of glass wastes. Biosciences Biotechnology Research Asia. 2015. 12(1). Pp. 661–669. DOI: 10.13005/bbra/1710
10. Erofeev, V.T., Bogatov, A.D., Bogatova, S.N., Kaznacheev, S.V. Stroitelnyye materialy na osnove otkhodov stekla [Building materials based on waste glass]. Mordovia University Bulletin. 2008. 4. Pp. 70–79.
11. Kryvenko, P., Rudenko I., Pawel, S., Myroslav, S., Konstantynovskyi, O., Kropyvnytska, T. Alkali-activated cements as sustainable materials for repairing building construction: A review. Journal of Building Engineering. 2024. 90. Article no. 109399. DOI: 10.1016/j.jobe.2024.109399
12. Liu, Y., Shi C., Zhang, Z., Li, N. An overview on the reuse of waste glasses in alkali-activated materials. Resources, Conservation and Recycling. 2019. 144. Pp. 297–309. DOI: 10.1016/j.resconrec.2019.02.007
13. Lu, J.-X., Poon, C.S. Use of waste glass in alkali activated cement mortar. Construction and Building Materials. 2018. 160. Pp. 399–407. DOI: 10.1016/j.conbuildmat.2017.11.080
14. Pascual, A.B., Tognonvi, T.M., Tagnit-Hamou, A. Optimization study of waste glass powder-based alkali activated materials incorporating metakaolin: Activation and curing conditions. Journal of Cleaner Production. 2021. 308. Article no. 127435. DOI: 10.1016/j.jclepro.2021.127435
15. Vinai, R., Soutsos, M. Production of sodium silicate powder from waste glass cullet for alkali activation of alternative binders. Cement and Concrete Research. 2019. 116. Pp. 45–56. DOI: 10.1016/j.cemconres.2018.11.008
16. Giro-Paloma, J., Barreneche, C., Maldonado, A., Royo, M., Formosa, J., Fernández, A., Chimenos, J. Alkali-Activated Cements for TES Materials in Buildings' Envelops Formulated With Glass Cullet Recycling Waste and Microencapsulated Phase Change Materials. Materials. 2019. 12(13). Article no. 2144. DOI: 10.3390/ma12132144
17. Kozhukhova, N., Zhernovsky, I., Voytovich, E. Aspects of application of industrial aluminosilicate wastes in production of zero-cement construction composites. IOP Conference Series: Materials Science and Engineering. 2018. 365(3). Article no. 032043. DOI: 10.1088/1757-899x/365/3/032043
18. Klimenko, V.G., Pavlenko, V.I., Gasanov, S.K. Otkhody stekloboya – kak vazhnyy komponent kompozitsionnykh materialov na osnove gipsovykh vyazhushchikh [Waste glass as an important component of composite materials based on gypsum binders]. Bulletin of BSTU named after V.G. Shukhov. 2014. 6. Pp. 33–38.
19. Kadir, A.A., Ismail, M.R., Al Bakri, A.M.M., Sarani, N.A., Hassan, M.I.H. The Usage of Glass Waste as Cement Replacement. Key Engineering Materials. 2016. 673. Pp. 95–104. DOI: 10.4028/www.scientific.net/kem.673.95

20. Afshinnia, K., Rangaraju, P.R. Sustainable use of recycled glass in Portland cement concrete. The Journal of Solid Waste Technology and Management. 2016. 42(1). Pp. 16–24. DOI: 10.5276/jswtm.2016.16
21. Kondratiev, V.V., Karlina, A.I., Guseva, E.A., Konstantinova, M.V., Gorovoy, V.O. Structure of Enriched Ultradisperse Wastes of Silicon Production and Concretes Modified by them. IOP Conference Series: Materials Science and Engineering. 2018. 463(4). Article no. 042064. DOI: 10.1088/1757-899X/463/4/042064
22. Elagra, H., Rustom, R. Effect of using glass powder as cement replacement on rheological and mechanical properties of cement paste. Construction and Building Materials. 2018. 179. Pp. 326–335. DOI: 10.1016/j.conbuildmat.2018.05.263
23. Cherkasova, T.G., Cherkasova, E.V., Tikhomirova, A.V., Gilyazidinova N.V., Gilyazidinova N.V., Klyuev R.V., Karlina, A.I., Skiba, V.Y. Study of Matrix and Rare Elements in Ash and Slag Waste of a Thermal Power Plant Concerning the Possibility of their Extraction. Metallurgist. 2022. 65(11–12). Pp. 1324–1330. DOI: 10.1007/s11015-022-01278-2
24. Yelemessov, K., Sabirova, L.B., Martyushev, N.V., Malozyomov, B.V., Bakhmagambetova, G.B., Atanova, O.V. Modeling and Model Verification of the Stress-Strain State of Reinforced Polymer Concrete. Materials. 2023. 16(9). Article no. 3494. DOI: 10.3390/ma16093494
25. Usmanov, R., Mrdak, I., Vatin, N., Murgul, V. Reinforced soil beds on weak soils. Applied Mechanics and Materials. 2014. 633–634. Pp. 932–935. DOI: 10.4028/www.scientific.net/AMM.633-634.932
26. Amran, M., Onaizi, A.M., Fediuk, R., Vatin N.I., Rashid, R.S.M., Abdelgader, H., Ozbakkaloglu, T. Self-Healing Concrete as a Prospective Construction Material: A Review. Materials. 2022. 15(9). 3214. DOI: 10.3390/ma15093214
27. Fastykovsky, A.R., Martyushev, N.V., Musatova, A.I., Savchenko, I.A., Karlina, A.I. Feasibility demonstration of normative models for sheet-rolling shop productivity. Message 1. Chernye Metally. 2024. 2024(1). Pp. 9–16. DOI: 10.17580/chm.2024.01.02
28. Kondrat'ev, V.V., Ershov, V.A., Shakhrai, S.G., Ivanov, N.A., Karlina, A.I. Formation and Utilization of Nanostructures Based on Carbon During Primary Aluminum Production. Metallurgist. 2016. 60(7-8). Pp. 877–882. DOI: 10.1007/s11015-016-0380-x
29. Rassokhin, A., Ponomarev, A., Shambina, S., Karlina, A. Different types of basalt fibers for disperse reinforcing of fine-grained concrete. Magazine of Civil Engineering. 2022. 109(1). 10913. DOI: 10.34910/MCE.109.13
30. Dudin, M.O., Vatin, N.I., Barabanshchikov, Y.G. Modeling a set of concrete strength in the program ELCUT at warming of monolithic structures by wire. Magazine of Civil Engineering. 2015. 54(2). Pp. 33–45. DOI: 10.5862/MCE.54.4

Information about the authors:

Anastasia Prisyazhnyuk,
ORCID: https://orcid.org/0009-0001-8467-6301
E-mail: vosxod1962@mail.ru

Victor Vorontsov,
ORCID: https://orcid.org/0009-0005-2057-6503
E-mail: victorvorontsov2012@yandex.ru

Received 02.06.2024. Approved after reviewing 29.05.2025. Accepted 31.05.2025.

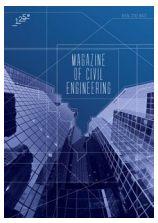

Magazine of Civil Engineering

ISSN 2712-8172

journal homepage: http://engstroy.spbstu.ru/

Research article

UDC 625

DOI: 10.34910/MCE.136.3

Using bio-oil as a rejuvenator for asphalt extracted from reclaimed asphalt pavement

A.A. Abdulmawjoud ✉ , ***M.K. Hammadi***

University of Mosul, Mosul, Iraq

✉ *aymanmawjoud@uomosul.edu.iq*

Keywords: bio oil, reclaimed asphalt pavement, rejuvenator, virgin asphalt, aged asphalt

Abstract. Every year, huge quantities of asphalt pavement resulting from road rehabilitation are crushed. To address the threat of waste accumulation and achieve a sustainable environment, the world has turned to recycling these asphalt wastes by treating them with renewable materials for reuse. In this research, bio-oil, which is a green liquid composed of oils extracted from biomass (corn oil, hill oil, sunflower oil, soybean oil, rapeseed oil and vegetable oil), was used. Many studies have employed different types of bio-oil as rejuvenators, showing good results for aged asphalt treated with bio-oil. Therefore, this type of bio-oil was used to demonstrate its effect on the physical condition and physical properties of bio-oil. One of the characteristics of the reclaimed asphalt was tested by adding bio-oil in different weight percentages (1 %, 2 %, 3 % and 4 %) to a blend of 70 % virgin asphalt and 30 % reclaimed asphalt to determine the ideal bio-oil proportion. Physical tests (penetration, softening point, ductility and viscosity) were conducted on the mixture. The results showed that adding bio-oil at an optimum rate of 1.31 % to the mixture increased penetration and ductility by 15.6 % and 34 %, respectively; reduced the softening point by 7 % and decreased viscosity at 135 °C and 165 °C by 33 % and 58 %, respectively. According to the results, aged asphalt can be renewed to a condition similar to virgin asphalt, offering both environmental and practical benefits by reducing waste.

Citation: Abdulmawjoud, A.A., Hammadi, M.K. Using bio-oil as a rejuvenator for asphalt extracted from reclaimed asphalt pavement. Magazine of Civil Engineering. 2025. 18(3). Article no. 13603. DOI: 10.34910/MCE.136.3

1. Introduction

Roads are the main arteries that connect cities, and their construction according to international standards is evidence of a country's development. Iraq has begun rehabilitating and rebuilding roads due to its economic openness to other countries. With this urban revolution in road rehabilitation and construction, the quantities of aged asphalt pavement waste have increased. As environmental sustainability gains prominence in academics and industry, and with the delayed use and accumulation of these materials, a way must be found to benefit from these materials and reuse them by mixing them with rejuvenators [1].

Recently the use of waste materials in construction as partial or complete replacement for virgin materials has increased for several reasons. Reclaimed asphalt pavement (RAP) materials are created by scraping off the top layer of aged asphalt pavements, which are then dumped in landfills, causing environmental issues [2]. During the recycling process, RAP components are mixed with virgin materials to create fresh asphalt mixture. Therefore, recycling RAP materials is a common approach to reducing manufacturing costs and energy consumption, as well as natural resources, while protecting the environment [3, 4].

As more RAP is used in asphalt mixes, concerns about the possible detrimental influence of the aged RAP binder on field performance are growing. To address these challenges, rejuvenators are increasingly

used to improve RAP mix performance. In [5], the effectiveness of waste vegetable oil (WVO) as rejuvenator in restoring the desired properties of recycled asphalt mixes. The effectiveness of rejuvenators was first evaluated based on aging resistance, rutting, and fatigue performance. Rejuvenated bitumen, when evaluated based on a linear amplitude sweep test, has shown inferior fatigue resistance compared to virgin bitumen. Such behavior of rejuvenated bitumen could be attributed to the presence of a high concentration of more reactive unsaturated fatty acids inherited from WVO. However, from indirect tensile fatigue tests on the asphalt mixes, it was found that the fatigue performance of rejuvenated recycled asphalt mixes is satisfactory.

In [6], the performance characteristics and workability of high RAP mixtures in the presence of a bio-modified binder was investigated. The data indicated that the addition of the bio-modified binder helped reduce the stiffness of the control mixture with 40 % RAP to a level closer to the stiffness of the same mixture without RAP. In addition, the presence of the bio-binder led to improving the workability of the mixtures, especially this was very evident at high-RAP content of 40 %. The data indicated that the bio-modified binder improved the fatigue properties and cracking characteristics and had no negative effect on the moisture susceptibility/rutting characteristics of the control mixture with 40 % RAP. Overall, data indicated that there was a good degree of blending between the virgin/bio-modified and RAP binders.

In [7], the recycling and restoration of RAP using two types of renovators, waste cooking oil (WCO) and asphalt cement (AC) 85–100, were studied. Five percentages (1 %, 1.5 %, 2 %, 2.5 % and 3 %) by weight of both types of renovators were added to the RAP, separately, for the purpose of rejuvenation. Marshall Test was performed on the renovated samples to obtain the optimum percentages, which will be adopted in subsequent tests, which include: indirect tensile strength, tensile strength ratio and duple punch shear strength test – to evaluate the performance of rejuvenated RAP mixes and compare them with the original RAP. The results indicated that 1.5 % of WCO and 2.5 % of AC 85–100 are the optimal percentages.

Other researches have been conducted to explore the use of materials, such as organic montmorillonite clay, fractionated bio-oil, cottonseed oil, crude glycerin and microalgae-derived bio-binders [8–11]. In [12], the effectiveness of an asphalt binder, produced from thermochemical conversion of swine manure, was examined. According to the test results, the addition of bio-binder can improve low temperature properties of asphalt binder significantly.

Bio-oil from renewable biomass can partially replace asphalt binder, because it is comparable to asphalt binder in terms of viscosity, elasticity, chemical composition and color [14, 15]. Adding bio-oil to asphalt binder may enhance its low-temperature properties and stress-cracking resistance [16–18].

In [19], it was found that adding 3–4 % of jatropha curcas oil (JCO) reduced age-hardening.

In [20], date seed oil (DSO) was used to modify binders containing different amounts of RAP binder varying from 20% to 40%. The moisture susceptibility, rutting performance, stiffness modulus and fatigue resistance of the mixtures were evaluated, and the results showed that the addition of DSO improved fatigue life of the specimens containing 20 % RAP up to 15 %.

This study uses a blend of 70 % virgin asphalt (VA) and 30 % RAP, following prior research [21].

The study's significance lies in mitigating environmental harm from obsolete asphalt waste, while repurposing it for road paving. The research will also help in establishing an economical and sustainable method for manufacturing RAP, which may ultimately lead to reducing waste and promoting greener infrastructure in the country.

The current study aims to study the effect of using bio-oil, consisting of a group of oils extracted from biological materials, on the properties of extracted asphalt RAP (30 %) mixed with VA (70 %) [1]. Various bio-oil ratios were tested to identify the optimal rejuvenation percentage. The methodology is outlined in Fig. 1.

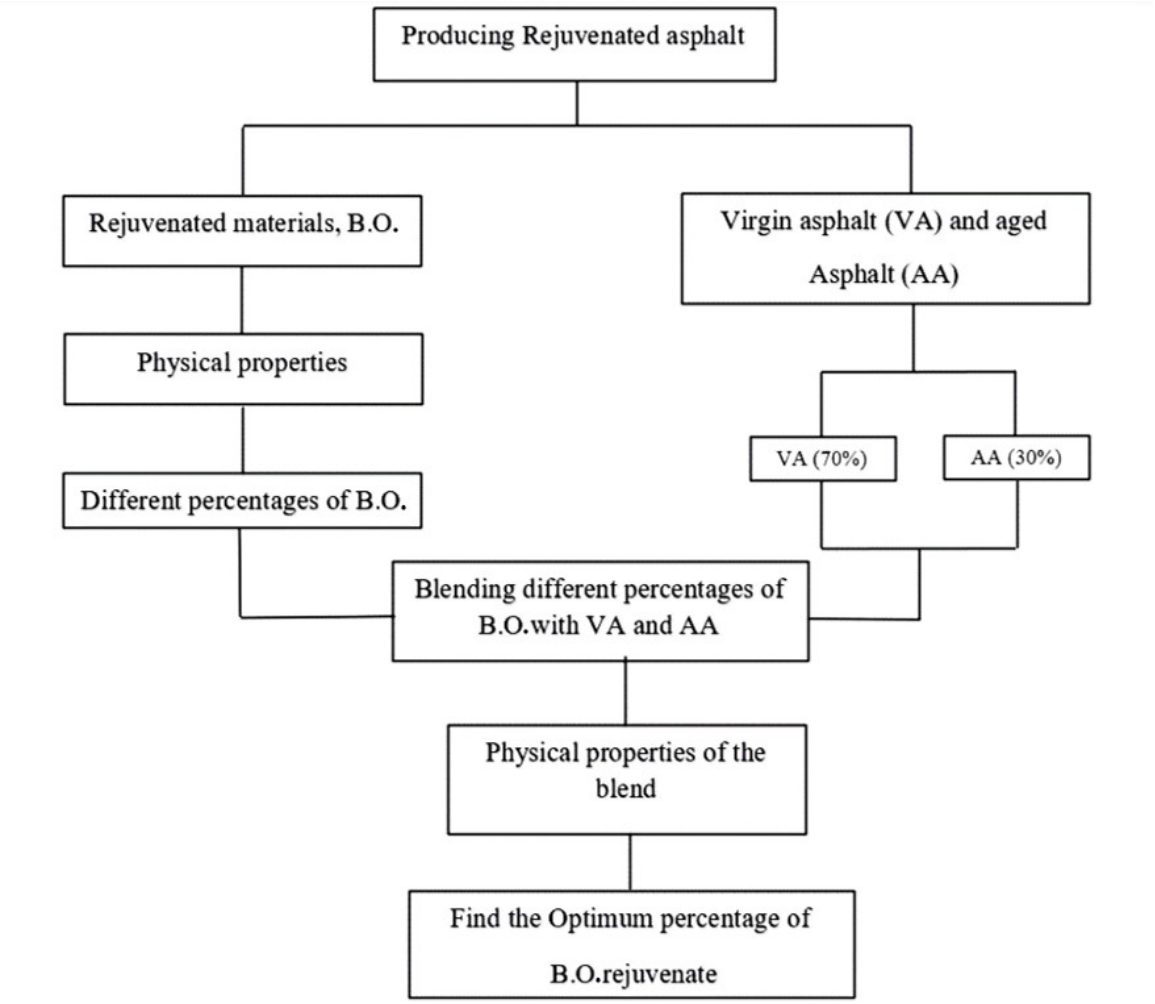

Figure 1. Research methodology.

2. Materials and Methods

2.1. Materials

Asphalt binder

Asphalt binder is the most widely used material for different types of paving in road construction [22]. In this study, 40–50 asphalt grade produced from AL-Daura refinery (Baghdad, Iraq) was used. The basic characteristics of this asphalt binder are shown in Table 1.

Table 1. Physical properties of the VA binder.

Physical properties	Value	Unit	Test condition	SCRB specification (2003)	ASTM standard
Penetration	43	1/10 mm	25 °C, 100 gm, 5 sec	40–50	D5
Ductility	145	cm	25 °C, 5 cm/min	> 100 cm	D113
Softening point	54	°C	Ring & ball	–	D36
Specific gravity	1.03	(25 °C/25 °C)	–	–	D70
Rotational viscosity	573	CP	135 °C	–	D4402
	143	CP	165		

Bio-oil rejuvenator

The bio-oil rejuvenator used in this study is a green liquid composed of several oils extracted from biomass (corn oil, tall oil, sunflower oil, soybean oil, rapeseed oil and vegetable oil), produced by SRIPATH Technology (LLC/ReLIXER). Physical and chemical properties are listed in Table 2.

Table 2. Physical and chemical properties of the bio-oil.

Property	Typical value	
Moisture, Vacuum oven	2 %	
Flash point	> 204 °C	> 400 °F
Density	0.9 kg/liter	7.5 lb/gal
Viscosity at 24 °C (75 °F)	0.05 Pa.s	50 cp
Insoluble	1 %	
Iodine value	115	

Reclaimed asphalt

The RAP used in this study was brought from one of the main roads in the city of Mosul, which connects the Al-Sukkar neighborhood intersection with the third bridge. This paving represents the binder asphalt layer and was created five years before its removal.

The aged asphalt was extracted from RAP using methylene chloride (CH_2Cl_2) as a solvent, according to the extraction test [23] and is shown in Fig. 2. The solvent methylene chloride was then separated from the aged asphalt using a rotary evaporator according to [24], as shown in Fig. 3. Research revealed that the centrifuge method was a reasonably safe and effective cold extraction technique [25]. Physical tests were conducted on the aged extracted asphalt, and the results are listed in Table 3.

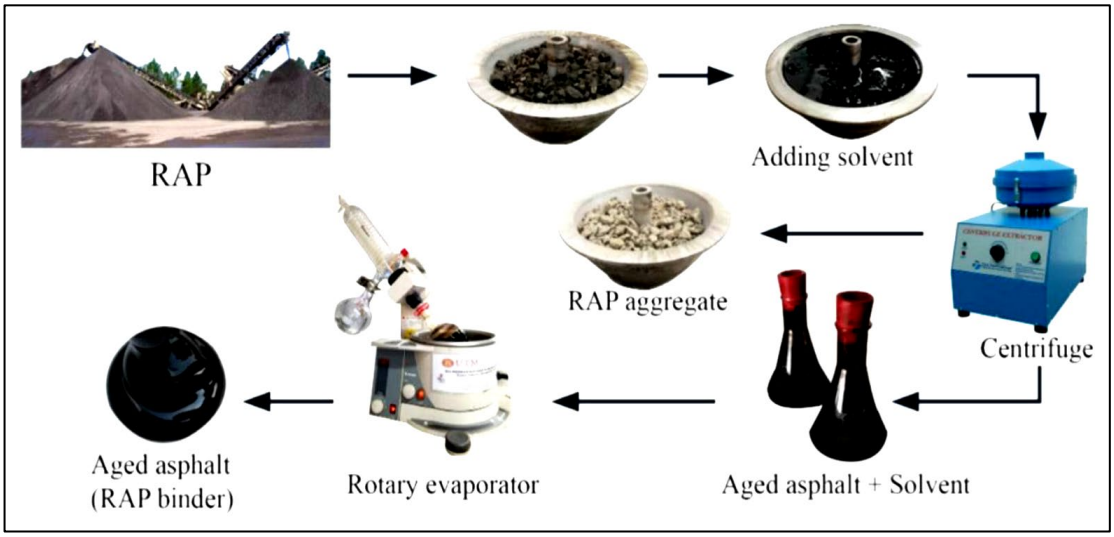

Figure 2. The process of extracting aged asphalt.

Figure 3. Rotary evaporator device.

Table 3. Physical properties of the aged asphalt binder.

Physical Properties	Value	Unit	Test Condition	SCRB Specification 2003	ASTM
Penetration	19.7	1/10 mm	25 °C, 100 gm, 5 sec	40–50	D5
Ductility	21	cm	25 °C, 5 cm/min	> 100 cm	D113
Softening point	67	°C	Ring & ball	–	D36
Rotational viscosity	1433	CP	135 °C	–	D4402
	986.1	CP	165		

2.2. Methods

Mixing bio-oil with VA and RAP

VA and RAP were placed in the oven at a mixing temperature of 150 °C for 60 min. Then, the samples of 30 % RAP with 70 % VA were placed at 150 °C in a shear mixer, and bio-oil was added in different proportions to VA and RAP and mixed at a rotational speed of 1000 rpm for 20 min [26], as shown in Fig. 4.

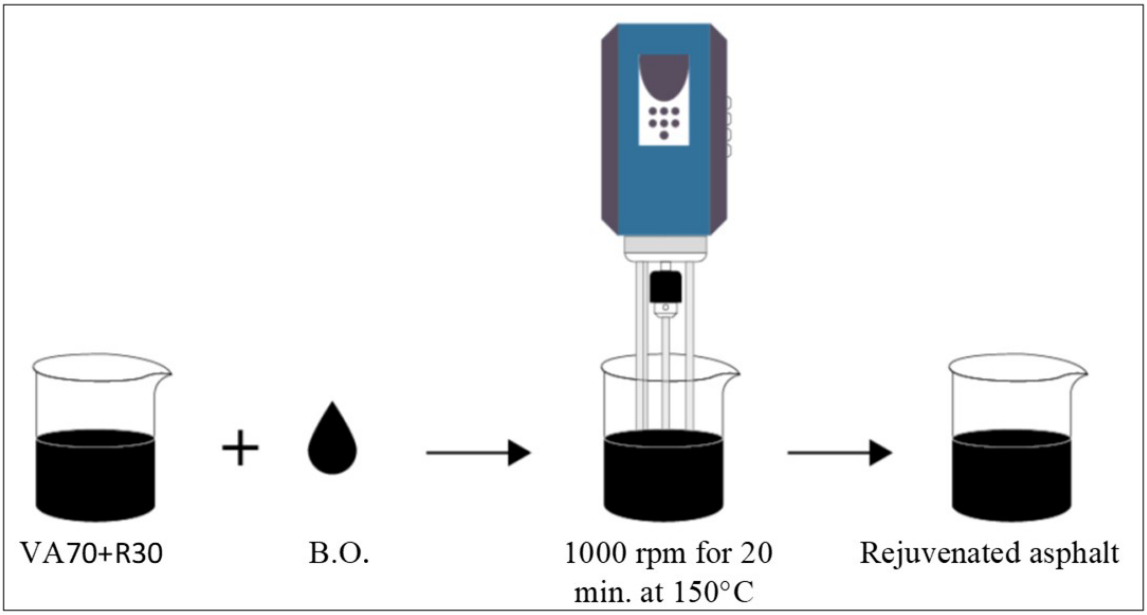

Figure 4. Preparing rejuvenated asphalt using high shear mixer.

Penetration, softening point, ductility and rotational viscosity tests

The penetration test was conducted according to [27] on different samples of VA and RAP (70 % of VA with 30 % of RAP), and several percentages of bio-oil (1 %, 2 %, 3 % and 4 %). The penetration test indicates the uniformity and resistance to deformation of the asphalt at 25 °C.

The softening points of different types of asphalt samples were examined according to [28]. The softening point test measures the temperature sensitivity of the binder when the temperature is increased at a heating rate of 5 °C/min.

The ductility test was performed on different asphalt samples according to [29]. This test is used to determine the elongation characteristics of asphalt binders, which must not be less than 100 cm for the asphalt to be considered successful and in compliance with the specifications.

Viscosity, which is the flow resistance that greatly affects the pumpability, mixability and workability of the binder, was measured using a rotational viscosity test that was performed on a variety of asphalt samples according to [30]. In this test, a cylindrical spindle with a specific diameter and effective length rotates inside a container filled with asphalt binder at a limited speed according to the specifications. The viscosity of the samples was measured at 135 °C and 165 °C.

3. Results and Discussion

Penetration

Fig. 5 shows the penetration results at different percentages of bio-oil. The results indicate that higher the percentage of bio-oil in the mixture leads to greater the penetration values due to the low viscosity of the bio-oil, which reduces the viscosity of the mixture and thus increases penetration [31, 32]. As shown in Fig. 5, the penetration value of 2 % is close to the penetration value of VA and falls within the limits of 40–50 grade specification.

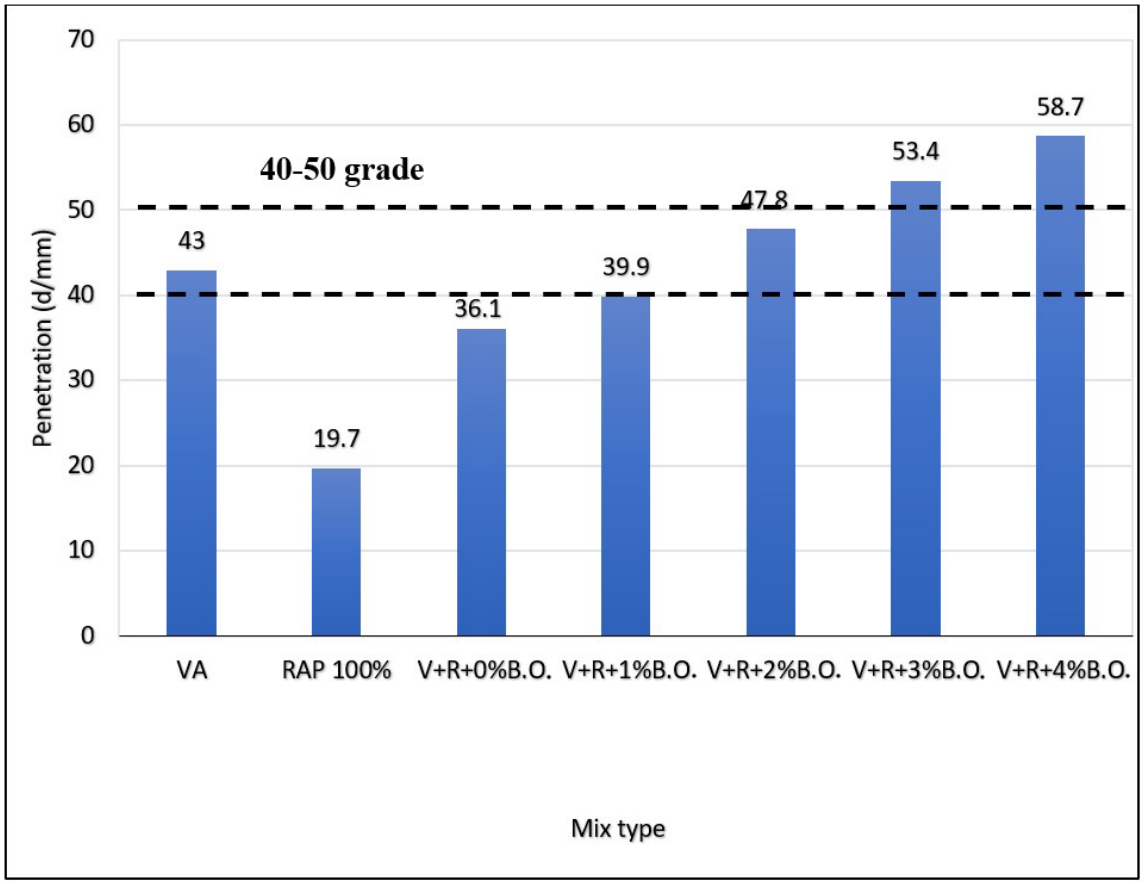

Figure 5. Penetration at different percentages of bio-oil (B.O.).

Softening point

Fig. 6 shows the softening point results at different percentages of bio-oil. The results indicate that the softening point of RAP was measured at 67 °C, a high value resulting from asphalt hardening with age. The softening point decreases consistently with increasing bio-oil content due to the increased sensitivity of the binder to temperature, when adding greater amount of bio-oil chemicals in bitumen, which reduces its softening point [33, 34]. Fig. 6 shows that the softening point value at 1 % is close to the softening point value for VA. It may be close to the optimal value of bio-oil that achieves regeneration of aged asphalt.

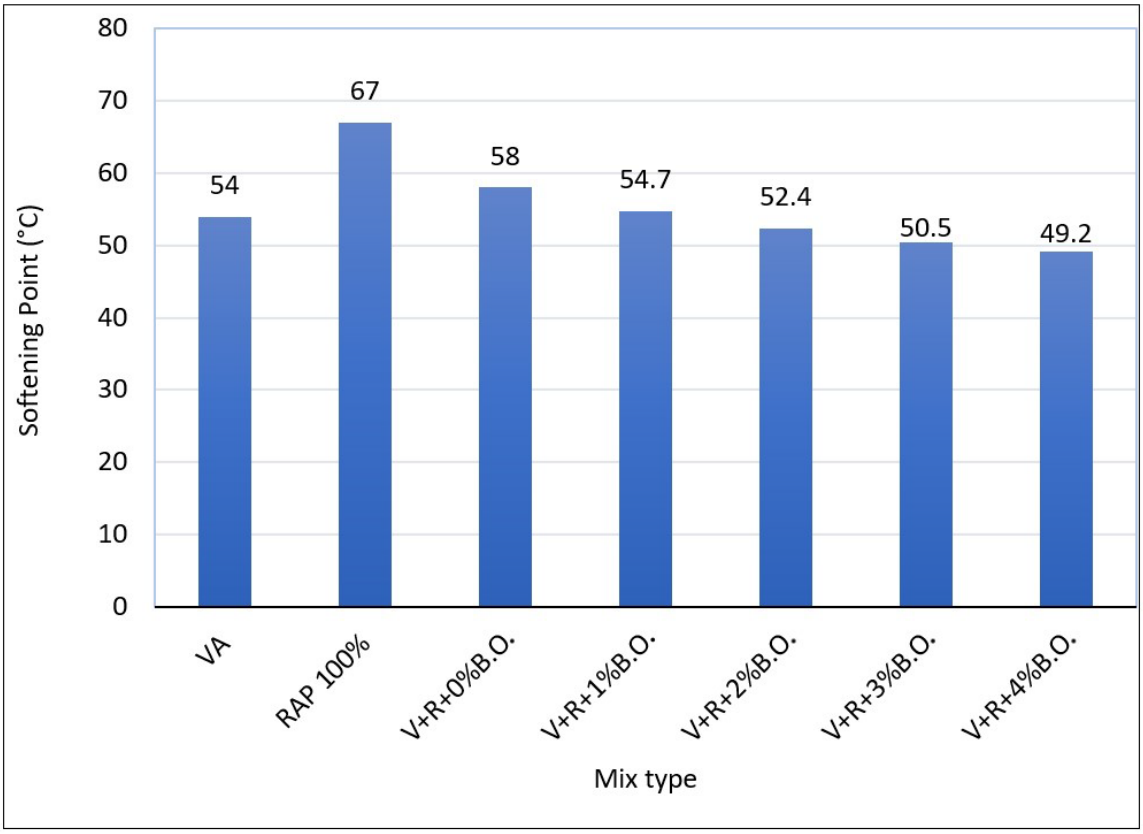

Figure 6. Softening point at different percentages of bio-oil (B.O.).

Ductility

Fig. 7 shows that the ductility value for RAP is 21 cm, which is less than the standard minimum of 100 cm. With the increase in the percentage of bio-oil in the bitumen, the ductility of the binder increases, thus improving the elongation properties of the aged binders and reducing the possibility of asphalt cracking at 25 °C. However, the ductility value begins to decrease, when the bio-oil content is more than 3 % due to reduced viscosity and increased sensitivity to temperature [33–35]. Notably, at 1 % bio-oil content, ductility exceeds 100 cm, meeting specifications and effectively rejuvenating the mixture.

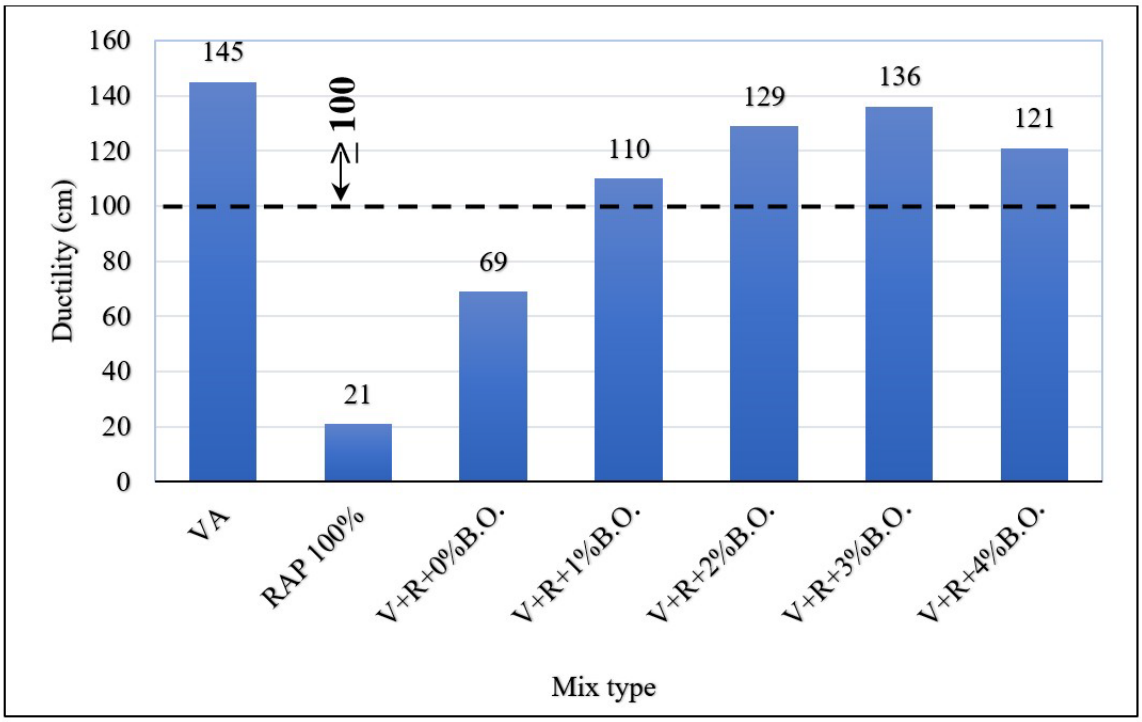

Figure 7. Ductility at different percentages of bio-oil (B.O.).

Rotational viscosity

Fig. 8 shows the results of the rotational viscosity test at different percentages of bio-oil. Compared to VA, RAP samples showed much higher viscosity. This viscosity increase in aged asphalt primarily results from changes in the asphaltene-to-maltene ratio during aging, which alters the internal structure of the asphalt [36]. This supports the results of the softening point and penetration tests. When 70 % VA with 30 % RAP was added, the mixture showed a reduction in the viscosity with further decreases observed at higher bio-oil percentages. Adding a large amount of bio-oil to the asphalt mixture may lead to a decrease in service performance, as the binder with low viscosity will be more susceptible to corrosion at the service temperature of the road, while the binder with high viscosity will be more susceptible to thermal cracking [37].

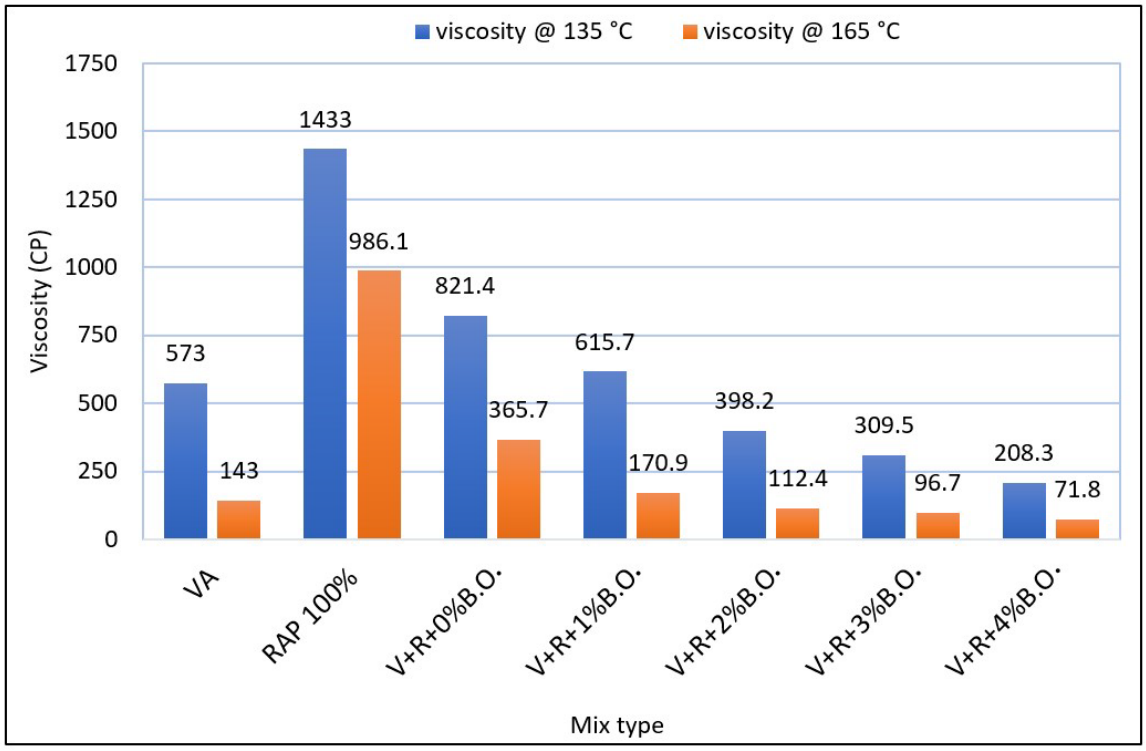

Figure 8. Rotational viscosity at different percentages of bio-oil (B.O.).

Finding the optimal ratio of bio-oil

To find the optimal percentage of bio-oil for rejuvenating aged asphalt to VA property, we compared penetration and softening point values (Figs. 10 and 11).

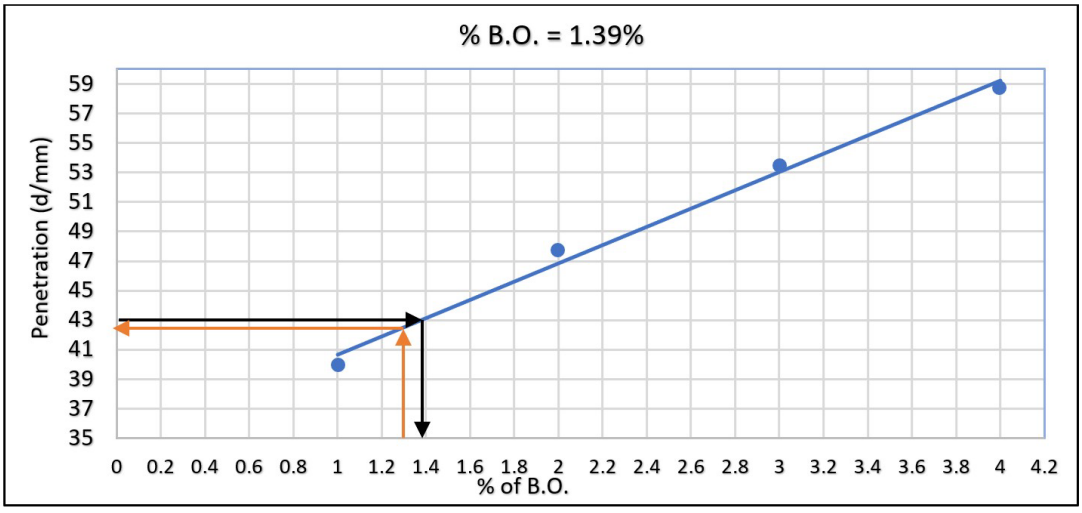

Figure 10. Penetration at different percentages of bio-oil (B.O.).

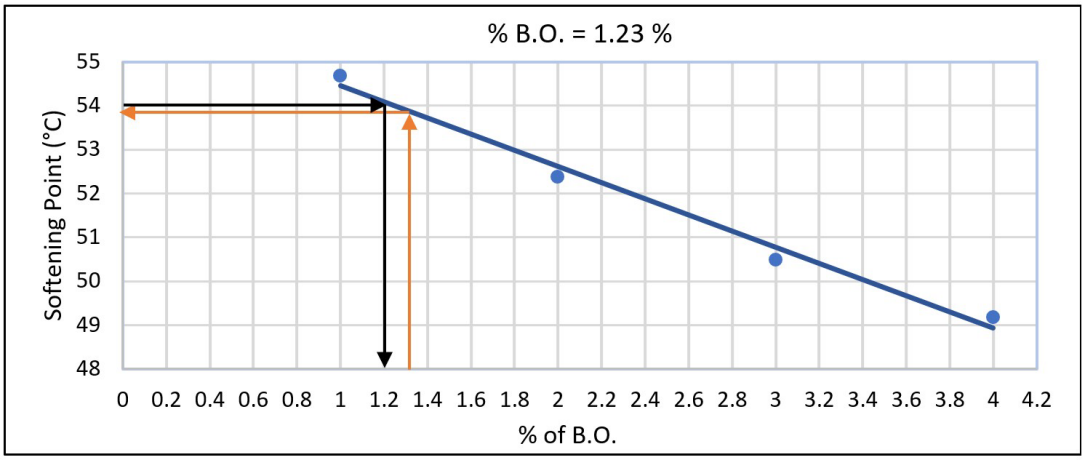

Figure 11. Softening point at different percentages of bio-oil (B.O.).

The optimal bio-oil percentages were 1.39 % for penetration and 1.23 % for softening point, yielding an average of 1.31 %. This value was then applied to all test plots (Figs. 12 and 13) and corresponding physical properties (Table 4).

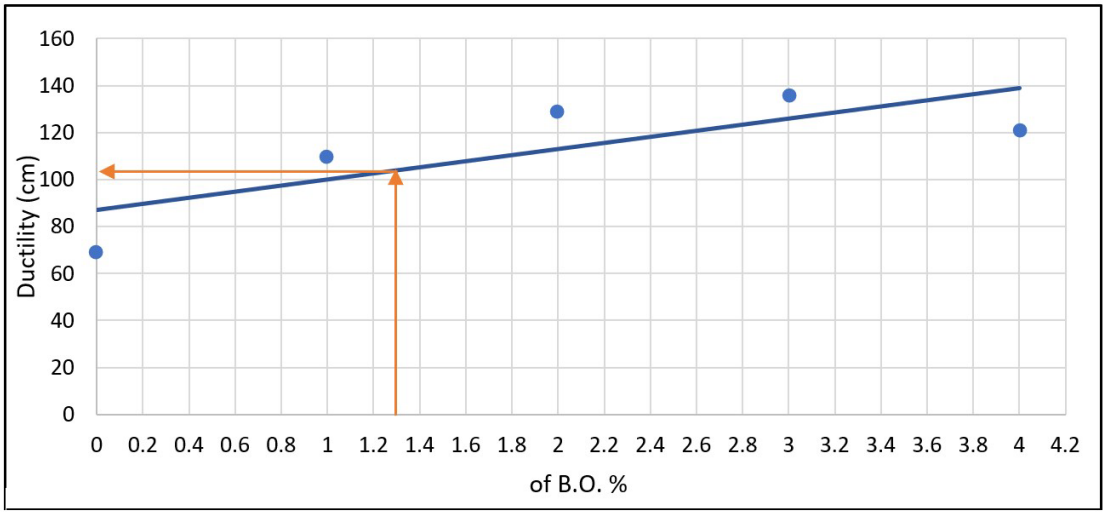

Figure 12. Results of the ductility for the optimal bio-oil percentage.

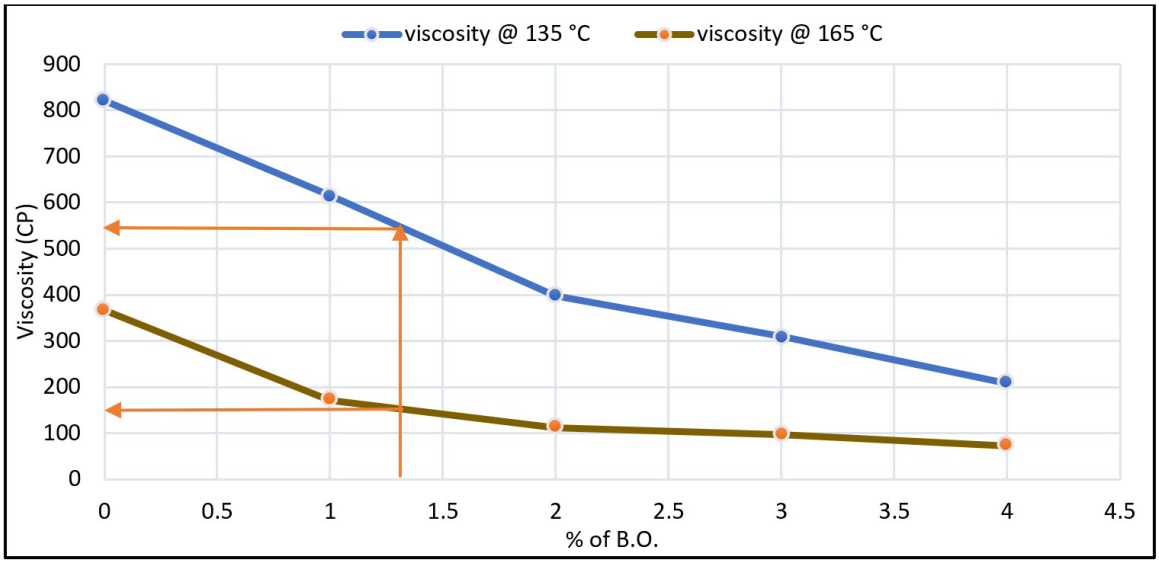

Figure 13. Results of the rotational viscosity for the optimal bio-oil percentage.

Table 4. Physical properties at the optimal bio-oil value.

Physical property	Bio-oil value
Penetration, d/mm	42.8
Softening point, °C	53.9
Ductility, cm	105
Rotational viscosity, CP	550
	150

Adding 1.31 % bio-oil to the mixture consisting of 70 % VA and 30 % RAP increases the penetration and ductility of the asphalt binder by 15.6 % and 34 %, respectively. It reduces the softening point by 7 % and viscosity at 135 °C and 165 °C by 33 % and 58 %, respectively. These results demonstrate that bio-oil addition effectively softens the asphalt mixture and enhances binder performance characteristics.

4. Conclusions and recommendations

This study investigated the physical properties of asphalt binder (70 % VA and 30 % RAP) modified with different percentages of bio-oil. Based on the results, the following conclusions can be drawn:

- The penetration and ductility values of RAP asphalt decrease by 54.2 % and 85.6 %, respectively, compared to VA. Meanwhile, its softening point increases by 24 %, and viscosity values rise by 150 % and 590 % at 135 °C and 165 °C, respectively. These changes result from the increased viscosity of aged asphalt, loss of binding properties, temperature variations and high traffic loads that cause hardening and brittleness, leading to road cracking and surface deterioration.
- Adding 1.31 % bio-oil to VA and RAP mixture increases penetration and ductility by 15.6 % and 34 %, respectively. It reduces the softening point by 7 % and viscosity at 135 °C and 165 °C by 33 % and 58 %, respectively. These improvements demonstrate that bio-oil effectively restores aged asphalt properties, including flexibility, viscosity and temperature tolerance, making it suitable for reuse in road construction.

These findings align with previous studies showing improved physical properties of asphalt treated with bio-oil composed of other bio-based materials [38–41].

Future studies should examine the performance of bio-oil rejuvenators in RAP mixtures for asphalt paving applications.

References

1. Abdulmawjoud, A.A. Performance Evaluation of hot mixture reclaimed asphalt pavement. Journal of Engineering Science and Technology. 2020.15(1). Pp. 477–492.
2. Hettiarachchi, C., Hou, X., Wang, J., Xiao, F. A comprehensive review on the utilization of reclaimed asphalt material with warm mix asphalt technology. Construction and Building Materials. 2019. 227. 117096. DOI:10.1016/j.conbuildmat.2019.117096
3. Behnood, A., Modiri Gharehveran, M. Morphology, rheology, and physical properties of polymer-modified asphalt binders. European Polymer Journal. 2019. 112. Pp. 766–791. DOI:10.1016/j.eurpolymj.2018.10.049
4. Nsengiyumva, G., Haghshenas, H.F., Kim, Y.R., Reddy Kommidi, S. Mechanical-chemical characterization of the effects of type, dosage, and treatment methods of rejuvenators in aged bituminous materials. Transportation Research Record: Journal of the Transportation Research Board. 2020. 2674(3). Pp. 126–138. DOI:10.1177/0361198120909110
5. Guduru, G., Goli, A.K., Matolia, S., Kuna, K.K. Chemical and performance characteristics of rejuvenated bituminous materials with high reclaimed asphalt content. Journal of Materials in Civil Engineering. 2021. 33(1). 04020434. DOI:10.1061/(ASCE)MT.1943-5533.0003540
6. Mogawer, W.S., Fini, E.H., Austerman, A.J., Booshehrian, A., Zada, B. Performance characteristics of high reclaimed asphalt pavement containing bio-modifier. Road Materials and Pavement Design. 2016. 17(3). Pp. 753–767. DOI:10.1080/14680629.2015.1096820
7. Joni, H.H., Al-Rubaee, R.H.A., Shames, M.K. Evaluating the mechanical performance properties of reclaimed asphalt pavement rejuvenated with different rejuvenators. Wasit Journal of Engineering Sciences. 2020. 8(1). Pp. 46–56. DOI:10.31185/ejuow.Vol8.Iss1.154
8. Chailleux, E., Audo, M., Bujoli, B., Queffelec, C., Legrand, J. et al. Alternative binder from microalgae: Algoroute project. workshop alternative binders for sustainable asphalt pavements. 2012. [Online]. URL: https://hal.science/hal-00851063v1 (01.08.2025)
9. Williams, R.C., Satrio, J., Rover, M., Brown, R.C., Teng, S. Utilization of fractionated bio oil in asphalt. Transportation Research Board 88th Annual Meeting. 2009
10. Guo, N., You, Z., Zhao, Y., Tan, Y., Diab, A. Laboratory performance of warm mix asphalt containing recycled asphalt mixtures. Construction and Building Materials. 2014. 64. Pp. 141–149. DOI:10.1016/j.conbuildmat.2014.04.002
11. Yang, F., Hanna, M.A., Sun, R. Value-added uses for crude glycerol – a byproduct of biodiesel production. Biotechnology for Biofuels and Bioproducts. 2012. 5(13). DOI:10.1186/1754-6834-5-13

12. Fini, E.H., Yang, S.H., Xiu, S. Characterization and application of manure-based bio-binder in the asphalt industry. Transportation Research Board 89th Annual Meeting. 2010
13. Fini, E.H., Al-Qadi, I.L., You, Z., Zada, B., Mills-Beale, J. Partial replacement of asphalt binder with bio-binder: characterization and modification. International Journal of Pavement Engineering. 2012. 13(6). Pp. 515–522. DOI:10.1080/10298436.2011.596937
14. Dhasmana, H., Ozer, H., Al-Qadi, I.L., Zhang, Y., Schideman, L., Sharma, B.K., Chen, W.-T., Minarick, M.J., Zhang, P. Rheological and chemical characterization of biobinders from different biomass resources. Transportation Research Record. 2019. 2505(1). Pp. 121–129. DOI:10.3141/2505-16
15. Raouf, M.A., Williams, R.C. Temperature and shear susceptibility of a nonpetroleum binder as a pavement material. Transportation Research Record. 2010. 2180(1). Pp. 9–18. DOI:10.3141/2180-02
16. Raouf, M.A., Williams, R.C. General rheological properties of fractionated switchgrass bio-oil as a pavement material. Road Materials and Pavement Design. 2010. 11(sup1). Pp. 325–353. DOI:10.1080/14680629.2010.9690337
17. Peralta, J., Raouf, M.A., Tang, S., Williams, R.C. Bio-renewable asphalt modifiers and asphalt substitutes. Sustainable Bioenergy and Bioproducts. 2011. Pp. 89–115. DOI:10.1007/978-1-4471-2324-8_6
18. Borghi, A., del Barco Carrión, A.J., Lo Presti, D., Giustozzi, F. Effects of laboratory aging on properties of biorejuvenated asphalt binders. Journal of Materials in Civil Engineering. 2017. 29(10). 04017149. DOI:10.1061/(ASCE)MT.1943-5533.0001995
19. Ahmad, K.A., Abdullah, M.E., Abdul Hassan, N., Usman, N., Ambak, K. Investigating the feasibility of using jatropha curcas oil (JCO) as bio based rejuvenator in reclaimed asphalt pavement (RAP). MATEC Web of Conferences. 2017. 103. 09013. DOI:10.1051/matecconf/201710309013
20. Foroutan Mirhosseini, A., Tahami, S.A., Hoff, I., Dessouky, S., Ho, C.-H. Performance evaluation of asphalt mixtures containing high-RAP binder content and bio-oil rejuvenator. Construction and Building Materials. 2019. 227. 116465. DOI:10.1016/j.conbuildmat.2019.07.191
21. Abdulmawjoud, A.A. Performance evaluation of hot mixture reclaimed asphalt pavement. Journal of Engineering Science and Technology. 2020. 15(1). Pp. 477–492
22. Al-Mohammed, M.A., Al-Hadidy, A.I. Durability and rutting resistance of SBS-modified asphalt mixtures containing blowdown as a sustainable filler. Al-Rafidain Engineering Journal (AREJ). 2023. 28(2). Pp. 48–57. DOI:10.33899/rengj.2023.142194.1273
23. ASTM D2172-05. Standard test methods for quantitative extraction of bitumen from bituminous paving mixtures. American society for testing and materials (ASTM), 2010. 13 p. DOI:10.1520/D2172-05
24. ASTM D5404-03. Standard practice for recovery of asphalt from solution using the rotary evaporator. American society for testing and materials (ASTM), 2010. 3 p. DOI:10.1520/D5404-03
25. Mikhailenko, P., Ataeian, P., Baaj, H. Extraction and recovery of asphalt binder: a literature review. International Journal of Pavement Research and Technology. 2020. 13. pp. 20–31. DOI:10.1007/s42947-019-0081-5
26. You, Z., Dai, Q., Xiao, F. Advanced asphalt materials and paving technologies. Applied Science. Basel. 2018. 430 p. DOI:10.3390/books978-3-03842-890
27. ASTM D5-06. Standard test method for penetration of bituminous materials. American society for testing and materials (ASTM), 2017. 4 p. DOI:10.1520/D0005-06
28. ASTM D36/D36M-12. Standard test method for softening point of bitumen (ring-and-ball apparatus). American society for testing and materials (ASTM), 2014. 4 p. DOI:10.1520/D0036_D0036M-12
29. ASTM D113-99. Standard test method for ductility of bituminous materials. American society for testing and materials (ASTM), 2010. 3 p. DOI:10.1520/D0113-99
30. ASTM D4402/D4402M-15(2022). Standard test method for viscosity determination of asphalt at elevated temperatures using a rotational viscometer. American society for testing and materials (ASTM), 2023. 4 p. DOI:10.1520/D4402_D4402M-15R22
31. Ren, J., Zang, G., Xu, Y. Formula and pavement properties of a composite modified bioasphalt binder considering performance and economy. Journal of Materials in Civil Engineering. 2019. 31(10). 04019243. DOI:10.1061/(ASCE)MT.1943-5533.0002888
32. Cao, X., Wang, H., Cao, X., Sun, W., Zhu, H., Tang, B. Investigation of rheological and chemical properties asphalt binder rejuvenated with waste vegetable oil. Construction and Building Materials. 2018. 180. Pp. 455–463. DOI:10.1016/j.conbuildmat.2018.06.001
33. Su, N., Xiao, F., Wang, J., Cong, L., Amirkhanian, S. Productions and applications of bio-asphalts – A review. Construction and Building Materials. 2018. 183. Pp. 578–591. DOI:10.1016/j.conbuildmat.2018.06.118
34. Dong, Z., Tao, Z., Luan, H., Wang, H., Xie, N., Xiao, G. Performance evaluation of bio-based asphalt and asphalt mixture and effects of physical and chemical modification. Road Materials and Pavement Design. 2020. 21(6). Pp. 1470–1489. DOI:10.1080/14680629.2018.1553732
35. Sang, Y., Chen, M.Z., Wen, J., Leng, B.B., Wu, S.P. Effect of waste edible animal oil on physical properties of aged asphalt. Key Engineering Materials. 2014. 599. Pp. 130–134. DOI:10.4028/www.scientific.net/KEM.599.130
36. Noferini, L., Simone, A., Sangiorgi, C., Mazzotta, F. Investigation on performances of asphalt mixtures made with Reclaimed Asphalt Pavement: Effects of interaction between virgin and RAP bitumen. International Journal of Pavement Research and Technology. 2017. 10(4). Pp. 322–332. DOI:10.1016/j.ijprt.2017.03.011
37. Zaumanis, M., Mallick, R.B., Frank, R. 100% recycled hot mix asphalt: A review and analysis. Resources, Conservation and Recycling. 2014. 92. Pp. 230–245. DOI:10.1016/j.resconrec.2014.07.007
38. Asli, H., Ahmadinia, E., Zargar, M., Karim, M.R. Investigation on physical properties of waste cooking oil – Rejuvenated bitumen binder. Construction and Building Materials. 2012. 37. Pp. 398–405. DOI:10.1016/j.conbuildmat.2012.07.042
39. Al-Omari, A.A., Khedaywi, T.S., Khasawneh, M.A. Laboratory characterization of asphalt binders modified with waste vegetable oil using SuperPave specifications. International Journal of Pavement Research and Technology. 2018. 11(1). Pp. 68–76. DOI:10.1016/j.ijprt.2017.09.004
40. Ahmad, K.A., Abdullah, M.E., Abdul Hassan, N., Nda, M., Usman, N. Effect of bio based rejuvenator on permanent deformation of aged bitumen. International Journal of Integrated Engineering. 2018. 10(9). Pp. 135–139. DOI:10.30880/ijie.2018.10.09.025
41. Zeng, M., Pan, H., Zhao, Y., Tian, W. Evaluation of asphalt binder containing castor oil-based bioasphalt using conventional tests. Construction and Building Materials. 2016. 126. Pp. 537–543. DOI:10.1016/j.conbuildmat.2016.09.072

Information about the authors:

***Ayman A. Abdulmawjoud**, PhD*
E-mail: aymanmawjoud@uomosul.edu.iq

***Mahmood K. Hammadi**,*
E-mail: amahmood.22enp4@student.uomosul.edu.iq

Received: 11.06.2024. Approved: 05.11.2024. Accepted: 10.12.2024.

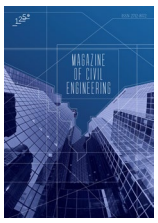

Magazine of Civil Engineering

ISSN 2712-8172

journal homepage: http://engstroy.spbstu.ru/

Research article

UDC 624.011.1

DOI: 10.34910/MCE.136.4

Pore pressure in the core of ultra-high earth core rockfill dam at consideration of stress-strain state

M.P. Sainov ✉, ***B.A. Boldin***

Moscow State University of Civil Engineering (National Research University), Moscow, Russian Federation

✉ *mp_sainov@mail.ru*

Keywords: pore water pressure, earth core rockfill dam, soil consolidation, filtration, dam core, stress-strain state, numerical modeling, Nurek dam

Abstract. In the clayey core of the rockfill dam, pore pressure always appears, which may present a serious threat to the dam safety. Therefore, in the middle of the 20th century, there started the development a theory of clayey soil consolidation in cores of earth core rockfill dams; analytical methods were developed to calculate pore pressure. However, these methods are approximate; they do not permit modeling complicated processes of soil consolidation in the structure. The published data of field measurements at the ultra-high dam of Nurek HPP give evidence about the fact that the processes of accumulation and dissipation of pore pressure in the core soil have a complicated character. At the initial stages of construction, there observed a gradual growth of pore pressure due to the weight of the overlying soil layers. But at the completion stages, pore pressure rapidly decreased, and its values approached the values, which are characteristic for the regime of steady seepage. These effects cannot be explained and simulated by a traditional method of analysis. The rate of seepage is too small to provide occurrence of so rapid processes. Therefore, for study of the processes of pore pressure formation in the core of Nurek dam, a more complicated and accurate method was used, i.e. the method of numerical modeling. Numerical modeling permits joint solving the tasks related to stress-strain state and seepage regime in the structure. Use of numerical modeling permitted us with sufficient accuracy to simulate the pore pressure formation process in the core of Nurek dam, as well as to analyze the causes of the observed effects. It was revealed that the main role in pore pressure formation is played not by the process of water seepage but by the process of the dam stress-strain state formation. Decrease of increased pore pressure due to dead weight loads takes place due to the dam lateral expansion. Increase of pore pressure before the seepage pressure is due to soil deformation under the action of force loads from the upstream side. The considered analytical method of analysis does not take into account the peculiarities of formation of stress-strain state of the rockfill dam earth core, it does not consider appearance of pore pressure from the upstream loads. Therefore, the real processes of the core soil consolidation cannot be simulated with its aid.

Citation: Sainov, M.P., Boldin, B.A. Pore pressure in the core of ultra-high earth core rockfill dam at consideration of stress-strain state. Magazine of Civil Engineering. 2025. 18(4). Article no. 13604. DOI: 10.34910/MCE.136.4

1. Introduction

Pore pressure is pressure in the liquid phase of soil. It may exceed the hydrostatic pressure corresponding to groundwater level at the steady seepage regime. Such pressure we will cause increased pressure (or surplus pressure).

It is known that increased pore pressure may present a serious danger for safety of embankment dam structures. Namely, it was pore pressure in the clayey soil layer, which became the cause of failures of embankment dams Chingford (1937) and Muirhead (1941) in Great Britain. At these dams immediately

after completion of construction, there happened the loss of clayey soil bearing capacity and break of integrity of the dam structure [1].

Special urgency in study of pore pressure in structures of embankment dams aroused in the middle of the 20th century with use of earth core rockfill dams (ECRDs), whose core was constructed of clayey soil. Many of them had considerable height, therefore, the clayey soil in them was subject to great loads. In 1939, the height of an ECRD for the first time exceeded 100 m. This is 131.7 m high Mud Mountain dam in the USA.

The danger of increased pore pressure in the cores of high ECRD is related to the fact that it may cause crack formation in them. Numerical modeling of stress-strain state (SSS) shows that pore pressure creating a wedging action, contributes to formation of separation cracks in the core [2] or shear surfaces [3]. Pore pressure may be one of the causes of the core hydraulic fracturing, which happened at several dams.

In the 21st century, a number of high ECRDs was built : Karkheh (H=127 m, Iran, 2001) [4–6], Masjed-e-Soleyman (H=177 m, Iran, 2002) [3], San Roque (H=210 m, Philippines, 2003), Tehri (H=260.5 m, India, 2006), Qiaoqi (H=125.5 m, China, 2006) [7], Pubugou (H=186 m, China, 2010) [8], Maoergai (H=147 m, China, 2011) [7], Nuozhadu (H=261.5 m, China, 2012) [9–11], Upper Gotvand Dam (H=180 m, Iran, 2012), Changheba (H=240 m, China, 2017) [9]. Dams San Roque, Tehri, Nuozhadu, Changheba refer to ultra-high dams; their height exceeds 200 m. At construction stage is the dam of Rogun HPP (Tajikistan), which should be the highest in the world.

To provide safety of high ECRDs, it is necessary to carry out studies of pore pressure in the core clayey soils. Approximately from the 1950s, pore pressure started to be studied experimentally, in field conditions at the constructed structures. In [12], there published the data of field measurements of pore pressure at several dams constructed in the 20th century. Monitoring of pore pressure is carried out at all high ECRDs [3, 11, 13].

Analysis of field measurements shows that processes of the core soil consolidation on different dams take place in different ways. In some dams (Aswan, Pachkamar), pore pressure did not exceed hydrostatic pressure and the processes of soil consolidation were quick [12]. In the clay core of Talbingo dam, pore pressure reached considerable values and dissipated slowly [12].

Therefore, it is urgent to develop methods of calculating the process of soil consolidation in ECRD core, so that they can predict formation of pore pressure.

In this connection, of special interest are studies of pore pressure in the core of the highest embankment dam in the world, i.e. the dam of Nurek HPP. Sensors were installed in the core of this dam, which permitted carrying out monitoring of pore pressure during construction and operation. The results of field measurements were published in [14]. With this regard, it is interesting to compare the results of calculations with the results of field measurements and estimate accuracy of calculation methods.

The theory of forming pore pressure and soil consolidation has been developed over the last one hundred years.

The pioneer in study of pore pressure is K. Terzaghi, who provided the basis for the theory of soil consolidation [15]. K. Terzaghi proposed to consider soil as a multi-phase system consisting of solid, liquid, and gaseous phases. And in 1925, he proposed to solve a one-dimensional problem of soil water saturated layer compaction due to the process unsteady seepage.

For development of consolidation theory of great importance was solving the problem of the effect of presence in soil pores of compressible gaseous phase on the value of pore pressure. In 1939, American researchers J. R. Bruggeman, C. N. Zanger, J. H. A. Brahtz proposed determining pore pressure based on the assumption of equality of pore pressure in liquid and gaseous phases using equations of R. Boyle and E. Mariotte law (on air compressibility) and W. Henry law (on dissolubility of air in water). In 1948, J. W. Hilf published the equation based on Boyle–Mariotte law, which permitted determining pore pressure without consideration of consolidation process. This equation became the basis for analytical methods of analysis. A.W. Skempton introduced the methodology of calculating coefficients of pore pressure, which reflects connection between the total stresses and pore pressure with consideration of pore liquid compression and the degree of pore water saturation [16].

The consolidation theory was developed in the works of N.M. Gersevanov, V.A. Florin, M. Biot et al.

In 1937, a Russian scientist V.A. Florin proposed the equation for solving a 2D problem of seepage consolidation applicable to the case of non-compressible liquid. Then, he developed the methods of solving consolidation problems also with consideration of solid phase creep.

In 1941, M. Biot published the proposed by him system of equations of seepage consolidation for a more common case, i.e. for the case of compressible skeleton of soil and compressible liquid [17].

Analytical methods of analysis propose creation of closed analytical solution of the indicated equations, permitting calculation of the pore pressure value and its variation with time.

Analytical solving of the problem related to formation and dissipation of soil pore pressure in the dam core was obtained by A. A. Nichiporovich and T.I. Tsybulnik. They mark two types of pore pressure: pore pressure from the weight of overlying soil layers and pore pressure from water filtration (penetration of the upstream water in the core). A. A. Nichiporovich and T.I. Tsybulnik proposed mathematical formulae, which permits determining distribution pore pressure in the core for each moment of time [18, 19].

In this analytical method, the initial pressure from the weight is determined based on J. W. Hilf equation (via pore pressure coefficient), and the process of pore pressure dissipation is described by V.A. Florin equations. However, at that, a number of simplifying assumptions was accomplished, which makes this method of analysis approximate.

From the middle of the 20th century, the methods of numerical modeling started to be used for solving the problems on soil consolidation. They permit solving joint static-seepage problems simultaneously modeling the process of forming SSS of the structure and its seepage regime. Numerical methods permit solving complicated tasks of soil consolidation not only for particular, previously assigned conditions.

Already in the 1970s, the numerical analyses of pore pressure by the finite element method were carried out at designing Mica dam (Canada, 1973, 243 m high) [20]. It was shown that the results of numerical modeling greatly differ from the results of analyses by the analytical method due to variation of mass stress state in the process of consolidation.

In the 1980s, Yu.K. Zaretsky and V.N. Lombardo[1] fulfilled prognostic modeling of pore pressure in the core of Nurek dam (1980, the USSR, – Tajikistan, 300 m high). The finite difference method was used for solving a joint static-seepage problem for the dam cross section.

At present at designing high ECRD, numerical modeling of processes forming pore water pressure (PWP) and SSS is always fulfilled. Publications [3, 11, 21–24] are devoted to this issue. Rater often analysis has the aim of checking the core crack resistance [11, 21, 23].

For fulfilling analyses, there were used different software packages: FLAC 3D [3, 21], PLAXIS [22, 24], GeoStudio [23]. With the aid of software package FLAC 3D, there was fulfilled numerical modeling of SSS and PWP for several dams in Iran: Masjed-e-Soleyman [3], Siah Sang [21]. Calculations in [13] and [3] were carried out in 3D formulation. Not always for determining pore pressure there modeled the process of soil consolidation, in [22], a simplified approach is used for determining pore pressure.

Publication of [21] is devoted to numerical modeling of SSS and PWP for Siah Sang dam (33 m high) in Iran. Analyses showed rapid dissipation of pore pressure.

Of the most interest are publications [11, 3], devoted to studies of ultra-high ECRD.

The article [11] is devoted to numerical modeling of SSS and PWP for Nuozhadu dam in China. Analyses were conducted based on consolidation theory of M. Biot with use of parabolic model of soil. For obtaining results, adequate data of field measurements, calibration of the structure model was required. At the soil seepage factor value $(2\div5)\cdot10^{-6}$ cm/s, measured in laboratory and field conditions, at numerical modeling, the pore pressure quickly dissipated, which were not observed in real dam. Correspondence to the field data was reached at seepage factor value $(1.5\div5)\cdot10^{-9}$ cm/s [11].

The article [3] is devoted to studies of PWP and SSS for Masjed-e-Soleyman dam in Iran. By the results of field measurements, there observed high pore pressure in the dam core, and its dissipation was sufficiently slow. At the end of the first reservoir impoundment, the crest settlement amounted to 2,2 m. numerical modeling of SSS and PWP showed that due to pore pressure, there is a danger of the core soil shear strength.

These examples demonstrate urgency of study of pore pressure formation and dissipation, as well it shows that they have not been sufficiently studied by present.

The aim of our study is estimation of adequacy of pore pressure analyses results, obtained by different methods, estimation of adequacy of representation by them of the processes in core soil consolidation, which are observed in a real structure.

---

[1] Zaretsky Yu.K., Lombardo V.N. Statics and dynamics of embankment dams. M.: Energoatomizdat, 1983. 255 p.

Analysis will be conducted by two methods: analytical method and the finite element method. They will be shown on the example of Nurek HPP, where field measurements of pore pressure in the core have been conducted for already 40 years.

Consequently, the tasks of the study are as follows:

- fulfill analysis of data on field measurements of pore pressure in the core of Nurek dam;
- fulfill analysis of pore pressure in the core of Nurek dam by the analytical method;
- carry out numerical modeling of Nukek dam SSS and seepage regime;
- compare the results of analysis obtained by different methods, formulate conclusions and recommendations on peculiarities of pore pressure formation and for reliability of the analysis results.

2. Materials and Methods

2.1. Subject of Study

The subject of study, i.e. Nurek dam, is an ECRD. It has a 269 m high core made of sandy loam (Fig. 1). The core rests on a thick concrete block. The dam shells are made of gravel-pebble soil.

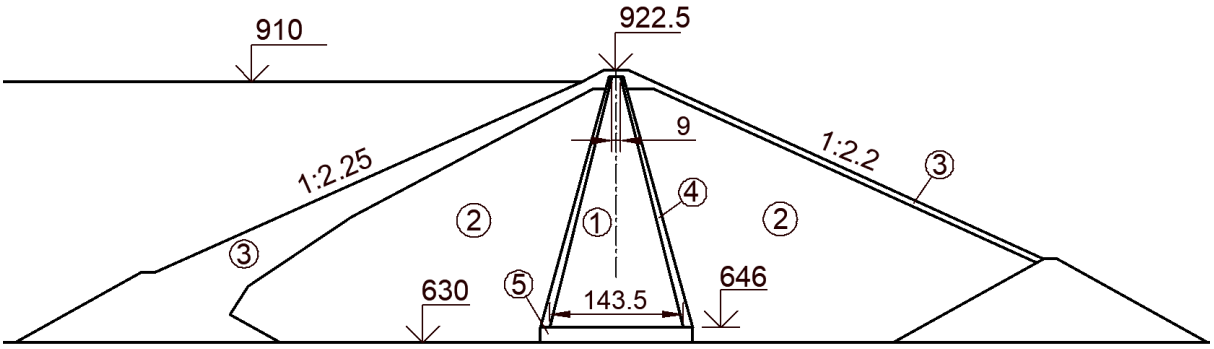

Figure 1. Design scheme of earth core rockfill Nurek dam structure in vertical section: 1 – sandy loam core; 2 – shells of gravel-pebble soil; 3 – protection against rockfill; 4 – transition zone; 5 – concrete plug.

2.2. Description and Analysis of Results of Pore Pressure Field Measurements

Several dozens of sensors were installed in the core for measuring pore pressure. Multiple sensors were installed on the surface of concrete block. Besides, vibrating wire piezometers were installed inside the dam core in 7 vertical measuring sections at different elevations. For example, in the riverbed section (measuring section 5), the sensors are installed at elevations 686, 774.5, 799 m.

Measurements were carried out from the start of construction (since 1973). In [14], there given the data of pore pressure field measurements during the period of construction. In 1973, when the core was constructed for the height of 104 m, pore pressure reached 1,8 MPa (Fig. 2a), and in 1977, when the core was constructed for the height of 209 m, it reached 2,99 MPa (Fig. 2b). For these moments of time, the vertical pressure from the soil weight amounts to 2.4 and 4.8 MPa respectively. This means that on the liquid phase of soil (pore liquid), there transferred accordingly 75 and 62 % of maximum possible pressure (for pressure coefficient α=0.75 and 0.62).

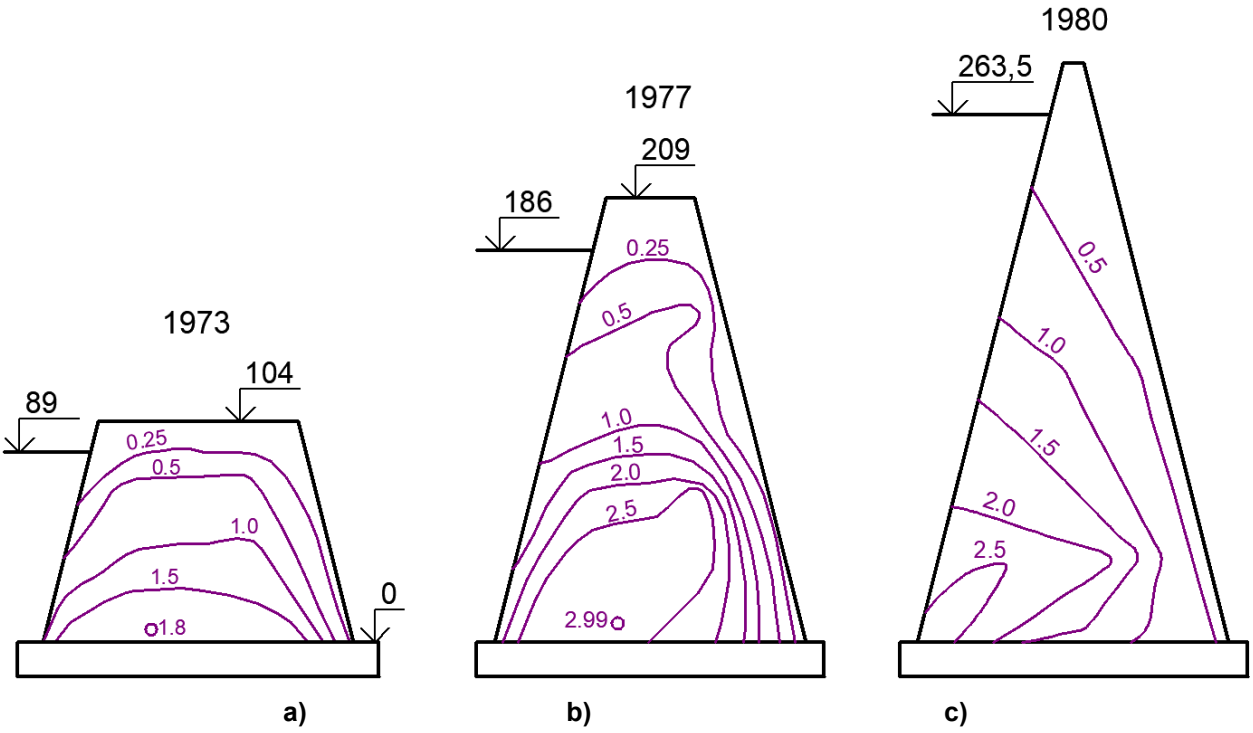

Figure 2. Pore pressure in the dam core by the data of field measurements (values are in MPa): a – after 2 years from the start of construction; b – after 6 years from the start of construction; c – after 9 years from the start of construction. Relative elevations are indicated.

For us, of the most interest is the riverbed vertical cross section No. 5, having maximum height. After completion of the dam construction and the reservoir impoundment (in 1981) in this section, the maximum value of pore pressure was reached in sensor No. 1314 [14]. In this sensor at ∇686 m, it amounted to 2.48 MPa (Fig. 2c). As compared to maximum possible value (5.4 MPa), the pore pressure is 46 %.

This simple analysis evidences that during the period of construction, intensive dissipation of pore pressure and soil consolidation took place. During the operation period, these processes continued. In the same sensor No. 1314 by 2014, pore pressure decreased to 1.47 MPa [14], i.e. by 40 %.

The data of field measurements show complicated character of pore pressure distribution in the dam core. In the core, upper part considerably less portion of load is transferred to water than in the lower part. Already during construction period (1977), piezometric levels in the upper sensors turned to be less than in the lower one; in future this tendency maintained.

Plotted by the data of field measurements, distribution of pore pressure for the moment of construction completion (Fig. 2c) proves that by the start of operation period, dissipation of the most part of surplus pore pressure took place, and it approached the values, which corresponded to the steady seepage flow.

The described above pattern of distribution and variation of pore pressure obtained in the field is abnormal from the point of view of theoretical concepts, and the causes of such rapid soil consolidation are debatable. In publication [14], it is affirmed that rapid dissipation of pore pressure in the core lower part may be explained by permeability of the concrete block. By the results of numerical modeling of the process of non-steady seepage in the core of the ultra-high dam, fulfilled by N.A. Aniskin [25], the process of water penetration inside the dam core should usually occur very slowly, i.e. during several decades the boundary of seepage area should advance only for several meters from the upstream face. Consequently, consolidation process should take place for decades or hundreds of years.

Our study is an attempt to explain the causes of effects in distribution of pore pressure in the core of Nurek dam, revealed by field measurements during construction period.

Specially mentioned should be the results of field measurements of the core soil permeability, which are also published in [14]. Values of the core soil seepage factor were determined by calibration of the mathematical model. It was obtained that with time, the values of the core soil seepage factor decreased. If in 1984, it amounted to $(0.4 \div 4) \cdot 10^{-6}$ cm/s, afterwards, it decreased approximately by an order [14]. However, the value of seepage factor $1.2 \cdot 10^{-6}$ cm/s =0.001 m/day seems to be very high for the clayey soil.

2.3. Analytical Method of Analysis

Design formulae of the analytical method, proposed by A. A. Nichiporovich and T.I. Tsybulnik, are given in [2, 18, 19, 25]. They permit determining two types of pore pressure: pore pressure appearing under the action of weight of overlying layers and seepage pore pressure of water from the upstream side penetrating inside the core.

This analytical method is approximate; it is based on a number of assumptions. The following assumptions may be distinguished:

- the core operates independently from the dam shells, it is independently subject to the load from the weight of overlying soil layers;
- total stresses in the core in vertical direction are equal to the pressure from the weight of overlying soil layers;
- soil deformations occur only in vertical direction; soil is a linearly deformed material;
- initial pore pressure (in the initial moment of time) is determined by total stresses with the aid of J. W. Hilf equation, corresponding to conditions of fluid efflux (“closed system”);
- dissipation of pore pressure occurs due to water seepage in horizontal direction;
- the rate of the structure construction height-wise, the rate of the upstream level growth at the reservoir impoundment are constant.

Due to the made assumptions, the analytical method is approximate. Therefore, we used the method of numerical modeling.

2.4. Method of Numerical Modeling

Numerical modeling of the structure was accomplished based on the finite element method in the software package MIDAS. The problem of soil consolidation was solved by M. Biot equations.

These calculations are also approximate because only the dam vertical section is considered and the dam soil is assumed to be linearly deformed.

The used for analyses finite element model of the dam section is shown in Fig. 3. It comprises 6975 nodes and 6906 finite elements.

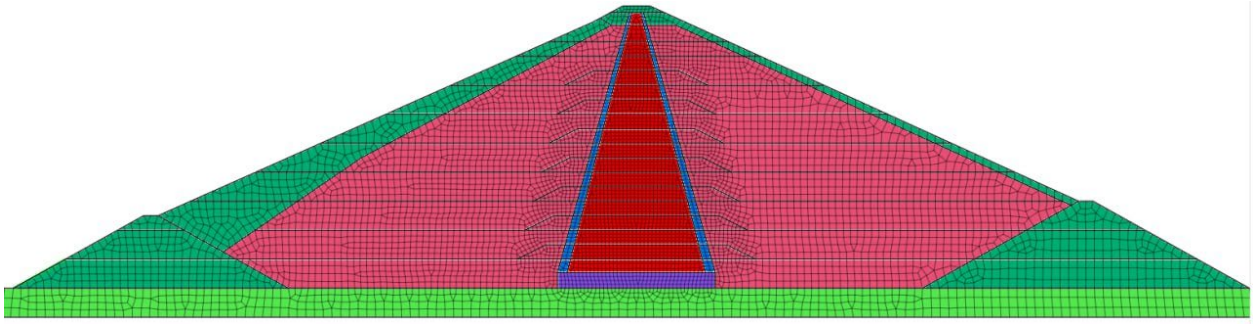

Figure 2. Finite element discretization of the designed section.

During analyses, the following types of loads were considered:

- loads from the structure dead weight;
- loads on soil from the buoyant action of water;
- volumetrically distributed loads from filtering water.

Only construction period was considered, whose duration was 9 years.

The sequence of dam construction was simulated (with consideration of its construction by horizontal layers) and the reservoir impoundment. It is shown in Fig. 3 as a diagram, reflecting growth with time of the dam top elevation and the upstream level.

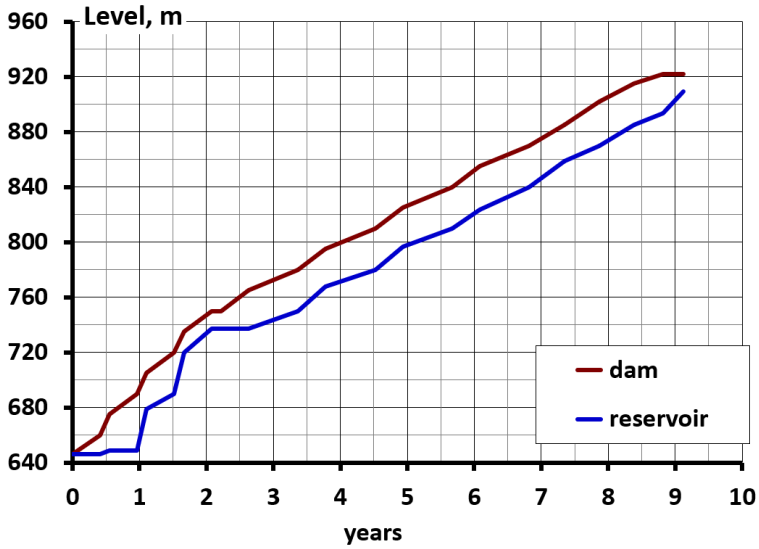

Figure 3. Design diagram of sequence of the dam construction and the reservoir impoundment (for numerical modeling).

At modeling behavior of soil, Coulomb–Mohr model was used envisaging linear deformation. Physical-mechanical properties of soils adopted in the analysis are in Table 1. The core soil seepage factor was assumed to be several times less than that by data of [14].

Table 1. Design physical-mechanical characteristics of soils.

Material	ρ_d t/m^3	ρ_{sat} t/m^3	E MPa	ν	k_f m/day
Sandy loam	2.10	2.28	40	0.32	$8.64 \cdot 10^{-5}$
Soils of transition zones	2.10	2.20	55	0.3	20
Gravel-pebble soil of shells	2.16	2.35	150	0.27	100
Weightening rock mass	1.96	2.22	150	0.27	100

Designations: ρ_d – density in dry state, ρ_{sat} – density in water saturated state, E – modulus of linear deformation, ν – Poisson's ratio, k_f – seepage factor.

3. Results and Discussions

3.1. Results of Analysis by Analytical Method

At analysis by the analytical method of A.A. Nichiporovich and T.I. Tsybulnik for a number of moments of time, there was determined pore pressure from soil dead weight and from the seepage flow, out of which the greatest was selected. The rate of the dam growth height-wise and the rate of the reservoir impoundment were assumed to be constant due to peculiarities of this method.

Analysis results on pore pressure in the core by the analytical method are presented in Fig. 4. They show that pore pressure is mainly caused by the dead weight of the overlying soil layers, while the seepage pore pressure is small.

The results of analysis are in bad correlation with the data of field measurements at the initial stages of the dam construction (Figs. 4a, 4b), though design values slightly exceed the field values. For example, for the moment of time for the year of 1977, the maximum value of pore pressure according to calculation amounts to 3.5 MPa, and by field data it is 2.99 MPa (Fig. 4b). It should be stressed that by the results of analyses, made by Yu.K. Zaretsky and V.N. Lombardo, the maximum pore pressure comprised 2.77 MPa. Thus, the results of analyses are in satisfactory correlation.

However, for the time of construction completion (1980), divergence of design and field data is considerable. The difference is not only in absolute values of pore pressure but also in the pattern of their distribution and variation with time. In the data of field measurements, the most part of pore pressure due to the soil dead weight has already dissipated, and by the results of analysis, it is not decreased but increases. By field data, the maximum value of PWP is about 2.5 MPa (Fig. 2c), and by the results of analysis, it reaches 4.5 MPa (Fig. 4c).

Such difference in the results of field measurements and calculations testifies about disadvantages of the design model. Therefore, it is interesting to estimate the results of analysis with the aid of numerical modeling.

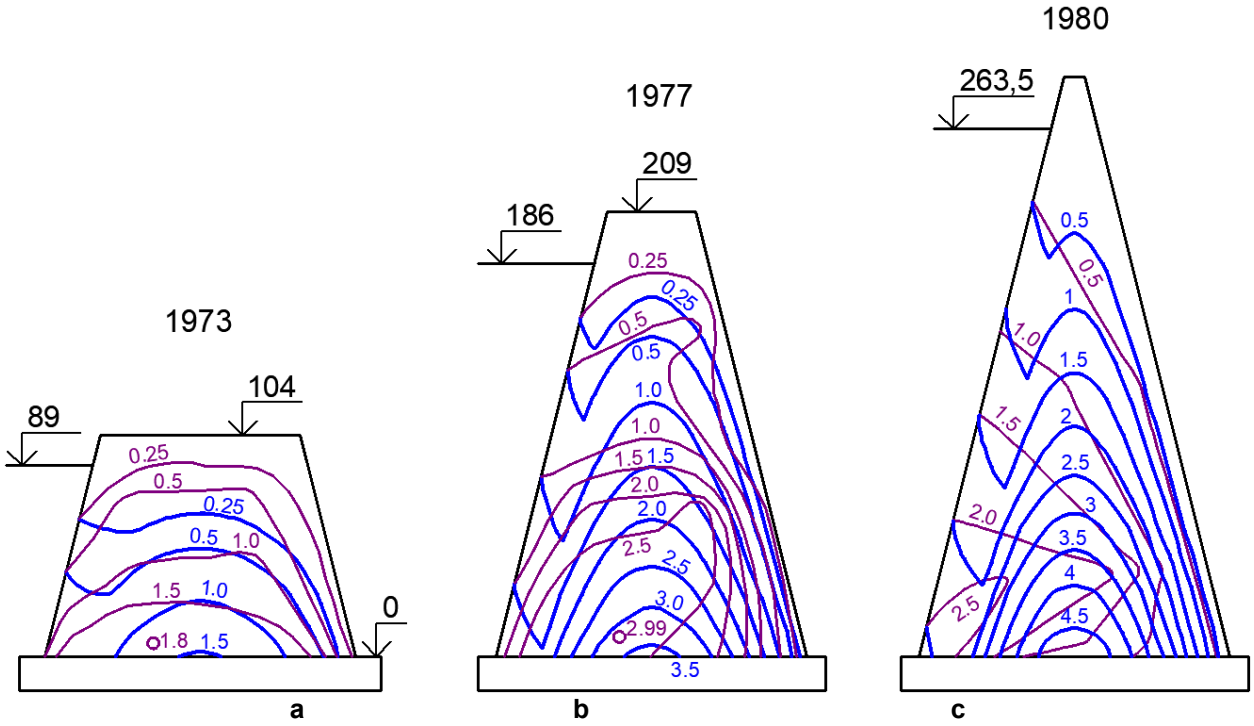

Figure 4. Pore pressure in the dam core by the results of analyses by the analytical method (values are given in MPa):
a – after 2 years from the start of construction; b – after 6 years from the start of construction; c – after 9 years from the start of construction. Violet color shows isolines of pore pressure by the results of field measurements, blue color – by the results of analyses with use of the analytical method. The indicated elevations are relative.

3.2. Results of Numerical Modeling

The dam stress state for the moment of construction period completion, obtained by numerical modeling, is shown in Figs. 5–10. Construction settlements and displacements of the dam are shown (with consideration of construction sequence), as well as distribution of vertical and horizontal stresses.

Obtained in the analysis construction settlements reach maximum in the core central part (Fig. 5). The maximum settlement amounts to 3.35 m, which is slightly more than by the results of field measurements (3.0 m).

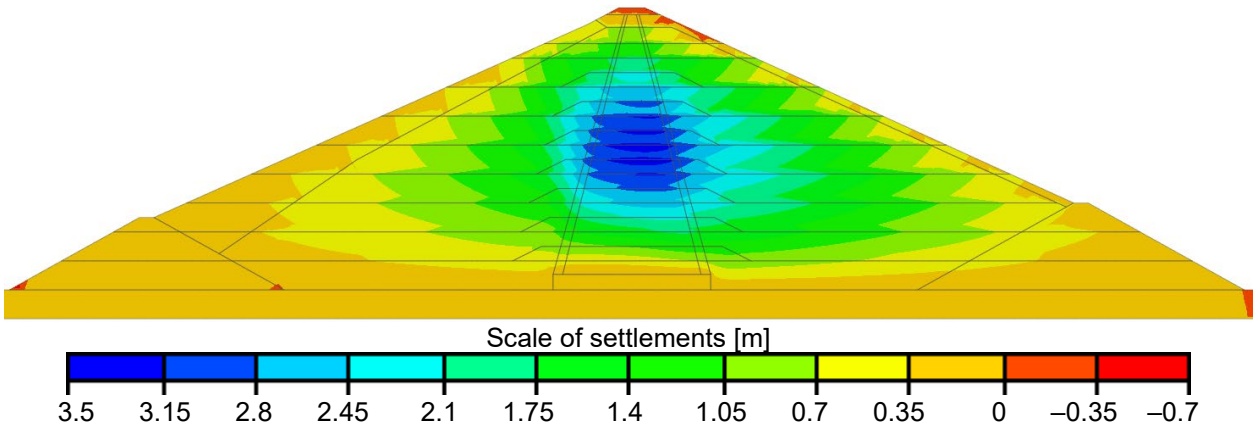

Figure 5. Dam settlements by the results of numerical modeling (for the moment of construction completion).

Design horizontal displacements are directed towards the downstream side. Their maximum value 2.5 m is in core central part (Fig. 6). It is several times more than field settlements (0.8 m). This difference

is explained by the fact that analyses were conducted in 2D formulation for the dam vertical section, while SSS of a real dam was formed in spatial conditions.

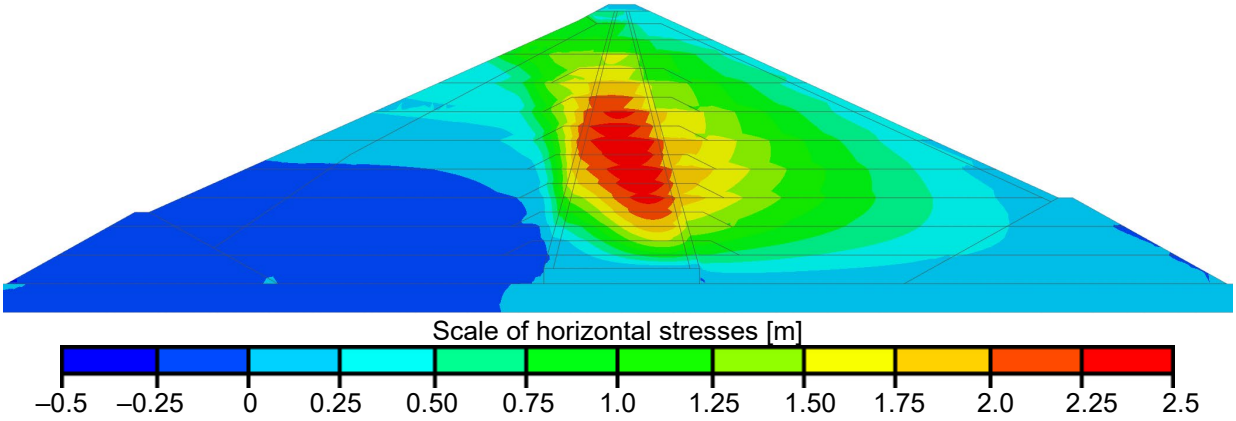

Figure 6. Dam horizontal displacements by the results of numerical modeling (for the moment of constriction completion).

Arch effect is characterized for distribution of vertical total stresses (Fig. 7). Compressive stresses in the core do not reach 2.5 MPa, while in the shells, they exceed 8 MPa. As compared to maximum possible pressure from the soil weight (6.3 MPa), compressive forces amount to only 40 %. Thus, the effect of the core “hanging up” on the shells takes place.

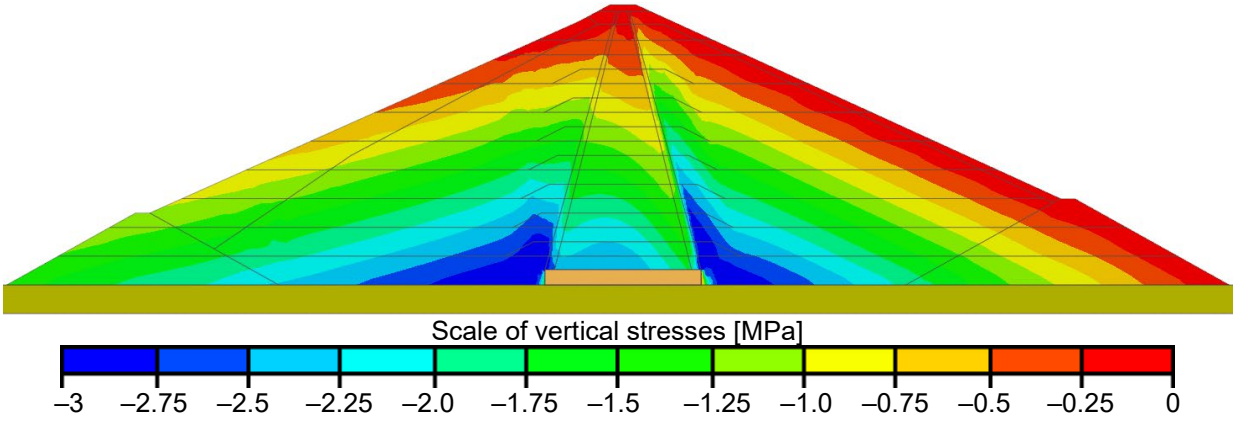

Figure. 7. Vertical total stresses in the dam body by the results of numerical modeling (for the moment of constriction completion).

Horizontal stresses are considerably lower than the vertical ones. They do not exceed 4.3 MPa (Fig. 8). The level of compression gradually decreases in the direction from the upstream slope to the downstream one. The most intensive drop of compressive stresses occurs in the core lower part.

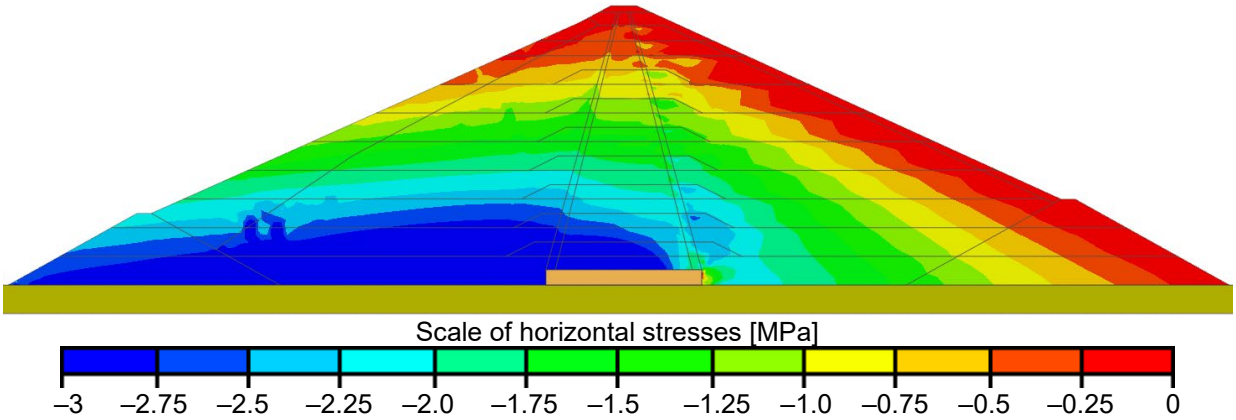

Figure. 8. Horizontal total stresses in the dam body by the results of numerical modeling (for the moment of constriction completion).

Fig. 9 shows distribution of pore pressure in the core for three characteristic moments of time obtained by numerical modeling. For convenience of comparison, Fig. 10 shows isolines (isobars) of pore pressure, obtained by analysis and field measurements.

The pattern of pore pressure distribution at the initial stages of construction, obtained with aid of numerical modeling, is similar to that obtained by the analytical method. It is formed mainly by pressure of the overlying soil weight. PWP maximum is reached closer to the center of the core lower part. PWP maximum values are also similar. For example, for the moment of time for the year of 1977, it amounts to: by the method of numerical modeling, it is 2.7 MPa (Fig. 9b), by the analytical method, it is 3.5 MPa (Fig. 4b). These values are close to the values obtained in the field conditions (2.99 MPa, Fig. 2b). PWP decrease, obtained by numerical modeling, among others is explained by the effect of the core “hanging up” on the shells.

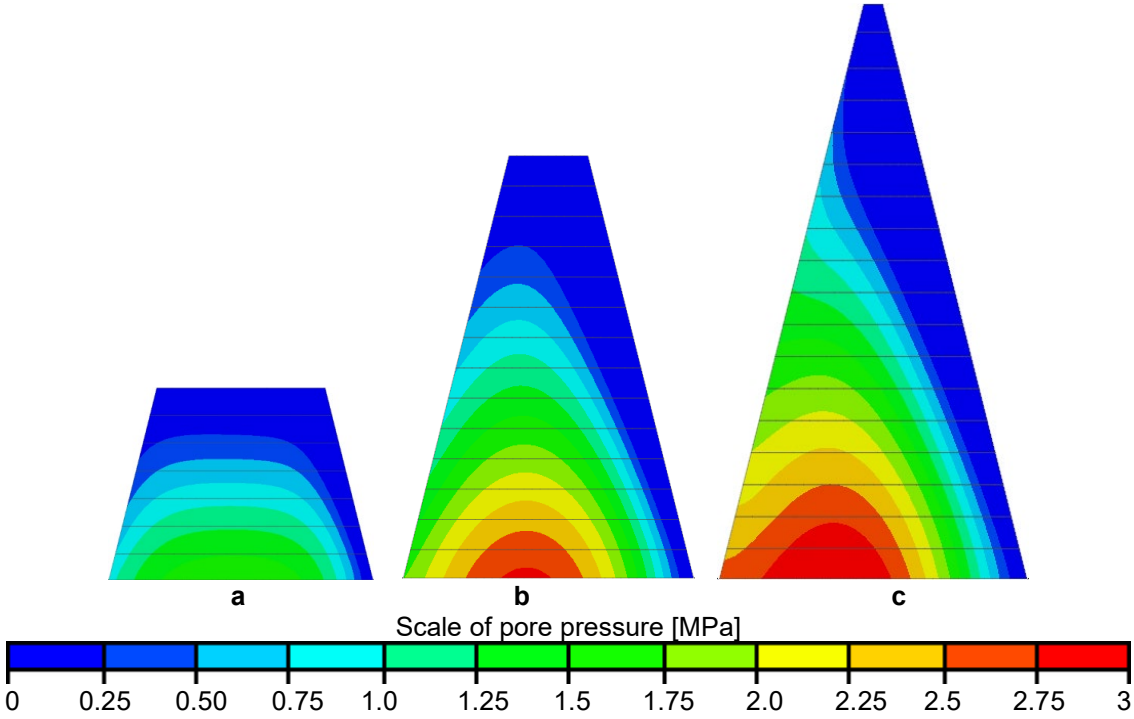

Figure 9. Pore pressure in the dam core by the results of numerical modeling (with consideration of the reservoir impoundment):
a – after 2 years from the start of construction; b – after 6 years from the start of construction;
c – after 9 years from the start of construction.

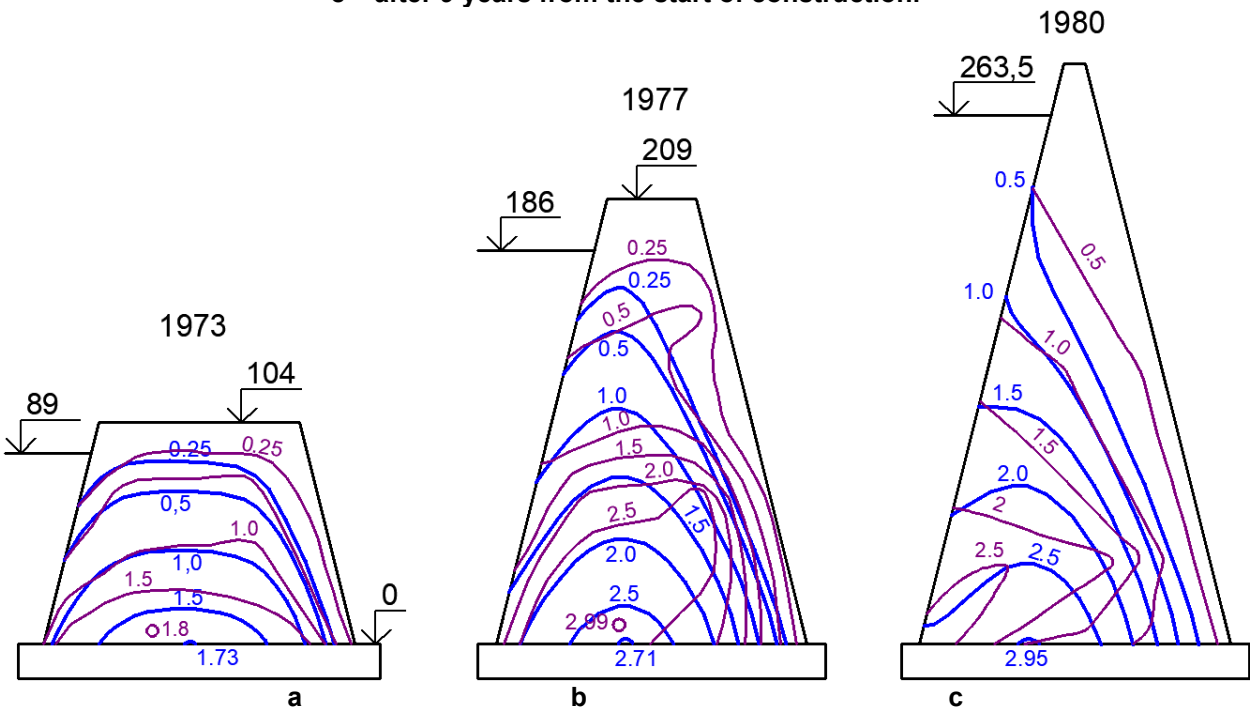

Figure. 10. Comparison of the results of numerical modeling with the results of pore pressure field measurements in the dam core:
a – after 2 years from the start of construction; b – after 6 years from the start of construction;
c – after 9 years from the start of construction. Violet color shows isolines of pore pressure by the

results of field measurements, blue color – by the results of numerical modeling. The indicated elevations are relative.

For the moment of construction completion (1980), the results of numerical modeling greatly differ from the results of analysis by the analytical method. The pattern of PWP distribution is much closer to that, which corresponds to the seepage pressure (Figs. 9c, 10c). PWP maximum value according to the analysis amounted to 2.95 MPa (Fig. 10c), which is less that by the analytical method (4.5 MPa, Fig. 4c). Obtained by numerical modeling pattern, pore pressure is much closer to that, which was obtained by field measurements. Maximum value of designed PWP is approximately by 15 % higher than by field data.

In order to determine the mechanism of pore pressure formation, reveal its rapid variation at the completion stage of construction, additional analysis was carried out. This SSS analysis was performed at loads only from the dead weight, without consideration of the reservoir impoundment. The obtained for this design scheme PWP distribution is shown in Fig. 11. It principally differs from that, which was obtained with consideration of the reservoir impoundment.

At the completion period of construction, the pore pressure does not increase with time but decreases. Namely, the maximum value of PWP after 6 years from the start of construction amounts to approximately 2.2 MPa (Fig. 11b), and after 9 years, it is about 1.8 MPa (Fig. 11c). PWP decrease is well illustrated in Fig. 12, where variation of pore pressure is shown for several points (where sensors are installed).

The pore pressure value under loads is much less then with consideration of the reservoir impoundment. Under loads from only the dead weight at the completion stage of construction, PWP maximum value was only 1.8 MPa (Fig. 11c), and with consideration of the reservoir impoundment, it was 2.95 MPa (Fig. 10c).

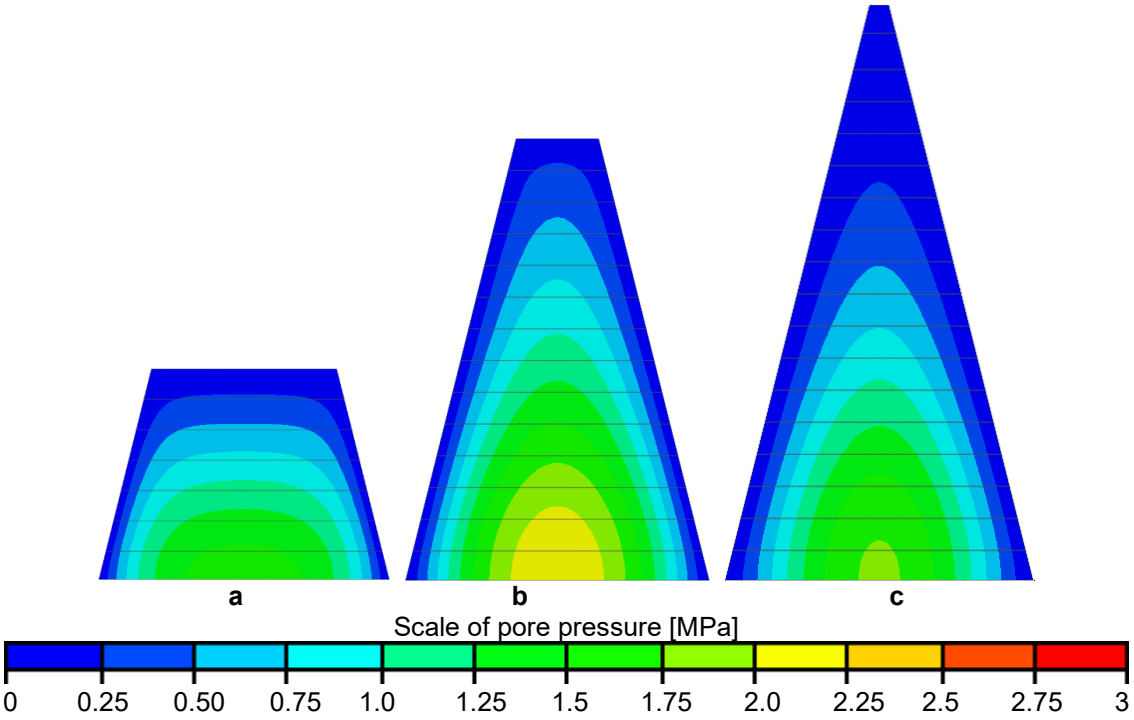

Figure. 11. Pore pressure of the dam core by the results of numerical modeling (without consideration of the reservoir impoundment):
a – after 2 years from the start of construction; b – after 6 years from the start of construction; c – after 9 years from the start of construction.

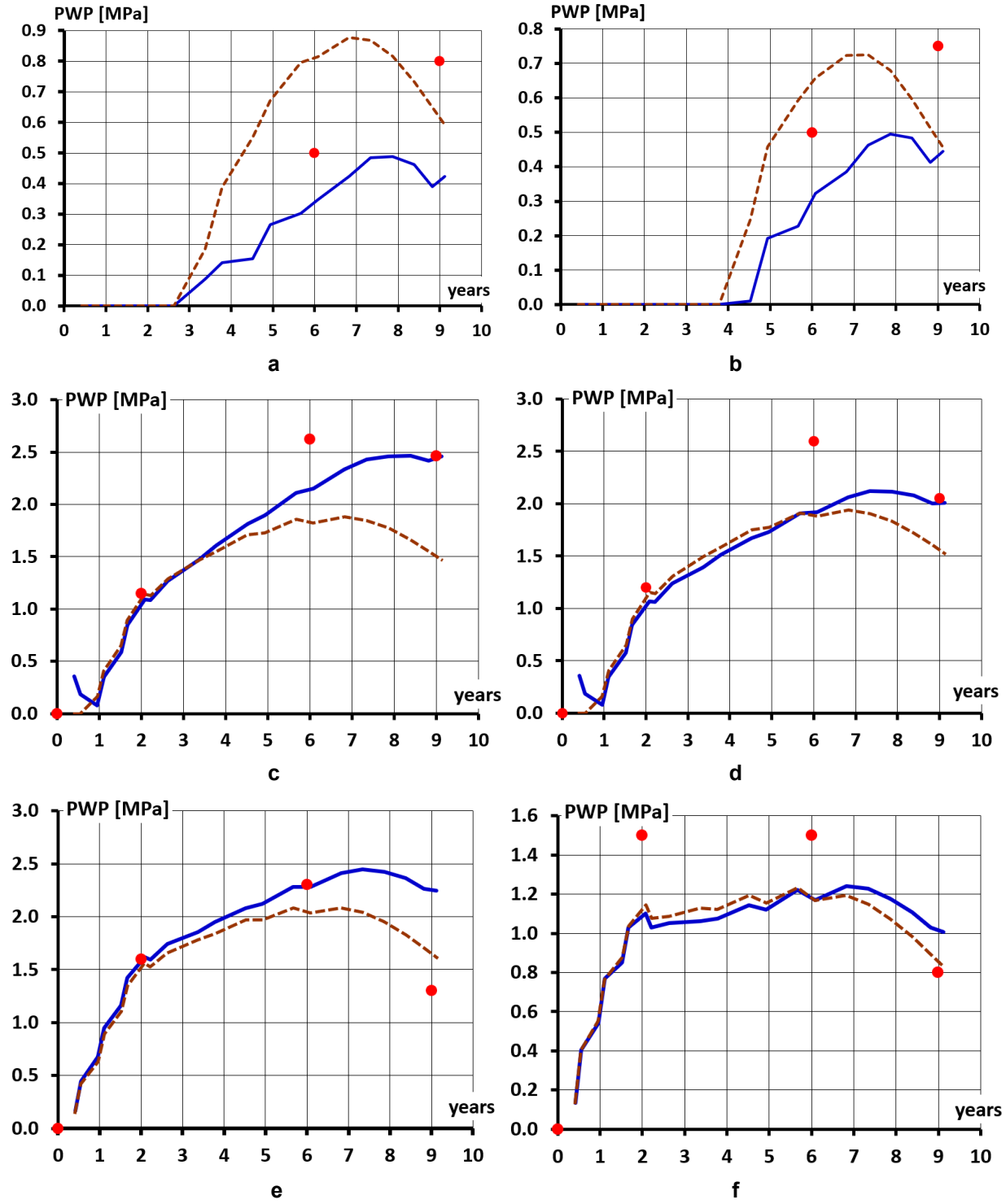

Figure. 12. Pore pressure variation with time in several points: a – sensor 1370; b – sensor 1357; c – sensor 1314; d – sensor 1315; e – sensor 1304; f – sensor 1305. Red points show the results of field measurements; the blue continuous line shows the results of numerical modeling with consideration of the reservoir impoundment; the brown dotted line shows the results of numerical modeling without consideration of the reservoir impoundment.

This comparison testifies that:

- in pore pressure formation, the role of pressure from the dead weight is much less, and the role of the reservoir impoundment is much greater than it is proposed in the analytical method of analysis;
- growth of seepage pressure in the core is sufficiently rapid.

These effects are explained by specific features of the dam SSS formed by the action of external forces.

Decreased values of pore pressure from dead weight, obtained by numerical modeling, are explained by several reasons. One of the causes is the effect of the core “hanging up”, as a result of which the load on the core decreases. The main cause is the dam lateral expansion at perception of loads, which leads to increase of porosity and, consequently, to decrease of PWP. This is the evidence due to the studies, which we have conducted earlier and described in [26].

Rapid increase of PWP at the reservoir impoundment occurs not just due to the process of water filtration inside the core but more due to compression deformations, to which the dam is subject at perceiving horizontal loads. To the two known types of PWP in the dam (PWP from the dead weight, filtration PWP) the third one may be added, i.e. PWP from horizontal loads.

Comparison of the character of core pressure variation in time, obtained by the results of numerical modeling (Fig. 12) and by the results of field measurements, shows their satisfactory conformity (with consideration of the fact that other factors also affect the processes of PWP formation in field conditions).

4. Conclusion

Analysis of field observations of Nurek dam state evidences that formation of pore pressure in the core soil was not always in the way predicted by the analytical methods of analysis of consolidation process. In real conditions, the soil consolidation process is more rapid than it is prognosed by analytical methods.

1. At the initial stages of construction, pore pressure increased, mainly due to weight increase of the overlying soil layers. At these stages, the process of soil consolidation is well described by analytical methods. At the completion stages of construction, the surplus pore pressure dissipated and filtering water penetrated inside the core. However, it happened much quicker than analytical methods predict. Already by the moment of construction completion, pore pressure from the dead weight already dissipated to a great extent and became close to seepage pressure. These effects cannot be explained only by long duration of construction and the reservoir impoundment (9 years).
2. Numerical modeling of the dam SSS jointly with modeling the seepage regime permitted to simulate rather accurately the process of pore pressure formation in Nurek dam core during construction period. In spite of proximity of the design scheme, we managed to reflect a special character of soil consolidation process, which was recorded by field measurements.
3. Analysis of numerical modeling results permits disclosing mechanisms of pore pressure formation in the core of ECRD, revealing the effect of the most important factors. Rapid decrease of pore pressure from the dead weight occurs not only due to its dissipation but mainly due to deformations of the dam lateral expansion. Due to these deformations in spite of dam height growth, cubic deformations do not increase but decrease. Rapid penetration of seepage pressure inside the core occurs not due to water filtration but due to those horizontal loads, to which the core is subject from the upstream water.
4. Analytical method of the core soil consolidation analysis does not take into account the enumerated above peculiarities in formation of the rockfill dam earth core SSS, therefore, it is applicable only for approximate estimations.
5. Results of numerical modeling are approximate because there were not considered non-linearity of soil deformation and special character of the dam SSS formation.

References

1. Penman, A.D.M. On the embankment dam. Geotechnique. 1986. 36(3). Pp. 303–348.
2. Sainov, M.P. Assessment of crack resistance of ultra-high earth core rockfill dam by pore pressure. Magazine of Civil Engineering. 2022. 114(6). Article no. 11411. DOI: 10.34910/MCE.114.11
3. Akhtarpour, A., Salari, M. The deformation mechanism of a high rockfill dam during the construction and first impounding. Scientia Iranica A. 2020. 27 (2). Pp. 566–587. DOI: 10.24200/sci.2018.20778
4. Hosseini, S.M.M.M., Fard, R.A. Pore pressure development in the core of earth dams during simultaneous construction and impounding. Electronic Journal of Geotechnical Engineering. 2003. 8. Pp. 1–13.
5. Razavi, B., Parehkar, M., Gholami, A. Investigation on Pore Water Pressure in Core of Karkheh Dam. International Journal of Civil and Environmental Engineering. 2011. 5(11). Pp. 539–542.
6. Balanji, S.G., Davoudi, S., Merufinia, E. Investigation the Effects of Pore Water Pressure and Arching on Karkheh Earth Dam Considering the Instrumentation Results. Advances in Environmental Biology. 2014. 8(12). Pp. 1345–1353
7. Feng, R., He, Y.-L., Cao, X.-X. Different Deformation Patterns in High Core Wall Rockfill Dams: A Case Study of the Maoergai and Qiaoqi Dams. Advances in Civil Engineering. 2019. 2019(2). Article no. 7069375. DOI: 10.1155/2019/7069375
8. Guo, Q., Pei, L., Zhou, Z., Chen, J., Yao, F. Response surface and genetic method of deformation back analysis for high core rockfill dams. Computers and Geotechnics. 2016. 74. Pp. 132–140. DOI: 10.1016/j.compgeo.2016.01.001
9. Ma, H., Chi, F. Major Technologies for Safe Construction of High Earth-Rockfill Dams. Engineering. 2016. 2(4). Pp. 498–509. DOI: 10.1016/J.ENG.2016.04.001
10. Lv, X., Chi, S. Strain Analysis of the Nuozhadu High Rockfill Dam during Initial Impoundment. Mathematical Problems in Engineering. 2018. 2018(2). Article no. 7291473. DOI: 10.1155/2018/7291473

11. Wu, Y., Zhang, B., Yu, Y., Zhang, Z. Consolidation analysis of Nuozhadu high earth-rockfill dam based on the coupling of seepage and stress-deformation physical state. International Journal of Geomechanics. 2016. 16(3). Article no. 04015085. DOI: 10.1061/(ASCE)GM.1943-5622.0000555
12. Rasskazov, L.N., Yadgorov, E.K., Nikolaev, V.B. Field Observations of Soil Settlements, Displacements, and Pore Pressure in Dams. Power Technology and Engineering. 2018. 51(6). Pp. 611–620. DOI: 10.1007/s10749-017-0804-1
13. Salari, M., Akhtarpour, A., Ekramifard, A. Hydraulic fracturing: a main cause of initiating internal erosion in a high earth-rock fill dam. International Journal of Geotechnical Engineering. 2018. 15(6). DOI: 10.1080/19386362.2018.1500122
14. Rasskazov, L.N., Yadgorov, E.Kh., Burenkov, P.M. Pore Pressure Dissipation in the Core of the Nurek Dam. Power Technology and Engineering. 2016. 50(1). Pp. 54–56. DOI: https://doi.org/10.1007/s10749-016-0658-y
15. Verruijt, A. Consolidation of Soils. Encyclopedia of Hydrological Sciences. Chichester: John Wiley & Sons, Ltd., 2008. Pp. 1–16. DOI: 10.1002/0470848944.hsa303
16. Skempton, A.W. The pore pressure coefficients *A* and *B*. Geotechnique. 1954. 4(4). Pp. 143–147. DOI: 10.1680/geot.1954.4.4.143
17. Biot, M.A. General Theory of Three-Dimensional Consolidation. Journal of Applied Physics. 1941. 12(2). Pp. 155–164. DOI: 10.1063/1.1712886
18. Tsybulnik T.I. Opredeleniye porovogo davleniya v yadre vysokoy plotiny pri peremennykh znacheniyakh kharakteristik grunta [Determining pore pressure in the core of a high dam with variable soil characteristics]. Trudy VODGEO, Gidrotekhnika. 1965. 11. Pp.35-45.
19. Nichiporovich A.A., Tsybulnik T.I. Odnomernaya zadacha konsolidatsii glinistogo grunta pri napryazhennom sostoyanii, sootvetstvuyushchem sluchayu ploskoy deformatsii [One-dimensional problem of consolidating clay soil in a stressed state corresponding to the plane deformation case]. Trudy VODGEO, Gidrotekhnika. 1972. 34. Pp. 5–25.
20. Eisenstein, Z., Law, S.T.C. Analysis of consolidation behavior of Mica dam. ASCE Journal of Geotechnical Engineering Division. 1977. 103(8). Pp. 879–895.
21. Rashidi, M., Heidari, M., Azizyan, Gh. Numerical Analysis and Monitoring of an Embankment Dam During Construction and First Impounding (Case Study: Siah Sang Dam). Scientia Iranica A. 2018. 25(2). Pp. 505–516. DOI: 10.24200/sci.2017.4181
22. Soroush, A., Pourakbar, M., Nabizadeh, A. 3D numerical analyses of behavior of a high rockfill dam with clay core in narrow canyon. 16th Asian Region Conference on Soil Mechanics and Geotechnical Engineering, Taipei, 2019.
23. Komasi, M., Beiranvand, B. Study of Hydraulic Failure Mechanism in the Core of Eyvashan Earth Dam with the Effect of Pore Water Pressure and Arching. Journal of Stress Analysis. 2020. 4(2). Pp. 55–67. DOI: 10.22084/jrstan.2020.20022.1110
24. Undayani, C.S., Sri P.R.W., Suharyanto, Windu P. Influence of pore water pressure to seepage and stability of embankment dam (case study of Sermo Dam Yogyakarta, Indonesia). MATEC Web of Conferences. 2017. 101. Article no. 05007. DOI: 10.1051/matecconf/201710105007
25. Aniskin, N.A., Rasskazov, L.N., Yadgorov, E.K. Filtration, pore pressure, and settling from consolidation of an ultra-high dam. Power Technology and Engineering. 2017. 50(6). Pp. 600–605.
26. Sainov M.P., Boldin A.A. Formirovaniye porovogo davleniya v yadre kamenno-zemlyanoy plotiny ot sobstvennogo vesa [Formation of pore pressure in the earth-core rockfill dam due to the dead weight]. Gidrotekhnika. 2024. 2(75). Pp. 10–14.

Information about the authors:

***Mikhail Sainov**, Doctor of Technical Sciences*

ORCID: https://orcid.org/0000-0003-1139-3164

E-mail: mp_sainov@mail.ru

***Aleksandr Boldin**,*

E-mail: alex.boldin2012@yandex.ru

Received 22.08.2024. Approved after reviewing 17.06.2025. Accepted 18.06.2025.

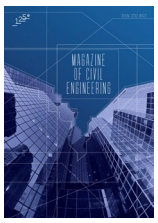

Magazine of Civil Engineering

ISSN 2712-8172

journal homepage: http://engstroy.spbstu.ru/

Research article

UDC 624.21

DOI: 10.34910/MCE.136.5

Probabilistic model for predicting the corrosion-fatigue durability of reinforced concrete railway bridges

G.A. Yefremov ✉ , ***D.A. Shestovitskiy***

Emperor Alexander I St. Petersburg State Transport University, St. Petersburg, Russian Federation

✉ *frost0077@mail.ru*

Keywords: reinforced concrete, durability, forecasting, numerical methods, service life, corrosion, fatigue of materials, fracture mechanics, probability, railway bridges, Paris law.

Abstract. This study proposes a probabilistic model for assessing the service life of a reinforced concrete railway bridge based on the criterion of corrosion-fatigue durability, taking into account the dynamics of the moving load. Currently, there is no similar methodology approved in the standards of the Russian Federation, as well as in the Eurocodes, while corrosion-fatigue destruction of reinforcement is typical in conditions of chloride-aggressive environments and repetitive loads. In this model, total service life of reinforced concrete superstructure is sum of three periods: corrosion initiation period, crack nucleation period, and crack propagation period. In each period, stochastic variables are specified by probability density functions. As an example of calculating the service life, one of the bridges developed during the design of the Moscow – St. Petersburg High-Speed Railway was chosen. Monte Carlo method was used as the way to modelling the stochastic nature of problem. Failure criteria was the critical crack growth, and crack growth process was modelled using Paris law. The form of the obtained probability density functions for each stage is lognormal; the greatest contribution to the total service life was made by the period of corrosion initiation. In the future, the use of the method will allow the engineer to design structures with a given durability, increase the service life of reinforced concrete bridge spans and more accurately plan funds for repairs of reinforced concrete bridges.

Citation: Yefremov, G.A., Shestovitskiy, D.A. Probabilistic model for predicting the corrosion-fatigue durability of reinforced concrete railway bridges. Magazine of Civil Engineering. 2025. 18(4). Article no. 13605. DOI: 10.34910/MCE.136.5

1. Introduction

This study focuses on the degradation of railroad bridge spans under chloride-containing environments. The combination of different effects, in this case chloride ions and repeated load, can lead to the corrosion pit growth and stress concentration in concrete beam reinforcement. Furthermore, repeatable train load can cause nucleation and growth of fatigue crack and rebar failure if crack length will reach its maximum allowed value.

Next some approaches to solving the corrosion-fatigue durability of bridges problem will be presented. For example, condition of working reinforcement under variable load under corrosion conditions is considered in the paper [1], which concludes that the fatigue characteristics of a reinforced concrete girder are reduced as a result of pitting corrosion. European document DuraCrete [2] provides various models of degradation of the span structure under the action of negative climatic factors. S. K. Verma et al. [3] proposes to estimate the service life as the sum of two periods: corrosion initiation and corrosion development period. Some publications are also devoted to the study of bonding of reinforcement with concrete under conditions of corrosion of working reinforcement [4, 5]. One of the first to apply the provisions of fracture mechanics and metal corrosion to calculate the corrosion-fatigue life of a reinforced concrete bridge was E. Bastidas-Arteaga [6]. J. Sun et al. indicated that corrosion, along with temporary

loading are the prevailing causes of collapse of reinforced concrete structures [7]. C. Cui et al. consider the negative effects of carbonization together with temporary loading [8]. The authors of a study on prestressed reinforced concrete beams of U-shaped urban rail transit exposed to chloride ions G. Chen et al. [9] indicate that the combined effect of temporary loading and chloride-containing environment can reduce the service life of the span by up to 61.2 %. T. Zhang et al. found that when reinforced concrete beams were jointly exposed to corrosion and repetitive loading, fatigue failure of longitudinal working reinforcement bars occurred [10].

From the above, it can be concluded that, firstly, with coupled action of chloride aggressive environment and repeatable loading, the corrosion-fatigue failure can be typical. Secondly, the problem of service life assessment is complex and currently it is not possible to collect all the developed models into a single methodology and provide a reliable prediction of the service life of reinforced concrete bridge spans. In addition, taking into account the dynamics of span structures is especially important in the calculation of bridges on high-speed highways. The resulting vibrations of the span structure during the passage of a train at high speeds can negatively affect the fatigue life of the span structure, which is not taken into account in the above-mentioned methods. Thus, this task is relevant and requires research. Therefore, in this study, the task was to develop a method for calculating corrosion-fatigue durability that could take into account the dynamic effect of temporary load, as well as the probabilistic natural parameters included in the calculation.

2. Methods

For chloride aggressive environment, pitting corrosion of reinforcement bars is often occurs. It has the most negative effect on the fatigue of reinforcement under the action of train loading [11]-[13]. The appearance of corrosion pits leads to stress concentration in the working reinforcement and fatigue crack initiation. Therefore, when assessing the service life of a span structure by the criterion of corrosion-fatigue durability, it is proposed to distinguish three main periods: the period of corrosion initiation, the period of corrosion pit growth and crack nucleation, and the period of fatigue crack growth until the failure:

$$T = t_{ini} + t_{cn} + t_{cg}. \tag{1}$$

Further we consider separately each of the periods in the probabilistic formulation of the problem.

3. Corrosion Initiation Period

The model of chloride ions penetration into the protective layer of the concrete of the span structure is based on Fick's II law of diffusion [14], [15]. In simplified form for one-dimensional case, it is written as follows:

$$\frac{\partial C}{\partial t} = D \cdot \frac{\partial^2 C}{\partial x^2}, \tag{2}$$

where C – chloride concentration at depth x, at time t; D – diffusion coefficient of chlorides into concrete.

Equation (2) was solved by the finite difference method using Mathcad Prime mathematical package. The scheme for solving equation (2) and the expression for the chloride diffusion coefficient are quite extensive, so we will limit ourselves to references to the corresponding works [6, 16].

The random nature of the parameters included in the equation was taken into account by means of Monte Carlo modelling [17]. This method involves solving this problem N times, each using randomly generated quantities according to their distribution laws. If the number of experiments N is large enough, the modeling results can be considered reliable.

As an example for the calculation, the rigid-framed reinforced concrete span shown in Figs. 1, 2 was used. The design of this overpass was considered as a variant on the Moscow – St. Petersburg High-Speed Railway.

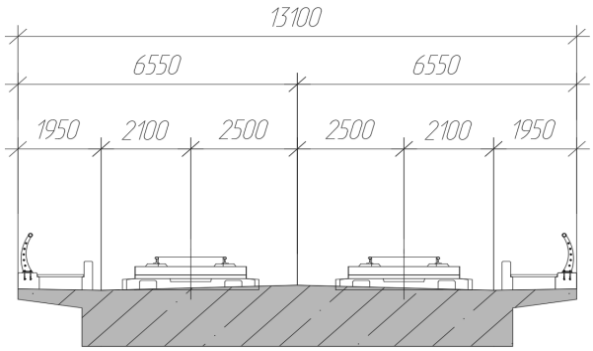

Figure 1. Cross-section of main span.

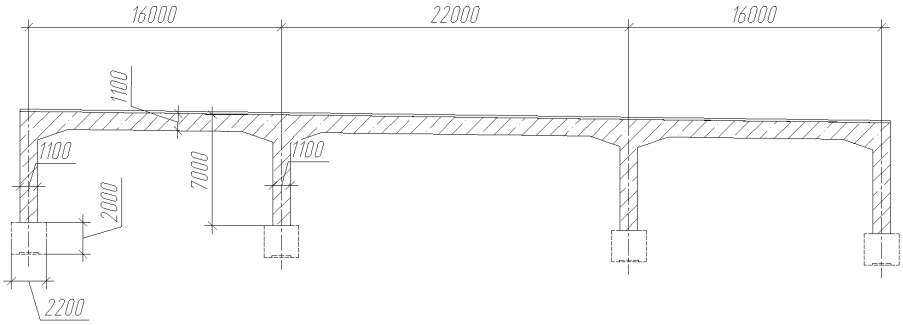

Figure 2. Longitudinal scheme of the bridge.

The initial parameters of the distributions of random variables are given in Table 1.

Table 1. Initial random variables for evaluating corrosion initiation time.

Parameter	Symbol	Probability density function	Expected value	Standart deviation
Water cement ratio	ω_c	Normal	0.4	0.04
Initial diffusion coefficient, m^2/s	$D_{cl,0}$	Normal	$3 \cdot 10^{-11}$	$0.6 \cdot 10^{-11}$
Activation energy of the diffusion process, kJ/mol	U	Normal	41.8	4.18
Protective layer of concrete, mm	c_t	Normal	50	7.5

The initial constant values are given in Table 2.

Table 2. Initial constant variables for evaluating corrosion initiation time.

Parameter	Symbol	Value
Number of experiments	N	1000
Maximum monthly average temperature, °C	T_{max}	26
Minimum average monthly temperature, °C	T_{min}	–5
Maximum monthly average humidity	W_{max}	0.79
Minimum average monthly humidity	W_{min}	0.72
Surface concentration of chlorides, kg/m^3	C_s	1.5
Binding constant	α	0.1185
Binding constant	β	0.09

The variability of air temperature and humidity is taken into account using the following equation:

$$f_{T,W}(t) = \frac{\varphi_{\max} + \varphi_{\min}}{2} + \frac{\varphi_{\max} + \varphi_{\min}}{2} \sin(2\pi t) + \lambda_{T,W}, \quad (3)$$

where $\varphi_{\max}$ is the maximum value of the parameter (temperature, humidity); $\varphi_{\min}$ is the minimum value of the parameter (temperature, humidity); t is time in years, $\lambda_{T,W}$ is a random parameter having normal distribution, mathematical expectation equal to 0 and standard deviation of temperature 3 °C and humidity 0.01. The graphs of these functions (3) are shown in Fig. 3. The sinusoids $T_0(t)$ and $W_0(t)$ are the mean values of these functions without considering monthly deviations, $T(t)$ and $W(t)$ take into account the random fluctuations of ambient temperature and humidity.

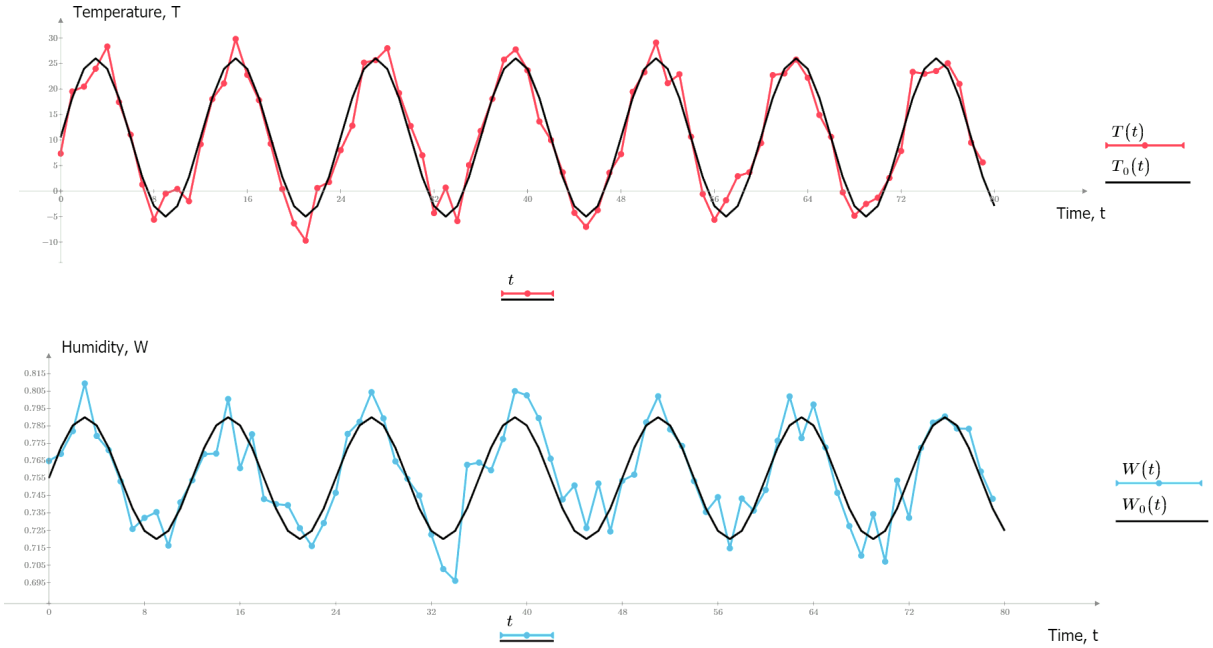

Figure 3. Plots of humidity and temperature dependence in deterministic and probabilistic form.

As a result of modeling 1000 iterations, in each of them, profiles of chloride concentration distribution along the depth of reinforced concrete span were obtained and the time, in which chloride concentration at the depth of concrete protective layer will reach the critical value, was calculated. The final function of the corrosion initiation time distribution is shown in Fig. 4.

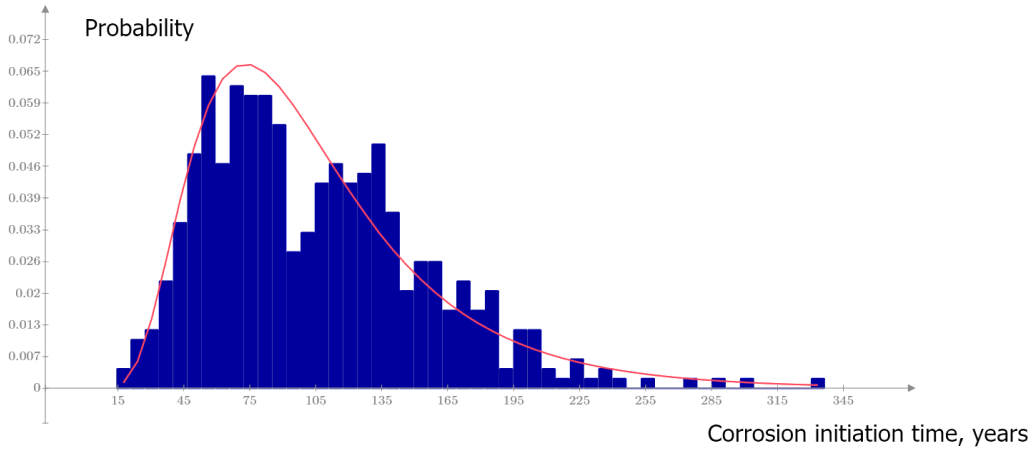

Figure 4. Distribution histogram and probability density distribution curve of corrosion initiation time of the working reinforcement of the span structure.

The graph shows the distribution histogram of the Monte Carlo simulation results and the theoretical probability density curve, which corresponds to a lognormal distribution with a mean value in these

conditions of 105.4 years, standard deviation of 55.9 years. The value, below which the corrosion initiation time does not fall with a 95 % probability or 5th percentile, is 41 years.

4. Time of Corrosion Pit Growth and Fatigue Crack Initiation

The second step in the total service life calculation is the calculation of the time, in which the stress concentration at the corrosion pit will lead to fatigue crack nucleation. The study [18] uses the following statement to calculate this time: for crack nucleation, it is necessary for the growth rate of the corrosion pit to coincide with the growth rate of the conditional crack at a point equal to the depth of corrosion development. In other words:

$$\frac{da}{dt} = \frac{dp}{dt}. \tag{4}$$

The left side of equation (4) represents the growth rate of the fatigue crack and is calculated using Paris's law [19, 20]:

$$\frac{da}{dt} = C_p \Delta K^{m_p} f, \tag{5}$$

where a is the crack size; C_p, m_p are coefficients depending on the material; ΔK is the stress intensity factor range [21]; f is the frequency of train loading (number of cycles per year).

The right part of equation (4) is the growth rate of the corrosion pit, calculated by the formula [22]:

$$p(t) = 0,00116a\int i_{corr}(t)\,\mathrm{dt}. \tag{6}$$

Thus, the growth time of the corrosion cavity before fatigue crack initiation is determined by equating (5) and (6) and solving with respect to t. The initial constants and random variables used in the solution are tabulated below.

Table 3. Initial random variables for evaluating crack nucleation time.

Parameter	Symbol	Probability density function	Expected value	Standart deviation
Corrosion initiation time, years	t_{ini}	Log-Normal	105.4	55.9
Concrete cover layer, mm	c_t	Normal	50	7.5
Paris law constant	C	Log-Normal	$1.8{\cdot}10^{-11}$	$1.118{\cdot}10^{-11}$
Paris law constant	m	Log-Normal	3.34	0.2
Water/cement ratio	ω_c	Normal	0.4	0.04
Pitting coefficient	α	Log-Normal	5.65	0.215

Table 4. Initial constant variables for evaluating crack nucleation time.

Parameter	Symbol	Value
Diameter of rebar, mm	d	32
Train load frequency, train/day	f	10
Average stress range in reinforcement	$\Delta\sigma$	75
Number of experiments	N	10000

The results of the Monte Carlo simulation in the form of a plot of the probability density function of the crack nucleation time are shown in Fig. 5.

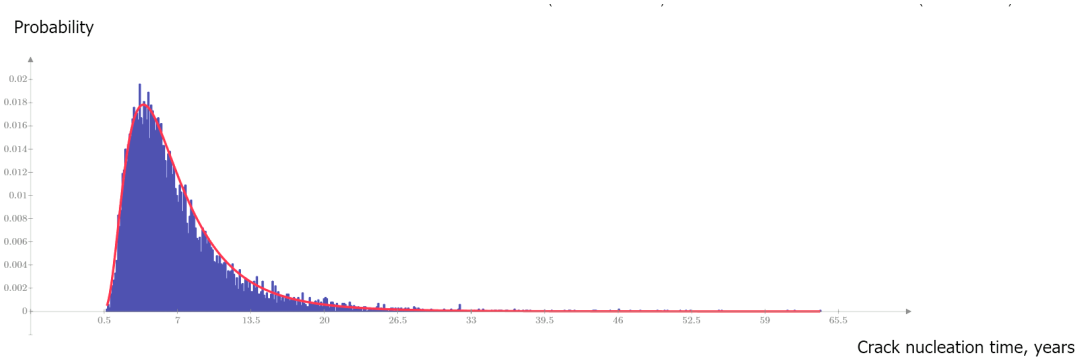

Figure 5. Distribution histogram and distribution density curve of the probability density function of crack initiation time in the working reinforcement of the span structure.

As in the case of corrosion initiation time, the fatigue crack initiation time is a lognormal distribution with mathematical expectation of 7 years, standard deviation of 4.6 years, and 5th percentile of 2.2 years.

5. Time of Crack Growth to Critical Value

The crack growth time to critical value is determined using Paris's law, see formula (5).

In this case, to calculate the stress intensity factor, it is also necessary to determine the stress difference arising from the train load. For this purpose, a nonlinear deformation model can be used; its basic provisions are given in [23]. The random nature of the parameters included in the calculation was also taken into account, see Table 5. The forces in the cross-section were found by dynamic calculation in the program complex realizing the finite element method [24]. The dynamic calculation is necessary to obtain the spectrum of the force factor and to take into account the contribution of each vibration of the spanning structure to the fatigue crack growth.

Table 5. Initial random variables to calculate stresses in reinforcement bars

Parameter	Symbol	Probability density function	Expected value	Standart deviation
Cross-section width, m	b	Normal	10.1–11.6	0.202–0.232
Cross-section height, m	h	Normal	1.64	0.016
Tensile reinforcement area, m^2	A_{s1}	Normal	0.05466	0.00137
Compressed reinforcement area, m^2	A_{s2}	Normal	0.03537	0.00088
Concrete Young's modulus, MPa	E_b	Normal	36000	2880
Steel Young's modulus, MPa	E_s	Normal	200000	6000
Cross-section center of gravity location, m	h_g	Normal	0.862	0.00862

Table 6. Initial constant variables to calculate stresses in reinforcement bars.

Parameter	Symbol	Value
Tensile strength of reinforcement, MPa	R_s	350
Design value of concrete compressive strength, MPa	R_b	20
Ultimate reinforcement strain	ε_s	0.025
Ultimate concrete compressive strain	ε_b	0.0035
Number of cross-section parts	n	30
Number of experiments	N	1000
Critical crack value, mm	a_{cr}	0.74·d

Similar to the previous steps, the probability distribution of the crack growth period was obtained and the 5th percentile was cut off, which amounted to 5.5 years (Fig. 6).

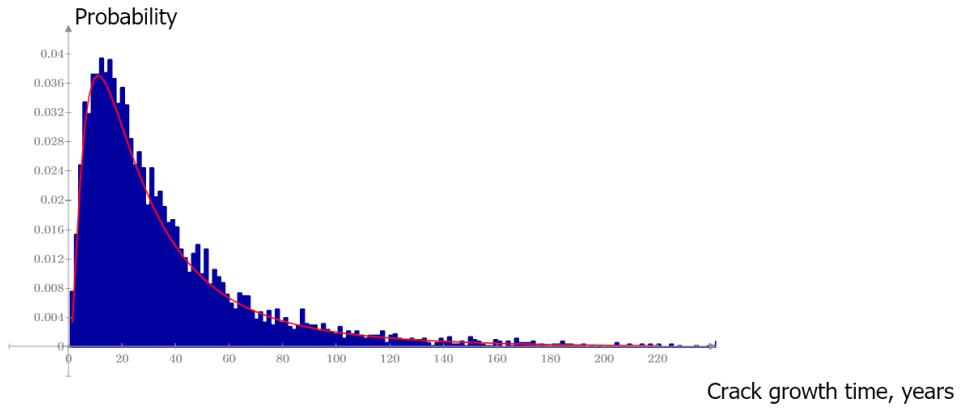

Figure 6. Distribution histogram and probability density distribution curve of crack growth time-to-failure probability in the working reinforcement of the spanwise structure.

6. Results and Discussions

To calculate the final service life of the structure, Monte Carlo simulation of the sum of three periods was performed, each of the periods was generated as a random variable based on the calculations performed. The final nature of the service life distribution can be seen in the figure below:

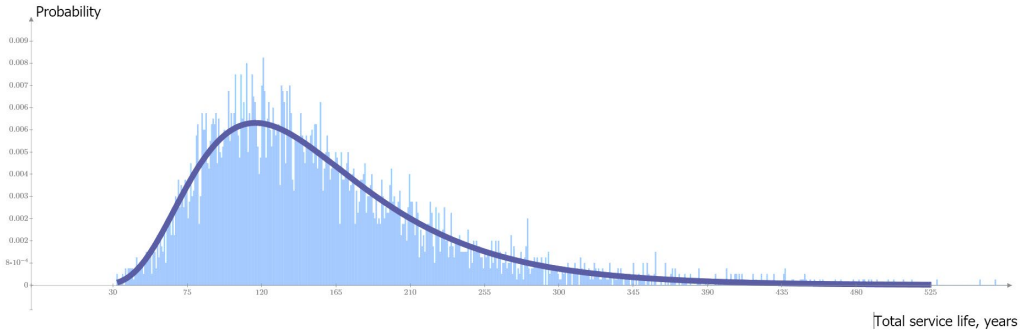

Figure 7. Distribution histogram and probability density distribution curve of the service life probability of the span structure based on the corrosion-fatigue life criterion.

Below is a summary table with the results of calculating the time of each of the periods and the total service life of the span structure.

Table 7. Results of calculating the time of crack initiation and growth before failure.

Parameter	Symbol	Probability density function	Expected value	Standart deviation	5th percentile
Corrosion initiation time, years	t_{ini}	Log-normal	112.5	62.8	42.5
Fatigue crack nucleation time, years	t_{cn}	Log-normal	7	4.6	2.2
Fatigue crack growth time, years	t_{cg}	Log-normal	38.2	43	5.5
Total bridge span service life, years	T	Log-normal	158.5	75.04	69.5

If we compare results with those available in various sources, we obtain a generally similar expected value of design service life, for example, in paper [25] for traffic load frequency 50/day and low-aggressive environment design service life of 157 years was obtain with standart deviation 57 years. The service life probability distribution density, obtained by the authors, also lognormal. However, with an increase in the frequency of load and the aggressiveness of the environment, the average service life drops to 20–40 years.

The authors [8] investigated corrosion-fatigue durability under carbonization and repeatable loading. Results show that the design service life of a 6-meter reinforced concrete plate superstructure is 162.1 years. However, the authors also conclude that corrosion-fatigue durability decreases by 67 % if traffic frequency increases from 1000 vehicles/day to 7000 vehicle/day.

A study of train loading coupled with aggressive environmental influences carried out by the authors [9] also showed a high corrosion-fatigue durability of 164.8 years with a low concentration of chloride ions and low load intensity, however, an increase in the concentration of chloride ions (from 2.5 kg/m^3 to 5.87 kg/m^3) reduced this value by 50 %, and an increase in train load (from 109 trains/day to 721 trains/day) – by 30 %.

In general, the possible dispersion of final results among different authors is associated with a large number of initial parameters of the model; the configurations of spans, the type and magnitude of the traffic load, climatic parameters, materials used, etc.

7. Conclusion

According to the results of the conducted research, we can conclude the following:

1. The corrosion initiation period, fatigue crack initiation time, crack growth time to failure, and the total service life of the span structure obey a lognormal distribution. The hypothesis that the sample from the Monte Carlo simulation results belong to the lognormal distribution is tested using Pearson's $\chi 2$ criterion of agreement, the critical value of the $\chi 2$ criterion is accepted for a significance level of 5 %.
2. The greatest contribution to the corrosion-fatigue durability is made by the corrosion initiation period, which indicates that if the working reinforcement is sufficiently protected from corrosion, it will be possible to significantly extend the service life of the structure. On the contrary, if the train moving load is significant and, for example, the protective layer is insufficient, the failure of the reinforcement can occur in a relatively short period of time.
3. The modern engineer has powerful tools for direct dynamic analysis of the structure, which, according to the proposed methodology, allows to estimate the contribution of each vibration of the span to the growth of fatigue crack, which can be used at the stage of design of artificial structures.
4. The service life of a structure, like everything in our world, has a probabilistic nature. In practice, probabilistic calculations are complicated and it is not reasonable to repeat them for each structure. Based on the results of this study, it is possible to calculate the reliability coefficient for the service life of the span structure for the example selected for the calculation. However, to develop a system of reliability coefficients for different initial data, further research on the influence of the variation of initial parameters on the statistical parameters of the service life of the structure is necessary.

References

1. Tamrazyan, A.G. Fatigue Behavior of Flexural Reinforced Concrete Beams under Corrosion Conditions. Reinforced Concrete Structures. 2024. 2(6). Pp. 24–36. DOI: 10.22227/2949-1622.2024.2.22-34
2. DuraCrete. Modelling of Degradation: Probabilistic Performance based Durability design of Concrete Structures. Document BE-1347. R4-5. 1998.
3. Verma, S.K., Sudhir, S.B., Saleem, A. Estimating Residual Service Life of Deteriorated Reinforced Concrete Structures. American Journal of Civil Engineering and Architecture. 2013. 1(5). Pp. 92–96. DOI: 10.12691/ajcea-1-5-1
4. Thajuddeen, H., Karthik, M. Fatigue Bond Life of Reinforced Concrete Beams with Low Reinforcement Corrosion. Proceedings of International Structural Engineering and Construction. 2024. 11(2). Pp. 1–6. DOI: 10.14455/ISEC.2024.11(2).STR-18
5. Zhou, H., Qi, X., Lin, Z., Filippo, M., Liu, J., Ma, C., Xing, F. An experimental study on bond behaviors of reinforced concrete under fatigue loading and corrosion. Structural Concrete. 2022. 24(1). Pp. 504–520. DOI: 10.1002/suco.202200684
6. Bastidas-Arteaga, E., Bressolette, P., Chateauneuf, A., Sanchez-Silva, M. Probabilistic lifetime assessment of RC structures under coupled corrosion-fatigue deterioration. Structural Safety. 2009. 31(1). Pp. 84–96. DOI: 10.1016/j.strusafe.2008.04.001
7. Sun, J., Ding, Z., Huang, Q. Corrosion fatigue life prediction for steel bar in concrete based on fatigue crack propagation and equivalent initial flaw size. Construction and Building Materials. 195. 2019. Pp. 208–217. DOI: 10.1016/j.conbuildmat.2018.11.056
8. Cui, C., Song, L., Liu, J., Yu, Z. Corrosion-Fatigue Life Prediction Modeling for RC Structures under Coupled Carbonation and Repeated Loading. Mathematics. 2021. 9. Article no. 3296. DOI: 10.3390/math9243296
9. Chen, G., Wang, M., Cui, C., Zhang, Q. Corrosion-Fatigue Life Prediction of the U-Shaped Beam in Urban Rail Transit under a Chloride Attack Environment. Materials. 2022. 15(17). Article no. 5902. DOI: 10.3390/ma15175902
10. Zhang, T., Zhang, X., Li, P., Li, H., Li, X., Zou, Y. Experimental Research on Fatigue Performance of Reinforced Concrete T-Shaped Beams under Corrosion. Fatigue Coupling Action. Materials. 2023. 16(3). Article no. 1257. DOI: 10.3390/ma16031257
11. Stewart, M.G. Time-dependent reliability of deteriorating reinforced concrete bridge decks. Structural Safety. 1998. 20(1). Pp. 91–109. DOI: 10.1016/S0167-4730(97)00021-0

12. Wang, H., He, S., Yin, X., Cao, Z. Experimental Study on Fatigue Performance of Reinforced Concrete Beams in Corrosive Environment with Cyclic Loads. Structural Durability & Health Monitoring. 2020. 14(2). Pp. 95–108. DOI: 10.32604/sdhm.2020.06595
13. Zhang, W., Song, X., Gu, X., Li, S. Tensile and fatigue behavior of corroded rebars. Construction and Building Materials. 2012. 34. Pp. 409–417. DOI: 10.1016/j.conbuildmat.2012.02.071
14. Liao, J., Wang, Y., Sun, X., Wang, Y. Chloride Penetration of Surface-Coated Concrete: Review and Outlook. Materials. 2024. 17(16). Article no. 4121. DOI: 10.3390/ma17164121
15. Sun, J., Jin, Z., Chang, H., Zhang, W. A review of chloride transport in concrete exposed to the marine atmosphere zone environment: Experiments and numerical models. Journal of Building Engineering. 2024. 84. Article no. 108591. DOI: 10.1016/j.jobe.2024.108591
16. Shalyy, E.E., Kim, L.V., Leonovich, S.N. Reinforced Concrete under Influence of Carbonization and Chloride Aggression: Probable Model of Service Life Calculation. Bulletin of Belgorod State Technological University named after. V. G. Shukhov. 2018. 6. Pp. 5–14. DOI: 10.12737/article_5b115a5ef027c2.76676320
17. Novák, D., Strauss, A., Novák, L., Lehký, D., Šomodíková, M., Lipowczan, M., Slowik, O., Doležel, J., Pukl, R., Sattler, F., Apostolidi, E. Nonlinear probabilistic structural assessment: Findings from Austrian and Czech bridges. EUROSTRUCT 2023: European Association on Quality Control of Bridges and Structures: Digital Transformation in Sustainability. 2023. 6(5). Pp. 1242–1251. DOI: 10.1002/cepa.2195
18. Chen, G., Wan, K., Gao, M., Wei R., Flournoy, T. Transition from pitting to fatigue crack growth modeling of corrosion fatigue crack nucleation in a 2024-T3 aluminum alloy. Materials Science and Engineering. 1996. 219(1–2). Pp. 126–132. DOI: 10.1016/s0921-5093(96)10414-7
19. Paris, P.C., Erdogan, F. A Critical Analysis of Crack Propagation Laws. Journal of Basic Engineering. 1963. 85. Pp. 528–533. DOI: 10.1115/1.3656900
20. Salah el din, A.S., Lovegrove, J.M. Fatigue of cold worked ribbed reinforcing bar – a fracture mechanics approach. International Journal of Fatigue. 1982. 4(1). Pp. 15–26. DOI: 10.1016/0142-1123(82)90016-0
21. Murakami, Y., Nisitani, H. Stress intensity factor for circumferentially cracked round bar in tension. Transactions of the Japan Society of Mechanical Engineers. 1975. 41. Pp. 360–369. DOI: 10.1299/kikai1938.41.360
22. Liang, M., Jin, W., Yang, R., Huang, N. Predeterminate model of corrosion rate of steel in concrete. Cement and Concrete Research. 2005. 35(9). Pp. 1827–1833. DOI: 10.1016/j.cemconres.2004.10.005
23. Trekin, N.N., Alekseytsev, A.V., Bobrov, V.V., Domarova, Ye.V. Raschet zhelezobetonnykh izgibayemykh konstruktsiy na osnove nelineynoy deformatsionnoy modeli. [Calculation of reinforced concrete bendable structures based on a nonlinear deformation model]. Moscow: MISI-MGSU Publishing, 2023. 63 p.
24. Efremov, G.A., Myachin, V.N., Shestovitskiy, D.A. Influence of cyclic loading on corrosion-fatigue life of concrete bridges superstructure. The Siberian Transport University Bulletin. 2023. 66(3). Pp. 51–59. DOI: 10.52170/1815-9265_2023_66_51
25. Bastidas-Arteaga, E. Reliability of Reinforced Concrete Structures Subjected to Corrosion-Fatigue and Climate Change. International Journal of Concrete Structures and Materials. 2018. 12. Article no. 10. DOI: 10.1186/s40069-018-0235-x

Information about the authors:

Gleb Yefremov,
ORCID: https://orcid.org/0000-0001-9311-3765
E-mail: frost0077@mail.ru

Dmitriy Shestovitskiy, *PhD in Technical Sciences*
E-mail: shestovitsky@mail.ru

Received 02.11.2024. Approved after reviewing 26.05.2025. Accepted 09.06.2025.

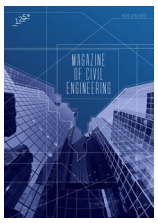

Magazine of Civil Engineering

ISSN 2712-8172

journal homepage: http://engstroy.spbstu.ru/

Research article

UDC 691

DOI: 10.34910/MCE.136.6

The effect of using internal curing on chloride penetration of self-compacting concrete

M. Rajabi Jorshari ✉, ***M. Malekzadeh***, ***A. Hajati Modaraei***

University of Guilan, Rasht, Iran

✉ *miladcivil.r84@gmail.com*

Keywords: self-compacting concrete, internal curing agent, superabsorbent polymer, chloride ion diffusion coefficient, recycled lightweight aggregate

Abstract. In recent years, the use of internal curing has received attention as a solution to reduce problems caused by shrinkage in self-compacting concrete (SCC). However, the use of internal curing agents increases the internal porosity of concrete, which can lead to durability issues in some environmental conditions. This study examines the effects of internal curing on the properties and durability of SCC incorporating recycled Lightweight aggregate (RLWA) and superabsorbent polymers (SAP) as internal curing agents. Mixtures containing 15 % and 30 % RLWA or 0.1 % SAP were evaluated under both saturated and 50 % relative humidity conditions. The tests included compressive strength and rapid chloride migration. The results indicated that under 50 % relative humidity, internal curing agents enhanced compressive strength by up to 6.8 % at 28 days and reduced the chloride ion diffusion coefficient by up to 18.4 % at 360 days. Using the chloride diffusion coefficients obtained, along with the Crank–Nielsen method, the phenomenon of chloride ion penetration in concrete was modeled, and the initiation time for reinforcement corrosion was estimated. SAP extended the corrosion initiation time by 25.8 % compared to Ref.-DW and demonstrated 17.2 % superior durability performance compared to 15RLWA-DW. The findings show that SAP is a more effective internal curing agent for improving the durability and corrosion resistance of SCC in unsaturated environments, offering a valuable approach to enhancing concrete durability.

Citation: Rajabi Jorshari, M., Malekzadeh, M., Hajati Modaraei, A. The effect of using internal curing on chloride penetration of self-compacting concrete. Magazine of Civil Engineering. 2025. 18(4). Article no. 13606. DOI: 10.34910/MCE.136.6

1. Introduction

Internal curing methods have gained significant attention as a solution to mitigate the drawbacks of self-compacting concrete (SCC). The higher paste volume and lower water-to-cement ratio in SCC increase the risk of shrinkage compared to conventional concrete [1, 2]. Common internal curing materials include natural lightweight aggregates (LWA) and superabsorbent polymers (SAP), which store water and release it gradually, reducing moisture loss in concrete pores and enabling prolonged curing [1–4].

Studies have shown that internal curing reduces concrete shrinkage and, consequently, the likelihood of cracking within structures. However, contradictory results have been reported regarding the effect of internal curing on the mechanical properties of concrete under saturated conditions. Rajamanickam and Vaiyapuri [5] found that incorporating 5 % LWA by volume reduced the compressive strength of SCC in saturated environmental conditions compared to control concrete. Conversely, Gopi and Revathi [6] observed that using 15 % saturated LWA improved the compressive strength of SCC in saturated conditions. Madduru et al. [7] reported that the tensile and flexural strengths of SCC containing

internal curing agents were reduced compared to control SCC under saturated conditions. These findings highlight a lack of consensus regarding the impact of internal curing on the strength characteristics of SCC.

Another critical aspect of internal curing materials is their influence on concrete permeability. Studies indicate that replacing natural aggregate with LWA increases concrete permeability due to higher internal porosity [8]. In general, research suggests that the application of internal curing in saturated environments increases concrete permeability [9–14]. However, as concrete in most structures exists in unsaturated conditions, investigating the mechanical properties and permeability of concrete with internal curing agents in such environments has become increasingly relevant. Despite this, limited research has been conducted on the permeability of concrete containing internal curing agents in unsaturated conditions.

Ahmadi et al. [15] investigated the characteristics of SCC containing LWA for internal curing in an unsaturated environment. Their findings revealed that, after demolding, the depth of chloride ion penetration in SCC with internal curing agents was lower than in SCC without them. However, this study substituted internal curing agents based on the weight percentage of natural fine aggregates and did not explore properties in water-saturated conditions. Similarly, Priya et al. [16] compared the effects of LWA and SAP as internal curing materials on SCC in laboratory environments, concluding that SAP was more effective than LWA.

Previous research has demonstrated that diffusion is the main mechanism of chloride transport in concrete exposed to chloride environments. Fick's second law is widely applied to model chloride ion penetration and estimate the initiation time of reinforcement corrosion. Among numerical approaches, the Crank–Nicolson method, based on the finite volume technique, has been frequently used in previous studies for such modeling purposes [17–20]. Therefore, in the present study, this method was adopted to evaluate the influence of internal curing materials on SCC.

This study investigates the impact of internal curing on the permeability properties of SCC in unsaturated environments with 50 % relative humidity. It evaluates and compares the effects of RLWA and SAP on the compressive strength and chloride ion diffusion coefficient of SCC under both saturated and unsaturated conditions.

2. Methods

2.1. Experimental Program

The cement used in this study was manufactured by Sepahan Cement Factory. Its composition included 24 % C_2S, 52 % C_3S, 9.5 % C_3A, and 9 % C_4AF, with a specific surface area of 2860 cm^2/g. The cement demonstrated a standard mortar compressive strength of 38.9 MPa and conformed to the ASTM C150 specifications for Type I cement regarding chemical composition, compressive strength, specific surface area, and setting time.

Concrete mixtures were prepared using P10N, a polycarboxylate ether-based superplasticizer from the Construction Chemicals Company, and tap water sourced from Rasht. Fine and coarse aggregates were procured from the North Pipe Factory. The natural fine aggregates (sand) had a saturated surface dry density of 2.61 g/cm^3, a water absorption rate of 13.3 %, and 1.14 % passing through a 200-mesh sieve. The coarse aggregates, with a nominal size of 12.5 mm, exhibited a saturated surface dry density of 2.65 g/cm^3, a water absorption rate of 1.74 %, and 0.16 % passing through a 200-mesh sieve. Both fine and coarse aggregates adhered to the ASTM C33 specifications.

Recycled lightweight aggregate (RLWA) particles used in this study were obtained from recycled autoclaved aerated concrete and ranged in size from 0.075 to 2.36 mm, with a saturated surface dry density of 0.836 g/cm^3. Particles smaller than 0.075 mm were excluded due to their powdery texture and insufficient water retention capacity.

The SAP employed was a polyacrylic polymer branded under TAISAP, with particle sizes ranging from 0.3 to 0.075 mm. A critical factor in using internal curing agents in concrete is quantifying the water released into the cement mixture. For LWA, the water released is calculated based on their water absorption percentage as outlined in ASTM C1761.

According to this standard, the water released by lightweight fine aggregates is determined by measuring the difference between their saturated surface-dry mass (achieved by removing them from water and gently drying the surface with a paper towel) and their stabilized mass at a relative humidity of 94 %. A controlled environment with 94 % relative humidity was maintained using a device equipped with temperature and humidity regulation. Results revealed that RLWA had a saturated surface dry water absorption of 19.3 %, and 66.3 % of the absorbed water was released under 94 % relative humidity conditions.

The adsorption and desorption behavior of SAP was evaluated using methods adopted from Huang et al. [21] and Lothenbach et al. [22]. The SAP was submerged in water for 72 hours, weighed, and then placed in a 0.7 mol/L sodium chloride solution for an additional 72 hours to assess mass loss, simulating the ionic conditions of cement pore solutions. Results showed that SAP absorbed water equivalent to 3.65 times its dry weight, with a desorption rate of 2.50 % in the sodium chloride solution. The 0.7 mol/L sodium chloride solution was selected to represent the typical ionic concentration of cement paste pore solutions prior to setting [19, 20].

2.2. Mixtures and Curing Methods

SCC mixtures were prepared with a water-to-cement ratio of 0.4 and a cement content of 500 (kg/m^3). The selected design was based on commercially available SCC mix designs provided by ready-mix concrete factories. The compositions of the studied mixtures are presented in Table 1. In addition to the control mixture, three other designs were prepared: one containing 0.1 % SAP by weight of cement (code S) and two mixtures with 15 % and 30 % by volume of natural fine aggregate replaced by RLWA (code RLWA).

Prior to mixing, the RLWA and SAP internal curing materials were soaked in water for 48 hours. To equalize the moisture content in these materials, they were placed on a drain for 3 hours, during which they were periodically moved to ensure even drainage. In accordance with ASTM C192, the moisture content of the aggregate materials was measured before concrete mixing. If necessary, adjustments were made to maintain a consistent free water-to-cement ratio in the mixtures. A portable moisture meter was used to measure the moisture content. In all mixtures, the dosage of high-range water-reducing admixture (superplasticizer) was kept constant to isolate and clearly observe the effect of SAP and RLWA on the fresh and hardened properties of SCC without the interference of other variables affecting workability.

The amount of internal curing agents in SCC was limited to avoid adverse effects on the fresh properties of the concrete. Excessive use of these agents can cause segregation in SCC.

The concrete was prepared using a pan-type mixer. After mixing, the specimens were molded following ASTM C192 specifications and stored in an environment with 95 % relative humidity for the first 24 hours. After demolding, the specimens were subjected to two different curing processes. In the external curing condition, the specimens were immersed in saturated lime water for up to 360 days. In the non-external curing condition, the specimens were kept in an environment with 50 % relative humidity and ambient temperature for up to 360 days.

2.3. Test Methods

In this study, the properties of fresh SCC, including the diameter of flow and flow rate, were assessed following the ASTM C1611 standard method.

Compressive strength tests were conducted in accordance with BS EN 12390 Part 3, under both saturated and unsaturated conditions. The tests were performed on three cubic specimens, each measuring 10×10×10 cm, at the ages of 28, 56, 90, 180, and 360 days.

Table 1. Concrete mixture proportions investigated in this study.

Mix Destination	W/B	Cement (kg/m^3)	Saturated Surface Dry aggregates (kg/m^3)			SAP (kg/m^3)	SP (%)	Internal curing water (kg/m^3)
			Fine Aggregate	Coarse Aggregate	RLWA			
Ref	0.4	500.0	988.0	669.0	0.0	0.0	1.19	0.0
0.1SAP	0.4	500.0	976.0	651.0	0.0	0.5	1.19	16.0
15RLWA	0.4	500.0	840.0	669.0	47.0	0.0	1.19	7.3
30RLWA	0.4	500.0	691.0	669.0	95.0	0.0	1.19	14.5

The Rapid Chloride Migration Test (RCMT) was performed in accordance with NTBuild 492 [23], under both saturated and unsaturated conditions. Three cylindrical specimens, each measuring 10 cm in diameter and 5 cm in thickness, were tested at the ages of 28, 56, 90, 180, and 360 days. During the test, one side of each specimen was exposed to a 10 % sodium chloride solution, while the opposite side was subjected to a 0.3 N sodium hydroxide solution. To accelerate chloride ion penetration, an electrical potential was applied, with the voltage determined based on the initial current passing through the specimen. The test setup is shown in Fig. 1.

After the test, the specimens were split, and a 0.1 N silver nitrate solution was applied to the exposed surfaces. The silver nitrate reacted with the chlorides, forming white silver chloride, which marked the

chloride penetration front. This visible boundary was used to identify the extent of chloride penetration, and the migration coefficient was then calculated using Equation 1 [23].

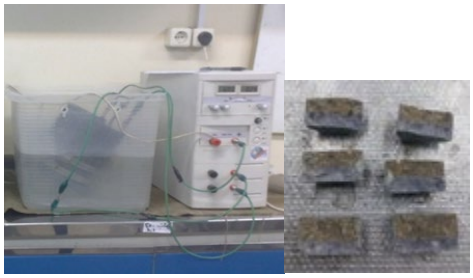

Figure 1. Test setup for rapid chloride migration test and splited specimens.

$$D_{nssm} = \frac{0.0239(273+T)L}{(U-2)t}\left(x_d - 0.0238\sqrt{\frac{(273+T)Lx_d}{U-2}}\right), \quad (1)$$

where D_{nssm} is non-steady-state diffusion coefficient (×10^{-12} m^2/s); U is absolute value of the applied voltage (V); T is average of the initial and final temperatures in the sodium chloride solution (°C); L is thickness of the specimen (mm); x_d is average value of the penetration depths (mm); t is test duration (hours).

3. Results and Discussion

3.1. Workability

Considering the constant amount of superplasticizer and water-cement ratio, the changes in the diameter of flow (slump flow) and flow rate are solely related to the effect of internal curing agents on the properties of fresh SCC. Table 2 presents the results for the diameter of flow and flow rate of the investigated mixtures. Fig. 2 shows the diameter of flow for the SCC of the control mixture.

The use of the internal curing agents studied did not have a significant effect on the diameter of flow and flow rate of SCC. The maximum reduction in diameter of flow was about 6 %, and the maximum increase in flow rate was about 4 %. The use of SAP caused a very small increase in the diameter of flow and a slight decrease in flow rate. Replacing 15 % by volume of natural fine aggregate with RLWA resulted in a decrease in diameter and an increase in flow rate. Increasing the replacement to 30 % by volume caused a further reduction in diameter of flow and an additional increase in flow rate. The effects of internal curing agents (RLWA and SAP) on the diameter of flow and flow rate of SCC are similar to the results obtained in the studies of Rajamanickam and Vaiyapuri [5], Kamal et al. [24], Madduru et al. [7], Ahmadi et al. [15], Gopi and Revathi [6], and Priya et al. [16].

It is noteworthy that the use of 30 % by volume of RLWA, due to the change in grain size, reduced the stability index and caused observed segregation in the SCC mixture. Although the amount of internal curing water required for this SCC is estimated to be about 30 liters per cubic meter, it is not possible to provide this amount of internal curing water with the lightweight fine aggregates under study as the requirements of SCC are not met.

Figure 2. Diameter of flow of Ref.

Table 2. Diameter of flow and the flow rate for concrete mixture studied.

Mix Destination	Diameter of flow (mm)	flow rate (Sec)	Visual Stability Index Values
Ref.	630	2.11	0
0.1SAP	633	2.06	0
15RLWA	615	2.12	0
30RLWA	592	2.21	1

3.2. Compressive Strength

The results of the compressive strength test are presented in Fig. 3 up to the age of 360 days. The results for the externally cured specimens (cured in lime water) up to the desired ages are labeled with code "W," while the specimens without external curing (stored in a relative humidity of 50 %) are labeled with code "D." As expected, the compressive strength of the concrete remained almost constant after the age of 90 days. The results show that exposure to a relative humidity of 50 % between the ages of 28 and 360 days caused a decrease of about 8 % in the compressive strength of SCC compared to the standard curing conditions. This decrease in strength is attributed to the formation of microcracks caused by the confinement of the aggregate due to shrinkage and a decrease in cement hydration reactions [2, 25].

It should be noted that the compressive strength of the reference mixture under conditions without external curing at the age of 360 days decreased compared to the age of 180 days. A similar trend was observed in mixtures containing internal curing agents. These results suggest that microcrack development between the ages of 180 and 360 days under the studied conditions caused a slight decrease in compressive strength.

The use of SAP slightly increased the compressive strength under both exposure conditions. Replacing 15 % by volume of fine aggregate with RLWA reduced the compressive strength under externally cured conditions. The use of 30 % by volume of RLWA as an internal curing agent at the age of 28 days in externally cured conditions reduced the compressive strength decrease by 12.1 %.

The use of 15 % by volume of RLWA at the age of 28 days under conditions without external curing increased the compressive strength by about 5.0 % compared to the control mixture. This is because the presence of RLWA helps prevent the reduction of internal moisture in the concrete, thereby promoting more hydration reactions compared to the control mixture. However, by the age of 90 days, the increase in strength for designs containing internal curing agents under non-curing conditions decreased compared to the control mixture. This is because, at 90 days, more moisture has been lost from the concrete mixture, and since the amount of internal curing water provided by these agents is less than the required amount, the rate of hydration reactions and prevention of microcracks caused by aggregate confinement decreases [2, 25]. The results show that despite the positive effect of the internal curing agent RLWA on compressive strength under non-curing conditions, its use cannot completely eliminate the reduction in the strength of SCC caused by inadequate curing.

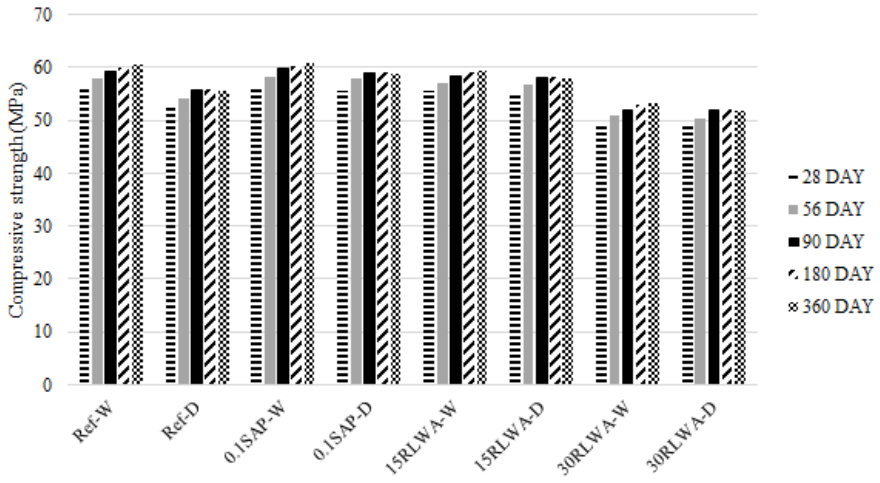

Figure 3. Compressive strength of mixture in saturated and unsaturated conditions.

In the study by Gopi and Revathi [6], it was also shown that the use of 15 % LWA improved the compressive strength compared to the conditions without external curing. However, the compressive strength of SCC with an internal curing agent was still lower than that of the control mixture cured under standard conditions. The results of the study by Rajamanickam and Vaiyapuri [5] show that increasing the amount of LWA replacement between 15 % and 25 % reduced the compressive strength of SCC under external curing conditions compared to the control mixture. It should be noted that the results of published studies on the effect of SAP and LWA curing agents in concretes with a low water-to-cement ratio indicate that, similar to the results obtained in the present study, the compressive strength of concrete under conditions without external curing was improved by using internal curing agents. However, the use of these materials could not eliminate the need for external curing [21, 26–32].

3.3. Chloride Diffusion Coefficient

Fig. 4 presents the results of the chloride ion diffusion coefficient. The chloride ion diffusion coefficient decreases with increasing age due to the progress of hydration reactions and the closure of the internal pores of the concrete. The use of the SAP curing agent caused a slight decrease in the chloride ion diffusion coefficient between the ages of 28 and 360 days under saturated conditions compared to the control mixture. However, the use of the RWLA curing agent led to an increase in the chloride ion diffusion coefficient between the ages of 28 and 360 days under saturated conditions compared to the control mixture. The results obtained in the study by Alaskar et al. [10] are consistent with those of the present study. In the study by Alaskar et al. [10], at the age of 28 days, the accelerated chloride ion permeability of reinforced concrete containing 20 % lightweight fine-grained aggregate as an internal curing agent under saturated conditions was 7 % higher than that of the control mixture.

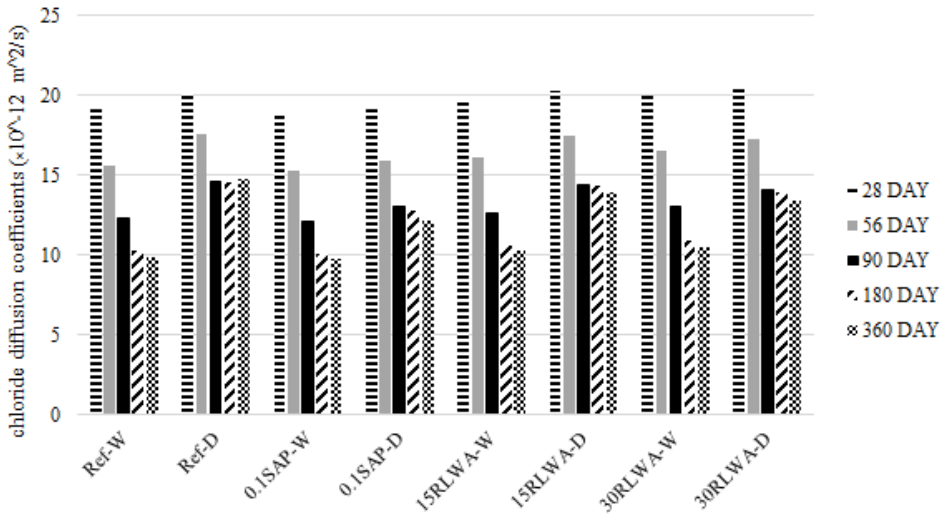

Figure 4. Chloride diffusion coefficient of mixture in saturated and unsaturated conditions.

The chloride ion diffusion coefficient of the control specimen placed in an environment with a relative humidity of 50 % at ages 28, 56, 90, 180, and 360 days increased by 5.8 %, 12.8 %, 18.7 %, 40.8 %, and

49.5 %, respectively, compared to the specimens in saturated conditions. The increase in the diffusion coefficient grew with increasing age. This is because the longer exposure to an environment with a relative humidity of 50 % causes the expansion of concrete microcracks and their greater interconnection [30]. As can be seen, the increase in the diffusion coefficient of Ref. mixture at the age of 180 days is significantly greater than at the age of 90 days. This is because, with increased exposure time in an unsaturated environment, the development of microcracks accelerates, and their interconnection increases. These results show that microcrack development after 90 days of exposure to the studied unsaturated environment significantly impacts the chloride ion diffusion coefficient. At the age of 360 days, the chloride ion diffusion coefficient of the Ref., 0.1SAP, 15RLWA, and 30RLWA mixtures in conditions of exposure to a relative humidity of 50 % increased by 49.5 %, 24.7 %, 35.0 %, and 27.6 %, respectively, compared to the diffusion coefficient of the specimens in saturated conditions. As seen, the use of internal curing in the 0.1SAP, 15RLWA, and 30RLWA mixtures reduced the increase in the chloride ion diffusion coefficient of specimens placed in an environment with a relative humidity of 50 %. However, it should be noted that the use of internal curing materials in saturated condition specimens did not reduce the chloride ion diffusion coefficient, and even the RWLA increased the chloride ion diffusion coefficient of concrete in the saturated condition specimens.

For SCC specimens placed in an unsaturated environment, the results obtained by Ahmadi et al. [15] also indicate that the use of a curing agent increases the resistance of concrete to chloride ion penetration compared to the control specimen. In the study by Mullem et al. [33], the diffusion coefficient for both the control mix and the SAP-containing mix with a water-to-cement ratio of approximately 0.36 was about 4.2. Their results indicate that at similar water-to-cement ratios, the addition of SAP does not significantly affect the chloride ion diffusion coefficient, which remains very close to that of the control mix.

3.4. Estimation of Corrosion Initiation of Rebar

Numerical modeling was employed to predict the time required for corrosion initiation in reinforcement embedded within concrete. The chloride ion penetration process was characterized using Fick's Second Law of Diffusion. Assuming a constant surface chloride concentration and a steady chloride diffusion coefficient, the differential equation governing Fick's Second Law was solved using the Crank–Nicolson numerical method, applying the finite difference approach as expressed in Equation 2 [18, 19]:

$$C(x,t) = C_i + (C_s - C_i)\left[1 - erf\left(\frac{x}{2\sqrt{D_a t}}\right)\right]. \quad (2)$$

Here, $C(x,t)$ represents the chloride concentration (as a percentage of the concrete's mass) at a depth x and the time t, C_i is the initial chloride concentration (% mass of concrete) before exposure to the chloride environment, C_s represents the surface chloride concentrations (% mass of concrete) on the exposed surface, erf is the error function, x is the depth below the exposed surface (m), t is the exposure time (s), and D_a is the apparent diffusion coefficient of chlorides m²/s.

The Crank–Nicolson method was employed to evaluate the resistance of concrete to chloride ion penetration, using data derived from the Rapid Chloride Migration (RCM) tests. The temporal variation in the chloride diffusion coefficient was determined according to Equation 3 [18, 19]:

$$D(t) = D_{ref}\left(\frac{t_{ref}}{t}\right)^m. \quad (3)$$

In this equation, $D(t)$ represents the concrete's diffusion coefficient at time t, D_{ref} is the concrete diffusion coefficient at time t_{ref}, and m is the aging factor. In this study, a constant chloride diffusion coefficient was assumed across the concrete cross-section to simplify the model and facilitate direct comparison among mixtures, consistent with the approach taken in many similar comparative investigations [18–20].

In this study, the critical chloride concentration was assumed to be 0.18 % of the concrete's weight, while the surface chloride concentration was set at 0.8 % of the concrete's weight [18, 19]. It is important to note that for submerged conditions in the Life 365 software, the surface chloride concentration is fixed at 0.8 % for specific scenarios [20].

In some structures, such as bridge decks or desalination tanks, concrete remains in an unsaturated state for an extended period before being exposed to chloride ions. In this study, it is assumed that the concrete was in an unsaturated environment for 360 days and then exposed to chloride ions. In this modeling, the corrosion initiation time is simulated for concrete in submerged conditions after contact with chloride ions. To calculate the age coefficient using the RCMT test results, tests were performed at ages of 450, 540, and 630 days according to the method described in Section 2-2. Only the specimens exposed to an environment with a relative humidity of 50 % were transferred into saturated lime water after 360 days, and the desired tests were conducted on them at the specified ages. Fig. 5 shows the diffusion coefficients obtained for these specimens. The abbreviation “DW” indicates that these specimens were first placed in an environment with 50 % relative humidity and then transferred into water. In Table 3, the aging factor (m) was calculated based on Equation 3, and the 360-day chloride diffusion coefficient obtained from the RCMT method is presented for use in the modeling.

The results in Fig. 5 show that between the ages of 360 to 630 days, the diffusion coefficient decreased with increasing age. It is noteworthy that the test specimens that were exposed to an environment with 50 % relative humidity before the age of 360 days and then placed in humid conditions exhibited a trend in chloride ion diffusion similar to the specimens that were in saturated conditions from the start. The aging coefficient calculated based on Equation 3 for the mixes is nearly identical.

Table 3. Aging factors and the reference diffusion coefficients.

Mix Destination	m	D_{ref} ($\times 10^{-12}$ m^2/s)
Ref-W	0.2692	9.9
Ref-DW	0.2574	14.8
0.1SAP-W	0.2706	9.7
0.1SAP-DW	0.2656	12.1
15RLWA-W	0.2691	10.3
15RLWA-DW	0.2604	13.9
30RLWA-W	0.2694	10.5
30RLWA-DW	0.2612	13.4

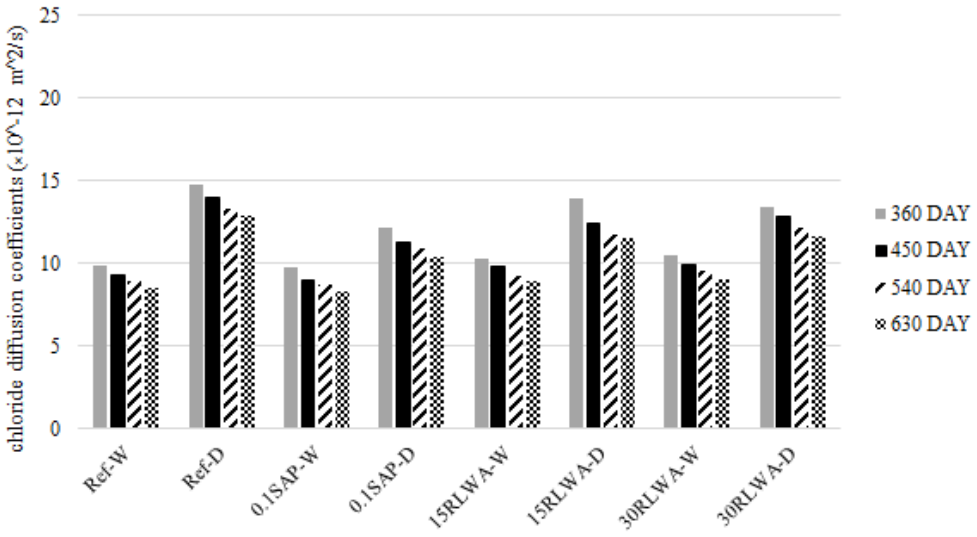

Figure 5. The chloride diffusion coefficient of mixtures used in modeling.

Fig. 6 shows the results of the estimated corrosion initiation time for the studied mixtures, with reinforcement at a depth of 5 cm. In a 5 cm cover, the estimated corrosion initiation times for the mixtures Ref-W, Ref-DW, 0.1SAP-W, 0.1SAP-DW, 15RLWA-W, 15RLWA-DW, 30RLWA-W, and 30RLWA-DW were 8.28, 5.25, 8.51, 6.61, 7.93, 5.64, 7.77, and 5.86 years, respectively. The results show that the use of internal curing for specimens that remain in saturated conditions decreases durability, causing these mixtures to initiate corrosion faster than the control mixture. Furthermore, exposure to an environment with a relative humidity of 50 % for one year before chloride ion penetration reduced the corrosion initiation time by approximately 40 %. This reduction in concrete durability is attributed to microcracks caused by shrinkage due to the loss of internal moisture. However, the use of internal curing improved the durability of concrete in these conditions. The corrosion initiation times for the 0.1SAP-DW, 15RLWA-DW, and 30RLWA-DW mixtures were 25.8 %, 7.4 %, and 11.6 % higher than that of the Ref-DW mixture,

respectively. Internal curing with SAP material was more effective in improving the corrosion initiation time than RLWA.

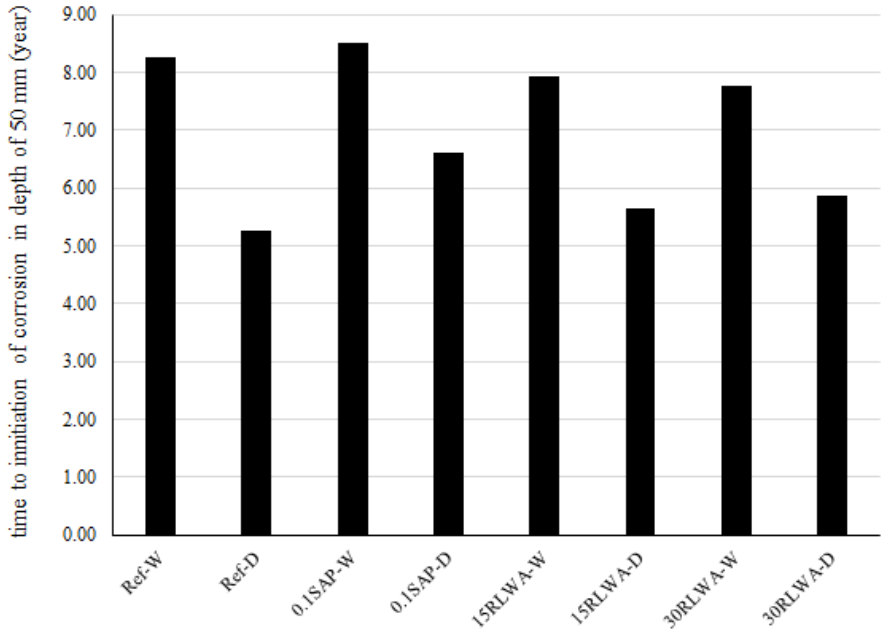

Figure 6. The predicted time of the corrosion initiation at depths of 50 mm.

4. Conclusion

Based on the findings of a laboratory study conducted on mixtures containing SAP internal curing agent and RWLA lightweight aggregates, the following results can be summarized:

1. The amount of internal curing agents in SCC is limited due to their potential influence on segregation.
2. The compressive strength and chloride ion diffusion coefficient of SCC containing SAP did not change significantly under saturated conditions compared to the Ref. mixture. However, mixtures containing RWLA exhibited a reduction in compressive strength by up to 12.1 % under saturated conditions at the age of 28 days. The chloride ion diffusion coefficient of mixtures containing RWLA increased by a maximum of 6.1 % under saturated conditions.
3. The use of internal curing materials in specimens placed in an environment with 50 % relative humidity improved compressive strength. The maximum enhancement in compressive strength with SAP internal curing agents was 6.8 % at the age of 28 days.
4. For specimens exposed to an environment with 50 % relative humidity, the use of internal curing materials resulted in a decrease in the chloride ion diffusion coefficient of concrete. The maximum reduction in the chloride diffusion coefficient of concrete containing internal curing agents was 18.4 % at the age of 360 days.
5. The results show that the predicted corrosion initiation time of Ref.-DW was reduced by 40 % compared to concrete exposed to saturated conditions. For specimens stored in an unsaturated environment, the use of an internal curing agent significantly improved the corrosion initiation time. The highest corrosion initiation time was observed for the 0.1SAP-DW mix, with a 25.8 % increase compared to the Ref.-DW mix.
6. In an environment with 50 % relative humidity, the performance of SAP in improving the mechanical properties and durability of SCC is better than that of RWLA.
7. The results show that the effect of the concrete placement environment on the concrete diffusion coefficient is significantly greater than its effect on the concrete compressive strength.
8. The results suggest that the application of internal curing agents can enhance the durability of SCC mixtures placed in unsaturated conditions prior to exposure to chloride environments. It also seems that exposure to an unsaturated environment for more than 90 days can have a significant impact on the durability of concrete. Therefore, it is recommended that concrete not be left in unsaturated

conditions for more than 90 days before being exposed to environments containing destructive ions. However, it is important to highlight that further research is required on this subject.

References

1. Athiyamaan, V. Admixture-based self-compacted concrete with self-curing concrete techniques: A state of art of review. Cleaner Engineering and Technology. 2021. 5. Article no. 100250. DOI: 10.1016/j.clet.2021.100250
2. Tang, C., Dong, R.R., Tang, Z., Long, G., Ma, G., Wang, H., Huang, Y. Effect of SAP on the properties and microstructure of cement-based materials in the low humidity environment. Case Studies in Construction Materials. 2024. 20. Article no. e03001. DOI: 10.1016/j.cscm.2024.e03001
3. Ma, X., Liu, J., Shi, C. A review on the use of LWA as an internal curing agent of high-performance cement-based materials. Construction and Building Materials. 2019. 218. Pp. 358–393. DOI: 10.1016/j.conbuildmat.2019.05.126
4. Yang, L., Ma, X., Liu, J., Hu, X., Wu, Z., Shi, C. Improving the effectiveness of internal curing through engineering the pore structure of lightweight aggregates. Cement and Concrete Composites. 2022. 134. Article no. 104773. DOI: 10.1016/j.cemconcomp.2022.104773
5. Rajamanickam, G., Vaiyapuri, R. Self-compacting self-curing concrete with lightweight aggregates. Građevinar. 2016. 68(4). Pp. 279–285. DOI: 10.14256/JCE.1137.2014
6. Gopi, R., Revathi, V. Influence of presaturated light expanded clay and fly ash aggregate in self-compacting concrete. Revista Romana de Materiale. 2019. 49(3). Pp.370–378.
7. Madduru, S.R.C., Shaik, K.S., Velivela, R., Karri, V.K. Hydrophilic and hydrophobic chemicals as self-curing agents in self-compacting concrete. Journal of Building Engineering. 2020. 28. Article no. 101008. DOI: 10.1016/j.jobe.2019.101008
8. Liu, Y., Wu, T., Hu, Y., Kou, D. Chloride ion diffusion in saturated lightweight aggregate concrete: A numerical investigation. Structures. 2023. 58. Article no. 105433. DOI: 10.1016/j.istruc.2023.105433
9. Güneyisi, E., Gesoğlu, M., Altan, I., Öz, H.Ö. Utilization of cold-bonded fly ash lightweight fine aggregates as a partial substitution of natural fine aggregate in self-compacting mortars. Construction and Building Materials. 2015. 74. Pp. 9–16. DOI: 10.1016/j.conbuildmat.2014.10.021
10. Alaskar, A., Alshannag, M., Higazey, M. Mechanical properties and durability of high-performance concrete internally cured using lightweight aggregates. Construction and Building Materials. 2021. 288. Article no. 122998. 10.1016/j.conbuildmat.2021.122998
11. Wang, X., Wang, W., Liu, Y., Duan, P., Liang, X., Zhang, H., Ge, Z. Enhancing chloride ion permeability resistance of recycled aggregate concrete through internal curing with glazed hollow beads. Construction and Building Materials. 2024. 438. Article no. 137293. DOI: 10.1016/j.conbuildmat.2024.137293
12. Gu, Y., Mohsenia, E., Farzadniac, N., Khayat, K.H. An overview of the effect of SAP and LWS as internal curing agents on microstructure and durability of cement-based materials. Journal of Building Engineering. 2024. 95. Article no. 109972. DOI: 10.1016/j.jobe.2024.109972
13. Jindal, A., Mehra, D. Effects of Inclusion of SAP as an Internal Curing Agent in Concrete, A Review. Civil Engineering Infrastructures Journal. 2024. 58(1). 1–13. DOI: 10.22059/CEIJ.2024.361854.1947
14. Kim, Y.J., Wang, J., Ji, Y. Characteristics and Chloride Permeability of Internally Cured Concrete. ACI Materials Journal. 2018. 115(1). Pp. 139–147. DOI: 10.14359/51701098
15. Ahmadi, J., Razavi, B.S., Amini, H., Moradi, M. Internal Curing Effect on Properties of Self-Compacting Concrete. IIOAB Journal. 2018. 9(S1). Pp. 45–53.
16. Priya, J.Sh., Chinnaraju, K., Jaganathan, V. Behavior of internally cured self-compacting concrete with fly ash under ambient curing conditions. Romanian Journal of Materials. 2021. 51(3). Pp. 464–471.
17. Ibragimov, R.A., Shakirzyanov, F.R., Kayumov, R.A., Korolev, E.V. Evaluation of the influence of an aggressive environment on the durability of the cement stone. Construction Materials and Products. 2024. 7(2). DOI: 10.58224/2618-7183-2024-7-2-4
18. Bagheri, A., Ajam, A., Zanganeh, H. Investigation of chloride ingress into concrete under very early age exposure conditions. Construction and Building Materials. 2019. 225. Pp. 801–811. DOI: 10.1016/j.conbuildmat.2019.07.225
19. Bagheri, A., Ajam, A., Zanganeh, H. Effect of very early age exposure on chloride ingress and service life performance of binary and ternary concretes. Construction and Building Materials. 2021. 289. Article no. 123137. DOI: 10.1016/j.conbuildmat.2021.123137
20. Ehlen, M.A. Life-365™ Service Life Prediction Model™ and Computer Program for Predicting the Service Life and Life-Cycle Cost of Reinforced Concrete Exposed to Chlorides. User's manual. Version 2.2.3. Life-365™ Consortium III, 2020. [Online]. URL: https://life-365.org/wp-content/uploads/2024/11/Life-365_v2.2.3_Users_Manual.pdf (reference date: 07.08.2025).
21. Huang, X., Liu, X., Rong, H., Yang, X., Duan, Y., Ren, T. Effect of Super-Absorbent Polymer (SAP) Incorporation Method on Mechanical and Shrinkage Properties of Internally Cured Concrete. Materials. 2022. 15(21). Article no. 7854. DOI: 10.3390/ma15217854
22. Lothenbach, B., Winnefeld, F. Thermodynamic modelling of the hydration of Portland cement. Cement and Concrete Research. 2006. 36(2). Pp. 209–226. DOI: 10.1016/j.cemconres.2005.03.001
23. NT Build 492. Concrete, Mortar and Cement-based Repair Materials: Chloride Migration Coefficient from Non-steady-state Migration Experiments. Nordtest. Finland, 1999. 8 p.
24. Kamal, M.M., Safana, M.A., Bashandya, A.A., Khalil, A.M. Experimental investigation on the behavior of normal strength and high strength self-curing self-compacting concrete. Journal of Building Engineering. 2018. 16. Pp. 79–93. DOI: 10.1016/j.jobe.2017.12.012
25. Korda, E., De-Schutter, G., Aggelis, D.G. Acoustic signatures of hydration and microcracking in early-age concrete. Developments in the Built Environment. 2024. 17. Article no. 100353. DOI: 10.1016/j.dibe.2024.100353
26. Arayeshgar, M., Madandoust, R., Ranjbar, M.M. A Comparative Study on Superabsorbent Polymer and Recycled Lightweight Aggregate as Internal Curing Agents for High-strength Concrete. International Journal of Engineering. 2025. 38(2). Pp. 452–461. DOI: 10.5829/ije.2025.38.02b.18
27. Abadel, A.A. Physical, Mechanical, and Microstructure Characteristics of Ultra-High-Performance Concrete Containing Lightweight Aggregates. Materials. 2023. 16(13). Pp. Article no. DOI: 10.3390/ma16134883

28. Alanazi, H., Elalaoui, O., Adamu, M., Alaswad, S.O., Ibrahim, Y.E., Abadel, A.A., Al-Fuhaid, A.F. Mechanical and Microstructural Properties of Ultra-High Performance Concrete with Lightweight Aggregates. Buildings. 2022. 12(11). Article no. 1783. DOI: 10.3390/buildings12111783
29. Venkateswarlu, K., Deo, S.V., Murmu, M. Effect of Super absorbent polymer on workability, strength and durability of Self consolidating concrete. International Journal of Engineering. 2021. 34(5). Pp. 1118–1123. DOI: 10.5829/ije.2021.34.05b.05
30. Kumar, P., Pasla, D., Saravanan, T.J. Self-compacting lightweight aggregate concrete and its properties: A review. Construction and Building Materials. 2023. 375. Article no. 130861. DOI: 10.1016/j.conbuildmat.2023.130861
31. Hong, S.-H., Choi, J.-S., Yuan, T.-F., Yoon, Y.-S. Mechanical and Electrical Characteristics of Lightweight Aggregate Concrete Reinforced with Steel Fibers. Materials. 2021. 14(21). Article no. 6505. DOI: 10.3390/ma14216505
32. Wu, Z., Wong, H.S., Chen, C., Buenfeld, N.R. Anomalous water absorption in cement-based materials caused by drying shrinkage induced microcracks. Cement and Concrete Research. 2019. 115. Pp. 90–104. DOI: 10.1016/j.cemconres.2018.10.006
33. Mullem, T.V., Brabandere, L.D., Voorde, E.V.D., Snoeck, D., Belie N.D. Influence of superabsorbent polymers on the chloride ingress of mortar measured by chloride diffusion and a quasi-steady-state migration test. Cement and Concrete Composites. 2024. 150. Article no. 105563. DOI: 10.1016/j.cemconcomp.2024.105563

Information about the authors:

Milad Rajabi Jorshari,
ORCID: https://orcid.org/0009-0008-4796-0785
E-mail: miladcivil.r84@gmail.com

Majid Malekzadeh, *PhD*
E-mail: Malekzadeh@guilan.ac.ir

Ataollah Hajati Modaraei,
ORCID: https://orcid.org/0009-0000-5678-640X
E-mail: dr.modaraei@gmail.com

Received 19.01.2025. Approved after reviewing 29.05.2025. Accepted 03.06.2025.

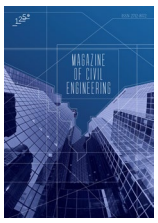

Magazine of Civil Engineering

ISSN 2712-8172

journal homepage: http://engstroy.spbstu.ru/

Research article

UDC 69

DOI: 10.34910/MCE.136.7

Effectiveness of wax additives in cast asphalt concrete mixtures

V.V. Yadykina [1] ✉, ***O.A. Mikhaylova*** [1], ***A.I. Karlina*** [2], ***N.I. Vatin*** [3], ***N.V. Martyushev*** [4] ✉

[1] *Belgorod State Technological University named after V.G. Shukhov, Belgorod, Russian Federation*
[2] *Moscow State University of Civil Engineering, Moscow, Russian Federation*
[3] *Peter the Great St. Petersburg Polytechnic University, St. Petersburg, Russian Federation*
[4] *National Research Tomsk Polytechnic University, Tomsk, Russian Federation*

✉ *martjushev@tpu.ru*

Keywords: cast asphalt concrete mix, bitumen binder, bitumen modifiers, waxes, mineral mix, characteristics of cast asphalt concrete

Abstract. The use of cast asphalt concrete mixtures makes it possible to produce road surfaces with very high wear resistance and water resistance. One of the problems of using cast asphalt concrete mixtures is the need for high temperature of their preparation. This significantly increases energy costs, worsens the labour conditions of workers and negatively affects the environment. Therefore, it is very important to search for effective methods to reduce the temperature of production of cast asphalt concrete mixtures without deterioration of their performance characteristics. One of the promising solutions to this problem is the use of synthetic waxes as additives that change the rheological properties of bituminous binder. Besides, the use of additives based on synthetic waxes makes it possible to improve the resistance of asphalt concretes to plastic deformations, which is very important for cast asphalt concrete pavements. In this paper, changes in the physical and chemical properties of bitumen binder modified with a new complex additive Viskodor PV-2 are investigated. In order to evaluate the effectiveness of this additive, these changes were compared with those observed when the well-known wax modifiers Licomont BS-100 and Sasobit were introduced into bitumen. The effect of these additives on the properties of cast asphalt concrete was also studied. It has been established that the introduction of 2.5 % of the investigated additives allows reducing the temperature of paving of cast asphalt concrete by at least 30 °C without reducing its strength characteristics. It is revealed that the use of Viscodor PV-2 in the composition of cast asphalt concrete contributes to the increase in the value of workability with a simultaneous decrease in the index of the die indentation depth. It is established that the efficiency of Viscodor PV-2, used as an additive to reduce the temperature of preparation of cast asphalt concrete mixtures, is not inferior to the known waxes Licomont BS-100 and Sasobit.

Acknowledgements: The research was carried out using the equipment of the High Technology Centre of Belgorod State Technological University named after V.G. Shukhov.

Citation: Yadykina, V.V., Mikhaylova, O.A., Karlina, A.I., Vatin, N.I., Martyushev, N.V. Effectiveness of wax additives in cast asphalt concrete mixtures. Magazine of Civil Engineering. 2025. 18(4). Article no. 13607. DOI: 10.34910/MCE.136.7

1. Introduction

The requirements for the strength characteristics of road surfaces are constantly increasing due to the increasing loads and traffic on motorways. In this regard, materials with improved performance are becoming more and more common. Cast asphalt concrete mixtures are one of them. Cast asphalt concrete mixtures differ from traditional asphalt concrete mixtures by the increased content of bitumen (7.5–10 %)

and mineral powder (20–30 %). In this regard, the main factors determining its strength characteristics are the rheological properties of bitumen binder and asphalt concrete microstructure [1].

Due to the high binder content and increased paving temperature, cast asphalt concrete mixtures have high mobility and do not require compaction. After cooling, a durable waterproof and crack-resistant pavement is formed, with residual porosity not exceeding 2 % [2]. The advantages of cast asphalt concrete are its high density, wear resistance, and corrosion resistance [3]. The use of cast asphalt concrete can significantly increase the service life of the road surface up to 15–20 years [4]. The main disadvantages of cast asphalt concrete mixtures are the need for high energy costs and the use of special transport equipment that provides constant mixing and heating of the mixture to maintain the temperature within 220–230 °C. Due to the high content of mineral powder and bituminous binder, the cost of such mixtures is higher than traditional asphalt concrete [5]. In addition, pavements made of cast asphalt concrete based on bitumen without the use of polymer modifiers have low shear stability, which leads to the formation of plastic deformations [6]. To improve the ability of cast asphalt concrete mixtures to resist plastic deformations, the binder is modified with polymers. Thus, the results of studies [7–10] confirm that the use of polymer-modified bitumen binders significantly improves the strength characteristics of cast asphalt concrete mixtures, increasing their resistance to mechanical loads and seasonal temperature fluctuations. According to [7] introduction of 4 % SBS increased viscosity of bitumen at 165 °C from 0.14 to 0.95 Pa*s, i.e. 6.8 times. As a result, in order to maintain the required mobility, there is a need for higher temperatures of preparation and placement, increasing the binder content. All this combined with the high cost of polymers leads to a significant increase in the cost of technology.

To solve this problem, additives are used to improve the mobility of the mixture. In Russia, additives based on surfactants that reduce bitumen viscosity in the range of process temperatures and are used in the production of warm asphalt concrete mixtures are widely used as temperature-lowering additives [11]. However, the introduction of these additives can reduce the resistance of cast asphalt concrete to plastic deformations. In European countries, organic additives based on waxes, such as Licomont BS-100, Sasobit, etc., are widely used to improve the technological properties of asphalt concrete mixtures. [12].

The introduction of wax-based modifiers reduces the viscosity of the bituminous binder at temperatures above the melting point of the wax, thereby increasing the mobility of the cast asphalt mixture. At the same time, waxes have the ability to crystallise at lower temperatures, forming structures that increase the viscosity and strength properties of the bituminous binder. Due to this, the introduction of Sasobit into asphalt concrete mixes allows to ensure the necessary mobility of the mix at a lower binder content, lower temperature of preparation and paving without reducing the quality characteristics of the road surface, which is proved in [12–14]. In the study of cast asphalt concrete mixtures [3], it was found that Sasobit introduced at a concentration of 0.3 % of the binder mass increased the workability index by 20 %. Researchers [15–17] found that the introduction of 2.0–4.0 % of Licomont BS-100 modifier into bituminous binder composition reduces viscosity at the temperature of asphalt concrete mixture preparation and structures the binder at pavement operation temperatures, which is expressed in the increase of softening and penetration temperature at 25 °C, thus increasing asphalt concrete resistance to plastic deformations.

Until recently, the Russian market has exclusively used expensive imported additives based on synthetic waxes, such as Licomont BS-100 and Sasobit, which significantly increased the cost, created difficulties with delivery and, as a consequence, limited the use of such modifiers in asphalt concrete. Thus, the task of development of the Russian modifier on the basis of waxes, not inferior in efficiency to imported additives, was actual. In this connection, Selena LLC together with the Department of Automobile and Railway Roads A.M. Gridchin of Belgorod State Technological University named after V.G. Shukhov developed the additive Viskodor PV-2, which is a complex composition including a mixture of waxes, plant-based plasticisers, and nitrogen-containing cationic surfactants. According to [18, 19], Viscodor PV-2 reduces the temperature of preparation of asphalt concrete mixtures and has structuring properties that increase the temperature range of plasticity of the binder. In this regard, studies on the use of Viscodor PV-2 in the composition of cast asphalt concrete mixtures are promising.

The subject of the study is the influence of these additives on the physicochemical properties of the binder and qualitative indicators of cast asphalt concrete mixtures. The aim of the research was: to study the influence of modifiers based on synthetic waxes on the properties of bitumen binder; to select the most effective dosage of the studied additives in binder for cast asphalt concrete mixtures; to evaluate the effectiveness of the new additive Viskodor PV-2 in cast asphalt concrete mixtures in comparison with imported wax additives Licomont BS-100 and Sasobit. The object of the study is bituminous binder samples

with Viskodor PV-2, Licomont BS-100, and Sasobit additives and cast asphalt concrete mixtures prepared with the use of binder modified in this way.

2. Materials and Methods

In this study, the effect of the complex additive Viscodor PV-2 (produced by Selena, Russia) on the properties of bituminous binder and cast asphalt mixture was investigated. For comparative purposes, the additives Sasobit (polyethylene wax produced by Fischer-Tropsch synthesis, manufactured by SasolWax, South Africa) and Licomont BS-100 (amide wax, manufactured by Clariant, Switzerland) were also tested and selected as the most widely used additives. For preparation of tested samples of binder and cast asphalt concrete mixtures, the bitumen of BND 70/100 grade produced by JSC Gazpromneft-MNPZ was used, which corresponds to Russian State Standard GOST 33133-2014 in its physical and chemical properties.

For preparation of cast asphalt concrete mixtures on the basis of bitumen BND 70/100 modified by investigated additives, crushed stone of fractions 8–16 and 4–8 mm and crushed sand of fractions 0–4 mm produced by Pavlovsk Nerud JSC and mineral powder MP-2 of Tsentr-Izvestnyak LLC were used. In order to study the effect of additives Viskodor PV-2, Sasobit, and Licomont BS-100 on bitumen properties and selection of rational concentration for testing in cast asphalt concrete mixtures, based on the experience of earlier studies [19], a number of bitumen binder samples were prepared with the introduction of each of the additives in different concentrations in the range from 2.0 to 3.5 % with a step increase – 0.5 %. Preparation of the modified binder was carried out using a laboratory stirrer, by mixing bitumen with the studied organic additives for 60 minutes at 150 °C.

The prepared samples of bituminous binder were tested for physical and chemical properties. Softening temperature of the ring and ball was determined in accordance with GOST 32054-2013, needle penetration depth at temperatures of 0 and 25 °C – according to GOST 33136-2014, ductility and maximum tensile force at temperatures of 0 and 25 °C – according to GOST 33138-2014, brittleness temperature – according to GOST 11507-78, adhesion of the binder to the mineral material was evaluated according to the method described in GOST 11508 with the use of granite sift of 0–4 mm fraction as a mineral material. Granulometric compositions of mineral materials used in the study were determined by dividing into fractions by sieving a sample of material through a set of appropriate sieves and determining the total residues on each sieve according to GOST 33029-2014. On the basis of grain compositions of mineral materials, the optimal composition of mineral part for cast asphalt concrete mixture LA 16 Vn was selected in accordance with GOST 54401-2020. Using initial bitumen and bitumen modified with investigated additives, as well as optimally selected mineral part, the compositions of cast asphalt concrete mixtures were prepared.

Further, according to GOST R 54400-2020, test specimens were made. The maximum density of the tested mixtures was determined in accordance with GOST R 58401.16; the bulk density of the tested samples was determined in accordance with GOST R 58401.8; the depth of stamp indentation was determined in accordance with GOST R 54400-2020 p. 11.4. The paving ability of the mixture was identified in accordance with GOST R 54400-2020 p. 11.9 and assessed by the value of the cone slump index. Each mixture was tested at temperatures of 185, 200, and 215 °C to determine the temperature-reducing effect of the investigated additives.

3. Results and Discussion

The results of tests of bitumen BND 70/100 modified by investigated additives are reflected in Tables 1, 2 and Figs. 1–4. The obtained data show that the introduction of all the studied additives is characterised by a decrease in penetration at 25 °C, an increase in the softening point, an increase in the plasticity interval, a decrease in ductility at temperatures of 25 and 0 °C, and an improvement in the adhesion properties of bitumen binder.

Table 1. Penetration of bitumen modified with investigated additives.

Binder composition number	1	2	3	4	5	6	7	8	9	10	11	12	13
Name of additive	Without additive	Viscodor PV-2				Licomont BS-100				Sasobit			
Additive concentration, %	0	2.0	2.5	3.0	3.5	2.0	2.5	3.0	3.5	2.0	2.5	3.0	3.5
Depth of needle penetration at 25 °C, 0.1 mm	81	72	70	63	55	68	63	61	54	54	52	50	48
Depth of needle penetration at 0 °C, 0.1 mm	28	32	31	28	27	30	29	27	25	25	25	24	23

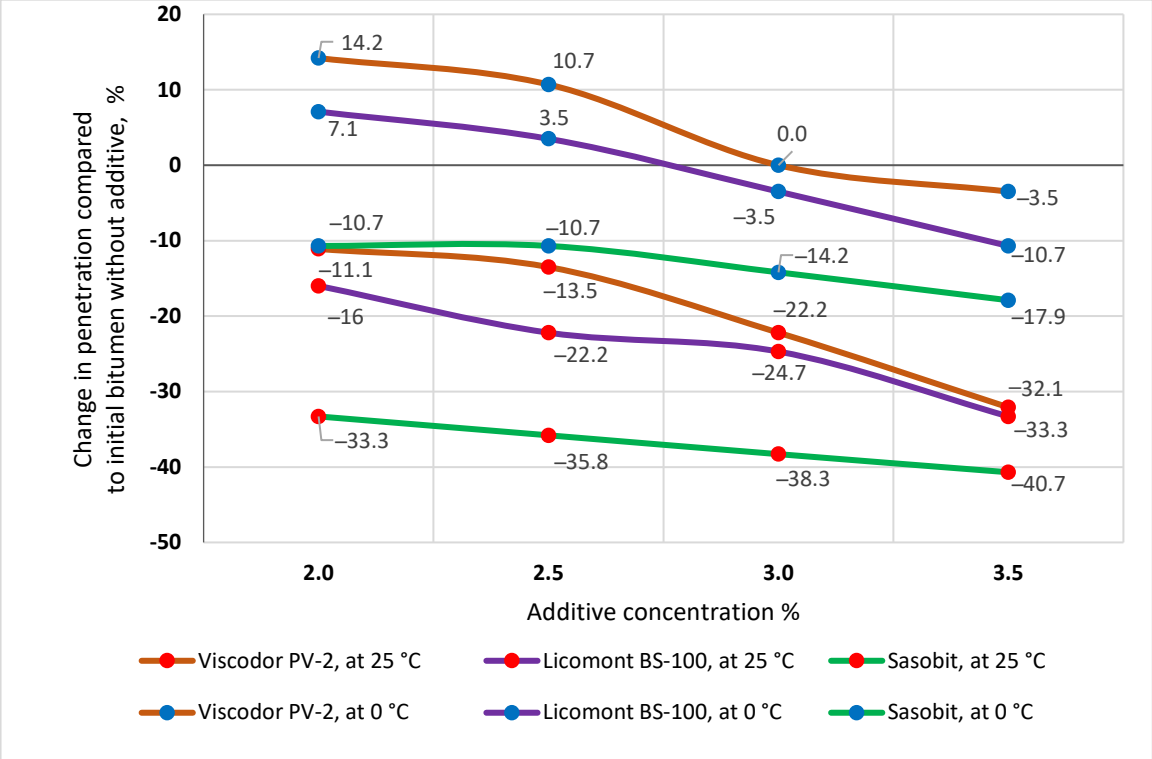

Figure 1. Change in penetration when bitumen is modified with additives.

Table 1 and Fig. 1 demonstrate the effect of the investigated additives on the change in needle penetration depth at temperatures of 25 and 0 °C.

According to the obtained data, all investigated additives when introduced reduce the needle penetration depth at 25 °C. With increasing concentration of additives, penetration index at 25 °C decreases, which is due to the ability of waxes to structure bituminous binder. The greatest decrease in needle penetration depth is observed at introduction of Sasobit additive. So, already at introduction of 2 % Sasobit, penetration of bitumen at temperature 25 °C decreases by 33.3 %, while introduction of the same amount of Licomont BS-100 gives a decrease in penetration depth by 16.0 %. Similar results of penetration reduction when comparing the effect of Licomont BS-100 and Sasobit on bitumen binder were obtained both by Russian and Western European researchers [17, 20–22] The lowest penetration reduction at all tested concentrations is observed when Viscodor PV-2 is added. Introduction of 3 % of this additive reduces penetration at 25 °C by 11.1 %. This is due to the presence of plasticising components in the composition of this additive. It should be noted that the intensity of penetration reduction when adding Viscodor PV-2 significantly increases at concentrations above 2.5 %. Thus, further increase in concentration leads to more intensive reduction of plastic properties of bitumen. It is revealed that in contrast to the additive Sasobit, the introduction of which even at 2 % reduces the penetration of bitumen BND 70/100 at 0 °C by 10.7 %, modifiers Viskodor PV-2 and Licomont BS-100 at a concentration of up to 2.5 % slightly increase this indicator, which will contribute to increasing the resistance of cast asphalt concrete to low temperatures of the winter period, and thus increase the service life of the roadway. Introduction of Viscodor PV-2 and Licomont BS-100 in concentration of 3 % and more causes a decrease in the depth of needle penetration at 0 °C in comparison with the indicator of the original bitumen, which indicates a deterioration of plastic

properties of the binder and therefore may be inappropriate for use in pavements operated in conditions of seasonal temperature change.

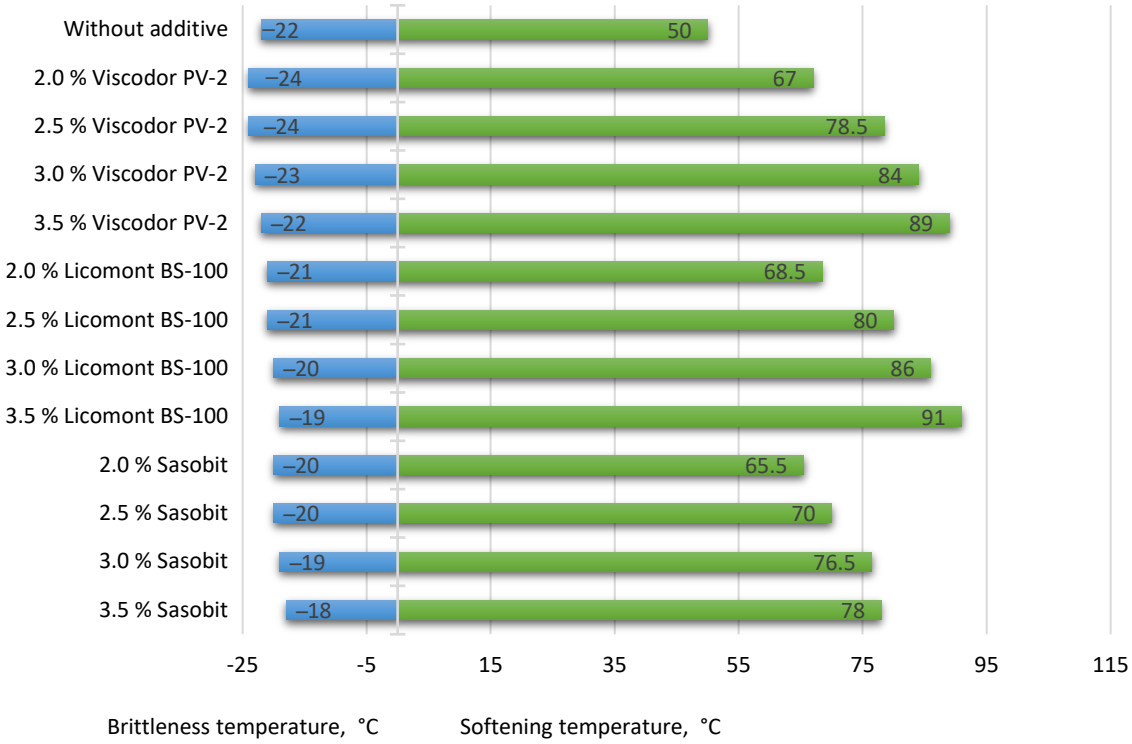

Figure 2. Change of plasticity interval of BND 70/100 after modification.

Temperature range of plasticity of modified bituminous binder in comparison with initial bitumen BND 70/100 without additives increases for all investigated additives due to a significant increase in softening temperature (Fig. 2). This is explained by the property of waxes to structure bituminous binder and will contribute to the decrease in the index of die indentation depth and resistance to plastic deformation of cast asphalt concrete mixtures. Common for the investigated wax additives is the dependence of the softening temperature increase and temperature interval of plasticity on the amount of the introduced additive. Thus, the plasticity interval for the initial bitumen – 77 °C, while the plasticity interval of bitumen modified with 2.0 and 3.5 % Viscodor PV-2 – 91 and 111 °C, with 2.0 and 3.5 % Licomont BS-100 – 89.5 and 110 °C, with 2.0 and 3.5 % Sasobit – 85.5 and 96 °C, respectively. The greatest increase in softening temperature is observed with the addition of Licomont BS-100 (2.5 % increase in softening temperature by 60 %), and the lowest for Sasobit (2.5 % increase in softening temperature by 40 %). However, both of these additives slightly increase the binder's brittleness temperature, which may adversely affect the low-temperature resistance of cast asphalt concrete. The greatest increase in the brittleness temperature is observed with the addition of Sasobit: 2 % of the additive increases this index by 2 °C, and further increase correlates with increasing concentration. The obtained results of temperature interval change at introduction of Licomont BS-100 and Sasobit additives correlate with literature data [14, 17, 21, 22]. Viscodor PV-2 at a concentration of up to 3 % reduces the brittleness temperature of bituminous binder due to the presence of plasticising agents in its composition. Further increase of Viscodor PV-2 input up to 3.5 % leads to increase of brittleness temperature up to the index of initial bitumen. Thus, the brittleness temperature of bitumen at the addition of 2–2.5 % Viscodor PV-2 decreases from –22 to –24 °C, while this indicator for the binder with 3.5 % of the additive is equal to –22 °C.

Table 2. Ductility of bituminous binder modified with investigated additives.

Binder composition number	1	2	3	4	5	6	7	8	9	10	11	12	13
Name of additive	Without additive	Viscodor PV-2				Licomont BS-100				Sasobit			
Additive concentration, %	0	2.0	2.5	3.0	3.5	2.0	2.5	3.0	3.5	2.0	2.5	3.0	3.5
Ductility at 0 °C, cm	4.2	3.7	3.6	3.0	2.4	3.4	3.2	2.6	1.8	2.1	2.0	1.9	1.7
Maximum tensile strength at 0 °C, N	115	159	160	171	172	135	150	160	168	175	177	178	180
Ductility at 0 °C, cm	130	64	61	52	49	62	58	49	46	61	55	51	45
Maximum tensile strength at 25 °C, N	1.0	5.1	5.8	6.0	7.1	5.5	6.0	6.5	6.8	5.1	5.9	7.7	8.2

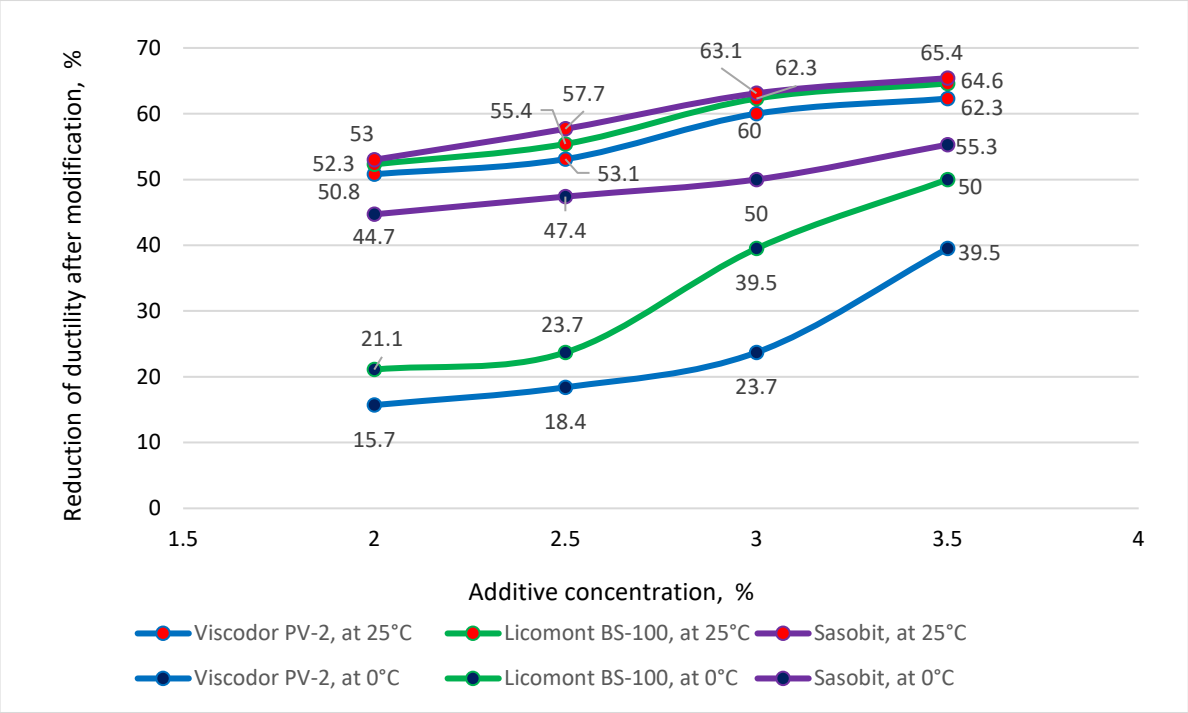

Figure 3. Reduction of bitumen ductility after modification.

Change of ductility of binder samples modified by the investigated additives is presented in Table 2 and Fig. 3. According to the results obtained, the studied organic additives reduce the ductility of bitumen both at 25 and 0 °C. The intensity of ductility reduction increases with increasing concentration of additives input, which is confirmed by the results of the study [22]. The decrease in ductility of the binder indicates an increase in its structuring as a result of increasing the content of synthetic waxes in bitumen. The most significant decrease in ductility both at 25 and 0 °C is caused by the introduction of Sasobit additive (purple lines in Fig. 3). The least significant reduction of ductility at 25 and 0 °C is observed at introduction of additive Viskodor PV-2 (blue lines in Fig. 3), which is due to the presence in the composition of surfactants and plasticising components. The maximum tensile strength recorded both at 25 and 0 °C indicates an increase in the cohesive strength of the binder, proportional to the increase in the concentration of the studied wax modifiers. Thus, the maximum tensile strength at 25 °C through modification of bitumen 2 % additives Viskodor PV-2, Licomont BS-100, and Sasobit increases by 410, 450, and 410 %, and the introduction of these additives in a concentration of 3.5 % increases this index by 610, 580, and 720 %, respectively. The maximum tensile force at 0 °C at the introduction of 2 % additives Viskodor PV-2, Licomont BS-100, and Sasobit increases by 38.3, 17.4, and 52.2 %, and with 3.5 % additives – by 43.0, 46.1, and 32.0 %, respectively. The increase in cohesive strength of the binder will contribute to the strength of the cast asphalt pavement.

It is important to note that when increasing the concentration of Viscodor PV-2 and Licomont BS-100 over 2.5 %, there is a more dramatic decrease in the ductility of bitumen at 0 °C, which in turn will lead to a decrease in the frost resistance of cast asphalt concrete.

Taking into account the above-mentioned, the concentration of Viscodor PV-2 and Licomont BS-100 – 2.5 % as the most rational and not leading to a significant decrease in low-temperature characteristics was chosen for the preparation of the investigated samples of cast asphalt concrete based on modified bitumen binder. In [21], when justifying the selection of Licomont BS-100 modifier dosage in bituminous binder BND 60/90 for cast asphalt concrete, it was also noted that the increase of modifier dosage more than 3 % is not reasonable and can adversely affect the strength of the road surface in winter.

In order to ensure comparability of the study results, a concentration of 2.5 % by weight of bitumen in the cast asphalt mix samples was also selected for the Sasobit additive.

a) **b)** **c)** **d)**

Figure 4. Appearance of granite sift covered with bituminous binder after boiling:

a) without additives; b) 2.5 % Viscodor PV-2; c) 2.5 % Licomont BS-100; d) 2.5 % Sasobit.

Fig. 4 shows the results of adhesion assessment of the initial bitumen and modified by the investigated additives at a concentration of 2.5 % to the mineral material according to GOST 11508. As a mineral material was used granite sifting 0–4 mm, as it is this material was further used for the preparation of experimental compositions of cast asphalt concrete mixtures. It is obvious that the introduction of the investigated additives gives an increase in the index of adhesion with the mineral material. So, the coverage of mineral material with initial unmodified bitumen after boiling was less than ¾ of the surface, which according to GOST 11508 corresponds to the sample No. 3, binder modified with Licomont BS-100 and Sasobit additives after boiling covers more than ¾ of the surface, and corresponds to the sample No. 2. Bitumen modified Viskodor PV-2 after boiling completely covers the surface of mineral material and corresponds to the sample No. 1. The greatest efficiency in improving the adhesion properties showed the additive Viskodor PV-2 as this additive contains in its composition cationic surfactants. The increase in adhesion of bituminous binder with the introduction of wax additives was noted earlier studies [17, 23, 24]. Increase of adhesion will improve such properties of road pavement as water resistance, frost resistance, wear resistance and increase the service life of road pavement.

Granulometric compositions of mineral materials used for preparation of the investigated cast asphalt concrete mixtures (mineral powder MP-2 produced by Tsentr-Izvestnyak LLC, crushed stone of fractions 8–16 and 4–8 mm, and crushed sand of fractions 0–4 mm produced by Pavlovsk Nerud JSC), determined by sieving on sieves according to GOST 33029-2014, are presented in Table 3.

Table 3. Grain composition of mineral materials.

No. n/a	Material name	Content of grains finer than this size, (mm) in % by weight								
		22.4	16.0	11.2	8.0	4.0	2.0	0.5	0.125	0.063
1	Crushed stone of fractions 8–16 mm	100.0	94.5	41.0	23.5	1.2	0.0	0.0	0.0	0.0
2	Crushed stone of fractions 4–8 mm	100.0	100.0	100.0	97.5	24.5	3.2	0.0	0.0	0.0
3	Sand of fractions 0–4 mm	100.0	100.0	100.0	100.0	97.7	71.1	30.1	9.2	4.7
4	Mineral powder	100.0	100.0	100.0	100.0	100.0	100.0	100.0	92.2	84.9

The optimal composition of the mineral part of the cast asphalt concrete mixture LA 16 Vn, selected on the basis of grain compositions in accordance with GOST 54401-2020, is shown in Table 4 and the graph of grain size distribution in Fig. 5.

Table 4. Selection of grain composition of the mineral part of the mixture.

No. n/a	Material name	Content, %	Content of grains finer than this size, (mm) in % by weight						
			22.4	16.0	8.0	4.0	2.0	0.5	0.063
1	Crushed stone of fractions 8–16 mm	39.0	39.0	36.9	9.2	0.5	0	0	0
2	Crushed stone of fractions 4–8 mm	11.0	11.0	11.0	10.7	2,7	0,4	0	0
3	Sand of fractions 0–4 mm	28.0	28.0	28.0	28.0	27.4	19.9	8.4	1.3
4	Mineral powder	22.0	22.0	22.0	22.0	22.0	22.0	22.0	18.7
Grain composition of the mineral part			100.0	97.9	69.9	52.5	42.3	30.4	20.0
Requirements of GOST R 54401-2020 for cast asphalt concrete mix LA 16 Vn		min	100	90	62	43	35	24	19
		max	100	100	78	61	50	41	28

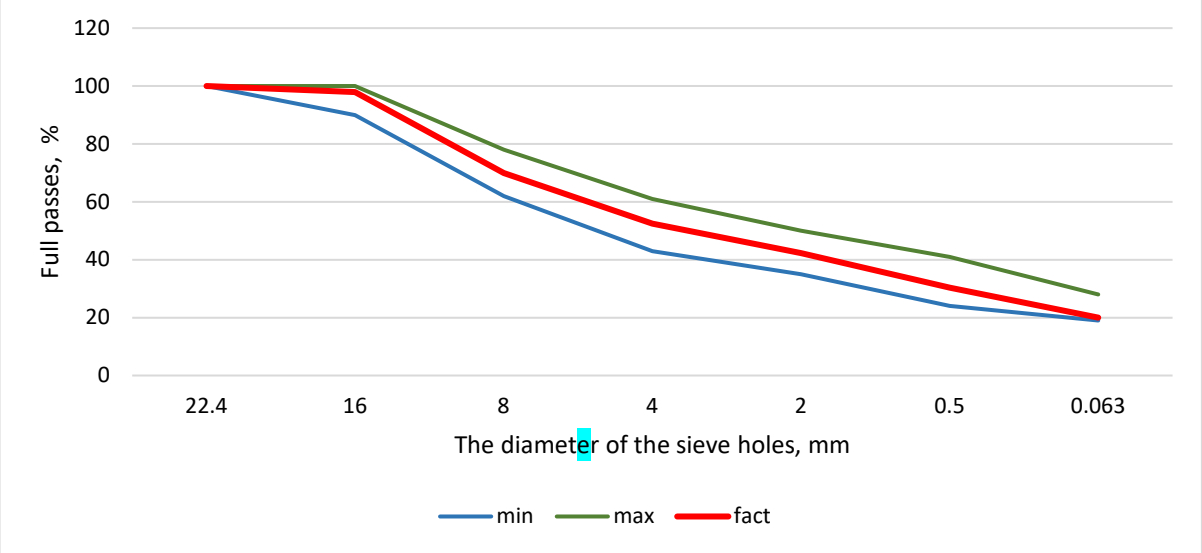

Figure 5. Granulometric composition curve.

On the basis of initial bitumen BND 70/100 without additives and bitumen modified with 2.5 % of investigated additives, as well as optimally selected composition of the mineral part of the mixture, LA 16 Vn asphalt concrete mixtures were prepared, the compositions of which are presented in Table 5.

Table 5. Compositions of cast asphalt concrete mixtures.

Components of bitumen binder composition in the mixture	Number of cast asphalt concrete mix					
	1	2	3	4	5	6
	Content, %, (over 100 % mineral content)					
Bitumen	9	9.5	10	8.775	8.775	8.775
Viscodor PV-2				0.225		
Sasobit					0.225	
Licomont BS-100						0.225
Total quantity of bitumen binder	9	9.5	10	9	9	9

The results of the study of physical and mechanical characteristics of the samples of cast asphalt concrete mixtures based on the original bitumen BND 70/100 and modified binders are presented in Table 6.

Table 6. Physical and mechanical properties of cast asphalt concrete mixtures.

Name of property		Requirements of GOST R 54401-2020 for cast asphalt concrete mixLA 16 Vn	Number of cast asphalt concrete mix					
			1	2	3	4	5	6
Maximum density of the mixture, g/cm^3		not regulated	2.4098	2.3977	2.3984	2.3981	2.3937	2.4031
Bulk density, g/cm^3		not regulated	2.3931	2.3834	2.3844	2.3852	2.3795	2.3902
Air void content, %		no more than 1.5	0.69	0.60	0.58	0.54	0.59	0.54
Paving ability, mm, not less, at temperature:	185 °C	not regulated	10	17	19	33	35	31
	200 °C	not regulated	17	25	28	39	42	36
	215 °C	not less than 30	26	35	40	49	55	43
Depth of stamp indentation, at 40 °C, mm		1.0–4.0	2.73	3.31	4.48	2.45	3.11	2.38
Increase of depth of stamp indentation after 30 min, mm		no more than 0.6	0.15	0.49	0.51	0.35	0.4	0.32

The analysis of the obtained data (Table 6) allows us to state that the control asphalt-concrete mixtures without additives (Nos. 1 and 3) with the binder content of 10 and 9 %, respectively, did not meet the requirements of GOST R 54401-2020. Thus, composition No. 1 containing 9 % bitumen at 215 °C had a paving ability of 26 mm, which is below the norm – not less than 30 mm, and composition No. 3 containing 10 % unmodified bitumen, with a satisfying the normative requirement paving ability of 40 mm at 215 °C, had depth of stamp indentation – 4.48 mm, which is above the required normative value – from 1 to 4 mm. Composition No. 2 containing 9.5 % of binder meets the requirements of GOST R 54401-2020 (paving ability of this mixture at 215 °C – 35 mm, depth of stamp indentation – 3.31 mm).

The introduction of the studied additives allowed to obtain mixtures with a lower content of bituminous binder – 9 %, meeting the normative requirements both in terms of paving ability and depth of stamp indentation.

The obtained results show that the quality of compaction, characterised by the index of air voids content, in samples Nos. 4, 5, and 6 using bitumen modified with the studied additives, improves in comparison with both sample No. 1, containing the same amount of binder but without additives, and with sample No. 2, containing a larger amount of binder (9.5 %). The best compaction was found in the samples containing Viscodor PV-2 and Licomont BS-100 (0.54 % air voids, compared to 0.69 % in the sample with the same amount of bituminous binder without additives and 0.60 % in the sample containing 9.5 % binder). The introduction of Sasobit reduced the amount of air voids to 0.59 %. Thus, the use of the investigated additives will improve the compactibility of asphalt concrete mixture without the need to increase the paving temperature and at a lower binder content.

The indicators of paving ability of the tested compositions at temperatures of 185, 200, and 215 °C allow to assert that the introduction of the investigated wax additives makes it possible to lower the temperature of mixture placement by 30 °C. Thus, even at 185 °C, the paving ability of the mixture with Viskodor PV-2 is 33 mm, with Sasobit – 35 mm, with Licomont BS-100 – 31 mm, which corresponds to the normative requirements for paving ability of cast asphalt concrete mixtures at 215 °C. The value of paving ability at 185 °C of the composition with Viscodor PV-2 is slightly higher than that of the composition with Licomont BS-100, which is due to the presence of surfactants and plasticisers in the composition of Viscodor PV-2. The Sasobit additive is the most effective in improving paving ability as this wax has a lower

melting point. The paving ability of control mixes with bitumen without additives at temperatures of 185 and 200 °C is less than 30 mm. The possibility of reducing the temperature providing the required mobility of cast asphalt concrete mixture to 180–185 °C by introducing wax additives was revealed earlier by the studies of the Moscow Automobile and Road State Technical University (MADI) [12].

It is worth noting that the depth of stamp indentation in the compositions No. 4 with Viscodor PV-2 and No. 6 with Licomont BS-100 are 10.3 and 12.8 % lower, respectively, than in the control composition No. 1 with the same amount of unmodified binder, which is explained by the high ability of amide wax, which is part of these additives, to structure the bituminous binder. Thus, the said additives will contribute to increase the strength properties of the cast asphalt concrete and the resistance to plastic deformation. The depth of stamp indentation for mix No. 5 with Sasobit additive is 13.9 % higher than that of sample No. 1 with equal amount of binder without additive but 6 % lower than that of sample No. 2 complying with the requirements of GOST R 54401-2020, with 9.5 % unmodified bitumen. This is due to the power ability of polyethylene wax Sasobit to structure the binder in comparison with the additives Viskodor PV-2 and Licomont BS-100, which have amide waxes in their composition. The reduction of the depth of stamp indentation with the introduction of additives based on synthetic waxes is confirmed by numerous studies [21, 25, 26].

4. Conclusion

Analysis of changes in the properties of modified bitumen binder and cast asphalt concrete mixtures with the use of investigated additives allows us to draw the following conclusions.

1. Modifiers Viscodor PV-2, Licomont BS-100, and Sasobit have a structurising effect on bitumen, which is expressed in the increase of softening temperature, decrease of penetration and ductility indices at 25 °C. This will increase the strength properties of cast asphalt concrete mixtures and improve their resistance to plastic deformations. The introduction of the investigated additives improves the adhesion of bitumen with mineral aggregate, which will increase the durability of cast asphalt concrete pavement.
2. The rational concentration of Licomont BS-100 and Viscodor PV-2 is 2.5 %, as further increase in the concentration of additives, leads to a decrease in the indicators of needle penetration depth at 0 °C, ductility at 0 °C and increase in the brittleness temperature of bituminous binder, which can lead to a decrease in the binder resistance to low operating temperatures.
3. The use of the investigated additives allows to reduce the binder content necessary to achieve the required mobility of cast asphalt concrete mixtures by 0.5 % without deterioration of their qualitative characteristics. Thus, at a temperature of 215 °C, the power ability of the sample of cast asphalt concrete mixture with 9 % unmodified bitumen is 26 mm, which does not meet the regulatory requirements, while the power ability for the composition with the same amount of binder modified Viskodor PV-2 – 49 mm, Sasobit – 55 mm; Licomont BS-100 – 48 mm, which meets the requirements of GOST R 54401-2020.
4. The investigated wax additives at a concentration of 2.5 % of bitumen weight allow to improve power ability and reduce the paving temperature of cast asphalt concrete mixture by 30 °C without loss of strength characteristics. Thus, at a temperature of 185 °C, the power ability of mixtures with binder modified by Viscodor PV-2, Sasobit, and Licomont BS-100 is 33, 35, and 31 mm, respectively, which meets the normative requirements for this indicator at a temperature of 215 °C. The power ability of cast asphalt concrete mixtures without additives at temperatures of 185 and 200 °C does not reach the required value at which paving is possible.
5. Licomont BS-100 and Viscodor PV-2 additives not only effectively improve the mobility of cast asphalt concrete mixtures but also increase their resistance to mechanical loads, which is characterised by lower indices of die indentation depth (2.45 and 2.38 mm, respectively) compared to control samples without additives Nos. 1 and 2 (2.73 and 3.31 mm).
6. Viscodor PV-2 as an additive for cast asphalt concrete mixtures is not inferior in effectiveness to the well-known wax modifiers Licomont BS-100 and Sasobit. In addition, due to the presence of plasticizing and surface-active substances in the composition of Viscodor PV-2, this additive has a greater positive effect on the power ability of cast asphalt concrete mixtures than Licomont BS-100, and the presence of amide wax in the composition of Viscodor PV-2 causes a lower the depth of stamp indentation and, consequently, a higher resistance to plastic deformations than the Sasobit additive.

References

1. Tiraturyan, A.N. Dissipation of dynamic deformation energy in pavements of automobile roads. Sustainable Development of Mountain Territories. 2024. 16(3). Pp. 909–920. DOI: 10.21177/1998-4502-2024-16-3-909-920
2. Shavakuleva, O.P., Grishin, I.A., Sedinkina, N.A., Fadeeva, N.V. The effect of preliminary reagent treatment of marble rubble on the screening efficiency. Sustainable Development of Mountain Territories. 2024. 16(3). Pp. 931–942. DOI: 10.21177/1998-4502-2024-16-3-931-942
3. Fadeev, A.A., Zaborskiy, E.N., Bagdasaryan, O.E. Digital solutions for drilling and blasting operations as a way to improve efficiency, safety of operations and reduce seismic impact during rock crushing. Ugol'. 2024. 12. Pp. 99–102. DOI: 10.18796/0041-5790-2024-12-99-102
4. Bosikov, I.I., Klyuev, R.V., Revazov, V.Ch., Martyushev, N.V. Analysis and evaluation of prospects for high-quality quartz resources in the North Caucasus. Mining Science and Technology (Russia). 2023. 8(4). Pp. 278–289. DOI: 10.17073/2500-0632-2023-10-165
5. Ermolovich, E.A., Ivannikov, A.L., Kongar-Syuryun, C.B., Tyulyaeva, Y.S., Khayrutdinov, M.M. Creation of a Nanomodified Backfill Based on the Waste from Enrichment of Water-Soluble Ores. Materials. 2022. 15(10). Article no. 15103689. DOI: 10.3390/ma15103689
6. Kozikov, I.O., Lupanov, A.P., Silkin, V.V. Prediction of Shear Resistance of Cast Asphalt Concrete Pavements. Transport construction. 2023. 3. Pp. 10–13.
7. Akishev, K., Aryngazin, K., Tleulessov, A., Bulyga, L., Stanevich, V. The use of simulation modeling in calculating the productivity of the technological system for the production of building products with fillers from man-made waste. News of the National Academy of Sciences of the Republic of Kazakhstan. Series of Geology and Technical Sciences. 2024. 4(466). Pp. 22–32. DOI: 10.32014/2024.2518-170x.422
8. Klyuev, R.V. Improving the energy efficiency of heat production during the utilization of coal mine methane in gas piston power plants. Ugol'. 2025. 1. Pp. 105–108. DOI: 10.18796/0041-5790-2025-1-105-108
9. Dossaliyev, K.S., Ibragimov, K., Nazarov, K.I., Ussenkulov, Zh.A., Aubakirova, F.Kh. Coarse-grained soils compaction at the experimental site during the construction of the earthen dam. News of the National Academy of Sciences of the Republic of Kazakhstan. Series of Geology and Technical Sciences. 2024. 3(465). Pp. 58–70. DOI: 10.32014/2024.2518-170x.409
10. Yelemessov, K., Sabirova, L.B., Martyushev, N.V., Malozyomov, B.V., Bakhmagambetova, G.B., Atanova, O.V. Modeling and Model Verification of the Stress-Strain State of Reinforced Polymer Concrete. Materials. 2023. 16(9). Article no. 3494. DOI: 10.3390/ma16093494
11. Yadykina, V.V., Akimov, A.E., Trautvain, A.I, Kholopov, V.S. Influence of DAD-TA temperature-reducing additive on physical and mechanical properties of bitumen and compaction of asphalt concrete. IOP Conference Series: Materials Science and Engineering. 2018. 327(3). Pp. Article no. 032006. DOI: 10.1088/1757-899X/327/3/032006
12. Kozikov, I.O., Lupanov, A.P., Silkin, V.V., Sukhanov, A.S. Influence of asphalt granulate and deflegmators on mobility of cast asphalt concrete mixtures. Transport Construction. 2023. 2. Pp. 27–29.
13. Yue, M., Yue, J., Wang, R., Xiong, Y. Evaluating the fatigue characteristics and healing potential of asphalt binder modified with Sasobit® and polymers using linear amplitude sweep test. Construction and Building Materials. 2021. 289. Article no. 123054. DOI: 10.1016/j.conbuildmat.2021.123054
14. Kolapkar, S., Sathe, S. Effect of Sasobit® as a WMA additive on mix design parameters. Materials Today: Proceedings. 2023. DOI: 10.1016/j.matpr.2023.03.253
15. Bosikov, I.I., Klyuev, R.V., Martyushev, N.V., Modina, M.A., Khekert, E.V. Analysis of the quality of underground mineral waters of terrigenous deposits of the hauteriv barremian aquifer of the lower cretaceous. News of the National Academy of Sciences of the Republic of Kazakhstan. Series of Geology and Technical Sciences. 2024. 2(464). Pp. 36-47. DOI: 10.32014/2024.2518-170x.392
16. Rodríguez-Alloza, A.M., Gallego, J., Pérez I. Study of the effect of four warm mix asphalt additives on bitumen modified with 15 % crumb rubber. Construction and Building Materials. 2013. 43(4). Pp. 300–308. DOI: 10.1016/j.conbuildmat.2013.02.025
17. Sigwarth T., Büchner J., Wistuba M.P. Bio-Degradable Wax to Modify Asphalt Binder for Warm Mix Asphalt. Sustainability. 2022. 14(16). Article no. 10219. DOI: 10.3390/su141610219
18. Arsenyev, I.D. Numerical simulation of the reaction of the geological environment for various variations of underground construction options. Ugol'. 2024. 12. Pp. 127–130. DOI: 10.18796/0041-5790-2024-12-127-130
19. Yadykina, V. V., Mikhailova, O. A. Effect of temperature-lowering additives based on synthetic waxes on bitumen properties. A. Influence of temperature-reducing additives based on synthetic waxes on bitumen properties. Bulletin of BSTU named after V.G. Shukhov. 2023. 3. Pp. 8–18. DOI 10.34031/2071-7318-2022-8-3-8-18 (rus)
20. Stienss, M., Szydlowski, C. Influence of Selected Warm Mix Asphalt Additives on Cracking Susceptibility of Asphalt Mixtures. Materials. 2020. 13(1). Article no. 202. DOI: 10.3390/ma13010202
21. Isametova, M.E., Nussipali, R., Martyushev, N.V., Malozyomov, B.V., Efremenkov, E.A., Isametov, A. Mathematical Modeling of the Reliability of Polymer Composite Materials. Mathematics. 2022. 10(21). Article no. 3978. DOI: 10.3390/math10213978
22. Gostev, D.V., Kryukova, A.A., Izmailov, A.M., Abdrakhimov, V.Z. Ecological, economic and practical feasibility of using ash slag in the production of wall material based on montmorillonite clay. Ugol'. 2023. 4. Pp. 49–53. DOI: 10.18796/0041-5790-2023-4-49-53
23. Myrzakulov, M.K., Dzhumankulova, S.K., Yelemessov, K.K., Barmenshinova, M.B., Martyushev, N.V., Skeeba, V.Y., Kondratiev, V.V., Karlina, A.I. Analysis of the Effect of Fluxing Additives in the Production of Titanium Slags in Laboratory Conditions. Metals. 2024. 14(12). Article no. 1320. DOI: 10.3390/met14121320
24. Nurpeissova, M.B., Orynbekov, E.S., Fedotenko, N.A., Estemesova, A.S. The influence of technological factors on density and the strength of ash gas concrete. Sustainable Development of Mountain Territories. 2024. 16(2). Pp. 669–678. DOI: 10.21177/1998-4502-2024-16-2-669-678
25. Popov, M.G., Sinegubov, V.Yu. Study of the properties of two-layer concrete-fiber-concrete structures at different ratio of layer thickness. Sustainable Development of Mountain Territories. 2024. 16. Pp. 70–82. DOI: 10.21177/1998-4502-2024-16-1-70-82
26. Artykbaev, D.Zh., Ibragimov, K., Aubakirova, F.Kh., Karatayev, M., Polat, E. Research and laboratory methods for determining coarse soils at the experimental site during the construction of an earth dam. News of the National Academy of Sciences of the Republic of Kazakhstan. Series of Geology and Technical Sciences. 2024. 2(464). Pp. 8–23. DOI: 10.32014/2024.2518-170x.390

Information about the authors:

Valentina Yadykina, *Doctor of Technical Sciences*
ORCID: https://orcid.org/0000-0001-8289-2361
E-mail: vvya@intbel.ru

Olga Mikhaylova,
ORCID: https://orcid.org/0009-0000-5896-5524
E-mail: mihaylovalymar@mail.ru

Antonina Karlina, *PhD in Technical Sciences*
ORCID: https://orcid.org/0000-0003-3287-3298
E-mail: karlinat@mail.ru

Nikolai Vatin, *Doctor of Technical Sciences*
ORCID: https://orcid.org/0000-0002-1196-8004
E-mail: vatin@mail.ru

Nikita Martyushev, *PhD in Technical Sciences*
E-mail: martjushev@tpu.ru

Received 23.01.2025. Approved after reviewing 17.06.2025. Accepted 20.06.2025.

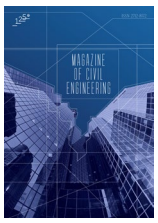

Magazine of Civil Engineering

ISSN 2712-8172

journal homepage: http://engstroy.spbstu.ru/

Research article

UDC 625.7/.8

DOI: 10.34910/MCE.136.8

Relative hysteresis as an indicator of structural condition of pavements

A.N. Tiraturyan ✉

Federal State-Funded Educational Institution of Higher Education Don State Technical University

✉ *tiraturjanartem@gmail.com*

Keywords: flexible pavements, mechanical properties, dissipated energy, hysteresis loop, fracture

Abstract. The paper is devoted to the experimental study of dynamic hysteresis under impact loading on the surface of flexible pavements. The relevance of the study is associated with the lack of informative indicators of the condition of pavements, which would allow for the assessment of their structural condition taking into account the mechanisms of viscoelastic deformation. A FWD PRIMAX 1500 falling weight deflectometer was used as the measuring equipment, which allows for the registration of dynamic hysteresis loops on the pavement surface under impact loading. Based on the recorded hysteresis loops, the values of dissipated energy, potential energy of deformation and relative hysteresis were determined. For the first time, the quantitative values of relative hysteresis characterizing energy absorption in different pavement layers have been determined. The regularities of change in the relative hysteresis value with increasing load transmitted by the impact loading unit have been established. It is shown that the curve of relative hysteresis change as the load increases contains two sections. A flat section, where its value is close to constant, and a section with a monotonic increase in the value of relative hysteresis, which suggests that the loads causing this monotonic increase are critical, forming a 'dangerous' fracture energy in the pavement. This result can be used in the preparation of short ultimate axial loads, as well as in the development of projects for the transport of heavy loads on public roads.

Funding: The research was supported by the Russian Science Foundation grant No. 24-29-00110 "Study of the mechanisms of deformation of layered media under the influence of dynamic load and improvement of the method of non-destructive testing of their condition (using highways as an example)". Available online: https://rscf.ru/project/24-29-00110.

Citation: Tiraturyan, A.N. Relative hysteresis as an indicator of structural condition of pavements. Magazine of Civil Engineering. 2025. 18(4). Article no. 13608. DOI: 10.34910/MCE.136.8

1. Introduction

Road pavements are an important structural element of a motorway, directly determining its durability and operational condition. The control of their condition during operation is carried out by various indicators, among which structural indicators play a special role. In the practice of the Russian Federation, the main such indicator characterising the structural properties of a motorway is the general modulus of elasticity, or the moduli of elasticity of materials of individual layers, established during non-destructive tests using FWD impact loading units [1–3].

However, it is known that pavements are characterised by a complex set of properties determined by their constituent materials that make them up. Evaluating these properties solely from the point of view of elastic characteristics, which should include both modulus of elasticity and the elastic deflection, from which the modulus of elasticity is directly derived, can lead to errors and distortion of information. Work on the development of new structural indices is being carried out continuously by different groups of scientists [4–6].

In a number of studies, the deflection bowl parameters, linking different deflection bowl zones with the structural condition of the corresponding structural elements, are used as the main indicators characterising road properties. Such parameters include surface curvature index (SCI), base curvature index (BCI), and others [7–9]. This approach is an empirical one, and its undoubted advantage is the possibility of assessing the structural condition of the pavement without any prior history of the pavement, i.e. without information on the materials of its structural layers, design characteristics, and previous repairs carried out.

Another well-known approach to determining the condition of a pavement is the 'backcalculation' method, which allows for estimating its individual structural parameters from the deflection bowl measured in the field, based on the solution of the inverse coefficient problem. These problems are described in detail with reference to static pavements in the following works [10–13], and in a dynamic formulation in the works [14–17].

At the same time, modern dynamic loading facilities allow, in addition to discrete characteristics of deformation of pavements, which are certainly deflection bowls, for the recording of continuous characteristics such as amplitude-time characteristic of displacements and the hysteresis loop in the coordinates 'displacement – load'. The hysteresis loop has a direct physical meaning, which is that its area is equivalent to the energy dissipated in the studied object. In terms of research of energy characteristics of deformation of road pavements determined in full-scale conditions, in domestic and foreign practice, there are separate works concerning changes in the shape and size of dynamic hysteresis loops in different periods of the year, as well as their application in relation to user parameters characterising the road condition. However, up to the present moment the issue of connection between energy characteristics of deformation and the structural condition of the pavement and its individual elements remains poorly studied [18–21].

In the laboratory practice of testing construction materials, studies concerning the energy parameters of deformation are much more widespread. A well-established approach is the study of strain energy dissipation in fatigue testing of asphalt concrete specimens in four-point loading and indirect tension facilities. The California Non-Rigid Pavement Design Method directly uses strain energy parameters determined on dynamic creep units to design new structures. Nevertheless, despite all the results associated with testing materials in laboratory conditions, it should be noted that the most reliable way to establish the design characteristics of the materials under study is to test them under in-situ conditions [22–24].

It should also be noted that studies related to the energy picture of deformation of various objects are widespread in many related fields. These are studies of dynamic instability of soils carried out by the scientific school of Prof. E.A. Voznesensky. Studies of reinforced concrete fracture based on full diagrams of its deformation, carried out under the guidance of Prof. V.M. Bondarenko. A significant body of research of fracture energy was carried out in the study of fatigue life of metals. In their fatigue tests, various hypotheses have been developed to establish the proportions of 'dangerous' and 'non-dangerous' deformation energy. Methods have been developed for predicting the fatigue life of various structural materials on the basis of the total dissipated strain energy [25–28].

All this together suggests that a gradual transition to the study of the energy picture of pavement deformation is an important and urgent task. The deformation energy expressed in the form of quantitative indicators allows for a comprehensive assessment of all structural processes that have occurred with the pavement and its individual layers during the period of operation. A quantitative assessment can be expressed by different indicators, in particular, the area of hysteresis loop, relative hysteresis (absorption coefficient) and potential deformation energy. The effective application of these indicators may allow for significant development both in the methods of non-destructive testing of road pavements and in creating prerequisites for the improvement of road pavement design methods.

Thus, the aim of this work is to investigate the quantitative parameters of the deformation energy, in particular the relative hysteresis recorded during in-situ measurements on the pavement surface, and to establish a qualitative relationship between the relative hysteresis value and the operational condition of the pavement.

2. Methods

Within the framework of this work, experimental studies were carried out using the FWD PRIMAX 1500 impact loading rig. This unit is a semi-trailer with a shock loading mechanism mounted on it and a beam with geophone sensors for recording the vertical component of displacements Fig. 1. The impact loading mechanism allows for reproducing impulse loading $F(t)$ with contact interaction time equal to 0.03 s. The shape of the loading impulse is close to sinusoidal Fig. 2. The range of possible loads is 10–

130 kN. The load value variation is done by changing the height of the load discharge. The sensors-geophones (D1–D10) allow for recording of vertical displacements in the time range – $u_i(t)$. The form of the amplitude-time characteristic is shown in Fig. 3.

Superimposition of the amplitude-time characteristic of displacements $u_i(t)$ on the time characteristic of the loading impulse allows for constructing a dynamic hysteresis loop Fig. 4. The area of the hysteresis loop characterises the energy irreversibly dissipated in the pavement structure under dynamic loading.

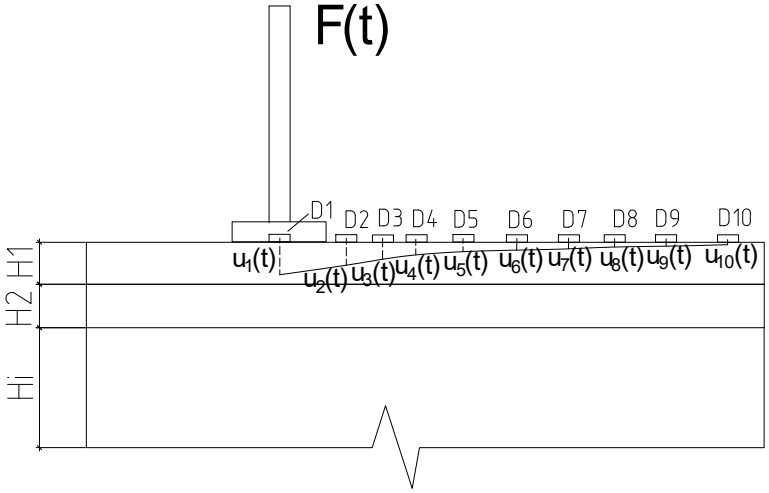

Figure 1. Registration of dynamic response on pavement surface by FWD unit.

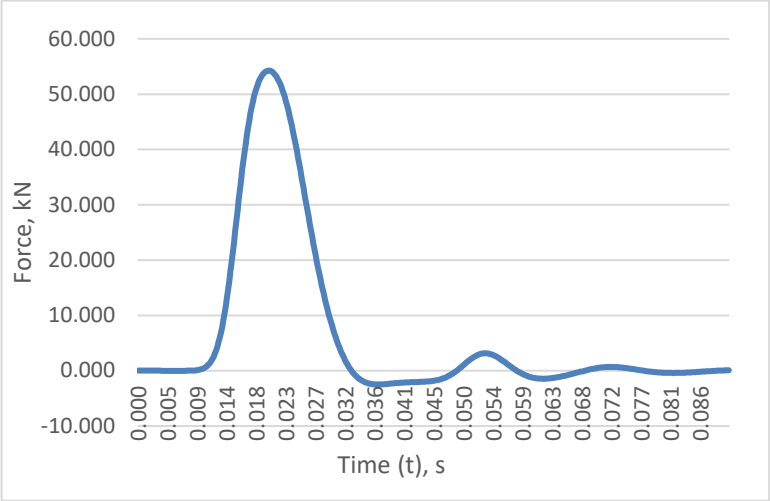

Figure 2. Pulse shape reproduced by the falling weight deflectometer.

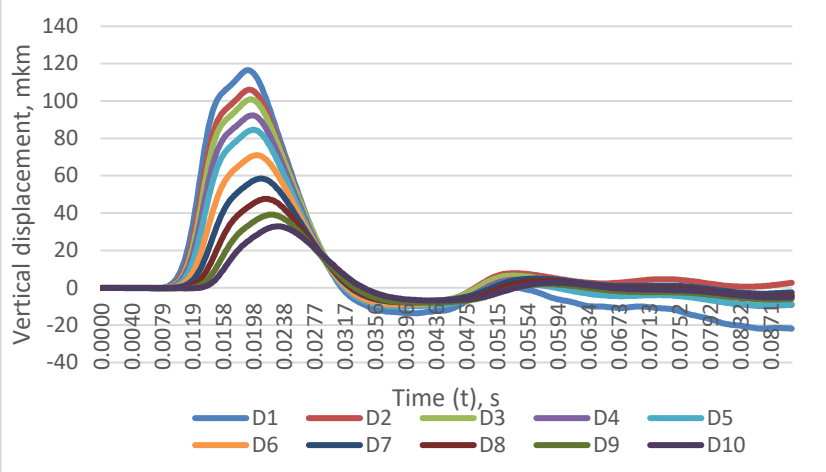

Figure 3. Shape of amplitude-time characteristic of displacements.

$$W = \int_0^t u_i(t) F(t) dt, \tag{1}$$

where $u(t)$ is the dependence of vertical displacements on time, $F(t)$ is time-dependent force impulse.

Taking into account that during field tests the amplitude-time characteristics of displacement and the impulse of impact loading are arrays of values, representing, in fact, the coordinates of the dynamic hysteresis loop this integral can be determined in accordance with the Gauss formula for the area of a polygon.

The potential energy of deformation is determined by the formula:

$$\Pi = \frac{1}{2} u^{\max} F, \tag{2}$$

where $u^{\max}$ is maximum value of vertical displacement on the surface of the medium under study, F is corresponding load value.

Relative hysteresis (absorption coefficient) η in this case is defined as:

$$\eta = \frac{W}{\Pi}. \tag{3}$$

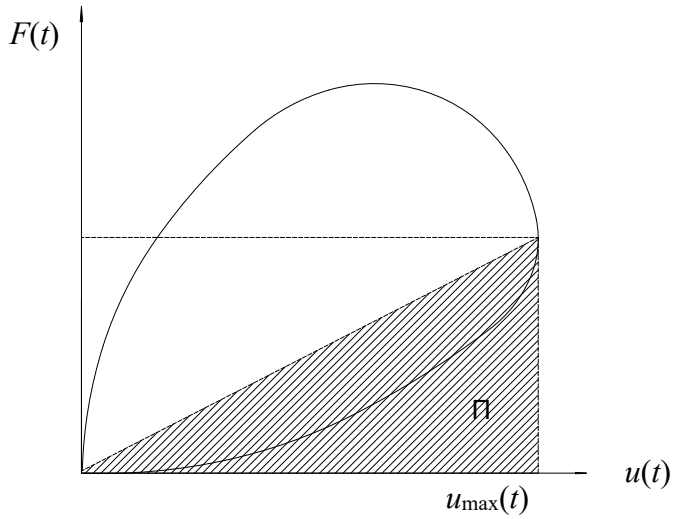

Figure 4. Dynamic hysteresis loop.

Experimental studies of deformation of pavements were carried out on different sections of motorways. In the first section, layer-by-layer tests were carried out as the pavement was constructed, starting from the crushed stone base layer and ending with the surface of the structure. The other three sections recorded dynamic hysteresis loops on the surface of the pavement to quantify energy dissipation, potential strain energy, and relative hysteresis. At the same time, the surveyed sections were in different transport-operational condition, which should allow for evaluating qualitative changes in the calculated parameters. The design of the test section where the layer-by-layer control was carried out is given in Table 1. The design of the operational sections where measurements on the pavement surface were carried out is given in Table 2, and the general view of their operational condition is given in Fig. 5.

Table 1. Pavement on monitoring station.

Layer no.		Layer name	Thickness, cm
Asphalt surface	1	SMA-16	5
	2	A32Lh (Lower layer of asphalt concrete pavement)	8
	3	A32Bh (Asphalt concrete base course)	12
Base	4	Stabilized base layer made of organomineral mixture HO 32 EM	22
	5	Crushed stone M800 crushed stone of 31.5–63 mm	36
Subbase		Medium coarse sand with a filter coefficient of more than 1 m/day,	20
Soil	6	Heavy dusty loam	–

Table 2. Structures of road pavements on maintained road sections.

Section 1		Section 2		Section 3	
Layer name	**Thickness, cm**	**Layer name**	**Thickness, cm**	**Layer name**	**Thickness, cm**
SMA-15	4	SMA-15	4	SMA-15	4
A32Lh (Lower layer of asphalt concrete pavement)	7	A32Lh (Lower layer of asphalt concrete pavement)	7	A32Lh (Lower layer of asphalt concrete pavement)	7
A32Bh (Asphalt concrete base course)	7	A32Bh (Asphalt concrete base course)	8	A32Bh (Asphalt concrete base course)	14
Crushed stone M800	41	crushed stone-gravel-sand mixture	18	crushed stone-gravel-sand mixture	16
Gravel-sand mixture	66	Gravel-sand mixture	41	Gravel-sand mixture	32
Heavy dusty loam	–	Heavy dusty loam		Heavy dusty loam	

Figure 5. Visual condition of the monitoring sections.

During the tests, 4 impacts were performed on each measuring point. The first impact was a test impact and the remaining impacts were measuring impacts. The specificity of the FWD dynamic loading unit operation implies constant hardware control of the measurement accuracy. In case the vertical displacement values for each measurement impact differ by more than 5 %, the measurement is rejected and repeated. After a successful series of measurements, the data for the three measuring strokes shall be averaged. The observation time, during which the amplitude-time characteristics of displacements and loading impulse are recorded, is 0.1 s. During this time, there is almost complete decay of deformation characteristics and the experimental loop of dynamic hysteresis corresponds to the curve shown in Fig. 4.

3. *Results and Discussion*

The general view of the dynamic hysteresis loops recorded at the test section on the surface of different structural pavement layers is shown in Fig. 6.

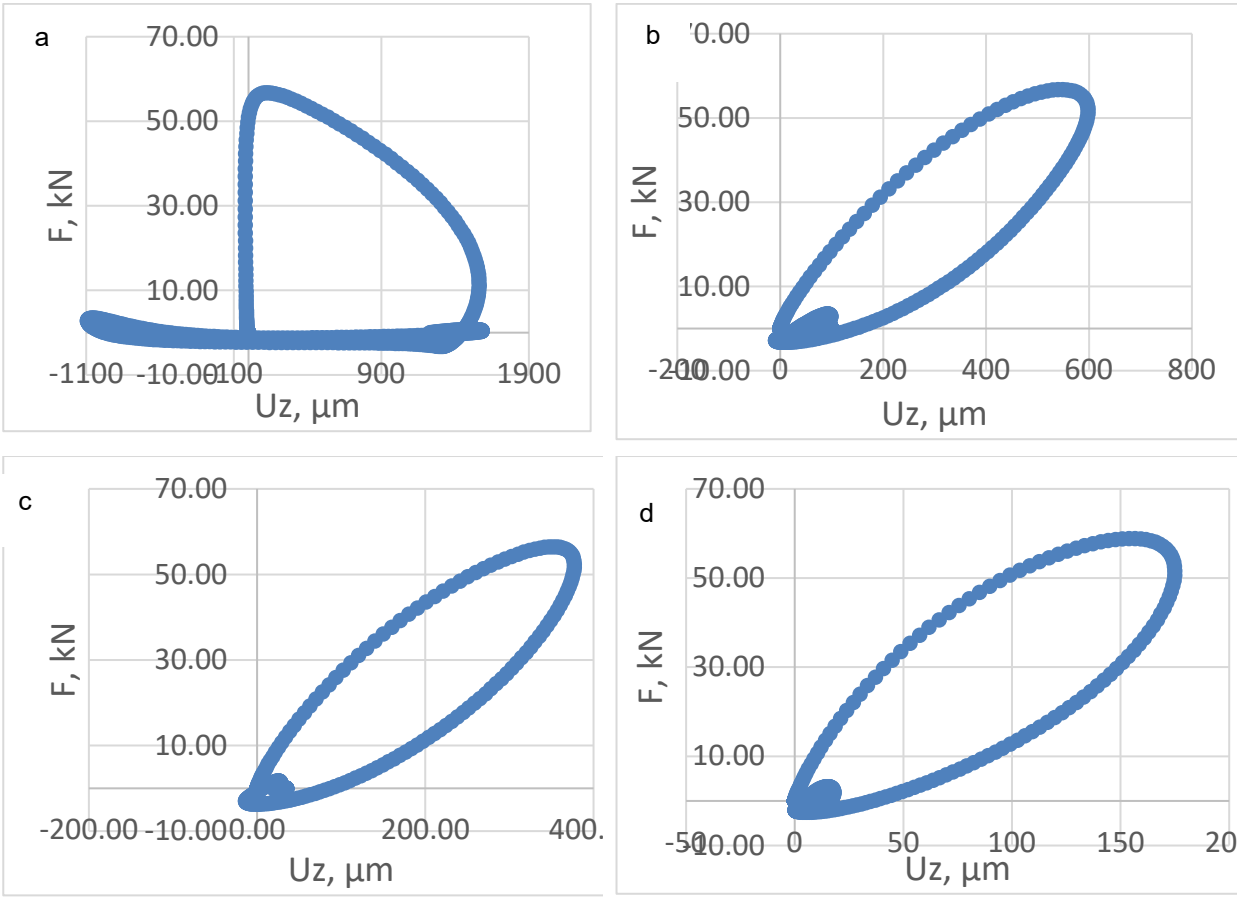

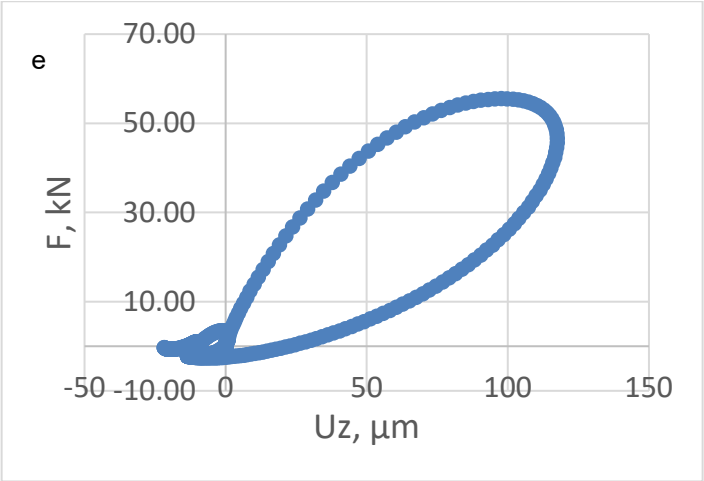

Figure 6. Hysteresis loop on surface pavement layers: a – on top layer no. 5, b – on top layer no. 4, c – on top layer no. 3, d – on top layer no. 2, e – on top layer no. 1.

The analysis of the results of experimental registration of dynamic hysteresis loops on the surface of each of the newly constructed pavements allows for drawing the following conclusions. On the surface of all layers, even under the condition of short-pulse loading of 0.03 s, the picture of dynamic deformation of each layer is highly non-linear. Thus, for example, on the surface of the crushed stone layer the loading curve increases sharply, while the value of vertical displacement practically does not increase. The maximum level of vertical displacement on the crushed stone base layer is reached at the moment when the load is about 24 % of the test loading value of 57.5 kN. On the surface of the other layers, the hysteresis loop tends to the classical ellipse shape, while also being slightly different. Thus, it can be seen that in all cases, the peak of loading does not coincide with the peak of vertical displacements and the width of the loop changes, which indicates a different magnitude of strain energy dissipation. Quantitative estimates of the dissipated energy, potential strain energy, and relative hysteresis are given in Table 3.

Table 3. Results of recording dynamic hysteresis loops on the pavement surface at the test section.

Layer no.		Layer name	Dissipated energy on surface layer – W, J/m^3	Potential energy on surface layer – П, J/m^3	Relative hysteresis, η
Asphalt surface	1	SMA-16	3.54	2.74	1.29
	2	А32Нт (Lower layer of asphalt concrete pavement)	4.63	4.51	1.03
	3	А32От (Upper layer of asphalt concrete pavement)	9.26	9.88	0.94
Base	4	Stabilized base layer made of organomineral mixture НО 32 ЕМ	15.14	15.47	0.98
	5	Crushed stone М800 crushed stone of 31.5–63 mm	72.2	9.5	7.6

Thus, it can be seen that the value of strain energy dissipation during the construction of the pavement structure changed approximately 7 times, from 72.2 J/m^3 characteristic of the unbound crushed stone base layer to 3.54 J/m^3 registered on the surface of the crushed stone-mastic asphalt concrete layer. The picture of the relative hysteresis variation is somewhat different. Taking the maximum value on the surface of the unbound crushed stone base layer, as more rigid frame layers of asphalt-granulose concrete and asphalt concrete of the upper base layer are arranged, it decreases to 0.94–0.98, after which, as more

viscous asphalt concrete layers of the lower pavement layer and the upper pavement layer are arranged, it increases again to 1.29.

Given the obvious relationship of relative hysteresis to the structural properties of the structural layer materials, it is of some interest to study this index as the test loading increases. For this purpose, an experiment was carried out on three sections of motorways with pavement structures listed in Table 2, which are in different operational condition, in order to study the change in relative hysteresis as the load increases from 30 to 110 kN.

On each of the above sections, tests were carried out using FWD impact loading rig and the dissipated energy, potential strain energy and relative hysteresis were determined. The calculation results are summarised in Table 4. The variation of the relative hysteresis index as a function of the applied load is shown in Fig. 7.

Table 4. Results of registration of energy parameters of deformation at the operated sections.

Load, kN	Section 1			Section 2			Section 3		
	Dissipated energy, J/m^3	Potential energy, J/m^3	Relative hysteresis	Dissipated energy, J/m^3	Potential energy, J/m^3	Relative hysteresis	Dissipated energy, J/m^3	Potential energy, J/m^3	Relative hysteresis
30	2.50	2.00	1.25	3.78	2.21	1.71	3.41	2.30	1.48
40	4.57	3.67	1.25	7.07	4.20	1.68	5.67	3.98	1.42
50	7.58	6.15	1.23	11.75	6.66	1.77	8.44	5.99	1.41
60	10.37	8.63	1.20	17.21	9.58	1.80	12.19	8.57	1.42
70	14.20	11.40	1.25	22.93	12.13	1.89	15.56	11.12	1.40
80	17.86	14.35	1.24	29.19	14.51	2.01	19.84	13.99	1.42
90	22.71	17.94	1.27	36.60	17.58	2.08	24.37	16.79	1.45
100	27.04	20.95	1.29	45.14	21.46	2.10	30.49	20.33	1.50
110	32.71	24.31	1.35	53.78	23.15	2.32	36.46	22.94	1.59

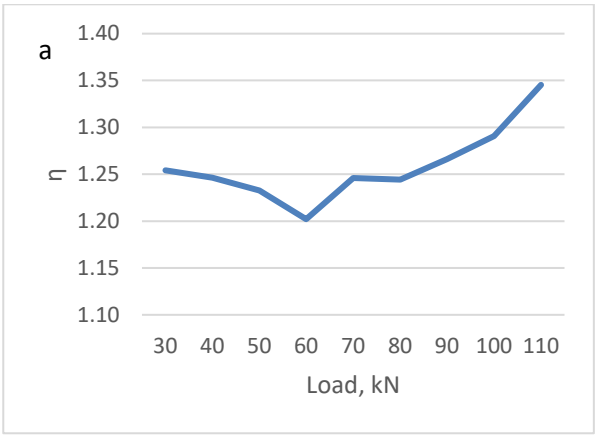

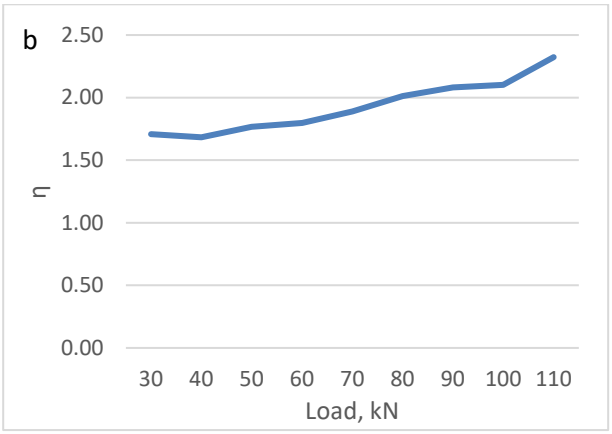

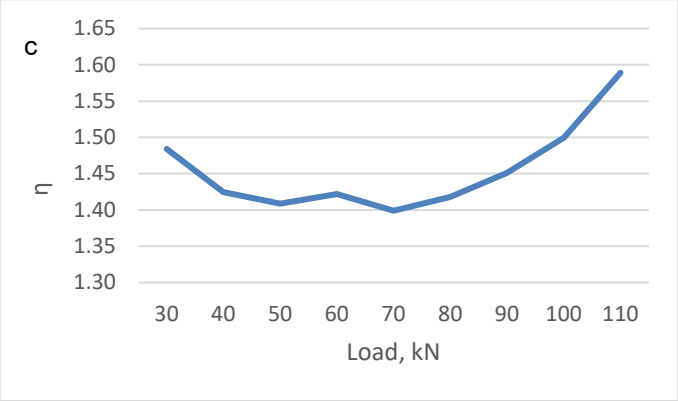

Figure 7. Variation of relative hysteresis with increasing test load: a – section 1, b – section 2, c – section 3.

As can be seen in the presented graphs, all of them have a similar tendency of change. At the beginning, with a gradual increase in load, the relative hysteresis varies non-monotonically, increasing or decreasing by some value. This can be seen in section 1 in the range from 30 to 80 kN, section 2 from 30 to 40 kN, and section 3 in the zone of 30 to 70 kN. After that, the magnitude of relative hysteresis starts to increase steadily with increasing load magnitude. This character of change allows for making an assumption that the load value, after which the relative hysteresis starts to grow steadily, is critical, and its further increase leads to an increase in the 'dangerous' fracture energy in the pavement, which is used for the development of defects in its structure. Based on this example, it can be noted that the values of the permissible load on the half of the vehicle axle of 80, 40, 70 kN proposed on the basis of the graphs generally correlate well with the current condition of the survey sections shown in Fig. 5.

Further development of this approach will allow for approaching a relatively simple express methodology for assigning ultimate axial loads, or critical loads from large vehicles travelling with excessive loads.

As a comparison with the presented approach can be considered the work [29], in which the ultimate load from the traffic flow is calculated based on the operational condition of the motorway according to the criterion of fatigue damage accumulation, and the depth of rutting. However, it is clear that this approach requires much more information and is generally much more labour intensive compared to the in situ test results presented in this study. There is also a domestic document ODM 218.6.002-2010 'Methodical Recommendations for Determining Allowable Axle Loads of Motor Vehicles in the Spring Period Based on the Results of Diagnostics of Public Roads of Federal Significance', which establishes the correspondence between the strength coefficient of the pavement and the maximum axle load. However, this approach also requires documented design information on the minimum required design total modulus of elasticity. In addition, the modulus of elasticity, being an elastic material characteristic, does not generally reflect the processes associated with the dissipation of deformation energy and the intensification of micro-destruction in the structure of pavement materials.

4. Conclusion

1. Experimental registration of dynamic hysteresis loops on the surface of pavement layers during its construction was carried out. The total energy dissipation, potential energy of deformation, and relative hysteresis on the surface of each layer were calculated.
2. It was found that the value of strain energy dissipation during the construction of the pavement structure changed approximately 7 times, from 72.2 J/m^3 characteristic of the unbound crushed stone base layer to 3.54 J/m^3 registered on the surface of the crushed stone-mastic asphalt concrete layer. It should also be noted that as the stiffer stabilized base layer frame layers and the asphalt concrete of the upper base course are placed, the relative hysteresis decreases to 0.94–0.98, after which it increases again to 1.29 J/m^3 as the more viscous asphalt concrete layers of the lower pavement and the upper pavement are placed.
3. Experimental studies of the relative hysteresis change, as the test load increases, have been carried out. It was found that with a gradual increase in the load, the relative hysteresis indicator changes non-monotonically, increasing or conversely decreasing by some value. Then the value of relative hysteresis begins to grow steadily with increasing load value. Such a character of change allows for making an assumption that the load value, after which the relative hysteresis began to grow steadily, was critical, and its further increase leads to an increase in the 'dangerous' fracture energy in the pavement, which was used for the development of defects in its structure.

References

1. Tiraturyan, A.N., Lyapin, A.A., Uglova, E.V. Improvement of the non-destructive method for determining the mechanical characteristics of elements of multilayer structures on the example of pavements. PNRPU Mechanics Bulletin. 2023. 1. Pp. 56–65. DOI: 10.15593/perm.mech/2023.1.06
2. Kuznetsova, A. Comparative trials of geosynthetic materials in the base of road pavement on the section of the Central Ring Road in the Moscow Region. Geotechnical Engineering Challenges to Meet Current and Emerging Needs of Society. CRC Press, 2024. Pp. 2400–2404. DOI: 10.1201/9781003431749-460
3. Babushkina, N.E., Lyapin, A.A. Solving the Problem of Determining the Mechanical Properties of Road Structure Materials Using Neural Network Technologies. Advanced Engineering Research (Rostov-on-Don). 2022. 22(3). Pp. 285–292. DOI: 10.23947/2687-1653-2022-22-3-285-292
4. García-Segura, T., Montalbán-Domingo, L., Sanz-Benlloch, A., Pellicer, E. Influence of pavement structure, traffic, and weather on urban flexible pavement deterioration. Sustainability. 2020. 12(22). Article no. 9717. DOI: 10.3390/su12229717
5. Shah, Y.U., Jain, S.S., Devesh Tiwari, Jain, M.K. Development of Overall Pavement Condition Index for Urban Road Network Procedia – Social and Behavioral Sciences. 2013. 104. Pp. 332–341. DOI: 10.1016/j.sbspro.2013.11.126
6. Yang, Z., Wang, L., Cao, D., Miao, Y., Yang H. Structural optimization design of semi-rigid base asphalt pavement using modulus matching criterion and multi-indicator range analysis. Journal of Traffic and Transportation Engineering (English Edition). 2024. 11(1). Pp. 131–159. DOI: 10.1016/j.jtte.2022.10.002
7. Andrews, J.K., Radhakrishnan, V., Koshy, R.Z. Evaluation of Deflection Bowl Parameters in Low-Volume Roads. Journal of Transportation Engineering, Part B: Pavements. 2023. 149(4). Article no. 04023021. DOI: 10.1061/JPEODX.PVENG-1273
8. Larsson, M., Niska, A., Erlingsson, S. Structural Stability of Cycle Paths – Introducing Cycle Path Deflection Bowl Parameters from FWD Measurements. Infrastructures. 2024. 10(1). Article no. 012018. DOI: 10.3390/infrastructures10010007
9. Simonin, J.M., Le Boursicaud, V., Hornych, P. Correction of deflection bowls measured by rolling devices using simple shape function. Transportation Engineering. 2021. 3. Article no. 100050. DOI: 10.1016/j.treng.2021.100050
10. Hamidi, A., Hoff, I., Mork, H. Elastic and viscoelastic back-calculation of pavement layers' moduli using data obtained from traffic speed deflection devices. Construction and Building Materials. 2024. 447. Article no. 138035. DOI: 10.1016/j.conbuildmat.2024.138035
11. Kazemi, N., Saleh, M., Lee, C.L. Effect of nonlinear stress-dependency and cross-anisotropy on the backcalculation outputs from the TSD deflection slopes and the effect on estimated pavement performance. International Journal of Pavement Engineering. 2024. 25(1). Article no. 2417967. DOI: 10.1080/10298436.2024.2417967
12. Coletti, K., Romeo, R.C., Davis, R.B. Bayesian backcalculation of pavement properties using parallel transitional Markov chain Monte Carlo. Computer-Aided Civil and Infrastructure Engineering. 2024. 39(13). Pp. 1911–1927. DOI: 10.1111/mice.13123
13. Kałuża, M., Kotasiński, M. Relationship between deflection basin parameters and backcalculated pavement layer moduli. Archives of Civil Engineering. 2024. 70(2). Pp. 149–162. DOI: 10.24425/ace.2024.149856
14. Tiraturyan, A.N. Backcalculation of Elastic Moduli for Layered Media Based on Dynamic Deformation Analysis (Example of Highways). Russian Journal of Nondestructive Testing. 2024. 60(8). Pp. 947–954. DOI: 10.1134/S1061830924602010
15. Wang, D., Luo, C., Li, J., He, J. Study on Dynamic Modulus Prediction Model of In-Service Asphalt Pavement. Buildings. 2024. 14(8). Article no. 2550. DOI: 10.3390/buildings14082550
16. Xiong, C., Yu, J., Zhang, X., Luo, C. Research on Multi-Parameter Error Model of Backcalculated Modulus Using Abaqus Finite Element Batch Modeling Based on Python Language. Buildings 2024. 14(11). Article no. 3454. DOI: 10.3390/buildings14113454
17. Cao, D. Zhu, M., Zhang, J., Zhao, Y. Feasibility of Dynamic Backcalculation on Pavement Performance Reduction Analysis. Journal of Beijing University of Technology. 2022. 48(6). Pp. 598–607. DOI: 10.11936/bjutxb2021120024
18. Diab, A., You, L., Topa, A. Saboo, N., Sukhija, M. Awed, A. Modeling linear and nonlinear viscoelastic oscillatory rheometric stress-strain hysteresis of asphalt binders. Scientific Reports. 2024. 14. Article no. 28499. DOI: 10.1038/s41598-024-78551-8
19. Noolu, V., Paluri, Y., Chavali, R.V.P., Reddy, B.S.K., Thunuguntla, C.S. Evaluation of a Clayey Soil Stabilized by Calcium Carbide Residue as Pavement Subgrade. Transportation Infrastructure Geotechnology. 9(4). Pp. 403–416. DOI: 10.1007/s40515-021-00185-4
20. Zhou, X., Song, W., Wu, H. Investigation on Fracture Performance of Hot-Mix Asphalt with Reclaimed Asphalt Pavement under Fatigue Loading. Coatings. 2023. 13(8). Article no. 1318. DOI: 10.3390/coatings13081318
21. Zhang, S., Cao, H., Xu, S., Tao, M. Mechanical responses of subgrade with natural hard crust through an accelerated laboratory loading test on pavements model. Case Studies in Construction Materials. 2023. 19. Article no. e02449. DOI: 10.1016/j.cscm.2023.e02449
22. Wu, R., Harvey, J., Lea, J., Jones, D., Louw, S., Mateos, A., Holland, J. Calibration of a Mechanistic-Empirical Cracking Model Using Network-Level Field Data. Transportation Research Record. 2022. 2676(12). 127–139. DOI: 10.1177/03611981221091561
23. Hernandez-Fernandez, N., Harvey, J.T., Underwood, B.S., Ossa-Lopez, A. Pavement Fatigue damage simulations using second-generation mechanistic-empirical approaches. Transportation Research Record. 2022. 2676(1). 1–17. DOI: 10.1177/03611981211027152
24. Mendoza-Sanchez, J.F., Alonso-Guzman, E.M., Martinez-Molina, W., Chavez-Garcia, H.L., Soto-Espitia, R., Delgado-Alamilla, H., Obregon-Biosca, S.A. A Critical Review of Pavement Design Methods Based on a Climate Approach. Sustainability. 2024. 16(16). Article no. 7211. DOI: 10.3390/su16167211
25. Kapustin, V.V., Vladov, M.L., Voznesensky, E.A., Volkov, V.A. Assessment of the Impact of Vibration Loads on Soil Masses and Structures. Seismic Instruments. 2022. 58(1). Pp. S135–S147. DOI: 10.3103/S074792392207012X
26. Fedorov, V.S., Levitsky, V.E., Isaeva, E.A. Basic principles in the theory of force and thermal force resistance of concrete. Structural Mechanics of Engineering Constructions and Buildings. 2022. 18(6). Pp. 584–596. DOI: 10.22363/1815-5235-2022-18-6-584-596
27. Panin, S.V., Moiseenko, D.D., Maksimov, P.V., Vlasov, I.V., Byakov, A.V., Maruschak, P.O., Vinogradov, A. Influence of energy dissipation at the interphase boundaries on impact fracture behaviour of a plain carbon steel. Theoretical and Applied Fracture Mechanics. 2018. 97. Pp. 478–499. DOI: 10.1016/j.tafmec.2017.09.010

28. Sendrowicz, A., Myhre, A.O., Yasnikov, I.S., Vinogradov, A. Stored and dissipated energy of plastic deformation revisited from the viewpoint of dislocation kinetics modelling approach. Acta Materialia, 2022. 237. Article no. 118190. DOI: 10.1016/j.actamat.2022.118190
29. Khazanovich, L., Lukanen, E., Tompkins, D. Evaluation of Bearing Capacity of Low-Volume Roads in Minnesota. Transportation Research Record. 2014. 2433(1). Pp. 79–86. DOI: 10.3141/2433-09

Contacts:

Artem Tiraturyan,
ORCID: https://orcid.org/0000-0001-5912-1235
E-mail: tiraturjanartem@gmail.com

Received 28.02.2025. Approved after reviewing 29.07.2025. Accepted 04.08.2025.

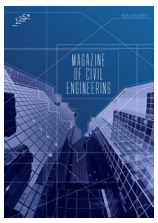

Magazine of Civil Engineering

ISSN 2712-8172

journal homepage: http://engstroy.spbstu.ru/

Research article

UDC 69.05.04

DOI: 10.34910/MCE.136.9

Method for developing a corporate BIM classification system

S.S. Zagorodnii [1]✉, ***M.V. Petrochenko*** [1], ***P.N. Nedviga*** [2]

[1] *Peter the Great St. Petersburg Polytechnic University, St. Petersburg, Russian Federation*

[2] *LLC ID Engineering, St. Petersburg, Russian Federation*

✉ *zagorodniy.serafim@mail.ru*

Keywords: BIM, building information modeling, BIM technologies, classification in construction, construction information classification system, classifier, classifier development method, building lifecycle, civil engineering, CAD

Abstract. The advancement of building information modeling (BIM) technologies is driving the implementation of construction information classification systems (CICS) to structure and standardize data across all phases of a project's lifecycle. This study aims to develop a formalized method for the formation of CICS, incorporate algorithms for selecting expert groups, develop the classification system, and assess its quality using the Delphi method. The proposed approach systematizes the classifier development process and ensures the incorporation of expert opinions, thereby enhancing the objectivity of evaluation and minimizing the risk of subjective distortions. The method consists of multiple iterative development cycles, each accompanied by testing and expert evaluation of the implemented improvements. To assess the effectiveness of the proposed approach, a comparative analysis was conducted, evaluating time and financial expenditures as well as the quality of the classification systems obtained using both the traditional and the newly proposed methods. The method was tested in a real-world production environment, where the CICS developed using the new method received 45 % higher expert ratings compared to traditional methods, while time and financial costs were reduced by 43 %. Thus, the application of the developed method optimizes the formation of CICS and enhances the quality of the final outcome, which is particularly relevant given the increasing complexity of construction projects and the accelerating digitalization of the construction industry.

Citation: Zagorodnii, S.S., Petrochenko, M.V., Nedviga, P.N. Method for developing a corporate BIM classification system. Magazine of Civil Engineering. 2025. 18(4). Article no. 13609. DOI: 10.34910/MCE.136.9

1. Introduction

In recent years, building information modeling (BIM) technologies have significantly transformed the processes of design, construction, and operation of buildings. Unlike traditional methods, where information is distributed among various participants, BIM creates a unified digital model that integrates data on geometry, materials, energy consumption, work schedules, costs, and other characteristics of the building. This model becomes the foundation for decision-making at all stages of the building's lifecycle – from initial design and detailed planning to its operation and subsequent maintenance. Thus, BIM contributes to the full digital transformation of construction processes, ensuring the relevance and availability of real-time information [1, 2]. This significantly enhances the accuracy of design decisions and reduces the number of errors occurring during data transfer between different project participants. As a result, collaboration among architects, engineers, builders, estimators, and other professionals becomes more coordinated and transparent, significantly reducing the time for project development and implementation, lowering costs and enhancing overall efficiency [3, 4].

An important feature of BIM is its ability to model not only the geometric and structural characteristics of buildings but also their operational attributes, such as energy efficiency and material durability, which enables the design of sustainable and energy-efficient buildings [5, 6]. Furthermore, the ability to create digital twins of buildings enables the simulation and testing of various operational scenarios, thereby significantly enhancing the predictability of building behavior over time, including potential emergency situations and repair needs [7, 8].

Against the backdrop of the global digitalization of construction processes, BIM technologies are being increasingly implemented in Russia. In particular, the Russian Federation Government Decree No. 331 dated March 5, 2021, mandates the compulsory use of BIM technologies for developers of multi-apartment buildings during the design phase, starting from July 1, 2024. Despite significant progress, according to data from DOM.RF as of January 14, 2025, only 30 % of Russian developers actively use or pilot BIM technologies, while 70 % of developers have yet to integrate these technologies into their processes [9].

One of the key stages in the implementation of BIM is the development and use of a construction information classification system (CICS), which ensures the structuring of data from information models. CICS is a tool that allows for the organization, systematization, and unification of information across all stages of the life cycle of a project. Unlike the traditional approach, where data tends to be fragmented and difficult to access, the classifier creates a structured and logically organized database, ensuring a unified data representation format. This simplifies access to information and makes it more comprehensible for all project participants, from designers to builders, reducing the likelihood of errors and misunderstandings related to the interpretation of information [10, 11].

Classification also allows for the prompt retrieval of necessary data, significantly speeding up the decision-making process. For example, when creating and managing projects, where each stage requires accurate and timely information, structured data prevents time-consuming searches and eliminates information duplication. In this context, the use of CICS not only increases work efficiency but also significantly improves communication among project participants, reducing the risks of errors and delays in construction and design processes [12]. This approach also fosters better interaction between various systems used for automating construction processes, such as project management systems, software solutions for cost estimation and schedule planning, as well as software for cost assessment and deadline control [13, 14].

Different construction and design processes require specific CICS, which determines their variety. For example, in 2020, a domestic CICS was developed by the Federal center of regulation, standardization and technical assessment of compliance in construction (FTSS FAU) for state expertise compliance. This classifier is responsible for the standardization of data to comply with regulatory requirements in construction. However, for other specialized tasks, such as the creation of work volume statements, the development of work schedules and cost estimation, corporate CICS are required, adapted to specific business processes and the employer's information requirements (EIR). It is important that such corporate classifiers may include not only standard data but also specialized categories unique to particular projects or companies, which allows for accounting for each construction object's distinct characteristics and operational requirements [15, 16].

For the effective implementation of corporate CICS, developers can select from several creation methods at the initial stages of BIM implementation, each characterized by distinct features and requirements. There are four primary strategies for developing corporate CICS: creating a classifier from scratch, modifying the existing CICS developed by FTSS FAU, adapting international classification systems, and using modified CICS from other Russian developers.

Each of these options has its advantages and limitations, and the choice depends on the specific conditions and needs of the developer. For example, creating a CICS from scratch requires significant effort and resources, as it not only involves the development of the classifier structure but also requires a comprehensive analysis of the company’s business processes and coordination with other participants in the construction process. In the case of modifying the CICS developed by FTSS FAU or adapting international classifiers, developers can save significant time since these classifiers already contain standardized data categories; however, they require further customization to fit specific conditions. Modifying CICS from other Russian developers is a less popular option since such classifiers are usually not published in the public domain, limiting the possibility of their use and further adaptation.

In this regard, an important aspect when choosing an approach for developing a corporate CICS is the evaluation of available international classification systems that have already proven their effectiveness on a global scale and can serve as a foundation for adaptation to the needs of the developer [17]. In the global construction practice, there are many well-known and proven classification systems, such as Uniformat, MasterFormat, OmniClass, Uniclass, CoClass, and others, each of which has its own specifics

and area of application. At the international level, these systems have gained wide recognition due to their functional flexibility and ability to meet diverse requirements in construction management [10, 18].

As a result of a comparative analysis of 12 existing classification systems [19], it was found that the CoClass, the CICS developed by FTSS FAU, Uniclass, and OmniClass represent the most suitable solutions for use in the practice of developers. These systems are characterized by a multifaceted structure that uses a functional grouping approach and are open standards in compliance with international norms. Among the systems considered, special attention should be given to OmniClass and Uniclass, which are widely applied in international practice and cover various aspects of construction activities. OmniClass has additional advantages over Uniclass since it includes recognized classifications, such as MasterFormat and Uniformat, which significantly increase its functional flexibility and areas of application. Moreover, OmniClass is supported by one of the leading international organizations in building information modeling – buildingSMART, which confirms its high relevance and alignment with the latest global trends in the standardization of construction information [20].

The CICS, developed by FTSS FAU, is a system designed for structuring and classifying data in the construction sector. The main objective of CICS is the standardization and unification of construction information, which facilitates its processing, storage, and use at various stages of the building life cycle. CICS includes the classification of construction materials, structures, equipment, and processes, enabling the effective organization and integration of information during the design and operational stages [21].

CoClass is a facet-based classification system based on the Swedish system Byggandets Samordning AB (BSAB). Developed in 1972, it was modified and presented as CoClass at the end of the BSAB 2.0 project. The system includes seven primary and two additional tables, with elements encoded using alphanumeric combinations. CoClass supports open standards, object-orientation and complies with ISO 12006-2, making it suitable for international use in the construction industry [22].

Uniclass is an international classification system developed in the United Kingdom in 1997 to organize the stages of the building life cycle. Initially, it adhered to ISO TR 14177, and later it was adapted to ISO 12006-2 [23]. The system consists of 11 tables, allowing the classification of more than 6,500 elements, such as pipelines, that can be used in various systems. Uniclass is applied for asset and facility management, providing an accurate link between construction elements and their functional roles [24].

OmniClass is a classification system covering the entire building life cycle, from design to demolition. Developed in 2006, it includes 15 tables, each with a multi-level coding system for precise identification of elements [25]. OmniClass integrates data from various classifications, such as Uniformat and MasterFormat, and is used for managing construction information within BIM systems. It complies with ISO 12006-2 and serves as the basis for the National Building Information Standard (NBIMS) and Construction Operations Building Information Exchange (COBie) standards.

Despite the possibility of creating corporate CICS based on international systems, such as OmniClass, Uniclass, and others, each of the proposed approaches is inevitably associated with high costs. This is due to the need to adapt international standards to the specifics of national legislation, the requirements of specific enterprises and the peculiarities of their business processes. Moreover, the lack of standardized methodological materials for developing CICS requires significant labor and financial investments, including the involvement of highly qualified specialists and the conduct of comprehensive research and design work [26, 27]. In this regard, the development of a method for forming a corporate CICS represents a relevant scientific task aimed at optimizing and standardizing the process of creating and implementing classification systems in the construction industry.

The aim of this research is to develop a method for forming a corporate CICS. To achieve this aim, the following research objectives have been formulated:

1. Analysis of existing traditional approaches to the development of a CICS.
2. Development of a new method for forming a corporate construction information classifier.
3. Comparative evaluation of the proposed method and the traditional approach in terms of the quality of the resulting classifiers, as well as the time and financial costs associated with each approach.

2. Methods

Currently, there are no detailed methodological guidelines available in open access for the development of corporate classifiers of construction information. Traditional approaches to the formation of such systems are generally based on expert evaluation methods for assessing the quality of CICS, including interviews, brainstorming sessions, and discussions. However, these methods often lack sufficient systematization and may be subject to subjective distortions, which reduces their reliability and objectivity.

In order to address these limitations and improve the quality of CICS development, a more formalized approach is proposed, incorporating structured consensus-building among experts. Within the framework of the proposed method, experts are selected based on objective criteria, such as the competence coefficient, which ensures a highly qualified expert group and enhances the credibility of its conclusions.

In order to minimize the impact of opinion discrepancies and ensure a high degree of objectivity in the evaluation process, the Delphi method is employed. This method is an effective tool for achieving consensus within an expert group as it involves multiple rounds of surveys with feedback, facilitating the refinement and alignment of viewpoints while reducing the influence of personal biases and group pressure. The application of the Delphi method in this approach not only systematizes the expert evaluation process but also enhances the reliability and objectivity of decision-making, making a significant contribution to the improvement of methodological guidelines for developing corporate CICS. However, it should be noted that this method has potential limitations related to its dependence on the qualification and competence of the selected experts, as well as the challenges associated with adapting the method for small companies with limited resources and expert group size. These factors may affect the comprehensiveness and quality of expert assessments, necessitating additional attention when implementing the method across diverse organizational contexts.

The method for forming a corporate CICS is a set of methods, principles, materials, and tools aimed at developing CICS. The method consists of three stages:

1. Selection of the expert group.
2. Development of the corporate CICS.
3. Quality assessment of the developed CICS based on the Delphi method.

The algorithm for selecting an expert group (Fig. 1):

4. Formation of a candidate list for the expert group. Based on methodological guidelines regarding the composition of the expert group and the list of employees from the developer, a candidate list is compiled with a reserve of approximately 10 % of the final number of experts.
5. Surveying the candidates. Candidates provide statements regarding the inclusion of individuals in the expert group. Each candidate may choose to include or exclude themselves from the expert group.
6. Completion of the survey result matrix. A template matrix is filled out with the results of the candidate survey:

$$x_{ij} = \begin{cases} 1, & if\ \ the\ j-th\ expert\ named\ \ the\ i-th\ expert, \\ 0, & otherwise \end{cases} \quad (1)$$

7. Expansion of the candidate list. If individuals not included in the initial list appear in the survey result matrix, the candidate list is updated, and steps 2–3 are repeated.
8. Calculation of the competence coefficient of candidates. The competence coefficient for each candidate is determined based on the data from the survey results matrix:

$$k_i = \frac{\sum_{j=1}^{m} x_{ij}}{\sum_{i=1}^{m}\sum_{j=1}^{m} x_{ij}}, \left(i = \overline{1, m}\right), \quad (2)$$

where k_i is the competence coefficient of the i-th expert, m is the number of experts. The competence coefficients are normalized so that their sum equals one:

$$\sum_{i=1}^{m} k_i = 1. \quad (3)$$

9. Interviewing the candidates. Candidates undergo interviews to assess their attitude toward expertise, constructive thinking, level of teamwork and creativity.
10. Selection and formation of the final expert group list. Based on the obtained individual characteristics of experts and the requirements for them, the final expert group list is compiled.

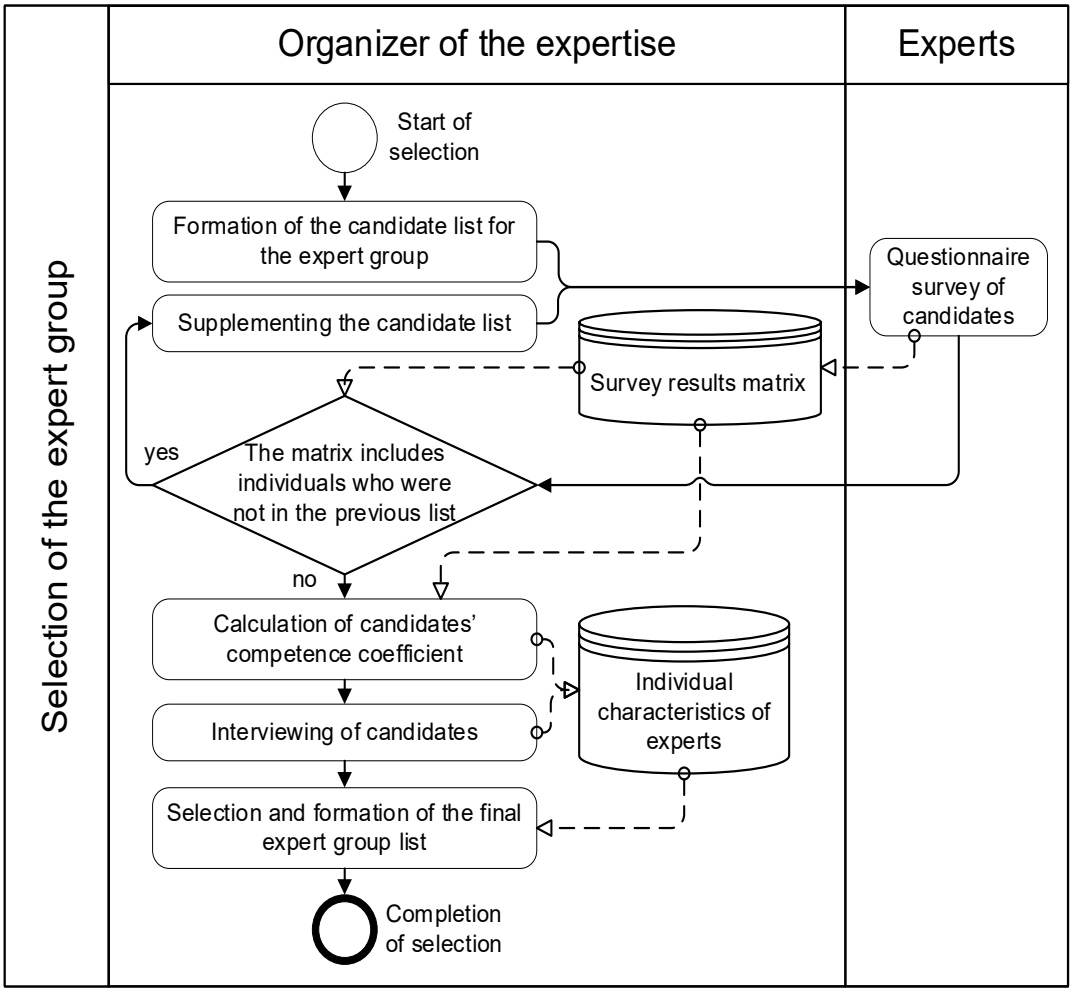

Figure 1. Algorithm for selecting the expert group.

The algorithm for developing a corporate CICS (Fig. 2):

1. Interviewing/brainstorming within the expert group. Interviews and brainstorming sessions are conducted with experts to determine the evaluation characteristics of the developed CICS.
2. Formation of the list of CICS characteristics. Based on methodological guidelines and the results of interviews and brainstorming sessions, a final list of characteristics for evaluating the developed CICS is compiled.
3. Analysis of CICS requirements. Requirements for the CICS are analyzed based on the terms of reference and the compiled list of CICS characteristics.
4. Development of the CICS. The CICS is created based on CICS templates and the CICS requirements.
5. Testing of the CICS. The system undergoes testing using tools for automatic classification of the information model according to the developed CICS.
6. Analysis and correction of CICS errors. If errors are detected during testing, an analysis is conducted, followed by error correction.
7. Expert evaluation of CICS characteristics using the Delphi method (described in detail later).
8. Definition of criteria for the final evaluation of CICS characteristics. After the first expert evaluation of the developed CICS (first iteration), criteria for the final assessment of CICS characteristics are determined.
9. Analysis of expert evaluations of CICS characteristics. If the evaluation of characteristics meets or exceeds the set criteria, the developed CICS is considered to satisfy all requirements, allowing the transition to the implementation phase. Otherwise, step 10 follows.
10. Refinement and modification of the CICS. Based on expert evaluations of CICS characteristics, modifications are made to the system, and the process returns to step 5.

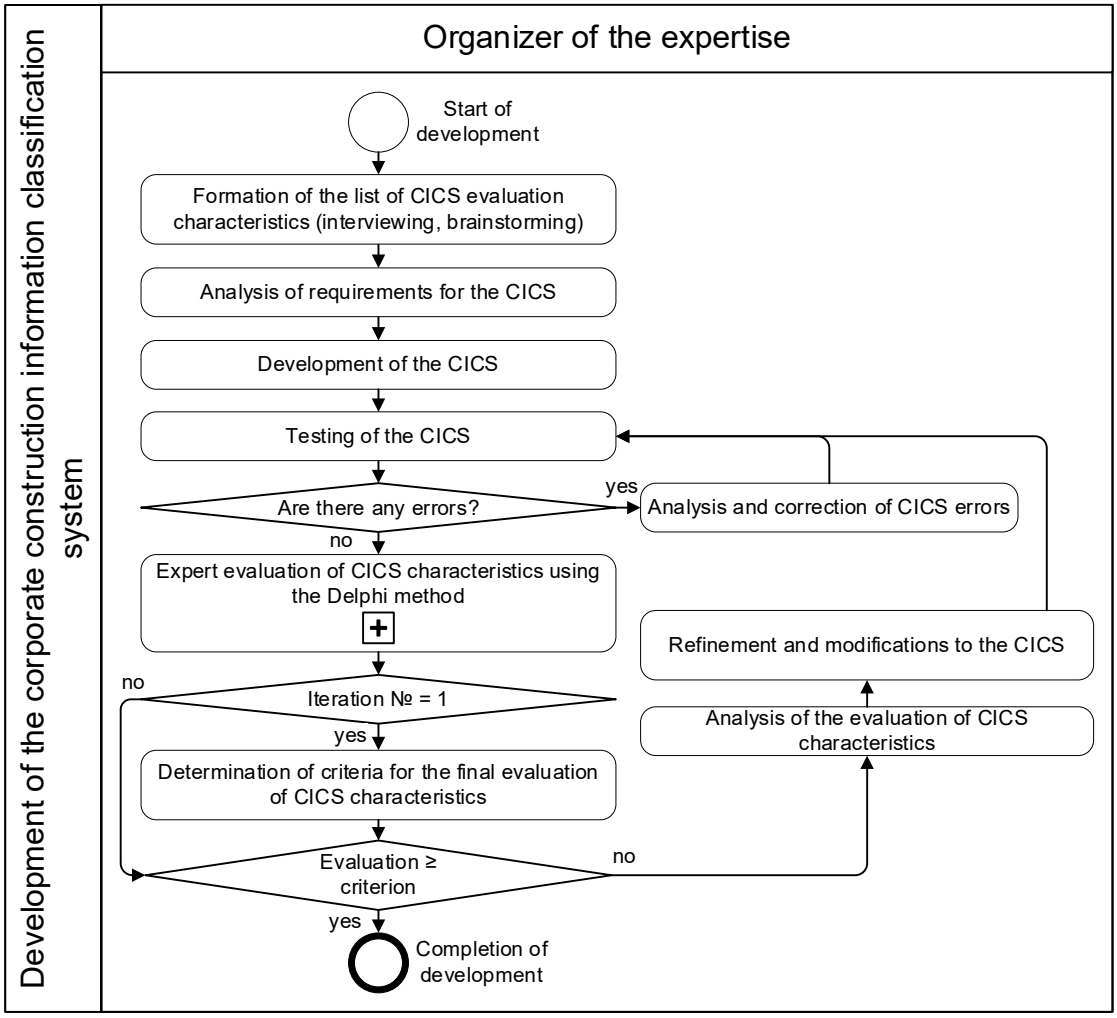

Figure 2. Algorithm for developing the corporate CICS.

Algorithm for evaluating the quality of the developed CICS based on the Delphi method (Fig. 3):

1. Development of a questionnaire for CICS evaluation. Based on questionnaire templates and the list of evaluation characteristics, a questionnaire is created to assess CICS using the Delphi method.
2. Expert survey. Experts are surveyed to obtain expert evaluations of CICS characteristics. The evaluation is conducted using a 10-point scale, where scores (ranks) may repeat. The survey results are compiled into a summary ranking matrix $\left\| r_{ij} \right\| \left(i = \overline{1, n}; j = \overline{1, m} \right)$, where r_{ij} is the rank assigned by the j-th expert to the i-th characteristic.
3. Rank restructuring. Since the summary ranking matrix contains tied ranks (identical ranking numbers), the ranks are recomputed to create a new matrix of recomputed ranks based on the following principles:
   - The expert evaluations of one expert are considered individually.
   - The smallest value is assigned rank 1, the next smallest is assigned rank 2 and so on.
   - The highest rank is assigned to the largest value.
   - If values are identical, they are assigned the same averaged rank (e.g., if two values share 4th and 5th places, both receive rank 4.5).
4. Statistical processing of survey results. The concordance coefficient of expert opinions and Pearson's chi-square statistic are calculated:
   - Concordance coefficient for tied (identical) ranks:

$$W = \frac{12 \cdot S}{m^2 \cdot \left(n^3 - n\right) - m \cdot \sum_{j=1}^{m} T_j}, \quad (4)$$

where S is the sum of squared deviations (calculated based on the recomputed ranks), T_j is the indicator of tied ranks in the j -th ranking (calculated based on initial ranks):

$$S = \sum_{i=1}^{n} \left(\sum_{j=1}^{m} r_{ij} - \bar{r} \right)^2, \quad (5)$$

where $\bar{r}$ is the mean sum of ranks:

$$\bar{r} = \frac{\sum_{i=1}^{n} \sum_{j=1}^{m} r_{ij}}{n}, \quad (6)$$

$$T_j = \sum_{k=1}^{H_j} \left(h_k^3 - h_k \right), \quad (7)$$

where H_j is the number of tied rank groups in the j -th ranking, h_k is the number of tied ranks in the k -th group of tied ranks in the j -th ranking.

- Evaluation of the concordance coefficient. The concordance coefficient W ranges from 0 to 1. A value of $W = 1$ indicates complete agreement among expert opinions, while $W = 0$ signifies the absence of agreement. If $W \geq 0.5$, the level of agreement among expert assessments can be considered satisfactory, whereas for $W \geq 0.7$, the agreement is deemed strong. If $W < 0.5$, expert assessments require refinement, and the process proceeds to step 5 [28].

- Computed value of Pearson's chi-square statistic χ^2_{calc} with $n-1$ degrees of freedom:

$$\chi^2_{calc} = m \cdot \left(n - 1\right) \cdot W. \quad (8)$$

- Expert agreement is considered sufficient if $\chi^2_{calc} \geq \chi^2_{0.05}$, where $\chi^2_{0.05}$ is the critical value of Pearson's chi-square test at the 5 % significance level. If $\chi^2_{calc} < \chi^2_{0.05}$, it indicates a lack of agreement among experts, making the final ranking results unreliable. In this case, an additional expert review is necessary, involving a larger number of experts and broadening their specialization, proceeding to step 5. Otherwise, proceeding to step 7 [28].

5. Compilation of a report indicating the dispersion of opinions. Based on the results of statistical processing, a report is generated that includes the dispersion of expert assessments.

6. Surveying the experts. Experts are provided with a report on the results of the previous survey and are subjected to a repeated survey. Experts whose assessments significantly deviate from the majority are required to justify their opinion or revise their decision with an explanation. Then, the process returns to step 3.

7. Comparison of expert evaluations for each CICS characteristic over the last two iterations of CICS development using the Mann–Whitney criterion. To determine the impact of the implemented improvements on the quality of CICS, a null hypothesis is formulated for each characteristic: there are no statistically significant differences between the expert evaluations of a CICS characteristic after the last two iterations of CICS development. To test this hypothesis, two independent samples of expert evaluations for each CICS characteristic are compared using the Mann–Whitney criterion:

   - Two samples of expert assessments for a single characteristic after the final and penultimate iteration of CICS development are taken. These samples are conceptually combined into one group, and the ranks within this group are reassigned according to the principle outlined in step 3.

   - The sum of the reassigned ranks is calculated separately for each sample.

- The sample with the highest sum of ranks is identified.
- The empirical value of the Mann–Whitney U_{emp}-statistic is calculated using the formula:

$$U_{emp} = n_1 \cdot n_2 + \frac{n_x \cdot (n_x + 1)}{2} - T_x, \quad (9)$$

where n_1, n_2 are the numbers of expert assessments in the first and second sample, respectively; n_x is the number of expert assessments in the sample with the highest sum of ranks; T_x is the highest sum of ranks.

- The empirical value of the Mann–Whitney U_{emp}-statistic is compared with the critical value U_{crt}. If the empirical value U_{emp} is less than or equal to the critical value (U_{crt}), the existence of statistically significant differences between expert assessments of CICS characteristic in the compared samples is recognized (i.e., the alternative hypothesis H1 is accepted). If the empirical value is greater than the critical value, the null hypothesis of no statistically significant differences is accepted. The significance of the differences increases as the empirical value U_{emp} decreases.
- Thus, the null hypothesis is tested for each CICS characteristic. If the null hypothesis of no statistically significant differences is supported for a characteristic, the latest improvements in CICS have not affected its quality, and this factor should be taken into account in future improvements. If the alternative hypothesis indicating the presence of statistically significant differences is supported, the latest improvements in CICS have influenced its quality.

8. Determination of generalized assessments of characteristics. Based on the results of statistical processing, generalized assessments of the characteristics are determined.
9. Report generation. A report is compiled on the assessment of the developed CICS.

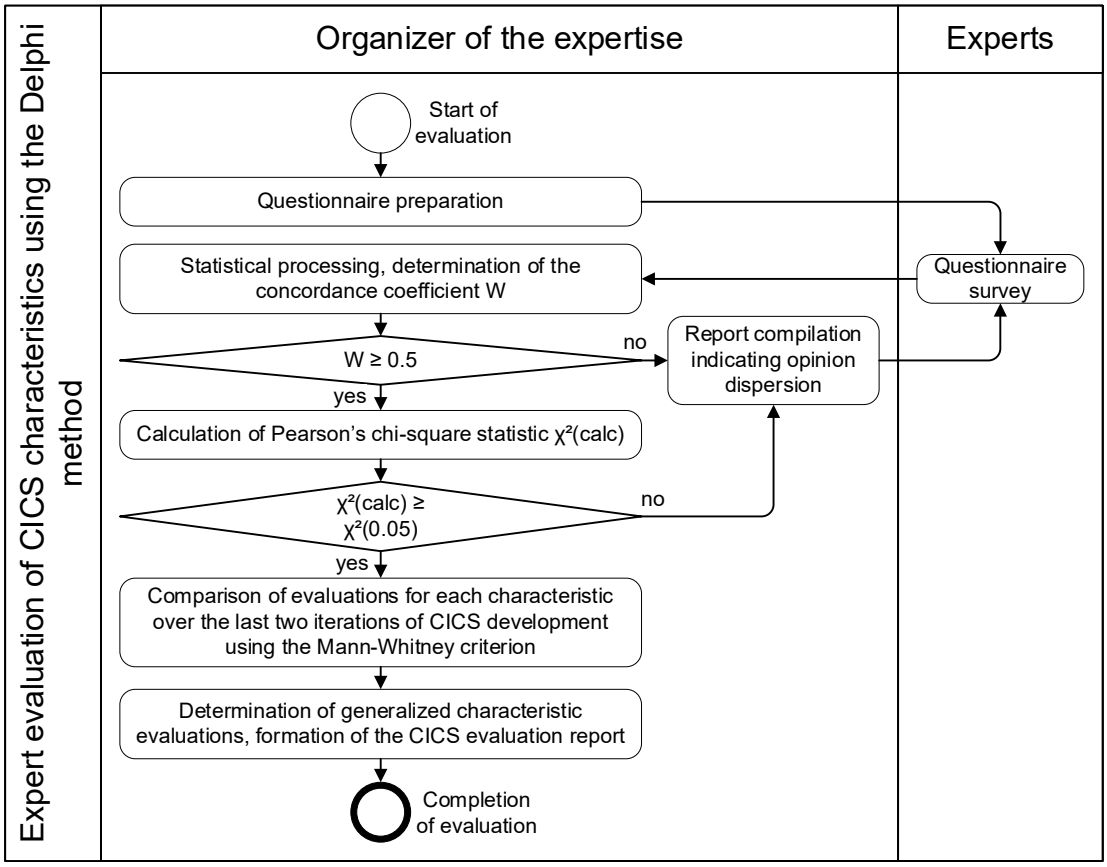

Figure 3. Algorithm for evaluating the quality of the developed CICS based on the Delphi method.

The validation of the developed method was conducted in a real-world production environment, specifically in the project department of the developer. As part of the comparative analysis, two versions of CICS were developed using different approaches: the traditional method and the proposed method, applied in two iterations.

To evaluate the effectiveness of the proposed approach and facilitate its further optimization, the following steps were implemented:

- Empirical determination of the time costs associated with classifier development using both the traditional and proposed methods.
- Calculation of financial costs for CICS development based on data on labor time expenditures, as well as information from Rosstat on the average monthly nominal accrued wages of employees working in information technology for the construction sector in Moscow for the period from January to October 2024.
- Evaluation of the quality of CICS developed using the traditional and proposed methods based on the Delphi method.
- Comparison of expert assessments of CICS characteristics formed using the traditional and proposed methods by applying the Mann–Whitney criterion. This made it possible to identify the impact of the developed method on the quality of the created CICS. During the analysis, a null hypothesis was initially formulated for each CICS characteristic, stating that there are no statistically significant differences between expert assessments of CICS characteristics obtained using the traditional and developed methods. The comparison was conducted following the principles outlined in step 7 of the “Algorithm for evaluating the quality of the developed CICS based on the Delphi method”, ensuring the objectivity and reproducibility of the obtained results.

3. Results and Discussion

As a result of the validation of the developed method, 15 candidates for the expert group were identified, and the competence coefficients of the candidates were determined (Table 1). Based on these coefficients, an expert group consisting of 12 members was formed, including design engineers, technical customer representatives, and BIM specialists (Table 2).

Table 1. Competence coefficients of candidates.

k_1	k_2	k_3	k_4	k_5	k_6	k_7	k_8	k_9	k_{10}	k_{11}	k_{12}	k_{13}	k_{14}	k_{15}
0.07	0.08	0.04	0.07	0.07	0.08	0.07	0.07	0.05	0.06	0.08	0.07	0.07	0.07	0.05

Table 2. Composition of the expert group.

Expert position	Expert department	Quantity
BIM coordinator/manager	BIM department	4
Engineer of production and technical department	Development department (technical customer)	2
Design engineer for construction organization project	Design department	2
Architect	Design department	1
Design engineer for electrical systems and equipment	Design department	1
Estimating engineer	Design department	2
	Total	12

Based on the results of interviews and brainstorming sessions with the expert group, a final list of characteristics for evaluating the developed CICS was compiled (Table 3).

Table 3. List of characteristics for evaluating the developed CICS.

№	Name	Description
C1	Hierarchy	The structure of the classifier should be organized in a hierarchy, where categories and elements are logically distributed across levels
C2	Logic and ease of use	The classifier should be intuitive and user-friendly, with a clear and logical structure that is easily perceived by users
C3	Scalability and flexibility	The classifier should support the possibility of expansion by adding new categories or elements and be flexible for adaptation to new requirements
C4	Compatibility of facets (aspects)	The ability to use different facets or aspects of classification within the same context without creating data conflicts
C5	Independence of facets (aspects)	Separation of classification aspects so that they are independent of each other and can function autonomously
C6	Compliance of information presentation aspects with user needs	Classification aspects should be oriented towards the needs and requirements of end-users, providing maximum value and convenience
C7	Ability to divide according to required sections	The classifier should support the ability to divide elements into various required categories and sections for detailed work
C8	Consistency with regulations and standards	The classifier must comply with current regulatory requirements and standards, ensuring conformity with industry and legal norms
C9	Rationality of using categories for elements modeled through other categories	When categories other than the primary ones are used for modeling elements, this should be justified in terms of logic and functionality
C10	Appropriateness of linking the classification parameter to type/instance	Classification parameters should be linked to the type or instance depending on their significance and the features of the objects they are intended for
C11	Consistency of parameter usage by specialists from different departments	Classification parameters should be coordinated between departments to avoid conflicts and misunderstandings in data usage
C12	Sufficient detail for linking with cost estimate items	The classifier should provide sufficient detail for accurate linking with cost estimate items, without unnecessary complexity or loss of accuracy
C13	Minimization of redundant detail for linking with cost estimate items	Redundant detail should be minimized to keep the classifier efficient and avoid overloading it with unnecessary data
C14	Sufficient detail for linking with work schedule positions	The classifier should provide sufficient detail for accurate linking with work schedule positions, without unnecessary complexity or loss of accuracy
C15	Minimization of redundant detail for linking with work schedule positions	Redundant detail should be minimized to keep the classifier efficient and avoid overloading it with unnecessary data
C16	Sufficient detail for linking with technical customer requests	The classifier should provide sufficient detail for accurate linking with technical customer requests, without unnecessary complexity or loss of accuracy
C17	Minimization of redundant detail for linking with technical customer requests	Redundant detail should be minimized to keep the classifier efficient and avoid overloading it with unnecessary data
C18	Sufficient detail for linking with expert requirements	The classifier should provide sufficient detail for accurate linking with expert requirements, without unnecessary complexity or loss of accuracy
C19	Minimization of redundant detail for linking with expert requirements	Redundant detail should be minimized to keep the classifier efficient and avoid overloading it with unnecessary data

To evaluate the effectiveness of the developed method, two versions of CICS were created: one using the traditional approach and the other developed through two iterations of the proposed method. The results of the quality assessment of the created CICS, conducted using the Delphi method – comparing the traditional method, the proposed method after the first iteration, and the proposed method after the second iteration – are presented in Table 4 and illustrated by histograms in Fig. 4.

Table 4 shows that in all three cases, the concordance coefficients were greater than 0.5, and the calculated Pearson criteria ($\chi^2_{calc} \geq \chi^2_{0.05}$) indicated that the degree of consistency in expert evaluations in all three cases can be considered satisfactory and sufficient.

Table 4. Quality evaluations of the developed CICS based on the Delphi method.

№ of charac-teristic	Traditional method		Proposed method (1st iteration)		Proposed method (2nd iteration)	
	Weight of characteristic	Average rank	Weight of characteristic	Average rank	Weight of characteristic	Average rank
C1	0.083	6.92	0.086	7.42	0.089	9.50
C2	0.034	4.75	0.045	5.75	0.035	7.67
C3	0.049	5.25	0.056	6.17	0.075	8.92
C4	0.091	7.17	0.074	6.92	0.068	8.67
C5	0.065	6.00	0.070	6.67	0.077	9.00
C6	0.061	5.75	0.056	6.17	0.060	8.42
C7	0.043	5.08	0.026	4.92	0.030	7.50
C8	0.082	6.92	0.076	7.00	0.073	8.83
C9	0.040	4.92	0.029	5.08	0.061	8.42
C10	0.045	5.08	0.045	5.75	0.057	8.33
C11	0.045	5.17	0.061	6.33	0.034	7.67
C12	0.082	6.83	0.080	7.17	0.070	8.83
C13	0.011	3.25	0.011	3.92	0.025	7.33
C14	0.049	5.33	0.051	6.00	0.042	7.92
C15	0.022	4.08	0.015	4.33	0.011	6.67
C16	0.059	5.75	0.072	6.75	0.078	9.08
C17	0.026	4.33	0.029	4.92	0.046	8.00
C18	0.067	5.92	0.067	6.67	0.035	7.67
C19	0.046	5.17	0.050	5.92	0.036	7.67
	W	0.617	W	0.618	W	0.608
	χ^2_{calc}	133.191	χ^2_{calc}	133.381	χ^2_{calc}	131.237
	$\chi^2_{0.05}$	28.869	$\chi^2_{0.05}$	28.869	$\chi^2_{0.05}$	28.869
	Number of iterations of expert evaluations	3	Number of iterations of expert evaluations	3	Number of iterations of expert evaluations	2
	Weighted average rank	5.86	Weighted average rank	6.38	Weighted average rank	8.50

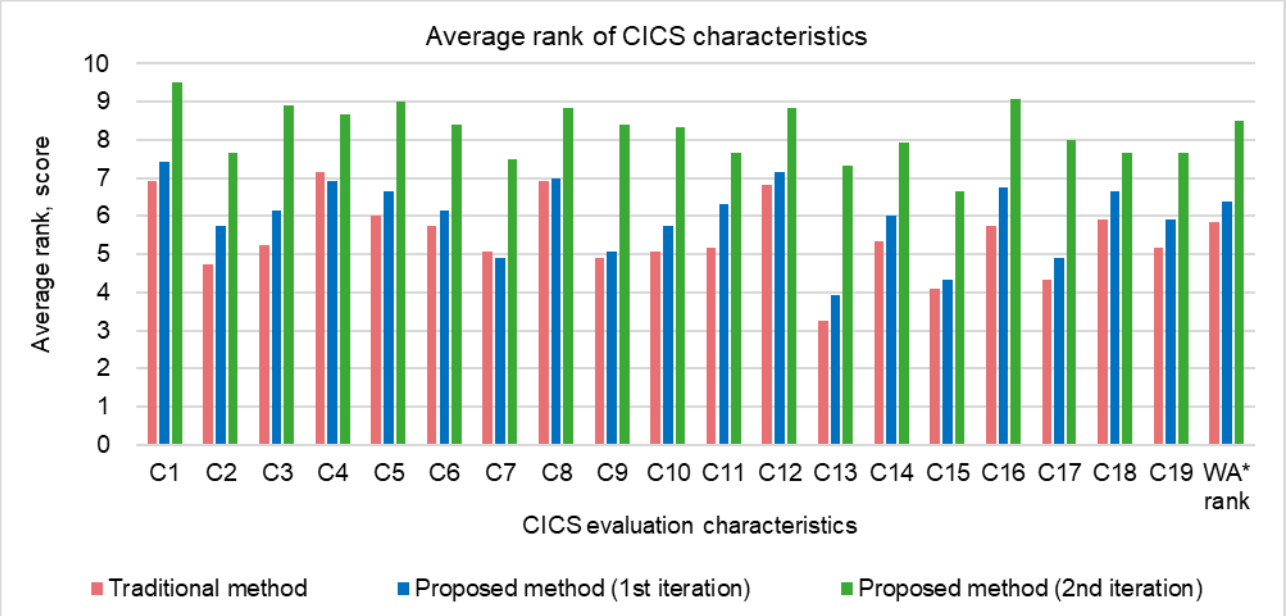

Figure 4. Average rank of CICS characteristics (*WA rank – weighted average rank).

Based on the histograms of the average ranks of CICS evaluation characteristics (Fig. 4), the following hypotheses were formulated:

1. When forming the CICS using the proposed method after the second iteration, the quality of the CICS improved across all characteristics.

2. When forming the CICS using the proposed method, a higher quality of the CICS was achieved across all characteristics compared to the traditional method.

To prove these hypotheses, the corresponding null hypotheses were formulated:

1. There are no statistically significant differences between the expert evaluations of CICS characteristics after the last two iterations of CICS development using the proposed method.
2. There are no statistically significant differences between the expert evaluations of CICS characteristics obtained using the traditional and proposed methods.

To test the hypotheses, we performed a comparison of two independent samples of expert evaluations for each CICS characteristic using the Mann–Whitney test (Table 5). From the table, it is evident that the obtained empirical value of the Mann–Whitney U_{emp}-statistic for each characteristic are lower than the critical value $U_{crt} = 42$, indicating the existence of statistically significant differences between the expert evaluations of CICS characteristics in the compared samples (i.e., the alternative hypotheses are accepted).

Table 5. Hypothesis testing using the Mann–Whitney test.

№ of charac-teristic	Hypothesis 1			Hypothesis 2		
	Sum of sample ranks		U_{emp}	Sum of sample ranks		U_{emp}
	Proposed method (1st iteration)	Proposed method (2nd iteration)		Proposed method (2nd iteration)	Traditional method	
C1	78.0	222.0	0	222	78	0
C2	80.0	220.0	2.0	222	78	0
C3	78.0	222.0	0	222	78	0
C4	84.0	216.0	6.0	216	84	6
C5	79.5	220.5	1.5	222	78	0
C6	81.5	218.5	3.5	222	78	0
C7	78.0	222.0	0	222	78	0
C8	86.0	214.0	8.0	214	86	8
C9	78.0	222.0	0	222	78	0
C10	78.0	222.0	0	222	78	0
C11	96.0	204.0	18.0	222	78	0
C12	90.5	209.5	12.5	212	88	10
C13	78.0	222.0	0	222	78	0
C14	90.5	209.5	12.5	222	78	0
C15	78.0	222.0	0	222	78	0
C16	81.0	219.0	3.0	222	78	0
C17	79.5	220.5	1.5	222	78	0
C18	98.0	202.0	20.0	218	82	4
C19	85.5	214.5	7.5	222	78	0
		U_{crt}	42		U_{crt}	42

Thus, the hypotheses we proposed are confirmed:

1. When creating the CICS using the proposed method, the improvements adopted after the first iteration contributed to the enhancement of the CICS quality across all characteristics.
2. When creating the CICS using the proposed method, a higher quality of the CICS was achieved across all characteristics compared to the traditional method.

As a result of testing the proposed method, the empirical time and financial costs for the development of the classifier using both the traditional and proposed methods were determined (Table 6). The cost reduction ratio of the proposed method amounted to:

$$d_{CRR} = \frac{T_{TM} - T_{PM}}{T_{TM}} \cdot 100\% = \frac{536 - 304}{536} \cdot 100\% = 43\%, \quad (10)$$

where T_{TM}, T_{PM} are the time or financial costs for the development of the CICS using the traditional method (TM) and the proposed method (PM), respectively.

Table 6. Time and financial costs for the development of CICS.

	Time costs, hours	Average daily salary, RUB	Financial costs, RUB
Traditional method	536	1,049	70,283
Proposed method	304	1,049	39,862

A theoretical study was also conducted to examine the relationship between the cost reduction ratio of the proposed method and the number of iterations in the development of the CICS (simulation of the processes of expansion and refinement of the CICS). From the graph (Fig. 5), it is evident that up to six iterations, the highest increase in the cost reduction ratio is observed, after which the growth slows down. The most cost-effective application of the proposed method occurs in processes with two iterations, with a reduction in costs of 50 %. This method is suitable for the development of a corporate CICS, typically involving between two and five iterations before commissioning.

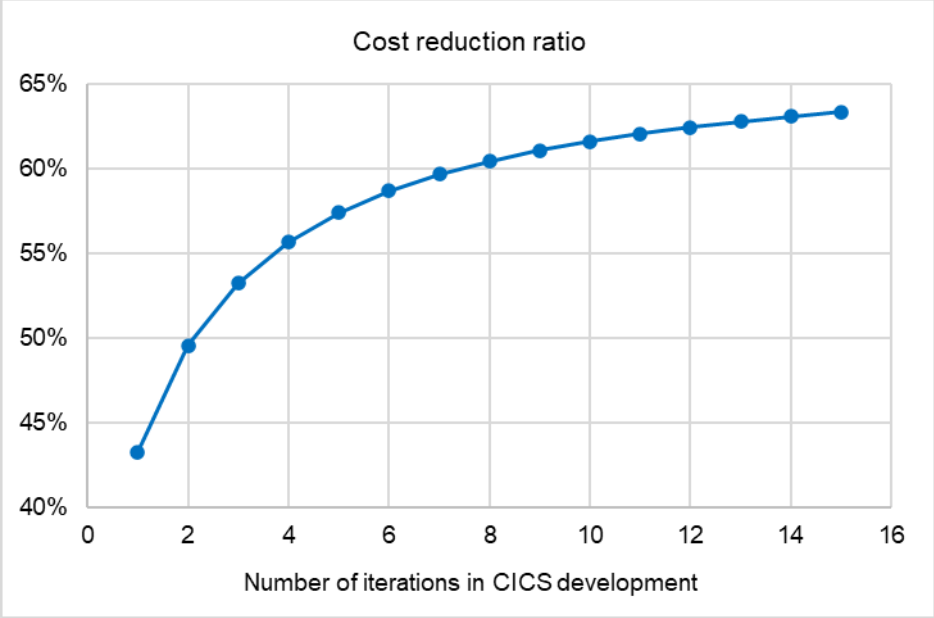

Figure 5. Dependence of the cost reduction ratio of the proposed method on the number of iterations in CICS development.

It is important to emphasize the originality of the present study. Despite a comprehensive literature review, no studies directly comparable to the presented results were identified at the time of this research. Consequently, a comparative analysis with findings from other authors could not be conducted.

4. Conclusions

The result of the conducted research is the developed method for forming a corporate CICS, which ensures improved quality, reduced time, and financial costs in the development and adaptation of the CICS compared to traditional approaches.

The main results obtained during the testing of the method are as follows:

- The weighted average expert evaluation of the CICS quality, formed using the developed method, was 8.50 points, which is 45 % higher than when using the traditional method (5.86 points), confirming the higher quality of the developed CICS.
- The time costs for creating the CICS using the proposed method amounted to 304 hours, while the traditional method required 536 hours. The reduction in costs using the new method was 43 %.
- The financial costs for the development of the CICS using the proposed method were 39,862 rubles, which is 43 % lower than the costs of the traditional method (70,283 rubles).

Additionally, a theoretical study was conducted to examine the relationship between the cost reduction ratio of the proposed method and the number of iterations in the development of the CICS. The analysis showed that the greatest increase in the cost reduction ratio occurs within the range of up to six iterations, after which the growth rate slows down. The optimal application of the proposed method is in processes involving between two and five iterations, where the cost reduction ratio of at least 50 % is achieved.

The application of the proposed method significantly reduces the costs associated with the development and maintenance of the CICS, while providing system flexibility in the context of the need for subsequent adjustments and expansions. The method is most effective when developing CICS with a larger number of iterations, which is particularly relevant for corporate systems that are in the stage of active development and adaptation to organizational needs.

In addition, the proposed method has the potential for implementation in various organizations and adaptation to diverse contexts, which expands its practical applicability across different sectors of the construction industry and allows for the consideration of specific requirements and features of corporate processes. It is particularly suitable for development companies and design bureaus that need to create and expand their own construction information classifiers for project and resource management. The method can also be effectively applied in companies that are at the initial stages of implementing BIM technologies, helping them to approach the formation and development of classification systems in a systematic manner with minimal time and financial expenditures.

References

1. Ariono, B., Wasesa, M., Dhewanto, W. The Drivers, Barriers, and Enablers of Building Information Modeling (BIM) Innovation in Developing Countries: Insights from Systematic Literature Review and Comparative Analysis. Buildings. 2022. 12(11). Article no. 1912. DOI: 10.3390/BUILDINGS12111912
2. Nguyen, T.D., Adhikari, S. The Role of BIM in Integrating Digital Twin in Building Construction: A Literature Review. Sustainability. 2023. 15(13). Article no. 10462. DOI: 10.3390/SU151310462
3. Wang, K., Zhang, C., Guo, F., Guo, S. Toward an Efficient Construction Process: What Drives BIM Professionals to Collaborate in BIM-Enabled Projects. Journal of Management in Engineering. 2022. 38(4). Article no. 04022033. DOI: 10.1061/(ASCE)ME.1943-5479.0001056
4. Qiu, Q., Zhou, X., Zhao, J., Yang, Y., Tian, S., Wang, J., Liu, J., Liu, H. From sketch BIM to design BIM: An element identification approach using Industry Foundation Classes and object recognition. Building and Environment. 2021. 188. Article no. 107423. DOI: 10.1016/J.BUILDENV.2020.107423
5. Gong, S. Performance Analysis of Application of BIM Technology and Two-Way Progressive Optimization Algorithm in Energy-Saving Design of Residential Buildings Based on BIM Technology. Journal of Electrical Systems. 2024. 20(4s). Pp. 252–265. DOI: 10.52783/JES.1911
6. Bhilare, S., Khatri, D., Rangnekar, S., Chen, Q. Using BIM to Facilitate Generative Target Value Design for Energy Efficient Buildings. Proceedings of the International Symposium on Automation and Robotics in Construction. Chennai, 2023. Pp. 667–674. DOI: 10.22260/ISARC2023/0093
7. Lemian, D., Bode, F. Digital twins in the building sector: Implementation and key features. E3S Web of Conferences. 2025. 608. Article no. 05004. DOI: 10.1051/E3SCONF/202560805004
8. Zhou, X., Sun, K., Wang, J., Zhao, J., Feng, C., Yang, Y., Zhou, W. Computer Vision Enabled Building Digital Twin Using Building Information Model. IEEE Transactions on Industrial Informatics. 2023. 19(3). Pp. 2684–2692. DOI: 10.1109/TII.2022.3190366
9. Tekhnologii informatsionnogo modelirovaniia | EISZHS [Information modeling technologies | EISZHS] [Online]. URL: https://clck.ru/3HS2gr (date of application: 10.02.2025).
10. Royano, V., Gibert, V., Serrat, C., Rapinski, J. Analysis of classification systems for the built environment: Historical perspective, comprehensive review and discussion. Journal of Building Engineering. 2023. 67. Article no. 105911. DOI: 10.1016/J.JOBE.2023.105911
11. Guven, G., Arceo, A., Bennett, A., Tham, M., Olanrewaju, B., McGrail, M., Isin, K., Olson, A.W., Saxe, S. A construction classification system database for understanding resource use in building construction. Scientific Data. 2022. 9(1). Article no. 42. DOI: 10.1038/s41597-022-01141-8
12. Petrov, A.E., Poshev, A.U.B. Increasing the productivity of construction projects with the use of technology BIM and blockchain. Modern Science: actual problems of theory and practice. Series: Natural and Technical Sciences. 2024. 7/2. Pp. 148–153. DOI: 10.37882/2223-2966.2024.7-2.26
13. Cerezo-Narváez, A., Pastor-Fernández, A., Otero-Mateo, M., Ballesteros-Pérez, P. Integration of Cost and Work Breakdown Structures in the Management of Construction Projects. Applied Sciences. 2020. 10(4). Article no. 1386. DOI: 10.3390/APP10041386
14. Luo, H., Gao, G., Huang, H., Ke, Z., Peng, C., Gu, M. A Geometric-Relational Deep Learning Framework for BIM Object Classification. Lecture Notes in Computer Science. 2022. 13807. Computer Vision – ECCV 2022 Workshops. ECCV 2022. Pp. 349–365. DOI: 10.1007/978-3-031-25082-8_23
15. Gelder, J.E. The Design And Development Of A Classification System For BIM. WIT Transactions on The Built Environment. 2015. 149. Pp. 477–491. DOI: 10.2495/BIM150391
16. Chung, T., Bok, J.H., Ji, H.W. A Multi-Story Expandable Systematic Hierarchical Construction Information Classification System for Implementing Information Processing in Highway Construction. Applied Sciences. 2023. 13(18). Article no. 10191. DOI: 10.3390/APP131810191
17. Lou, E.C.W., Goulding, J.S. Building and Construction Classification Systems. Architectural Engineering and Design Management. 2008. 4(3–4). Pp. 206–220. DOI: 10.3763/AEDM.2008.0079
18. Petrochenko, M.V., Nedviga, P.N., Kukina, A.A., Strelets, K.I., Sherstyuk, V. V. Machine learning model for the BIM classification in IFC format. Magazine of Civil Engineering. 2024. 126(2). Article no. 12602. DOI: 10.34910/MCE.126.2
19. Zagorodnii, S.S., Nedviga, P.N. Otsenka sootvetstviia sistem klassifikatsii stroitel'noi informatsii trebovaniiam zastroishchika [Assessment of compliance of construction information classification systems with the requirements of the developer]. Sbornik materialov vserossiiskoii konferentsii NEDELIA NAUKI ISI [Proceedings of the All-Russian Conference ISI SCIENCE WEEK]. 2024. Pp. 35–37. [Online]. URL: https://www.elibrary.ru/item.asp?id=67919329 (date of application: 12.02.2025).
20. BuildingSMART International. [Online]. URL: https://clck.ru/3JkALA (date of application: 15.02.2025).

21. Volkodav, V.A., Volkodav, I.A. Development of the structure and composition of a building information classifier towards the application of BIM technologies. Vestnik MGSU. 2020. 15(6). Pp. 867–906. DOI: 10.22227/1997-0935.2020.6.867-906
22. Svensk Byggtjanst. Om CoClass – nya generationen BSAB [About CoClass – the new generation BSAB]. 2019. [Online]. URL: https://coclass.byggtjanst.se/about#about-coclass (date of application: 01.03.2025).
23. Crawford, M., Cann, J., O'Leary, R. Uniclass: Unified Classification for the Construction Industry. 1st edn. RIBA Publications Ltd. London, 1997.
24. Pupeikis, D., Navickas, A.A., Klumbyte, E., Seduikyte, L. Comparative Study of Construction Information Classification Systems: CCI versus Uniclass 2015. Buildings. 2022. 12(5). Article no. 656. DOI: 10.3390/BUILDINGS12050656
25. CSI. OmniClassTM: A Strategy for Classifying the Built Environment. Introduction and User's Guide. 1st edn. 2006.
26. Saleeb, N., Marzouk, M., Atteya, U. A comparative suitability study between classification systems for BIM in heritage. International Journal of Sustainable Development and Planning. 2018. 13(1). Pp. 130–138. DOI: 10.2495/SDP-V13-N1-130-138
27. Lu, S., Yu, Z., Zhou, Z., Wei, L., Luo, Z. BIM Information Classification and Codification for manufacturing Heritage Buildings. Journal of Physics: Conference Series. 2022. 2261(1). Article no. 012020. DOI: 10.1088/1742-6596/2261/1/012020
28. Skvortsov, S. V., Khryukin, V.I., Skvortsova, T.S. Consistency analysis of specialist views under conditions of contradictory expert estimates of project alternatives. Vestnik of Ryazan State Radio Engineering University. 2021. 76. Pp. 53–64. DOI: 10.21667/1995-4565-2021-76-53-64

Information about the authors:

Serafim Zagorodnii,
ORCID: https://orcid.org/0009-0009-7500-7307
E-mail: zagorodniy.serafim@mail.ru

Marina Petrochenko, *PhD in Technical Sciences*
ORCID: https://orcid.org/0000-0002-4865-5319
E-mail: mpetroch@mail.ru

Pavel Nedviga,
E-mail: pavel.nedviga@gmail.com

Received 05.04.2025. Approved after reviewing 14.06.2025. Accepted 16.06.2025

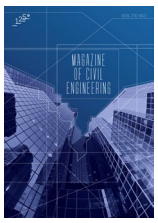

Magazine of Civil Engineering

ISSN 2712-8172

journal homepage: http://engstroy.spbstu.ru/

Research article

UDC 624.011.1

DOI: 10.34910/MCE.136.10

Numerical modeling of connected and disconnected piled raft foundation under seismic loading in clayey soil

M.O. Karkush ✉, ***S.N. Nafel***

University of Baghdad, Bagdad, Iraq
✉ *mahdi_karkush@coeng.uobaghdad.edu.iq*

Keywords: connected piled raft, disconnected piled raft, cushion, seismic loading, clayey soil, numerical analysis

Abstract. The disconnected piled raft foundation (DCPRF) is one of the newly introduced type of foundations in geotechnical engineering, which greatly reduces the moment and stress on the pile head. In addition, this type of foundation is an ideal choice in areas with seismic activity due to the presence of cushion material between the raft and the piles. This paper aims to present a numerical model in PLAXIS-3D software to simulate the behavior of the connected piled raft foundations (CPRFs) and DCPRFs with the same number and pattern of the piles, under the influence of seismic loading in clayey soil. The study will depend on the earthquake that struck Iraq in November 2017 in the Halabja region of strength 7.3 on Richter scale with PGA (0.1 g). To verify the results of the proposed numerical model, the settlement calculated from numerical is compared with field measurement for the Messe-Torhaus building in Frankfurt and the difference was 2 %. The horizontal displacement of the raft in the CPRF is less than the horizontal displacement of the raft in the DCPRF during seismic loading by 15 %. The vertical displacement in the DCPRF decreased by 7 % in comparison with the CPRF. For the DCPRF, the bending moment value is approximately equal to zero at the head of the piles, and the maximum bending moment value was in the middle of the pile.

Citation: Karkush, M.O., Nafel, S.N. Numerical modeling of connected and disconnected piled raft foundation under seismic loading in clayey soil. Magazine of Civil Engineering. 2025. 18(4). Article no. 13610. DOI: 10.34910/MCE.136.10

1. Introduction

When the raft foundation bearing capacity is sufficient to sustain the superstructure, but the raft's total and differential settlements exceed the allowable limit, a small number of piles can be used to control the settlements [1–3]. The pile heads are usually structurally connected to the raft to make a rigid connection. These piles should have sufficient bearing capacity and sufficient safety factor to avoid structural failure. Because high axial stress can develop in the piles and lateral forces from wind and earthquakes can destroy connections, even though structural failure can be prevented by using high-strength materials with a high factor of safety, this technique may be uneconomical. A new solution for solving such concerns has recently been presented, which involves isolating the raft from the pile with soil material that is strong enough to sustain the stresses imposed on it while also preventing or reducing the load seismic waves or shear forces on the pile's head. This void may be filled with suitable materials, which can be selected depending on the circumstances, such as types of loading and availability of materials [4]. Since the piles are not structurally attached to the raft, a smaller factor of safety may be utilized to protect the pile materials and prevent structural damage (as low as 1.3) [4–6]. As a result of the previous works, the disconnected piled raft foundation (DCPRF) that contains a cushion between the pile and the raft will increase the carrying load capacity of the foundation more than the connected piles group foundation. At the same time, it may be greater in carrying the loads compared with the connected piled raft foundation (CPRF), and this method leads to more economical results than others. Also, disconnected piles can be

used in buildings subjected to high horizontal loads, such as earthquakes or winds, especially in buildings containing basements and in buildings with weak soil that need to be strengthened, such as river sidewalks and ports.

Many researchers have studied the behavior of disconnected piles using the finite element method. Several characteristics (parametric study) of the parameters of this method were studied, such as pile stiffness, raft stiffness, cushion thickness, raft thickness, the behavior of the disconnected piled raft, and the distribution of axial loads on it. Wong et al. [4] are the first who proposed the DCPRF method. Cao et al. [7] studied the special properties of this method and the advantages and disadvantages of such a technique. According to Liang et al. [8] and Lee et al. [9], the cushion placed between the pile and the raft is either a sandy or a gravel soil material of high density to reduce the settlement that occurs in it. This cushion is considered a layer that transfers the loads to the soil and the piles below the mat and contributes to a certain amount of bearing the loads and the way of distributing the loads on the piles.

This research presents verification of the related connected piled raft with data measured in the field concerning the behavior of the connected piled raft under a building in Frankfurt subjected to static loading. After that, a numerical model is proposed to simulate the behavior of such a building under seismic loading and supported by DCPRFs. Then, a parametric study was presented for a DCPRF on the possibility of adding a cushion between the raft and the piles and studying the effect of the seismic loading on the proposed foundation.

2. Methods

In various geotechnical applications, numerical modeling is commonly utilized to simulate foundation behavior. The preponderance of finite element programs only captures the structure's linear behavior (i.e., up to the yielding of the design). These programs fail to capture post-peak behavior (e.g., ultimate load-displacement responses, failure modes, and fracture patterns). The interaction between the pile shaft and the surrounding soil, on the other hand, is nonlinear. In addition to nonlinearity, the program should be able to capture the structure's post-peak reaction. As a result, choosing a program that can accommodate this behavior is essential. PLAXIS is a 3D nonlinear finite element software package that includes commonly used constitutive models to represent soil behavior, pile behavior, and the interface between pile and soil, unlike other programs. PLAXIS can capture various pile structural loading conditions (e.g., static and seismic loads on the pile). Calculating the relationships between stress and strain in different soil models is one of the advantages of the PLAXIS 3D software, which allows loading and unloading behavior [10–12]. The most often used model for determining material plasticity is the Mohr–Coulomb model. It is a model that is linearly elastic, and perfectly plastic. Hooke's law describes the linear elastic element. At the same time, the Mohr–Coulomb failure criterion represents the completely plastic part whenever plastic deformations occur, irreversible strains, or permanent deformations, appear in the material yield function, which is introduced as a function that describes whether or not deformations occur. The material will stiffen or soften under plastic straining if the yield surface varies with plastic strain. As a result, a perfectly plastic model with a set yield surface is a constitutive model [13].

Interface elements are used to simulate the soil-structure interaction. The adjacent structural and soil elements may have to slide together if interface components are not present. Between them, there is no relative movement (slipping or gapping). An interface can be created next to a plate, between two soil volumes, or between two geogrids. Interfaces in PLAXIS 3D are made up of 12-node interface elements after meshing. Node pairs make up interface elements. One node in a node pair is related to the structure, while the other is associated with the soil. The interaction between these two nodes defines the soil-structure interaction. It is made up of two perfectly elastic-plastic springs. The strength reduction factor (R_{inter}) is used to define the strength of the interface. An elastic-plastic model describes the behavior of the interface. The following relationship can be used to compute the interface strength parameters [14]: Mohr–Coulomb is the most common and easy to use and does not require many parameters and is available compared with hardening soft soil model (HSS).

$$c_{inter} = R_{inter.} C' ; \tag{1}$$

$$tan\,\varphi_{inter} = R_{inter.}\, tan\,\varphi' ; \tag{2}$$

$$\psi_{inter} = 0.0 \quad for\ R_{inter} < 1; otherwise\ \psi_{inter} = \psi_{soil} . \tag{3}$$

Rinter is a program parameter that is either automatically determined by the software or manually selected by the user. When the first option is chosen, there will be no drop in interface strength compared to surrounding soil; strength and all other characteristics will remain unchanged, except the Poisson's ratio. Rinter has a value = 1, this option is activated by default. The amount of Rinter is manually entered in the

second option. In a real soil-structure interaction, the interface will be weaker and more flexible than soil, where R_{inter} has a value less than unity. The appropriate R_{inter} value for interaction could be chosen based on the type of soil. The strength reduction is greater in cohesive soil than for cohesionless soil, implying that the R_{inter} value for cohesionless soil is larger. Whenever the interface strength reaches its limit value as described by Rinter, it reduces to a residual strength described by R_{inter} residual strength. When the third option is chosen, the R_{inter} residual is enabled as shown in Figure 1.

When the geometry model is complete, it must be divided into a mesh of finite elements. To obtain accurate results in the calculations that are carried out within the PLAXIS 3D software, accurate meshes of soil and structure are used. However, they are not used with high accuracy, which leads to spending a long time in the calculation. The dimension of model is 250×250×100 m, X, Y, Z respectively. The same dimensions, properties, number of piles, and thickness. The program divided the model into 11867 elements and 19858 nodes and the types of mesh is medium as shown in Figure 2.

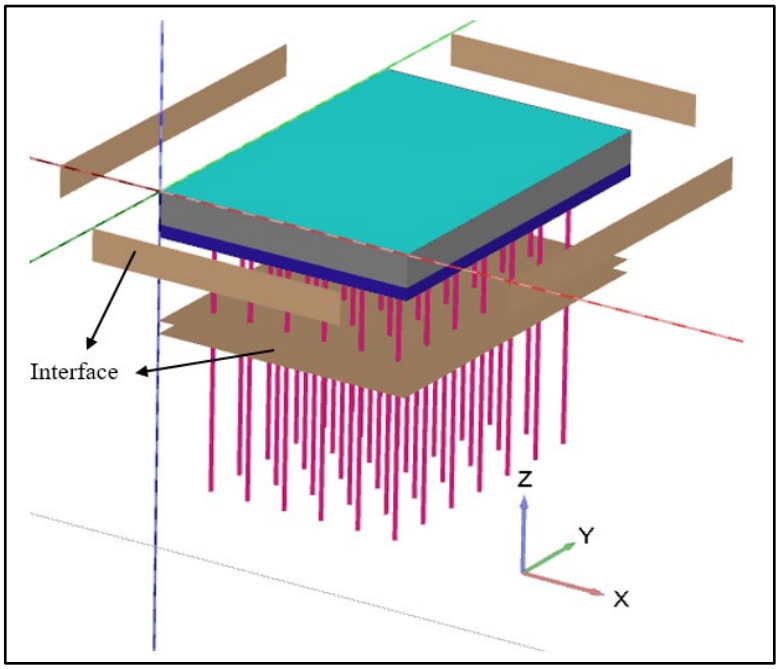

Figure 1. Modeling of interfaces.

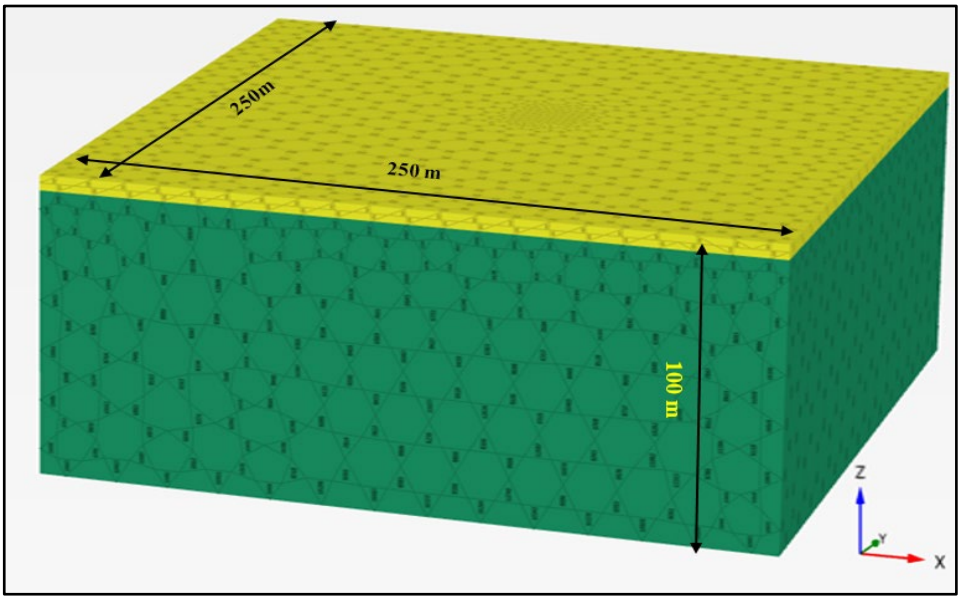

Figure 2. The mesh of finite element model used in this study.

2.1. Verification of Numerical Model

To verify the proposed numerical model, the foundation of the Messe-Torhaus building, Frankfurt, 1983–1985, under static loading was analyzed as an example of piled raft foundation [15]. The project is considered one of the first actual applications of piled raft foundation supporting a high-rise structure in

Germany. The proposed numerical model was formulated using PLAXIS 3D software. As a result, during the building phase, a monitoring program was rigorously implemented to watch the behavior of the piled raft foundation. This structure consists of 30 stories, split into two rafts 10 m apart. The rafts are constructed 3 m underneath the ground surface and have dimensions of 17.5×24.5 m. The structural load is 200,000 kN distributed evenly over the rafts to produce a stress of 466 kPa. The raft 2.5 m thick was attached to 42 drilled piles with a diameter of 0.9 m and a length of 20 m the groundwater level is 3 m below ground level as shown in Figure 3 [15]. The piles beneath each raft are evenly spaced with 3D to 3.5D spacing, where D is the pile diameter. Figure 4 shows the subsurface profile, consisting of 5 m of quaternary gravel and sand covering Frankfurt clay to a significant depth.

The properties of soil, cushion layer (sub-base), and geogrid used in the reinforcement of the cushion layer required in the proposed numerical model are listed in Tables 1 to 3 respectively. Figure 5 shows the piled raft foundation used in PLAXIS 3D. Reul and Randolph [16] presented an empirical equation to obtain the modulus of elasticity for the clay soils of the city of Frankfurt:

$$E = 45 + \left(tanh\left(z - 3015\right) + 1\right) \times 0.7z\,, \tag{4}$$

where E is modulus of elasticity (MPa) and z is depth below the surface (m).

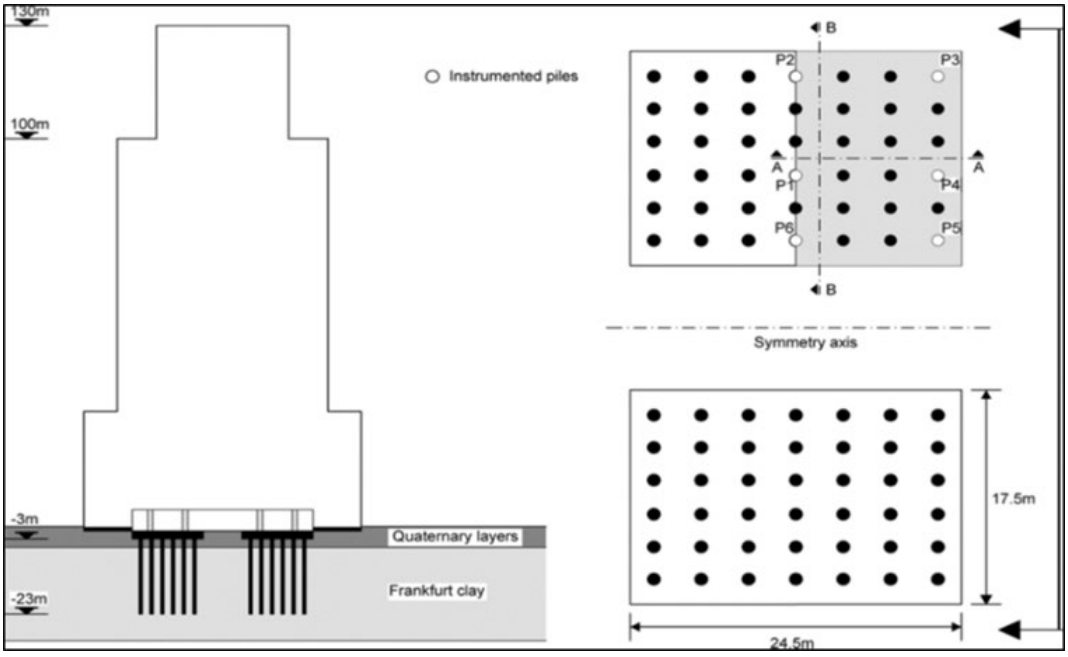

Figure 3. The piled raft system of the Messe-Torhaus building in Frankfurt [15].

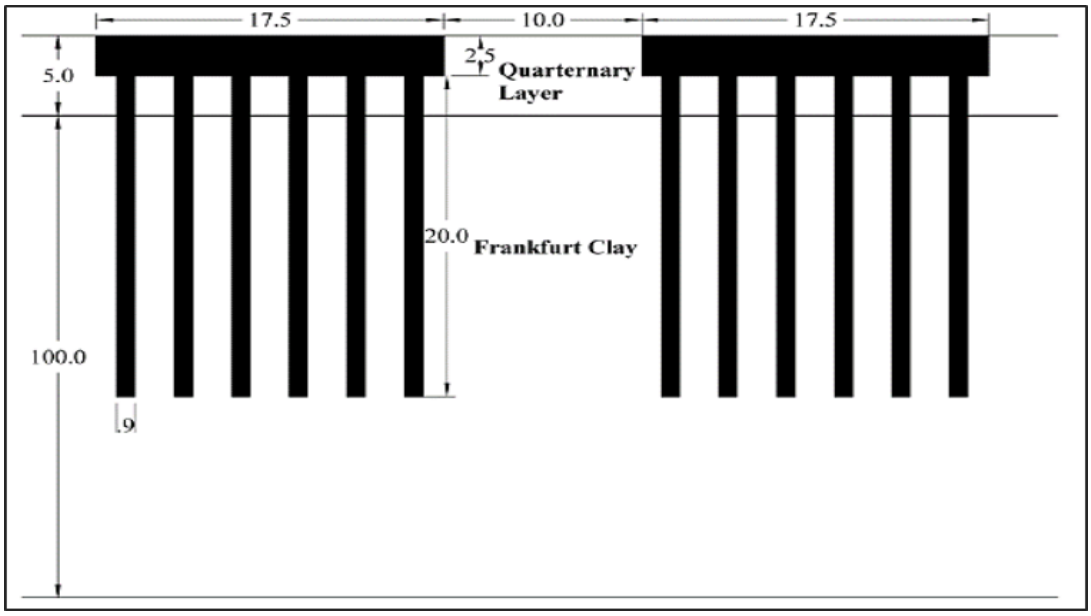

Figure 4. Soil layers support the foundation of the Messe-Torhaus building [15].

Table 1. Important parameters of the soil and piled raft for the Messe-Torhaus building [15].

Parameter	Quaternary gravel and sand	Frankfurt clay	Raft	Piles
Young's modulus, E (MPa)	75	50	34000	23500
Poisson ratio, v	0.25	0.35	0.2	0.2
Total unit weight (kN/m3)	18	19	25	25
Submerged unit weight (kN/m3)	–	9	–	–
Coefficient of lateral earth pressure at rest, k_o	0.72	0.46	–	–
The angle of internal friction, ∅′, degree	32.5	20	–	–
Cohesion, c (kPa)	0.1	20	–	–

Table 2. Properties of cushion layer used in the current study [17].

Property	Cushion layer
Modulus of elasticity, E (MPa)	60
The angle of friction, ∅ (degree)	19.4
Cohesion, c (kPa)	40
Dry unit weight (kN/m^3)	18.65

Table 3. Properties of geogrid used in the current study [18].

Parameters	Unit	Description or value
Material type	–	Elastic
Material behavior	–	Isotropic
Axial elastic stiffness (EA)	kN/m	110

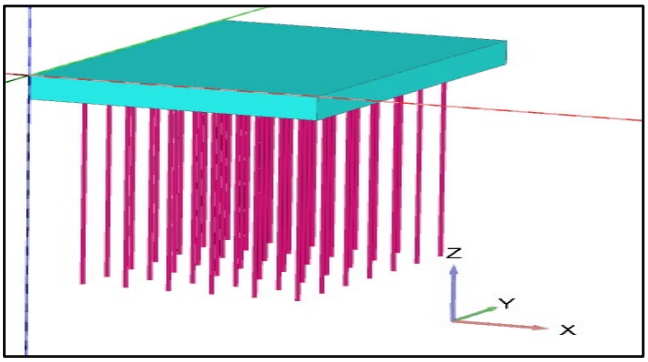

Figure 5. Modeling of Messe-Torhaus building in PLAXIS-3D software.

The maximum settlement recorded in the field due to the building's self-weight was 154 mm. For the same structural configuration and foundation characteristics (i.e., number of piles and raft dimensions), the numerical model predicted a settlement of 157 mm, demonstrating excellent agreement with the experimental observation (Figure 6). The deviation between the measured and simulated settlements is approximately 2%, indicating the reliability of the numerical model. In the foundation system of the Messe-Torhaus building, a 1 m-thick sand cushion layer (depicted in blue in Figure 7) was introduced to separate the piles from the raft. The influence of geogrid reinforcement within this cushion layer was also evaluated using the finite element software PLAXIS 3D. The geotechnical properties of the cushion layer are summarized in Table 2, where the elastic modulus of the sand layer was taken as 60 MPa [15].

.

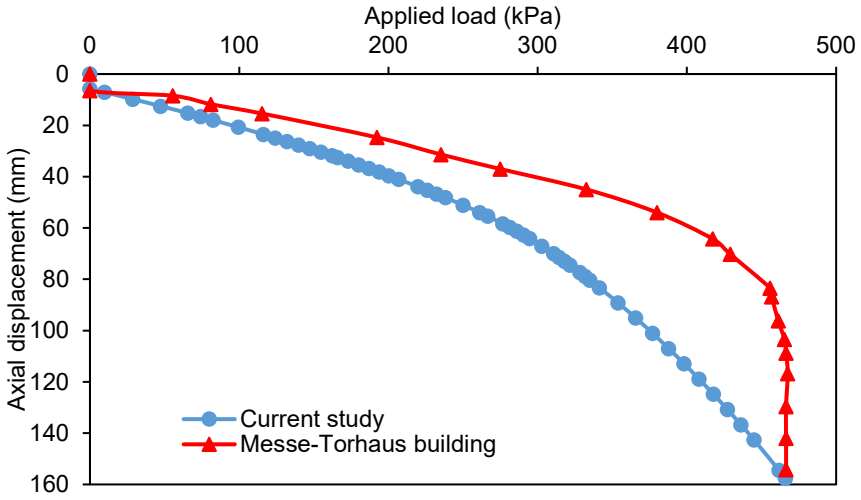

Figure 6. Verification of the settlement between the Messe-Torhaus building and the current study.

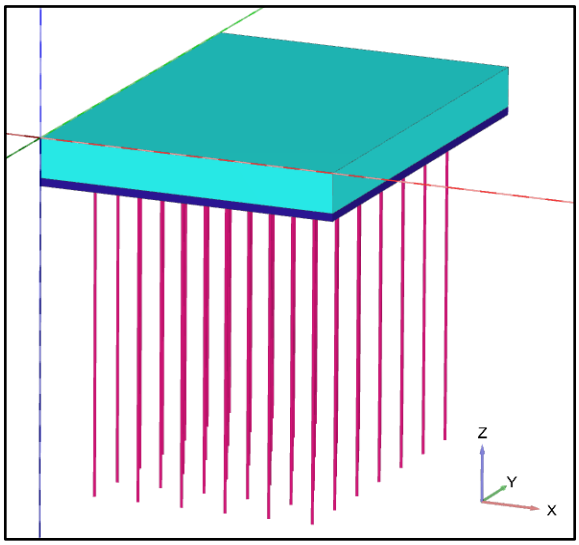

Figure 7. Disconnected piled raft model in PLAXIS 3D.

2.2. Seismic Loading

One of the most important and hazardous problems faced the geotechnical engineering is the presence of earthquakes that lead to damage or destruction of infrastructure as they affect the stability of facilities and foundations directly. Therefore, it is necessary to design the foundations in a strong manner that resists or limits the effect of earthquakes to preserve the safety of people from death. Recently, there has been an increasing interest in studying and understanding earthquake phenomena and trying to predict the time of their occurrence. Despite many studies having been conducted in this field, there was no accurate information on determining the time of earthquakes. Because Iraq is located within the earthquake-prone areas, where many earthquakes had hit Iraq over the past few years, where the eastern and northeastern regions witnessed many earthquakes, while the regions are stable in the south and southwest. This study will depend on the recorded data of an earthquake that struck Iraq in November 2017, in Halabja region, which killed many people and destroyed many structures. Halabja earthquake has a strength of 7.3 on the Richter scale (Peak ground acceleration, PGA = 1 m/sec^2) and its effect reached Baghdad city as shown in Figure 8 [19–25]. The behavior of the CPRFs and DCPRFs will be investigated under static and seismic loading.

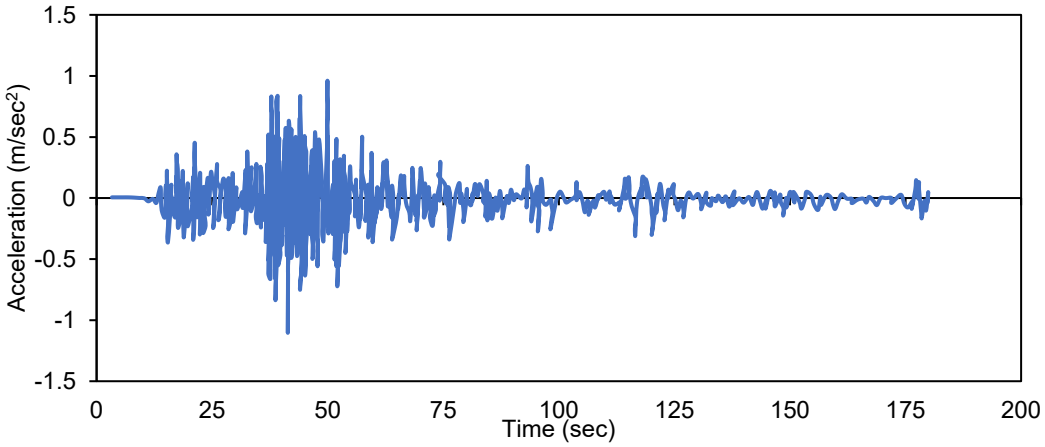

Figure 8. Acceleration–time history recorded in Baghdad for Halabjah earthquake.

3. Results and Discussion

The primary objective of this study is to evaluate the performance of the Disconnected Piled Raft Foundation (DCPRF) beneath the Messe-Torhaus building when subjected to seismic loading. This objective was achieved by analyzing the horizontal and vertical displacements of the foundation system and comparing the results with those obtained for a Connected Piled Raft Foundation (CPRF) under identical seismic conditions. The comparison aims to assess the effectiveness and seismic resistance behavior of the DCPRF.

3.1. Effect of Seismic Loading on Horizontal Displacement

To clarify the effect of the seismic load on the horizontal displacement during the static loads applied on the CPRFs and DCPRFs has been studied. Figure 9 shows the horizontal displacement of the raft caused by seismic loading in the CPRFs and DCPRFs.

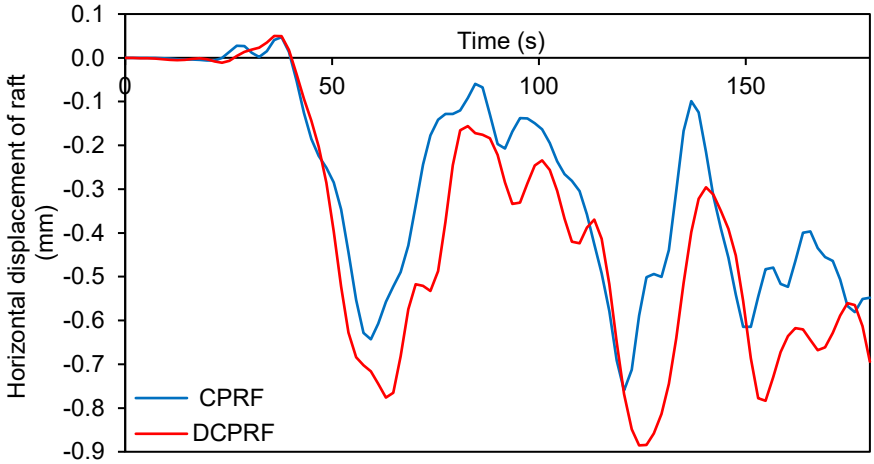

Figure 9. Horizontal displacement of the raft of the CPRF and DCPRF under seismic loading.

The horizontal displacement of the DCPRF is larger than the horizontal displacement of the CPRF by 15 %. This increase resulted from the lack of connection between the raft and piles or the piles behave as free head piles. When applying the Kobe earthquake with PGA (0.3 g), the horizontal displacement of the raft in the DCPRF increased by 45 % greater than the horizontal displacement in the CPRF as shown in Figure 10 due to increasing PGA from 0.1 g to 0.3 g.

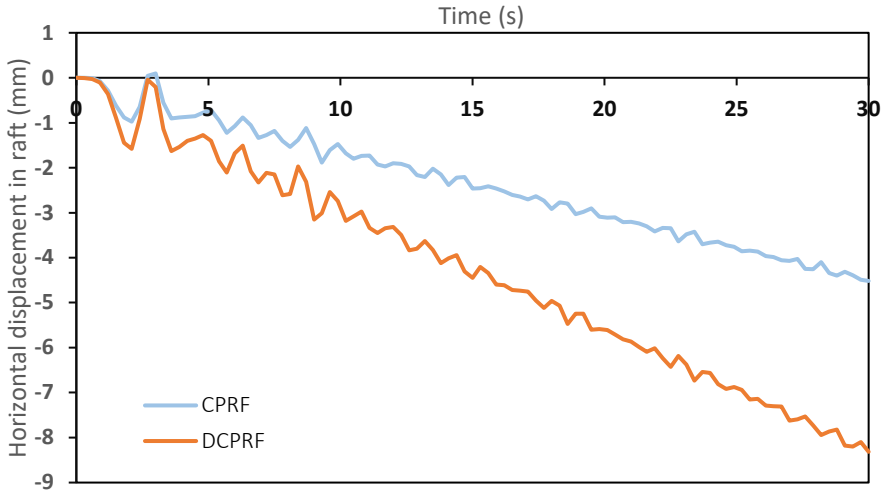

Figure 10. Horizontal displacement of the CPRF and DCPRF under seismic loading of Kobe.

3.2. Effect of Seismic Loading on Vertical Displacement

Figure 11 shows the effect of the seismic loading (Halabja earthquake) on the vertical displacement of the raft in the CPRF and DCPRF. The vertical displacement of the raft in the case of the CPRF is less than the vertical displacement of CPRF. The vertical displacement in the DCPRF decreased by 7 % from the CPRF because of the presence of the cushion layer, which plays an important role in the distribution of load between the soil and piles. Figure 12 shows the distribution of vertical settlement of the DCPRF under seismic loading obtained from PLAXIS 3D software. Applying the Kobe earthquake with PGA (0.3 g), the vertical displacement of the center of the raft in the CPRF increased by 38 % more than the displacement in the DCPRF as shown in Figure 13. Generally, increasing the intensity of the earthquake will increase the vertical displacement of the CPRF in comparison with the DCPRF.

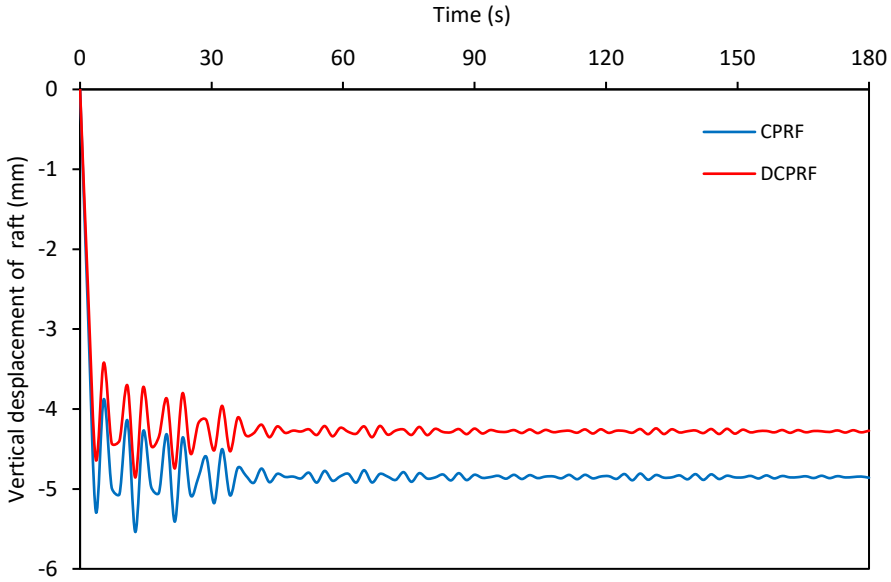

Figure 11. Vertical displacement at the center of the raft of the CPRF and DCPRF under seismic loading of Halabja earthquake.

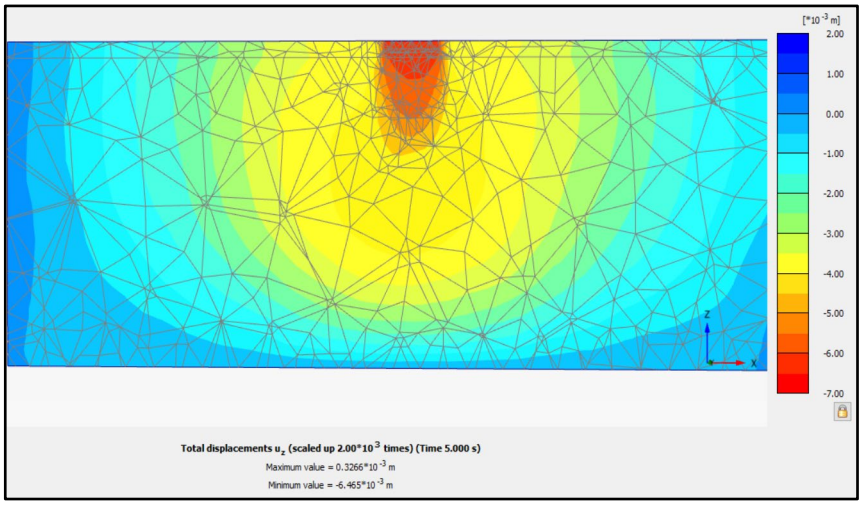

Figure 12. Distribution of vertical settlement of the DCPRF under seismic loading.

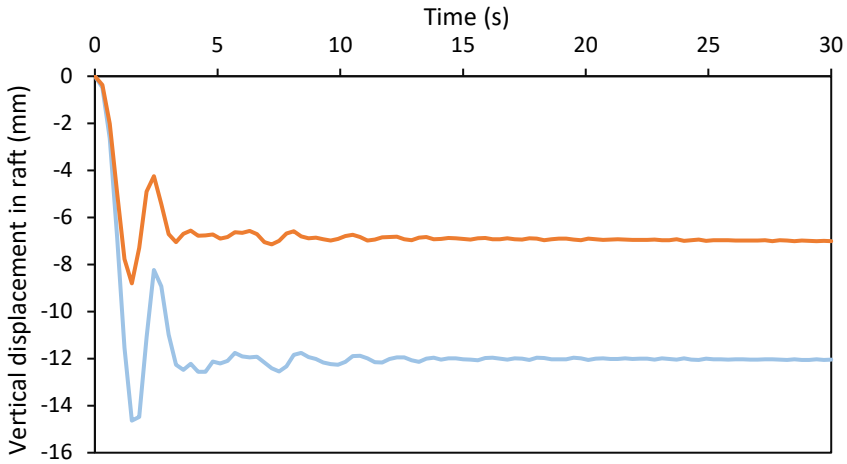

Figure 13. Vertical displacement at the center of the raft for the CPRF and DCPRF under seismic loading of Kobe earthquake.

Figure 14 shows the variation of the maximum vertical displacement under the raft foundation in both centerlines in long and short directions. The vertical displacement in the short direction at the edges is higher than that measured at the edges of the long direction of the raft. This decrease in vertical displacement is due to the difference in the dimensions of the raft foundation. While the vertical displacement at the center lines of long and short directions are almost the same.

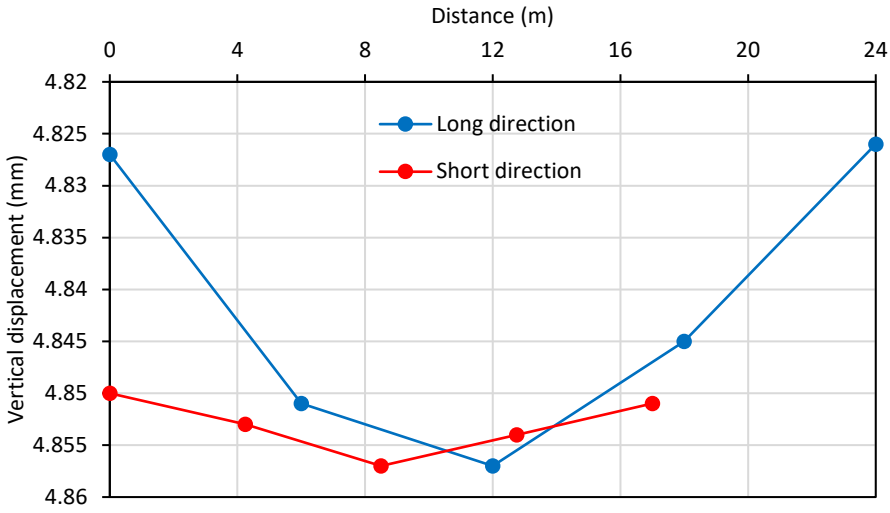

Figure 14. Vertical displacement of the raft foundation in the long and short directions under seismic loading.

The variation of axial load along the piles resulting from the seismic loading on the CPRF and the DCPRF is shown in Figure 15. In the case of the DCPRF, the axial force is less on the pile head compared to the CPRF by 44 %. In the case of the CPRF, the maximum axial load appears at the pile heal, and for DCPRF appears at the upper 1/5 of the pile length. The cushion layer will help to reduce the magnitude of axial load at the pile head, but the development of negative skin friction will increase the magnitude of axial load at the first quarter of the pile length.

The variation of shear force along the piles resulting from the effect of the seismic load on the DCPRF and CPRF is shown in Figure 16. At the pile head, the shear force is approximately equal to zero for the DCPRF, unlike the CPRF. The vanish in shear strength value results from the separation of piles from the raft by cushion layer, which change the situation of the pile head from fix pile head for the DCPRF to a free pile head. The DCPRF showed high variation in the shear force value along the pile length compared to the CPRF. From Figure 11, the shear force along the pile in the case of contact with the raft is less than it is in the pile disconnected from the raft. This decrease in shear force can be explained by the contact of the pile with the raft. At the pile tip, the shear force in the CPRF is higher than that in the pile head and higher than that in the DCPRF. The CPRF sustains low oscillation in the shear strength values which reflect the stability of such type of foundation.

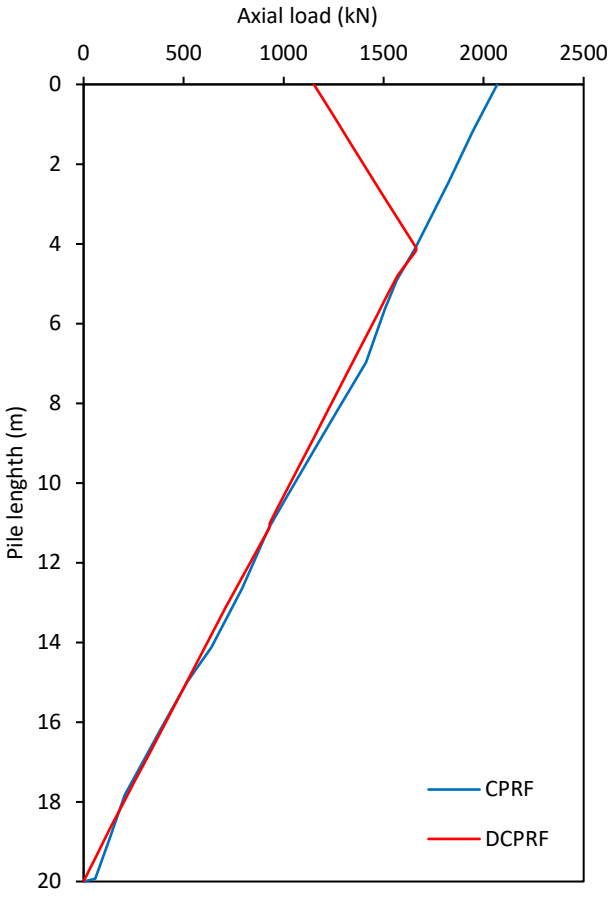

Figure 15. Variation of axial load along pile length of the DCPRF and CPRF system under seismic loading.

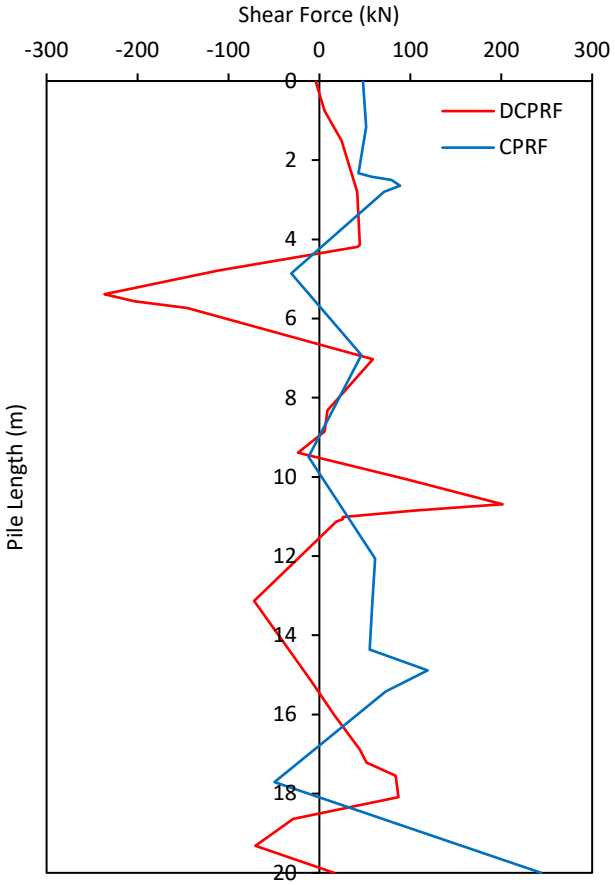

Figure 16. Variation of shear force of the DCPRF and CPRF system under seismic load at 180 sec.

Figure 17 shows the variation of the maximum bending moment along the pile under the influence of the seismic load in the connected and disconnected piled raft systems. In the connected piled raft system, the maximum bending moment value occurred at the head of the pile and then decreases with the depth. For the DCPRF, the bending moment value is approximately equal to zero at the head of the pile and the maximum value of the bending moment occurred in the upper quarter and middle of the pile. It is noticed from Figure 16 that the effect of the seismic load on the foundation compared to the vertical static load is small. While when use the DCPRF can solve the problems that damage the structural connections between the raft and the piles when an earthquake occurs.

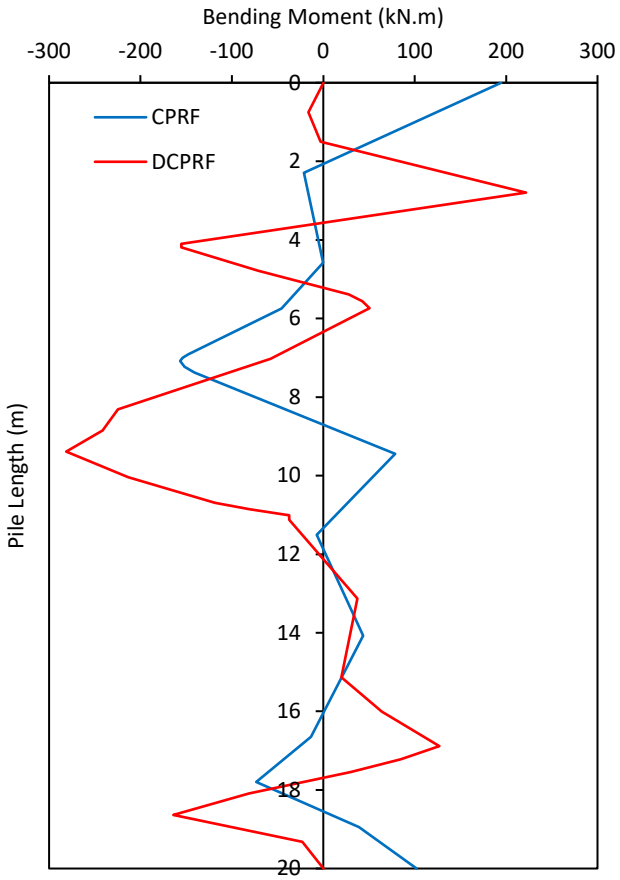

Figure 17. Bending moment of the DCPRF and CPRF system under seismic load at 180 sec.

4. Conclusions

The behavior of the proposed DCPRF is compared with the CPRF under the Messe-Torhaus building. Based on the results of the proposed numerical model simulating the behavior of the DCPRFs under seismic loading, the following points can be drawn out:

The verification of the proposed numerical model showed that the difference between the settlement calculated from numerical and field measurements for the Messe-Torhaus building in Frankfurt was 2 %.

The horizontal displacement of the raft in the CPRF is less than the horizontal displacement of the raft in the DCPRF during seismic loading by 15 %.

The vertical displacement in the DCPRF decreased by 7 % in comparison with the CPRF.

For the DCPRF, the bending moment value is approximately equal to zero at the pile head, and the maximum bending moment value occurred at the upper quarter and the middle of the pile.

The axial force at the pile head in the DCPRF is less on the pile head of the CPRF by 44 %.

References

1. Burland, J.B. Behaviour of foundations and structures on soft ground. Proceedings of the Ninth International Conference on Soil Mechanics and Foundation Engineering. 2. Tokyo, 1977. Pp. 495–546.
2. Karkush, M.O., Aljorany, A.N. Analytical and Numerical Analysis of Piled-Raft Foundation of Storage Tank. Lecture Notes in Civil Engineering. 2020. 84. Construction in Geotechnical Engineering. Pp. 373–384. DOI: 10.1007/978-981-15-6090-3_26
3. Karkush, M.O., Aljorany, A.N. Numerical Evaluation of Foundation of Digester Tank of Sewage Treatment Plant. Civil Engineering Journal. 2019. 5(5). Pp. 996–1006. DOI: 10.28991/cej-2019-03091306
4. Wong, I.H., Chang, M.F., Cao, X.D. Raft foundations with disconnected settlement-reducing piles. Design Applications of Raft Foundations. Thomas Telford. London, 2000. Pp. 469–486. DOI: 10.1680/daorf.27657.0017
5. Karkush, M.O., Sabaa, M.R., Salman, A.D., Al-Rumaithi, A. Prediction of bearing capacity of driven piles for Basrah Governatore using SPT and MATLAB. Journal of the Mechanical Behavior of Materials. 2022. 31(1). Pp. 39–51. DOI: 10.1515/jmbm-2022-0005
6. Karkush, M.O., Ahmed, M.D., Sheikha, A.A., Al-Rumaithi, A. Thematic Maps for the Variation of Bearing Capacity of Soil Using SPTs and MATLAB. Geosciences. 2020. 10(9). Article no. 329. DOI: 10.3390/geosciences10090329
7. Cao, X.D., Wong, I.H., Chang, M.F. Behavior of Model Rafts Resting on Pile-Reinforced Sand. Journal of Geotechnical and Geoenvironmental Engineering. 2004. 130(2). Pp. 129–138. DOI: 10.1061/(ASCE)1090-0241(2004)130:2(129)

8. Liang, F.Y., Chen, L.Z., Shi, X.G. Numerical analysis of composite piled raft with cushion subjected to vertical load. Computers and Geotechnics. 2003. 30(6). Pp. 443–453. DOI: 10.1016/S0266-352X(03)00057-0
9. Chan DH, Law KT, editors. Soft Soil Engineering: Proceedings of the Fourth International Conference on Soft Soil Engineering, Vancouver, Canada, 4-6 October 2006. CRC Press; 2006 Sep 28..
10. Fioravante, V. Load transfer from a raft to a pile with an interposed layer. Géotechnique. 2011. 61(2). Pp. 121–132. DOI: 10.1680/geot.7.00187
11. Polishchuk, A.I., Maksimov, F.A. Numerical Analysis of Helical Pile–Soil Interaction under Compressive Loads. IOP Conference Series: Materials Science and Engineering. 2017. 262(1). Article no. 012099. DOI: 10.1088/1757-899X/262/1/012099
12. Karkush, M.O., Ali, S.D., Saidik, N.M., Al-Delfee, A.N. Numerical Modeling of Sheet Pile Quay Wall Performance Subjected to Earthquake. Geotechnical Engineering and Sustainable Construction: Sustainable Geotechnical Engineering. Springer. Singapore, 2022. Pp. 355–365. DOI: 10.1007/978-981-16-6277-5_28
13. Gurtin, M.E., Anand, L. A theory of strain-gradient plasticity for isotropic, plastically irrotational materials. Part I: Small deformations. Journal of the Mechanics and Physics of Solids. 2005. 53(7). Pp. 1624–1649. DOI: 10.1016/j.jmps.2004.12.008
14. Datta, D., Varma, A.H., Coleman, J. Investigation of interface non-linearity on Non-linear Soil Structure Interaction analyses. Transactions. 24th International Conference on Structural Mechanics in Reactor Technology. SMiRT-24. Division 5. BEXCO. Busan, 2017.
15. Katzenbach, R., Arslan, U., Moormann, C. Piled Raft Foundations Projects in Germany. Design Applications of Raft Foundations. Thomas Telford. London, 2000. Pp. 323–391.
16. Reul, O., Randolph, M.F. Study of the influence of finite element mesh refinement on the calculated bearing behaviour of a piled raft. Numerical Models in Geomechanics: Proceedings of the 8th International Symposium NUMOG VIII. Rome, 2002. Pp. 259–264. DOI: 10.1201/9781439833797-c38
17. Alhassani, A.M.J., Aljorany, A.N. Parametric Study on Unconnected Piled Raft Foundation Using Numerical Modelling. Journal of Engineering. 2020. 26(5). Pp. 156–171. DOI: 10.31026/j.eng.2020.05.11
18. Taha, A., El Naggar, M.H., Turan, A. Experimental and numerical study on lateral behaviour of geosynthetic-reinforced pile foundation system. Geosynthetics International. 2014. 21(6). Pp. 352–363. DOI: 10.1680/gein.14.00023
19. Al-Taie, A.J., Albusoda, B.S. Earthquake hazard on Iraqi soil: Halabjah earthquake as a case study. Geodesy and Geodynamics. 2019. 10(3). Pp. 196–204. DOI: 10.1016/j.geog.2019.03.004
20. Karkush M, Almurshedi AD, AlSaadi KA, Al-Salakh AM. Behavior of partially connected piled raft foundation under seismic loading. Magazine of Civil Engineering. 2024;17(4)..
21. Tradigo, F., Pisanò, F., di Prisco, C. On the use of embedded pile elements for the numerical analysis of disconnected piled rafts. Computers and Geotechnics. 2016. 72. Pp. 89–99. DOI: 10.1016/j.compgeo.2015.11.005
22. Lin, C., Liu, Q., Su, Y., Yue, C., Zeng, L. Load transfer of the disconnected pile. Acta Geotechnica. 2024. 19(8). Pp. 5673–5684. DOI: 10.1007/s11440-024-02285-0
23. Tradigo, F., Pisanò, F., di Prisco, C., Mussi, A. Non-linear soil–structure interaction in disconnected piled raft foundations. Computers and Geotechnics. 2015. 63. Pp. 121–134. DOI: 10.1016/j.compgeo.2014.08.014
24. Halder, P., Manna, B. Load transfer mechanism for connected and disconnected piled raft: a comparative study. Acta Geotechnica. 2022. 17(2). Pp. 3033–3045. DOI: 10.1007/s11440-021-01409-0
25. Jawad, K.A., Salman, A.D. Effect of Rubber Scrap Tire Pads on the Behavior of Partially Connected Pile Raft Foundation System Subjected to Dynamic Loading. Journal of Engineering. 2024. 30(07). Pp. 15–34. DOI: 10.31026/j.eng.2024.07.02

Information about the authors:

***Mahdi Karkush**, Doctor of Technical Sciences*

ORCID: https://orcid.org/0000-0003-1304-0303

E-mail: mahdi_karkush@coeng.uobaghdad.edu.iq

***Sajjad Nafel**,*

E-mail: sajjad.nafil2001m@coeng.uobaghdad.edu.iq

Received 05.12.2024 Approved after reviewing 06.04.2025. Accepted 26.04.2025.